University of Nottingham Malaysia

Department of Mechanical, Materials and Manufacturing Engineering

Development and Characterisation of Thermal Responsive Shape Memory Natural Rubber

by Kow Yu Yang

Thesis submitted to the University of Nottingham for the fulfillment of the degree of Doctor of Philosophy, 2022

Abstract

Compared to the last century, research and development of smart materials are receiving more attention due to their ability to change shape in response to specific environmental conditions. Although the development of shape memory natural rubber is motivated by the higher recovery strain, low trigger temperature leads to poor shape memory performance typically when the surrounding temperature is increased. A new shape memory natural rubber fabrication method, prevulcanisation is proposed to maintain the crystalline structure of the rubber molecule at elevated temperature. The low molar fatty acid which is palmitic acid involves in the prevulcanisation process to increase the trigger temperature of shape memory natural rubber. The prevulcanised rubber is fabricated with various amount of palmitic acid and sulphur to evaluate its shape memory capability under different temperature conditions (various programming temperatures and recovery temperatures). A custom-made stretching apparatus is developed to measure the shape memory parameters (shape fixity and shape recovery) under strain-control mode. The shape memory experimental settings (200% deformation strain for the shape memory natural rubber with less than 60% palmitic acid loading) are determined from the swollen shape memory natural rubber experiment. According to the shape memory experiment of prevulcanised rubber, the outstanding shape fixity and shape recovery are found when the temperature is closer to the melting temperature of the palmitic acid during the programming and recovery process. A similar trend is observed when palmitic acid content is increased. However, the sulphur content (>1.0pphr) has a reverse effect, causing the prevulcanised rubber to behave like elastic rubber and immediately recover its shape after unloading. Apart from the shape memory experiment, other material properties such as rubber strength and stress relaxation are also investigated. Furthermore, a shape

memory behaviours prediction model is adopted to model the shape memory responses by using a standard linear solid model with Kelvin-Voigt element and a thermal strain model. The prediction model captured the shape memory behaviours appropriately and provided some insights on the stress-strain response of the respective segment phases for the shape memory process.

Acknowledgment

Foremost, I would first like to thank my principal supervisor, Dr Chai Ai Bao for the continuous support of my Phd study and research for her patience, motivation and effort in supervising my research works. I appreciate having a supervisor who leads me in every project stage.

I also would like to express my gratitude to my co-supervisor, Dr Ho Jee Hou, for his guidance and support on my research project. Without Dr Ho's assistance, my research work would never have been accomplished in this short span.

I am grateful to my family members, who always encourage me and provide me with emotional and financial support for my life. Without their encouragement and support, I would never start my research work or even had a wonderful postgraduate life. Although my late mother, Mdm Chee Chooi Leng would never have a chance to attend any of my graduations, I am thankful for her bring me to this world and have an amazing family.

List of Publications

1) Yu Yang Kow, Ai Bao Chai, Jee Hou Ho, “Relationship between swelling temperature and shape memory properties of palmitic acid-based shape memory natural rubber,” Journal of Rubber Research, Volume 23, Issue 1, PP. 13-22, 2020

2) Yu Yang Kow, Ai Bao Chai, Jee Hou Ho, “Development of shape memory natural rubber through prevulcanisation method,” IOP Conference Series: Earth and Environmental Science, Volume 442, Issue 1, 2020

3) Yu Yang Kow, Ai Bao Chai, Jee Hou Ho, “The effect of palmitic acid loadings on the shape memory cycle of shape memory natural rubber,” IOP Conference Series: Earth and Environmental Science, Volume 442, Issues 1, 2020

Table of Contents

List of Figures

List of Tables

Nomenclature

Abbreviations

ATA	3-amino-1,2,4-triazole
CGNR	Commercial grade vulcanised natural rubber
DMA	Dynamic mechanical analysis
DSC	Differential scanning calorimetry
DTG	Derivative thermogravimetry
ENR	Epoxidised natural rubber
KOH	Potassium hydroxide
MPT	Multi-Purpose Testware
NR	Natural rubber
NRL	Natural rubber latex
PCL	Poly(ε-caprolactone)
PEG	Poly (ethylene glycol)
POE	Polyolefin elastomer
S	Swelling ratio
SIC	Strain-induced crystallisation
SLS	Standard linear Solid
SMA	Shape memory alloy
SMC	Shape memory ceramic
SME	Shape memory effect

SMG	Shape memory gel
SMM	Shape memory material
SMNR	Shape memory natural rubber
SMP	Shape memory polymer
TGA	Thermal gravimetric analysis
T_g	Glass transition temperature
T_c	Trigger temperature
T_{high}	Heating temperature
T_{low}	Cooling temperature
T_m	Melting temperature
T_p	Programming temperature
T_r	Recovery temperature
TTS	Time-temperature superposition
TWSME	Two way-shape memory effect
WLF	Williams-Landel-Ferry
ZDA	Zinc diacrylate
ZDEC	Zinc Diethyldithiocarbamate
ZMBR	zinc 2-mercaptobenzothiazole
ZnO	Zinc Oxide

Parameters

B	Left Cauchy-Green deformation tensors
C	Right Cauchy-Green deformation tensors
C_1, C_2	Material constant of Mooney Rivlin
C_{T1},$C_{T2}, C_{T3}, C_{T4}, C_{T5}, C_{T6}$	Coefficients of the temperature algorithm
C_{sa1}, C_{sa2}	Material constant of Mooney Rivlin for soft active segment phase
C_{sf1}, C_{sf2}	Material constant of Mooney Rivlin for soft frozen segment phase
E	Total material stiffness
E_1, E_2	Material stiffness
E_R	Relaxed modulus
E_U	unrelaxed modulus
$\dot{\varepsilon}$	Strain rate
ε	Total strain
ε_h	Hard segment strain
ε_f	Fixed strain
ε_i	Initial strain
ε_l	Loaded strain
ε_p	Programming strain
ε_r	Recovery strain
ε_{r40},$\varepsilon_{r50}, \varepsilon_{r60}, \varepsilon_{r70}$	Recovery strain at the temperature of 40^{o}C ,50^{o}C, 60^{o}C, and 70^{o}C, respectively
$\varepsilon_{sa}, \varepsilon_{sf}$	Soft segment strain (active and frozen state)

ε_t	Thermal strain
F	Deformation gradient
k_b	Boltzmann constant
λ	Extension ratio
η	Material viscosity
p	Hydrostatic pressure
ρ_{nr}	Density of natural rubber
ρ_p	Density of palmitic acid
U	Activation energy
S_f	Shape fixity
S_r	Shape recovery
$\dot{\sigma}$	Stress rate
σ	Total stress
σ_h	Hard segment stress
σ_H	Upper boundary stress
σ_L	Lower boundary stress
σ_{SR}	Stress value measured from stress reduction equation
σ_{TH}	Stress value under the deformed strain of 200% at 70°C
σ_{sa}, σ_{sf}	Soft segment stress (active and frozen state)
τ'	Retardation time
$T_{r40}, T_{r50}, T_{r60}, T_{r70}$	The recovery temperature of 40°C ,50°C, 60°C, and 70°C, respectively

t_i	Time for undergoing strain change
T_H	Upper boundary of temperature
T_L	Lower boundary of temperature
V_h	Volume fraction of hard segment phase
V_p	Volume fraction of palmitic acid
Vs_a,Vs_f	Volume fraction of soft segment phase (active and frozen state)
W	Strain energy
wt%	Weight fraction
W_p	Weight fraction of palmitic acid
W_r	Weight fraction of natural rubber

1 Introduction

1.1 Research Background

Shape memory material (SMM) is emerging as a smart material because of its inherent characteristic which is shape memory effect (SME). SME offers the ability to retain the deformed shape and regain its original shape under specific environmental conditions. This characteristic encourages the development of SMM in medical application and electrical sensors [1]–[4]. By reviewing the past research works about the SMM, they are proven that SMM motion is predictable and controllable, even the imitation of animal locomotion possible implements under adopting SMM [5]–[7]. In addition, shape memory composite has shown to exhibit a two-way shape memory effect (TWSME) when subjected to multiple intermolecular phases change under a single weight load [8]–[10]. Unlike one-way shape memory effect (OWSME), TWSME offers the ability of switching two different shapes by responding to two different environmental conditions without involving any external stress.

Apart from shape recovery, self-healing is another popular area of research in the development of SMM [11]–[13]. Self-healing allows supramolecular assemblies or covalent bonding to repair thermal or mechanical damage on the material's surface [14]. The material properties could regain back to initial status by recovering surface damage. Other than that, self-healing also enhances the material lifetime and the possibility of ease of maintenance to the material. These benefits of self-healing ability have explored the diverse range of industrial applications, such as be the primary material of the aircraft to reduce the necessary repair work and overhaul [15], eliminating the crack propagation on the biological concrete [16], [17] and prolonging the lifetime service of smart battery [18]. However, SME is not an inherent feature for

a particular material group. SME properties are discovered into three common earth material groups, which are shape memory alloy (SMA), shape memory ceramic (SMC) and shape memory polymer (SMP).

In many engineering applications, the research on shape memory polymer (SMP) is more extensive than other SMMs, owing to the polymer's diverse range of methods to trigger the SME, including corrosion, fluctuating vibration, and even moisture level. SMP increases the sensitivity of polymer structures to react with complex and harsh environments to trigger shape memory effect. Beside the heat activation, magnetically triggered, electrically activated, and chemo-responsive are the other shape memory trigger methods discovered by studying the polymer phenomena of SMP [19]–[21]. Furthermore, some SMPs can be recognised as biocompatible and biodegradable materials, such as the blend composition of thermoplastic polyurethane and polylactic acid and the copolymerized polymer of methyl methacrylate and poly (ethylene glycol) dimethacrylate [22]–[24]. The wide range of polymeric materials allows SMP has a higher degree of freedom in material selection to meet particular application needs. However, in a relatively less explored area, natural rubber could be a viable means to be developed as one of the SMP.

Natural rubber (NR) as an elastomeric polymer is an attractive candidate for SMP development. Its unique properties include high elasticity, superior mechanical properties to withstand wear and tear force, and high corrosive resistance for organic and inorganic compounds. Due to this combination of traits, rubber products are widely used and growing fast in the automotive industries, food processing industry, and infrastructure field [25]–[28]. Moreover, the superior energy absorbing property enables NR to significantly contribute to vibration isolation or as a soundproof material [29]–[32]. The development of NR also involves the research of seismic isolation to minimise structural damage caused by earthquakes [33], [34]. This inflatable feature

allows rubber products to withstand impact force or eliminate the vibration forces. NR also reduces the risk of collision or injury when interacting with humans or the environment if NR is used as the SMM of soft robots [35].

Moreover, NR is an important raw material export from the Southeast Asia because 90% of world NR raw materials are supplied by ASEAN countries such as Malaysia, Thailand, and Vietnam [36]. Since the late 19th century, when the first rubber tree, *Hevea Brasiliensis* was transferred to Singapore, the rubber plantation in Southeast Asia has grown dramatically. Within 20 years, Southeast Asia become the world's largest NR vendor (93% of world supply) [37]. Although the invention of synthetic rubber had a significant impact on the rubber wealth in the mid of 20th century, the price trend of NR was gradually rebounded during the 1973 oil crisis [38]. Even today, NR research and development have a prominent position in Southeast Asia. For instance, Thailand, our neighbour country, investigates the greenhouse gas emission and carbon sequestration potential of rubber trees [39]–[41]. While Malaysia is the world's largest supplier of rubber products such as medical gloves and rubber catheters, it is turning away from raw material exports and moving toward the NR manufacturing segment [36], [42]. Research is establishing on practical usage for NR, and it is aligned with government policy of promoting and expanding NR usage across the community.

Even though NR material has been relatively well established with a variation of product family ranging from household items to industry applications, the research on shape memory natural rubber (SMNR) is less common than other SMP classes. SMNR is a thermo-responsive material which SME corresponds to the thermal properties of strain-induced crystallisation (SIC). Nevertheless, NR is an amorphous polymer with a relatively low glass transition temperature (-70^{o}C), far below ambient temperature. This lead to the crystal structures is unstable and vanish at

room temperature which deformed strain recover immediately after unloading [43]. In a result, none or low SME is exhibited, and this restricted ambient environment limits the SMNR implementation.

Nevertheless, the formation of SIC is influenced by different factors such as crosslink density, deformation level, and temperature [44]–[46]. Speciality modification and chemical synthesis such as epoxidized natural rubber (ENR) and blending with low molar mass organic compound are the solutions to increase the trigger temperature [47]–[49]. To improve the stability of SIC during the unloading process, incorporating palmitic acid as the reinforcement agent in SMNR fulfilled the economic purpose. High crystallinity of palmitic acid allows to retard the decrystallisation process to a higher temperature range to enhance the SME at room temperature. Moreover, oil palm is another large commodity in Malaysia. Diversifying the usage of palmitic acid on SMNR not only promotes Malaysia economy, but also fulfils Malaysia national policy on Industry 4.0, which more automation elements can be incorporated in the manufacturing sector.

This research works can be regarded as the first step toward a preliminary shape memory analysis of commercial rubber bands and natural rubber latex film on the swelling process. Besides investigating on the shape memory response under various swelling duration, the effect of the elongation strain and swelling temperature are also considered in shape memory analysis. A custom-made stretching apparatus is developed to capture the shape memory response of different swollen specimens under strain control mode. The second phase of experimental work focuses on the characteristics of the SMNR fabricated through prevulcanisation method. SMNR developed with various crosslinked density and palmitic acid content is inspected with the stretching device to measure the shape memory parameters. More precisely, a dynamic mechanical analysis (DMA) machine is utilised to investigate the shape memory characteristics such as trigger temperature and

the stress reduction that is caused by temperature change. The influence of the formulation on the mechanical characteristics of the SMNR is also investigated. Last but not least, a simple shape memory behaviour prediction model is proposed to model the shape memory behaviours of the SMNR.

1.2 Problem Statements

The lightweight and flexibility of natural rubber have motivated the research on SMNR. However, low trigger temperature is the primary obstacle in SMNR development. NR as an amorphous polymer, the trigger temperature of the SMNR is corresponding to its glass transition temperature which far below room temperature. This relatively low glass temperature leads to NR exhibits poor SME above room temperature.

In addition, mechanical degradation is another concern in SMNR development. To improve the SME, filler and reinforcement agent are commonly incorporated to fabricate SMP, similar to SMNR. Nevertheless, weak interfacial adhesion and the degradation from overflowing solvent not only constrain the stretching ratio, but also might lead to reduce shape performance like low strain recoverability (plastic deformation involved) or instantly recovery (without go through reheating or unable to fix the deformed strain).

The development of shape memory prediction system for SMNR is limited and rare compared to other SMP. The nonlinear mechanical response and low trigger temperature increase the complexity on simulating the shape memory behaviour. In consequence, the development for SMNR is much slower than other SMP. Hence, this project is conducted to develop and characterize thermally responsive SMNR with wider working temperature.

1.3 Aim and objectives

This project aims to develop a thermal responsive palmitic acid-based SMNR. To achieve the aim of this project, the objectives of this research project are layout as follows:

1. To develop a temperature-responsive palmitic acid-based SMNR
2. To characterise the shape memory response of the SMNR developed
3. To investigate the mechanical characteristics of SMNR developed.
4. To propose a shape memory prediction model to demonstrate the shape memory behaviours of SMNR.

1.4 Significance of Research

This thesis presents a novel SMNR fabrication under prevulcanisation to exhibit the shape memory effect above the room temperature. Prevulcanised NR allows to shift the trigger temperature to around the melting temperature of the fatty acid by mixing the new fatty acid soap (potassium palmitate) with natural rubber latex solution under dispersion form. To avoid the occurrence of coagulation when latex solution is reacting with acid compound, the palmitic acid has to go through the saponification reaction before mixing process. In the process of developing this SMNR, the significant contributions have been made:

- The shape memory experiment allows to review and analyse the component effect (various sulphur and palmitic acid content) on shape memory properties under swelling and prevulcanisation fabrication method.

- Thermal effect is another primary corner within this research work. Beside the swelling temperature effect for swollen specimen, the working temperature, programming temperature and recovery temperature, are also inspected in the shape memory experiment for prevulcanised specimens.

- The mechanical properties of SMNR are characterised within this research project. The prevulcanised SMNR have the complete different tensile behaviour as they are examined under room temperature and 70^{o}C. Although the tensile stress is enhanced with the palmitic acid content, the elongation at break is deteriorated with increasing amount of palmitic acid.

- This project adopts a phase transition model to simulate the shape memory behaviour under different palmitic acid content. It is the first constitutive model to simulate the SME for prevulcanised SMNR. Besides the thermal strain, the change of volume fraction between the palmitic acid and natural rubber also been taken into account for this shape memory prediction system.

1.5 Layout of the thesis

The thesis is organized as follows: Chapter 1 provides the background and motivation to develop the SMNR. The objectives and scope of the research works are also listed within this chapter.

Chapter 2 describes the relevant literature review corresponding to the SMM and SMNR. This section starts with the general review on SMM and shape memory mechanism of each SMMs. Subsequently, the fabrication methods and trigger methods of SMP are reviewed. Moreover, the factors influence the trigger temperature and the growth of SIC are also included in Chapter 2. The past research works about shape memory prediction mechanisms and their frameworks are also mentioned within this chapter.

The research methodology is presented in Chapter 3. The details and experimental procedures of the characterisation and investigation on the SME for rubber specimen with and without palmitic acid under swelling and prevulcanisation condition, are discussed. It includes specimens' preparation, experimental setup, the development of the custom-made stretching apparatus, and the experiment process. In addition, the mechanical response experiments which is prepared to establish the shape memory behaviour prediction model are also mentioned. The description and algorithm model of the shape memory behaviour prediction system also presented in this chapter.

Chapter 4 is the result and discussion section on the shape memory characteristics of both specimens. The modelling results and parameters selection are reported in Chapter 5. Lastly, Chapter 6 summarises the current research works and suggests some investigation directions for future research works.

2 Literature Review

SMM has emerged as an intelligent multifunctional material because of its unique capability to memorize its original shape even after seemingly plastic deformation. They can change their physical shape or chemical properties in response to specific stimuli. This action series is termed as SME, is divided into two stages, which are shape programming and shape recovery. The former occurs as a result of the action of retaining the temporary shape, whereas the latter is triggered by the elastic behaviour of particles, as illustrated in Figure 2.1. Driven by the requirements of engineering applications, researchers have actively researched on SMM to explore new functionality and enhance their performance over the last few decades. Due to the high intelligence and ease of maintenance, SMM has increased its popularity in a variety of material groups, including SMA [50]–[52], SMC [53]–[55] and SMP [56], [57].

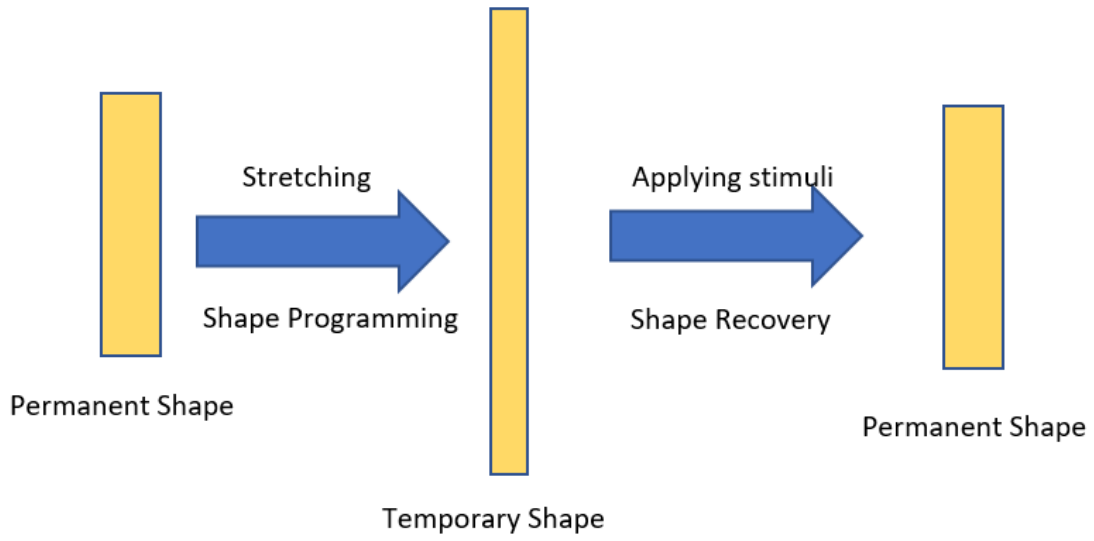

Figure 2.1: The action series of SME

Although the driving mechanism of SME is similar for each SMM, they are exposed to different structural phases to demonstrate the SME. For example, SMA and SMC rely on the crystalline microstructure which are martensitic and austenite to exhibit the SME. Figure 2.2 refers to the structural phases of object for each shape process under variation in temperature, stress and strain. For OWSME process, the shape programming occurs after object deformed under martensitic phase in low temperature (below austenite-start-temperature, A_s). Once the object is heated to above A_s, the shape recovery process is triggered which the martensitic phase began to transform into austenite phase. Although, reversible SME or TWSME is feasible by maintaining the temperature in between the martensitic phase temperature and austenite phase temperature, it exhibited poor result in recoverable strain for SMAs [58]. Pseudoelasticity or superelasticity is another distinguished property which have been found on SMA. As the temperature raised to above austenite-finish-temperature, A_f, it offers the ability of reverting to original form upon removing the external load without the need for any thermal activation. This characteristic behaves as like rubber band.

Whereas the SMP exhibits SME under polymeric segmental phase transitions, which are soft and hard segment phases. Due to presence of the stimulus, the orientation of soft segment phase is different on each shape memory process, but the location of the hard segment phase is fixed and await for triggering the shape recovery process. The structural phase change allows each SMM to recover in different mechanical aspects. For example, the SMA recovers from the passive energy and dynamic load [59], the SMC recovers from the crack grown [60]–[62], and the SMP recovers from elongated length.

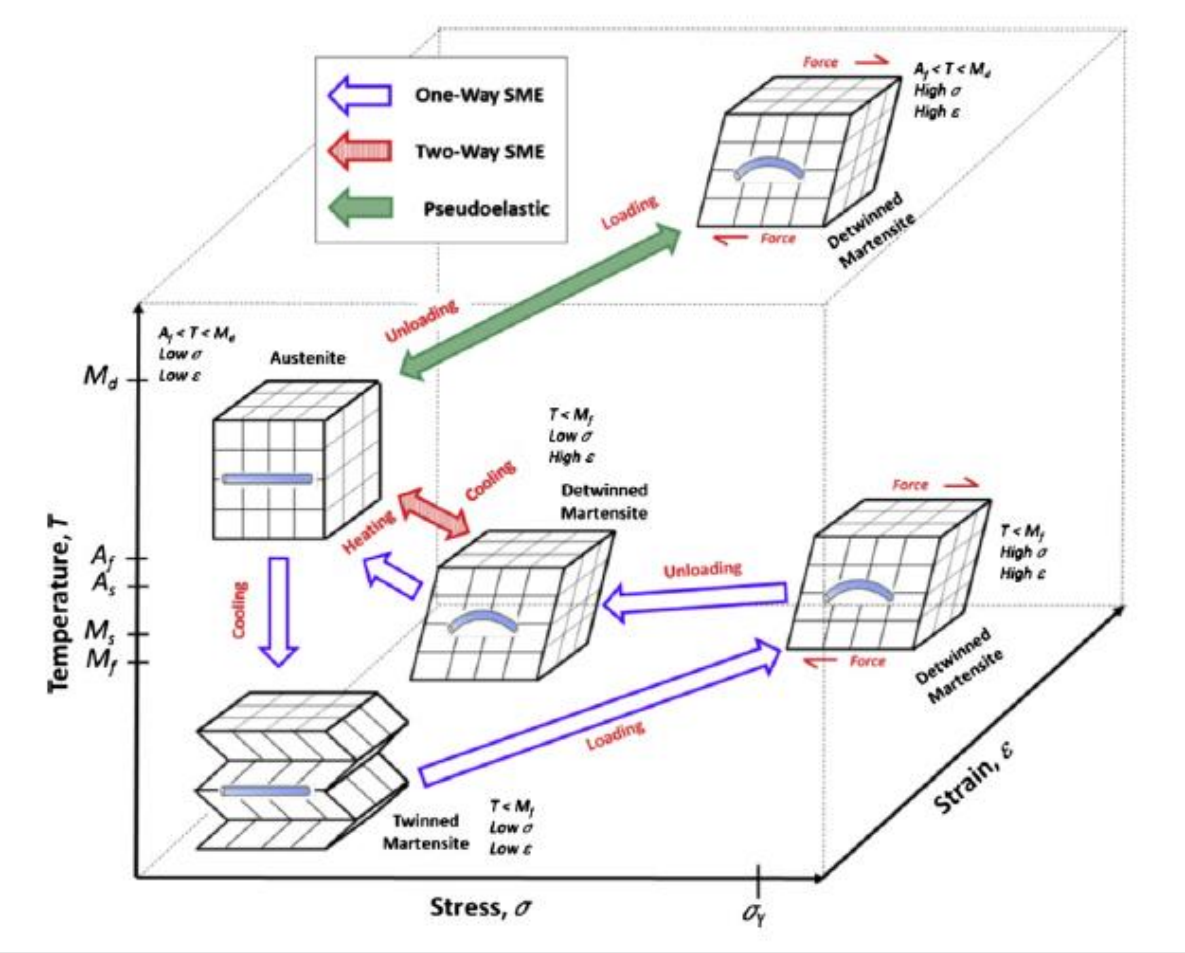

Figure 2.2: Shape memory mechanism of SMA and SMC [63]

2.1 Shape Memory Polymer (SMP)

SMP is classified as one of the smart materials due to its capacity to hold a temporary shape and recover to its original shape under specific and tailored environmental conditions such as temperature triggered, electrically activated, or chemo-responsive [64]–[66]. Compared to other SMMs, SMP stands out with the advantage of exhibiting high recoverable strain, which is up to 800% of deformed strain [67]. It has a wide and flexible choice of chemical composition to demonstrate shape memory behaviours [68]–[70]. Due to low intermolecular force between the polymer molecular, most SMPs have a lower trigger temperature than SMA. In consequence, it

requires less thermal energy to exhibit SME compared to other SMMs. Besides that, the lightweight and diverse trigger mechanisms are the critical features in promoting SMP research. The material properties and shape memory characteristics for each form of SMM are listed in Table 2.1.

Table 2.1: Shape memory characteristics for SMMs

Material	Shape Memory Alloy (SMA) [63]	Shape Memory Polymers (SMP)/ Shape Memory Gel (SMG [71]	Shape Memory Ceramic (SMC) [72]
Recovery strain	8%	50~600%	Below 0.5%
Recovery stress	150~300MPa	1~3MPa	100MPa
Phase Transformations	Martensitic transition	Glass transition / Crystallisation	Martensitic transition
Trigger temperature	Above 400^{o}C	Below 100^{o}C	0~1200^{o}C
Density	6~7g/cm^{3}	~1g/cm^{3}	7.5g/cm^{3}
Fabrication Cost (Material and process)	Expensive	Cheap	Cheap

In contrast to SMA and SMC, SMP operates on a completely different shape memory principle that exhibits SME during polymeric segmental phase transition. The two phases are formed by the molecular switching (soft segment) and netpoints (hard segment) in the polymer structure. They contribute to dimensional stability through crystallisation (shape programming process) and molecule reformation under decrystallisation (shape recovery process) [73]. The mobility of molecular under SME is shown in Figure 2.3. This indicates that the SME occurs due

to the glass phase transition, in which rigid molecular (soft frozen segment phase) retain temporary shape at low temperature and netpoints (hard segment) snap back the elastic molecular switching (soft active segment phase) into the initial position at high temperature. Hence, thermo-responsive is a common SME trigger method for SMP. The trigger temperature is determined by the glass transition temperature (T_g) or the melting temperature (T_m) of particular composites of the SMP [74].

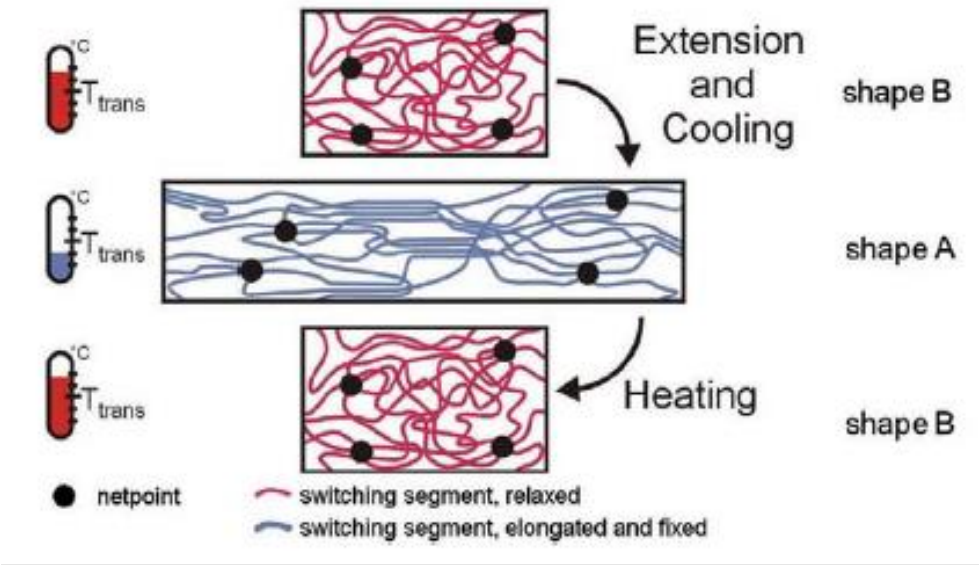

Figure 2.3: Polymeric segment transition during SME [73]

Other than just memorising single intermediate shape, SMP could perform multiple ways SME by increasing the number of discrete reversible phase transitions (have multiple T_g or T_m). For example, Bellin and co-worker evaluated triple SME by mixing poly (ethylene glycol) (PEG) (T_m of PEG=38^{o}C) and poly(ε-caprolactone) (PCL) (T_m PCL>50^{o}C) [75], [76], Du et al. proposed a triple SME polyolefin elastomer (POE) (T_g=100^{o}C) by blending with stearic acid (T_g=75^{o}C) [77]. In addition, the multiple ways SME is also feasible even merely contain one broad reversible phase transition. Xie reported that the quadruple SME can be exhibited under discrete recovery

temperature ranges [78], which is displayed in Figure 2.4. The recovery strain is constrained by the partial crystalline melting process, which restores only a part of the strain by reheating to a particular temperature range. These beneficial features are a result of the polymer structure and morphology of SMP. Hence, studying the polymer characteristics of the mixing component is important for investigating the shape memory behaviour.

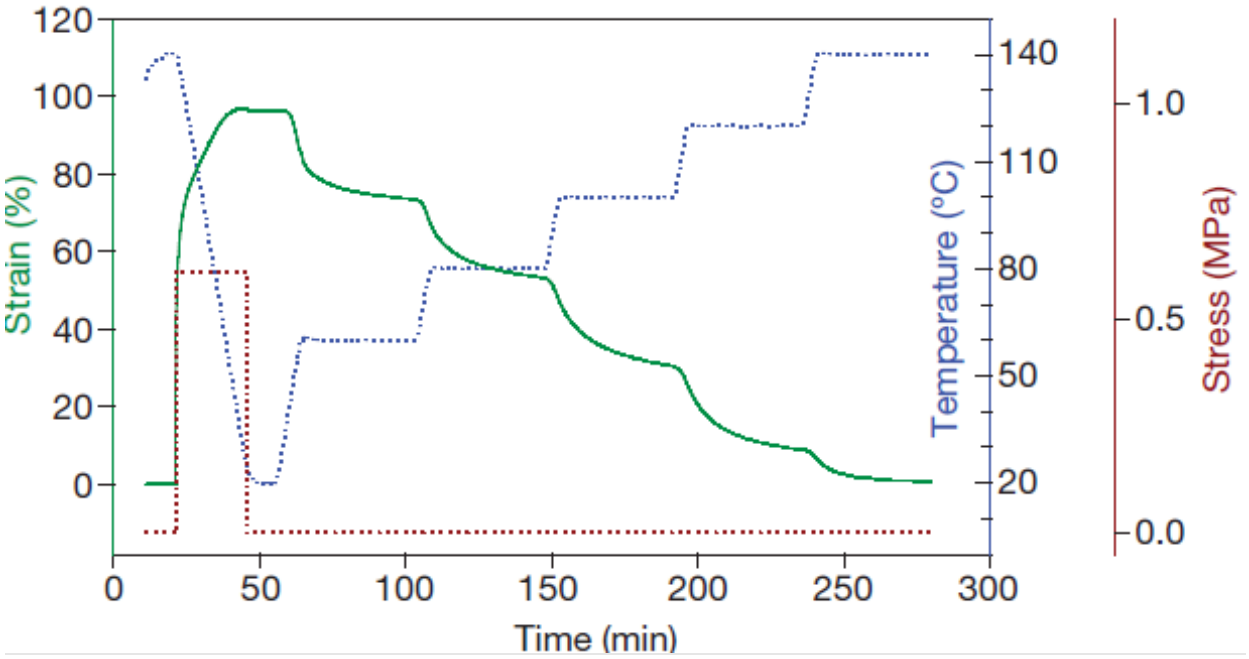

Figure 2.4: Discrete recovery process under a board reversible phase transition [78]

In addition, SMPs that can restore the mechanical properties by itself is termed as self-healing polymer. During the polymeric segmental phase change, the mobile molecule diffuses toward the defect site, enclosing the defect and mending the mechanical damage on the polymer surface [14]. Those self-healing polymers not only repair microscopic damage such as wearing and surface scratches, but they may also fully recover from macroscopic cracks. For example, Xiao proposes a graphene polymer composite to increase the crack resistance and recover the scratching

damage on the surface [11], Luo and his coworkers utilised the bleeding of molten PCL to bridge a crack gap [79], Rodrigues et al. illustrated the crack closure and crack rebonding within single heat treatment [80]. Figure 2.5 shows the self-healing capability on neat SMP and SMP composite. Although combining with a thermoplastic additive (self-healing composites) may affect the structural load carrying capacity [81], it reduces the overall maintenance activity owing to machine breakdown. However, the research into self-healing polymer has a profound impact on mendable engineering constructions

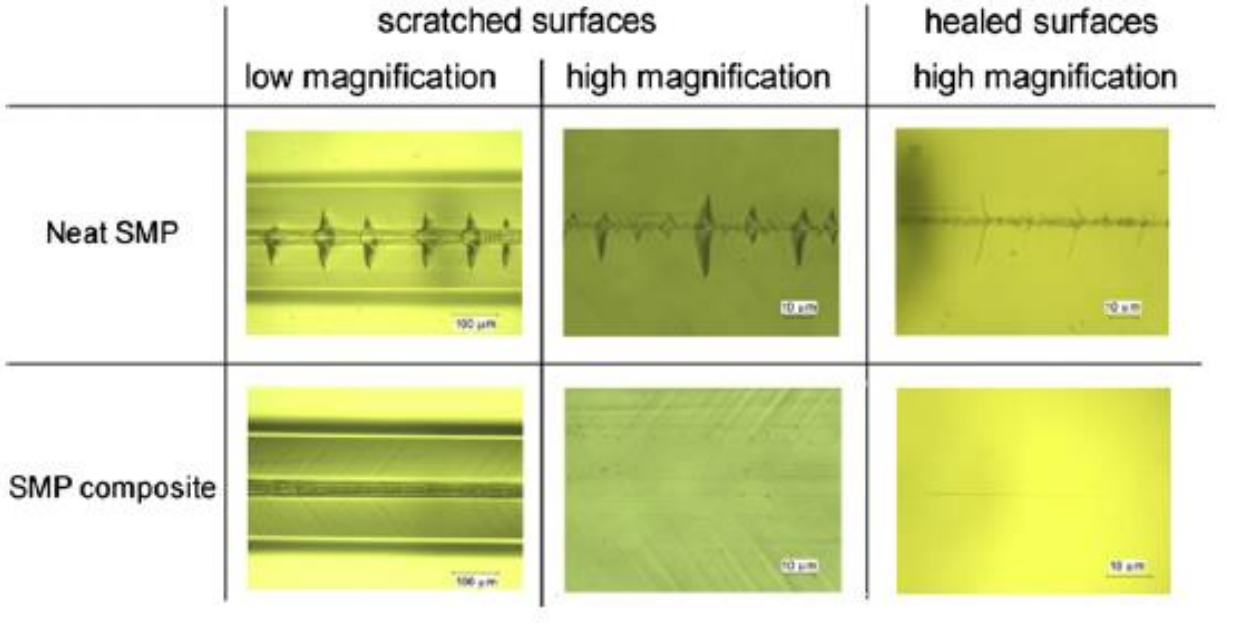

Figure 2.5: The self-healing capability on neat SMP and SMP composite [82]

2.2 Shape Memory Natural Rubber (SMNR)

NR as an elastic material has also emerged as a sustainable renewable resource. Although it is composed of thousands of isoprene monomers, unlike other polymers, it is synthesised by using natural rubber latex (NRL). Figure 2.6 shows the chemical structure of NR. The term “NRL”

refers to the milky sap liquid that is extracted from the tropical tree *Hevea Brasiliensis*. By tapping an incision into the bark of rubber trees, the white sap liquid will exude in a spiral pattern and flow down to the collecting cup. After the NRL is collected and sent to rubber manufacturing factory, "*Caoutchouc*" which is as the scientific term of NR is produced. Although this tropical agriculture has 6 years of immature period, the economic lifespan of rubber trees could extend up to 25 years. Therefore, NR is considered a sustainable and renewable resource.

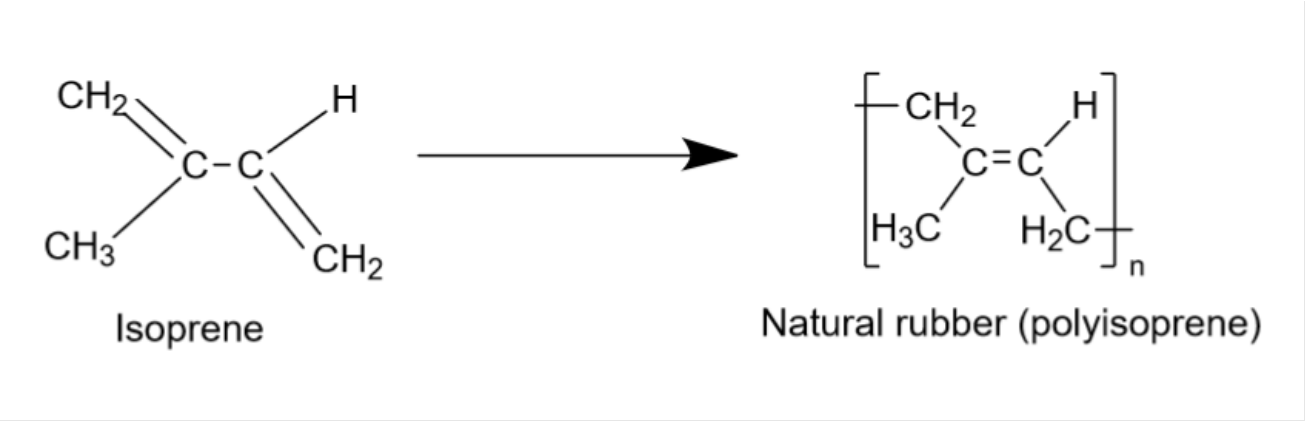

Figure 2.6: Chemical structure of polyisoprene

Historically, the NR tree was discovered in the early sixteen century, and the NRL was widely used as clothing and footwear because of its waterproof ability [37]. Due to lack of chemical knowledge regarding the rubber properties, the inherent drawback of NRL product which is sensitive to environmental temperature. This unsolved issue remained until the first vulcanised rubber using sulphur was discovered by Charles Goodyear in 1839. Figure 2.7 compares the rubber molecular structure before and after vulcanisation. Apart from enhancing the thermal resistance, vulcanisation with the term of curing causes the sulphur particles to crosslink between polymer chain segments to increase the rubber strength and durability of the NR. When the filler effect is considered, the tensile strength of vulcanised NR could be up to 30 MPa [83]. The discovery of

vulcanisation is not merely infused a revolution in the NR industry but also becomes a milestone in NR research and development.

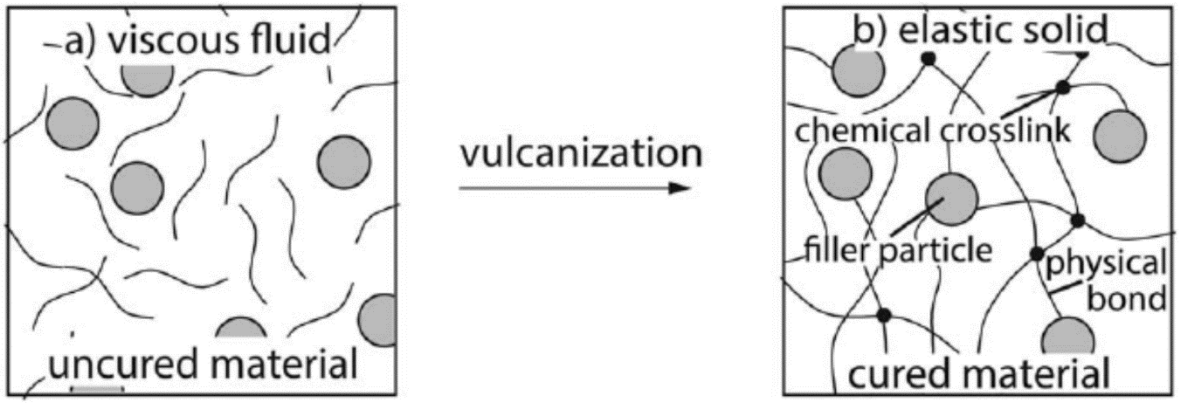

Figure 2.7: Molecular structure of rubber particles a) before vulcanisation b) after vulcanisation [84]

Innovative materials with novel properties have been a research priority in today's society, and SMNR is one of those. SMNR is an elastomer material with the superior capability of holding the temporary shape and reforming to its permanent shape when the appropriate environment is met. Although NR is an amorphous polymer, with those unstable crystal structures at room temperature, the crystalline upon strain term of strain-induced crystallisation (SIC) provides the state-of-the-art feature (SME) [85]. SIC halts the flow of the stretched macromolecules to undergo shape programming and then allows for shape recovery as the SIC has vanished at elevated temperatures. According to this distinct feature, the shape memory activation has been extended to additional stimuli by either indirect thermal response or direct actuation.

2.2.1 Strain-induced Crystallisation (SIC)

Along with vulcanization, SIC is another profound phenomenon for NR research. NR is an amorphous polymer that is unable to crystallise at ambient temperature under normal conditions. Nevertheless, a high elongation force stretches the rubber molecular into an orientated structure is known as SIC. Crystal form upon strain, offering self-reinforcement ability, whereas restores to original properties after crystals vanish during unloading. As shown in Figure 2.8, rubber molecular pack together to form and enlarge the size of dark bots to block the light through the sample during the stretching process. Once the loading is removed, the rubber molecular are released and more light is able to go through the sample. This indicate the nucleation and growth of SIC is began at the loading process and vanished during the unloading process.

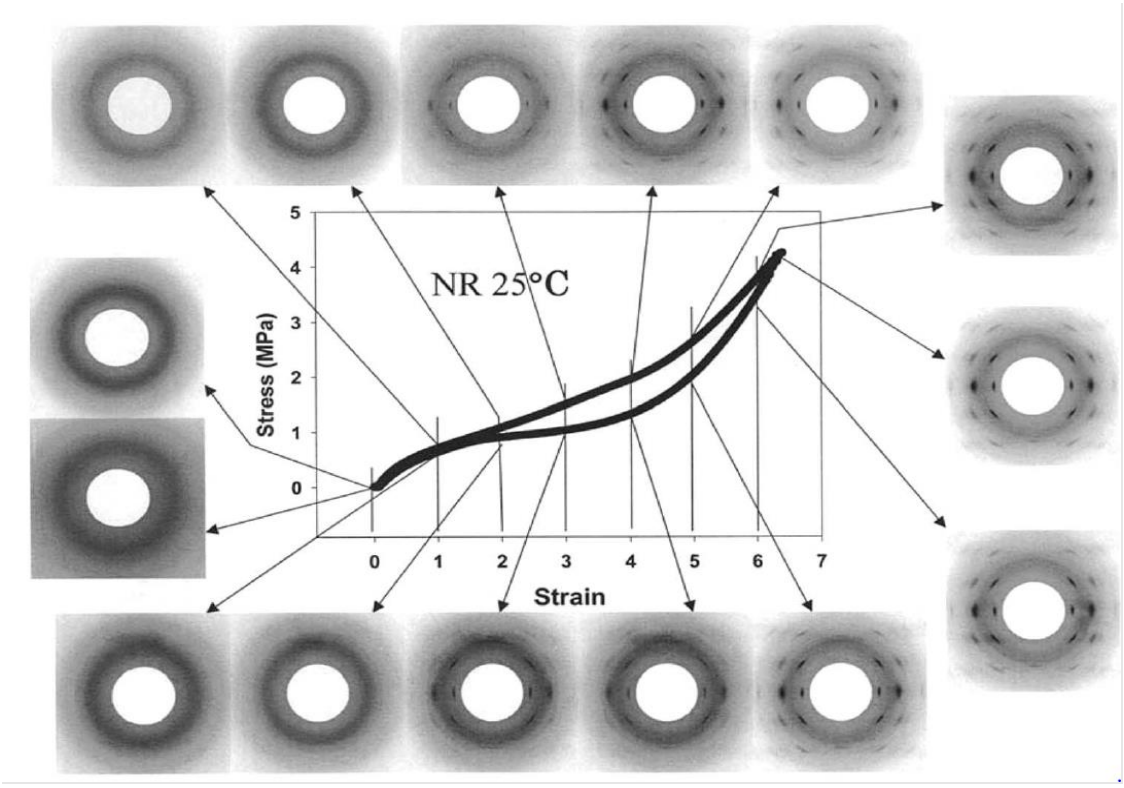

Figure 2.8: The SIC corresponding with different loading degrees (SIC formed as loading, vanished as unloading) [46]

The beneficial of SIC increases the tensile strength without adding the filler in high deformed loads [86]. SIC is a typical phenomenon during loading, but its self-reinforcement nature has drawn attention from researchers. Increasing the mechanical properties without modifying the chemical structure is a miracle in polymer material. In addition, the occurrence of SIC may act as a barrier to crack propagation [87]–[90]. Cracks are always challenging for hard and brittle materials because the crack length often promotes fatigue. Due to the presence of SIC, NR improves the crack resistance by strengthening the tensile strength that can withstand the high macroscopic stress at the crack tip section.

Besides the self-reinforcement effect, SIC also offers another unique capability known as SME. This is an inherent phenomenon for SMP [73], including amorphous elastomer (SMNR) [43]. During the deformation process, molecular switching is entangled with other soft segments to allow crystallisation. In contrast, rigid netpoints restrain the plastic deformation to prevent the molecular switching being stretched too far away from the interpenetrating network. The grown crystalline structure inhibits molecule switching mobility, and the temporary shape is persisted even after the applied stress is removed. SIC begins to degrade upon applying stimulus. Without the retaining force from SIC, the molecular switching is retracted by netpoints, and the deformed length is restored to its original shape. The nucleation and growth of SIC during the deformation stage are depicted in Figure 2.9. SIC research related to SME for SMNR is limited because SIC is unstable above room temperature, in which the rubber loading condition and composition affect the SIC nucleation and growth. For example, Brüning and his coworker stated that the crystallinity of SIC is increasing with the strain level [91], Sun et al. observed due to the pseudo-end-linked network within the NR molecule, higher crystallites is formed at those NR/IR blends with higher NR content. [92], and Plagge et al. also reported that the high portion of filler (carbon block)

impede the crystallization, which lead to low degree of crystallinity is induced at large strain [93]. However, those elements are less well-documented or are not yet included in the studies about SME or SMNR; those factors should be incorporated into the SMNR development.

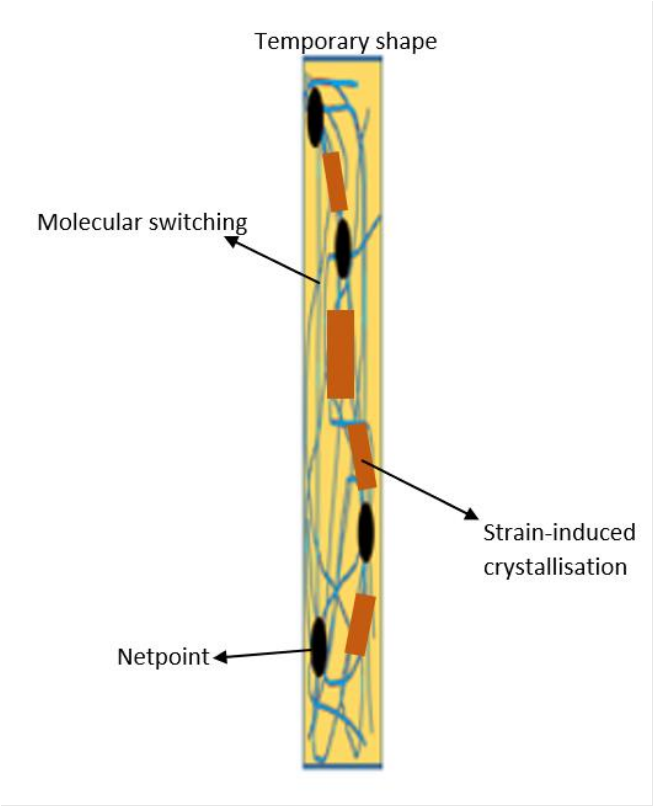

Figure 2.9: The SIC growth during the deformation stage

2.2.2 Trigger Temperature (T_c)

Trigger temperature, T_c refers to the particular temperature at which SMP exhibits the shape memory ability, as shown in Figure 2.10. A cycle of SME begins from heating up the object to above T_c at stage ①. Due to the SIC is formed during the deformation process (stage ②), the shape programming constrains the mobility of the molecule in a strained state at $T<T_c$ (③ →④)

even the force is removed. The end of the SME cycle is started when the SIC is vanished by the entropy at $T>T_c$ (⑤ →①) to trigger the shape recovery process. According to the shape memory mechanism of SMP, the T_c is typically set at transition temperature between the glass phase and the rubbery state, in which the T_g is for amorphous polymers or T_m for crystalline polymers [94]. However, the T_c can also be influenced by changing environmental conditions such as moisture level. Yang and his coworkers had the experiment with investigating the relationship between the T_c of polyurethane SMP and the water content in polymer structure (free water and bonded water) [95], [96], and he also proposed a water-driven SMP [97] as shown in Figure 2.11. While water acts as a plasticiser, it increases polymer chain mobility resulting in low entropy energy is required to initiate the SME. Although the T_c is critical in exhibiting the SME, it is easily influenced by changing environmental conditions. According to this shape memory feature, tuneable T_c is feasible and variable thermal stimuli were developed.

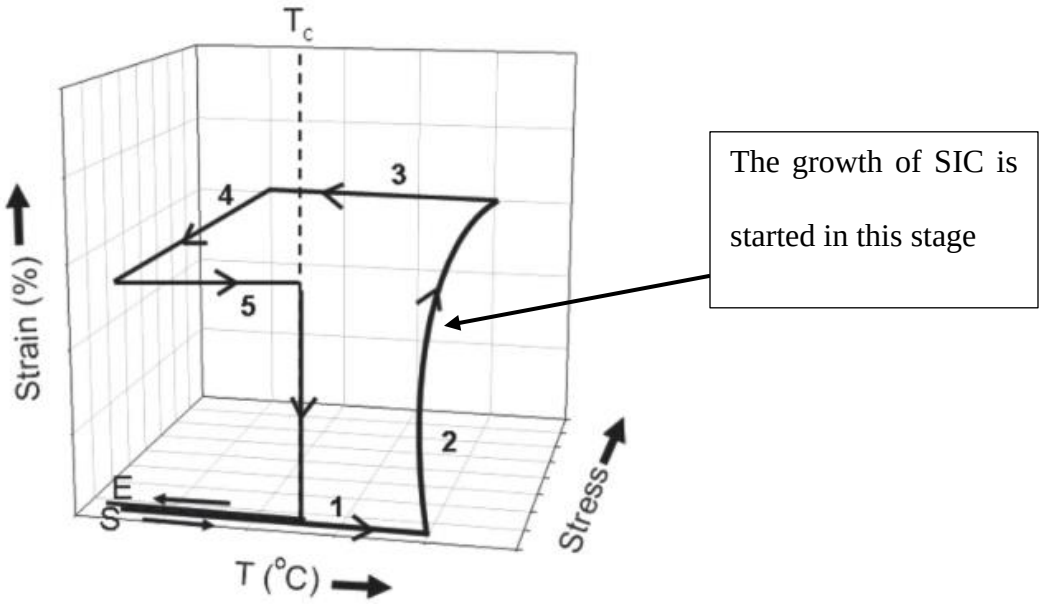

Figure 2.10: 3D graph of shape memory process (S refers as start of cycle, E defines as end of cycle) [98]

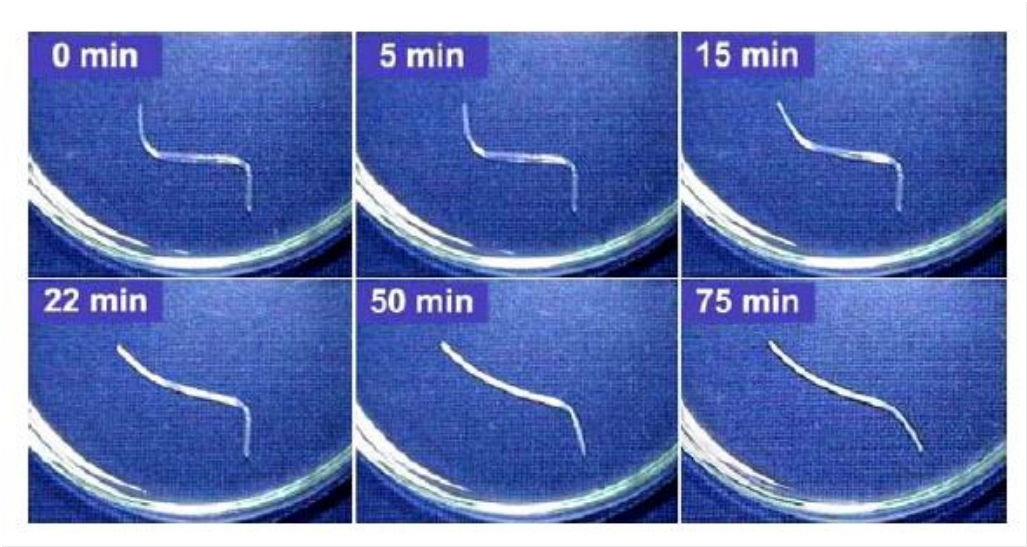

Figure 2.11: The shape recovery of water-driven SMP in different time zone [99]

Other than reducing the T_c by water molecule, indirect heating is another strategy to trigger the SME without increasing the surrounding temperature. Instead of transferring the thermal energy through the convection method, heat induced within the object is more efficient and consumes less energy. This concept is well demonstrated in a variety of applications, including electrically actuated polyurethane composites (T_c=55^{o}C) [100], magnetic response on SMP using nanocomposites (T_c=74^{o}C for temperature-memory polyurethane with nanocomposites) [101], and infrared light-induced SME on epoxy-based SMP (T_c=73.3^{o}C-107.8^{o}C) [102]. Due to the nanoparticle generates heat when it is exposed to a magnetic field or converts light energy to thermal energy, as shown in Figure 2.12, the internal temperature of SMP increases and approaches to T_c for exhibiting SME. Instead of heating up entire specimen, it also allows the SME occurs on specific position by laser as shown in Figure 2.12a. Merely the middle segment of the specimen activates the SME (wave shape) when the laser point to reacted position. Not only the nanoparticle

strengthens its own properties, but also acts as the heat source to allow the SMP undergoing 'self-heating' for triggering SME without any directly thermal activity involved.

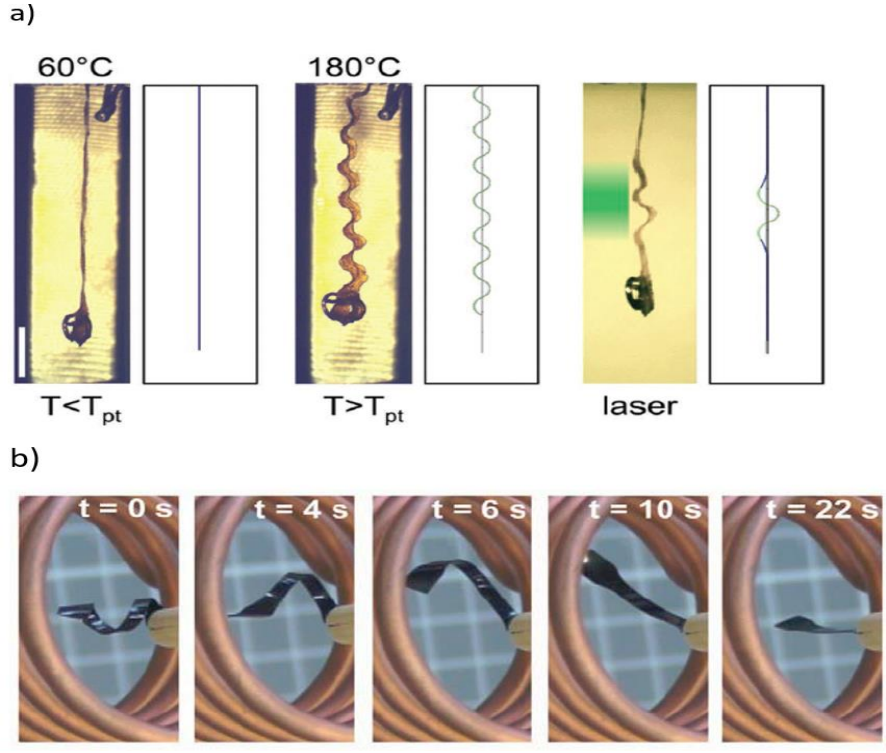

Figure 2.12: a) Light-induced SME [103] b) Magnetically induced SME [73]

The chemical composition is also a consideration in influencing the T_c. Although it is generally established that carbon black and nanotubes reinforce NR composites to increase their rubber strength, research on SME is relatively less common. This is because carbon black and nanotube hinder the SIC formation [93] with the result in deteriorating the SME at ambient temperature. Nevertheless, by reducing the crosslink density to 0.14%, the SMNR exhibits superior shape memory performance at a temperature slightly above room temperature (T_c=38.4^{o}C) under large deformed strain (95% of fracture strain) with a high strain rate (1000% per second) [104]. In addition, the shape programming happens without any heat treatment is known as cold

programming. It is feasible for lightly crosslinking SMNR. Due to the interaction between the entropy and internal energy of rubber molecule during deformation (exothermic process in stretching and endothermic process when retraction), the supercooling up to 20°C is observed under 1000% of elongation strain with 0.4% crosslink vulcanised NR [105]. The SMNR is a thermally responsive polymer, and its SIC behaviour corresponds to the temperature. The huge temperature change has a significant influence on the SME. For example, as shown in Figure 2.13, 80% of shape recovery difference is found within 1°C under the cold programmed SMNR [106]. To achieve the cold programmability, the T_c of SMNR must be around ambient temperature, which allows glass-rubbery state transition to be completed within a short period.

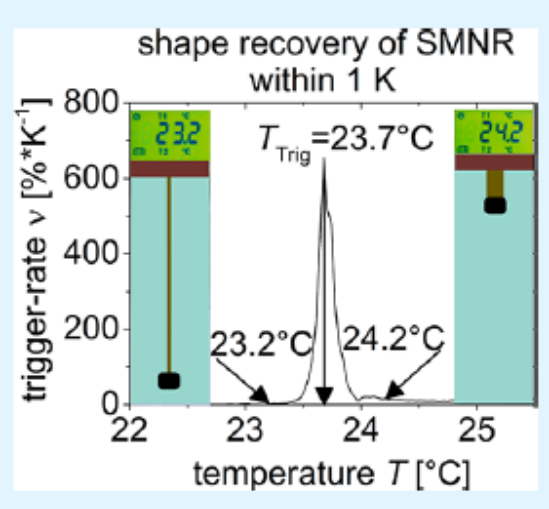

Figure 2.13: The difference in shape recovery within 1°C [106]

Other than the effect from composition of SMNR, the growth of the SIC is influenced by changes in the environment during or after the shape programming. Benjamin et al. gave the idea of tuning T_c (up to 45°C) by applying transverse stress [107], and Quitmann et al. also demonstrated the variation on stress recovery of the SMNR by applying different solvents vapour

and pressure after the shape programming process [108], [109]. Due to the external factor influences the nucleation and growth of SIC, SME could be triggered under varying temperatures. Combining the effect from light crosslink density, the trigger temperature range of SMNR might be further extended.

However, the investigation of T_c is essential for developing a new SMNR. By identifying the T_c of new SMNR, researcher could easily find out the optimum temperature range of the SMNR to examinate the shape memory performance during the shape programming and shape recovery process. In general, T_c is aligned to T_g or T_m of the SMP, but the amount of the filler and additive agent might alter the thermal behaviour of SMNR, especially for nucleation of SIC. Moreover, external environmental condition such as stress-strain condition and the thermal condition also influences the growth of SIC. In consequence, variable trigger temperature range is feasible for a similar SMNR group. Therefore, to study the shape memory behaviour of new SMNR, the investigation on the composition effect, the stress-strain conditions and the thermal conditions is essential.

2.2.3 SMNR Fabrication Process

Apart from the T_c, the crosslinks network plays another vital role in the SMNR. Based on thermally responsive SMP, the structures of SMP can be classified into four categories: chemically crosslinked glassy polymers, chemically crosslinked semi-crystalline polymers, physically crosslinked glassy polymers, and physically crosslinked semi-crystalline polymers [110]. Most chemically crosslinked SMPs have a single kind of molecular segment (homopolymer) to exhibit the shape memory behaviour. In contrast, physically crosslinked SMPs have multi-block structures such as copolymer, which possess two or more phases of thermal transition. Glassy and semi-crystalline polymers could be identified from their molecular constituents in the polymer structure.

Although SMNR is an amorphous polymer, crystalline upon strain allows the SMNR to exhibit SME. Therefore, most SMNRs are classified into chemically and physical semi-crystalline polymers. Several SMNRs under chemically crosslinking with excellent shape memory effect have been published. For example, Yuan et al. developed a fully biobased SMNR by chemically bonding polylactic acid (managing the recovery process) with NR (storing the elastic elongation strain) [111]. Figure 2.14 shows the shape recovery sequence of spiral and V shape for the specimen of neat PLA, D65/35 (65% of PLA and 35% under dynamic vulcanisation), and D40/60 (40% of PLA and 60% under dynamic vulcanisation) at their trigger temperature (60^{o}C). Moreover, Lin and his worker proposed a SMNR fabricated by Oxa-Michael reaction to chemically crosslink the ENR with zinc diacrylate (ZDA) [49]. The results indicated that the T_c increases as the crosslinking agent increases. At the same time, Chang et al. reached a similar conclusion by using the 3-amino-1,2,4-triazole (ATA) as the crosslinking agent [112].

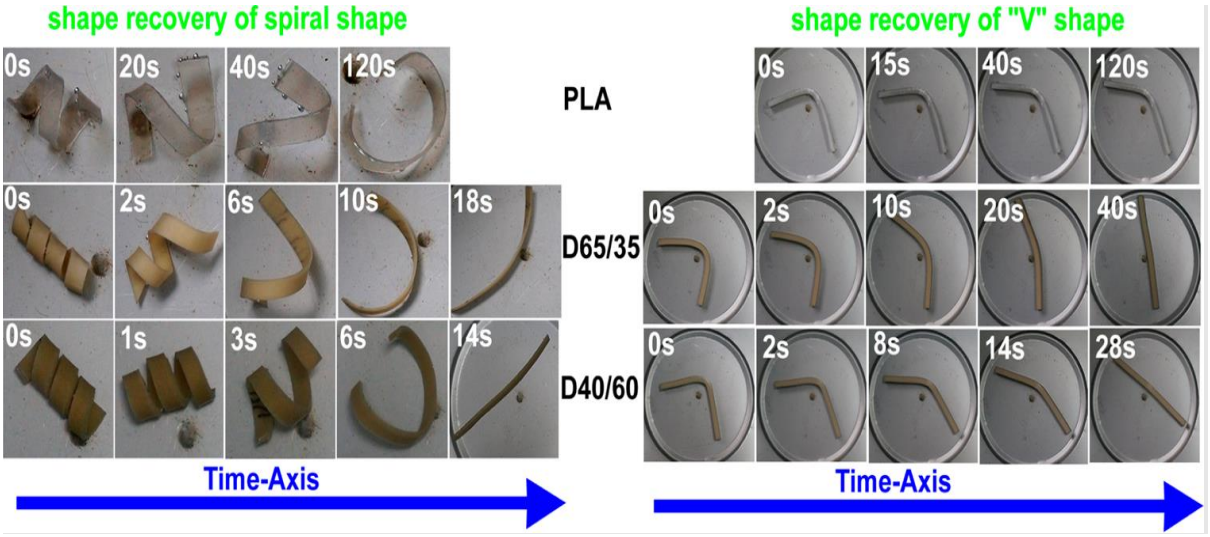

Figure 2.14: The shape recovery sequence for the fully biobased SMNRs under different testing shape [111]

Compared to chemically crosslinking, physically crosslinking SMP is more straightforward and effective. Weiss et al. proposed an ionomer bonding SMP, which is an elastomer mixture with low molar mass fatty acid salt [113]. Fatty acid salt is physically bonded with the elastomeric ionomer, which acts as the barrier to restrict the chain motion at low temperature and allow the elastic recovery by an external stimulus. With the presence of fatty acid, the T_c is shifted to the T_g or T_m of fatty acid [114]. Moreover, the swelling process has potential to transform commodity rubber into SMNR, which exhibits shape memory behaviour under physically crosslinking. For example, Brostowitz and his coworkers demonstrated outstanding shape fixation and high shape recovery (100%±10%) at the T_c (T_c=75^{o}C) by swelling a rubber band in molten stearic acid [115]. Fatty acid forms a percolated crystalline platelet network among rubber molecular, immobilising the segment during shape programming and triggering the recovery upon reheating to T_g or T_m of fatty acid. The swelling process not only streamlines the SMNR fabrication process but also widely extends the range of T_c by choosing suitable fatty acid temperature. However, the low repeatability and thermal degradation should be migrated before commercialising the physically crosslink SMNR.

The linkage of physically crosslinking is unstable and weak, which the shape memory performance is easily degraded within a short period or under particular environmental conditions. Swelling process allows the solvent diffuses into porous rubber to be readily crystallised during stretching and recovery upon reheating. Nevertheless, the fatty acid is also likely expelled from swollen SMNR, and the blooming effect is detrimental in particular to the programming process [48]. Jeff et al reported a similar outcome which, the reswelling process is required to retain the shape memory capability after a short period [114]. The reduction in solvent loading leads to the swollen SMNR exhibiting poor repeatability on SME after a few cycles. In addition, thermally

ageing might be accelerated during swelling at high temperature. Due to rubber with high crosslink density has a low permeability [116], the swelling process can be accelerated by increasing the temperature [117], [118]. In consequence, an undesirable reaction of reduction on effective crosslink term “chain scission” can occur due to overflow of solvent loading and long period exposure in high temperature environment [119], [120]. In addition, solvent easily dominates the rubber properties once the solvent is excess in the rubber molecule. For example, Marcos stated high solvent loading of SMNR (>50% wt) is likely failure at high loading shape memory test [48]. Moreover, it impacts on the material characteristics which causes the material to be more brittle. However, these degradations should be validated and verified as developing SMNR.

To enhance the shape memory capability of SMNR, this project has proposed a SMNR fabrication method through prevulcanisation with palmitic acid incorporation. Compared to conventional vulcanization, prevulcanisation allows rubber particles to undergo curing without further heating [121]. The compounding and mastication process occurs under dispersion form in the aqueous phase of latex and awaits the mixture solution to migrate into rubber form. Due to its simplicity and low manufacturing cost, prevulcanisation process is extensively implemented in the application, such as dipped goods and adhesives [122]. Prevulcanisation has a similar mechanical characteristic with conventional vulcanisation in which the rubber strength is improved by adding filler or increasing the crosslink density [123]. However, the rubber properties change over time because of the presence of the active accelerator and sulphur particles [124]. Although the prevulcanisation process could accelerate the vulcanisation process by increasing temperature during the compound process, it might lead to lower colloidal stability [125].

Despite the bulk of the research on prevulcanisation related to its mechanical response and colloidal stability, none are correlated to SME because of low crystallinity at room temperature.

The branched crosslink structure constrains crystal nucleation and crystal growth in rubber molecular [126]. In consequence, none or low shape memory performance is exhibited. The high homogenous sulphur-based linkage, polysulfide incorporated with palmitic acid might address this issue. Polysulfide has a more flexible netpoints, which promotes the initiation of SIC [127], [128], but uneven accelerator distribution with a long cure time easily increases the volume fraction of monosulfide and disulfide cross-link during conventional vulcanisation [129], [130]. In addition, reducing the particle size of sulphur and accelerator, which dissolved in dispersion form, not only enhance the efficiency of the compounding process, and it increases the homogeneity of crosslink structure [131]. In consequence, more polysulfide is formed in rubber molecular to increase the degree of SIC formation.

Despite the fact that prevulcanisation has improved the SIC formation, it still retains the low decrystallisation temperature. To overcome this issue, the prevulcanised SMNR is fabricated under the incorporation of palmitic acid. Fatty acid, a material with high crystallinity, is widely adopted as a reinforcing material in SMPs to increase the T_c, such as swollen polyurethane foam with stearic acid [132], methacrylate fatty acid (Oleic acid and lauric acid) synthesis [133], [134], and blending POE to lauric acid. Fatty acid acts as a filler, hindering the movement of polymer molecular at low temperatures. It also acts as a plasticiser, releasing the molecular back to its original position once the temperature is above the T_m of fatty acids [135]. Palmitic acid classifies as a saturated fatty acid with the T_m of ~63^{o}C, is the perfect candidate to be the SMNR reinforcer for this research. Moreover, it is also utilised as the physically crosslink agent of SMP under the studies of Jeff [114] and Pantajo [48]. However, the prevulcanised SMNR incorporated with palmitic acid has never been reported yet.

2.3 Constitutive Models of SMPs

The SME of SMP depends highly on the polymer morphology and operating conditions but the investigation of SME under build-and-test approach is inefficient and time consuming. To improve the efficiency of SMP development, several shape memory behaviours prediction models are proposed. For example, Zhang and Ni reported a bending deflection algorithm to describe the shape recovery activity [136], Haiyang et al. modelled the shape memory behaviour of triple SME by combining a phase transition model and generalized Maxwell model [137]. Qi Ge et al. displayed a shape memory behaviour prediction model by describing the crystal-melt transition during the shape memory process [138]. To simulate the shape memory behaviour, these constitutive models are established under a combination of mechanical response model with a thermal equation which written as Equation (2.1),

$$F = F_m . F_T \qquad \text{Equation (2.1)}$$

where F is total deformation gradient, F_m is deformation gradient under mechanical approach, F_T is deformation gradient under thermal approach

The mechanical approach refers to the stress-strain changing due to the deformation process and the material properties. The thermal approach is taking into account for the molecular state which are crystallinity and phase state during the shape programming and shape recovery process. By invoking a reliable shape memory prediction system, the material properties such as viscosity, stiffness, and thermal expansion are obtaining from other thermal and mechanical experiments (stress relaxation, Dynamic Mechanical analysis, and tensile test).

Since the first thermal dependent model of SME which is proposed by Liu et al. [139], the development of shape memory prediction system for SMP can be roughly divided into two categories: thermoviscoelastic modelling approaches and phase transition modelling approaches

[140], [141]. The primary difference between these two modelling approaches is the description of the deformation gradient on mechanical part. The theoretical framework of the former models the SME process under a decomposition into elastic and viscous parts which as shown in Equation (2.2),

$$F_m = F_e . F_v \qquad \text{Equation (2.2)}$$

where F_e is the deformation gradient under elastic part, F_v is the deformation gradient under viscous part.

While the standard liner solid (SLS) model is the generalized model to describe this viscoelastic relationship. Referring to the viscoelastic rules, the mobility of molecular is retained and generates internal stress due to shape programming at $T<T_c$, but once the temperature is reached as $T>T_c$, the viscosity is reduced to allow the internal stress driving the shape recovery process. To fulfill this rheological feature, the algorithm system often establishes under vary arrangement type of the spring and damping connection (series connection for Kelvin-Voigt element or parallel connection for Maxwell element) for predicting the shape memory behaviour [142]–[144]. Moreover, those mechanical parts of the thermoviscoelastic modelling approaches are temperature-dependent which merely focuses the change of the chain mobility under different temperature range. In order to incorporate the time-dependent effect during the shape programming and shape recovery processes, the thermal mechanisms (thermal expansion and entropic elasticity of the rubber network) are involved in the thermoviscoelastic modelling approaches. According to time-temperature superposition (TTS) principle, the viscoelastic behaviour in different time function is able to determine by a shift factor (α_T) where the Williams-Landel-Ferry (WLF) is adopted to measure the shift factor above $T>T_c$,

$$log\alpha_T(T) = \frac{-C_1(T-T_o)}{C_2+T-T_o} \qquad \text{For } T>T_c \qquad \text{Equation (2.3)}$$

and Arrhenius equation for $T<T_c$

$$log\alpha_T(T) = -\frac{U}{k_b}\left(\frac{1}{T}-\frac{1}{T_c}\right) \qquad \text{for } T<T_c \qquad \text{Equation (2.4)}$$

where C_1 and C_2 are the WLF constants for the reference temperature, T_o. While U is defined as activation energy and k_b is referred as the Boltzmann constant.

Combining the algorithm on describing strain change under the mechanical and thermal approach, a clear picture of the stress strain evolution during the shape programming and recovery response can be provided [145]–[147]. Due to the thermoviscoelastic model is highly adaptable to each material circumstance with requiring fewer material parameters, it has been widely adopted and extended with other thermal algorithms to simulate the shape memory behaviours of SMP, such as the modified Arrhenius equation to describe the stress-strain behaviour below the T_c [147] or time function is involved in the description of stress relaxation during the shape memory process [148].

Compared to thermoviscoelastic modelling approaches, phase transition modelling approaches treat SMP as a composite material composed of many molecular phases, frozen and active segment phase simultaneously operating at a single temperature range which shown as Figure 2.15. Under phased transition modelling approaches, three distinct phases are possible to exhibit on the shape memory process, which are the rubber phase at a temperature above T_c, glassy phase at a temperature below T_c, and glassy-rubber phase temperature between the upper boundary of Tc and lower boundary of T_c (for the SMP has wide T_c range). According to this phenomenological description, the SME kinetic process halts the molecular mobility (shape programming) during the cooling and restoring its movement (shape recovery) during heating.

Although the volume fraction of constituent phases is interchangeable and corresponding to the temperature, both phases have different stress-strain behaviour [149]. Within a small strain framework, both phases experience similar stress state, but the change of strain is involved in the thermal strain, frozen and active phases which written in Equation (2.5a-c),

$$\sigma = \sigma_a = \sigma_f \quad \text{Equation (2.5a)}$$

$$\varepsilon = V_f \varepsilon_f + V_a \varepsilon_a + \varepsilon_T \quad \text{Equation (2.5b)}$$

$$V_f = 1 - V_a \quad \text{Equation (2.5c)}$$

where σ is stress, ε is the strain, V is the volume fraction while the subscripts of 'a', 'f' and 'T' are defined as active phase, frozen phase, and thermal, respectively

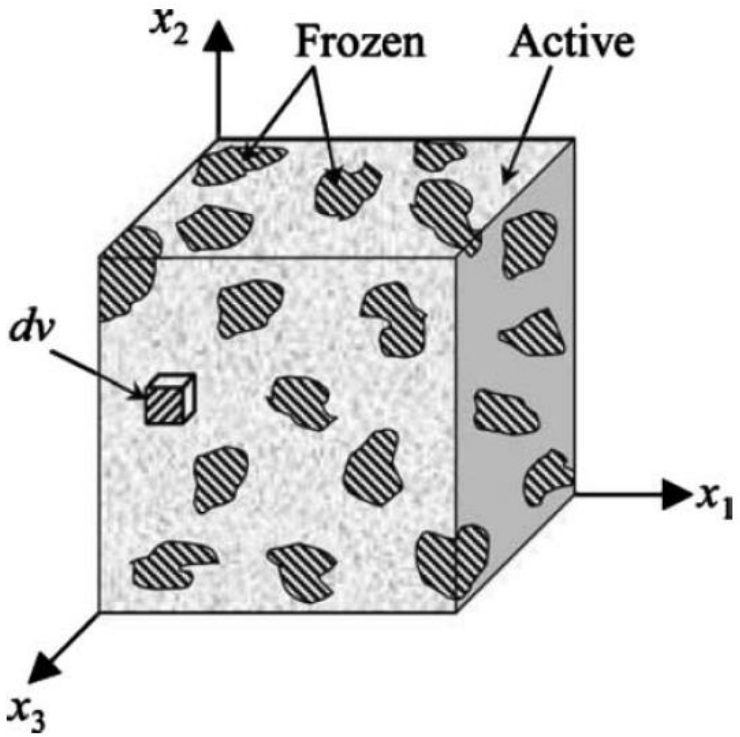

Figure 2.15: Schematic of a multi-phases structure SMP (active and frozen segment phase) at T_g [141]

To determine the volume fraction of each phase (frozen and active phase), variety of volume fraction algorithm have been suggested by the researchers [150]–[153] but the relationship between parameters and material properties or thermal condition remain uncertain [154]. Therefore, the volume fraction function is established under phenomenology approach (obtaining after material experiment). Due to each phase is represented to different material behaviour, SME behaviour is typically simulated under coupled thermomechanical model which is the combination of the hyperelastic model (Mooney Rivlin, Neo-Hookean and Arruda-Boyce) and viscoelastic model (Maxwell and Kelvin Voigt) [154]–[156]. In addition, both modelling approaches have adopted the similar thermal functions (WLF, Arrhenius and thermal expansion equation) to account of the strain effect coming the temperature change. Instead of just providing single overall stress-strain graph for a SMP material (under thermoviscoelastic modelling approaches), phase transition modelling approach could describe a clear vision to describe the stress-strain evolution of the respective segment phases (hard and soft segment phases). Hence, it has been widely implemented in modelling the shape memory behaviour of SMP composites.

3 Methodology

The literature review has shown that research and development of the SMNR are limited. Hence, this research is conducted to develop a thermal responsive palmitic acid-based SMNR and analyse the shape memory characteristic of the SMNR. The specimens are prepared from two different fabrication methods: swelling process and prevulcanisation process. The specimens are used to explore SME under various material formulations and testing conditions such as degrees of deformation and temperatures.

The specimens' preparation procedures, design of the custom-made stretching apparatus, measurement of the shape memory parameters, and detail of the mechanical response experiment are described in this chapter. Next, the shape memory responses of the SMNR are modelled under the phase transition approach. To simulate the shape memory behaviour of SMNR, the model algorithm is established under a viscoelastic model extended with a hyperelastic equation for the mechanical approach, and a temperature law governing the thermal response. The shape memory prediction system and their material coefficients are presented within the end of this chapter. These are conducted as a first attempt to understand and model shape memory responses in the SMNR. The flow chart of the research work is shown in Figure 3.1.

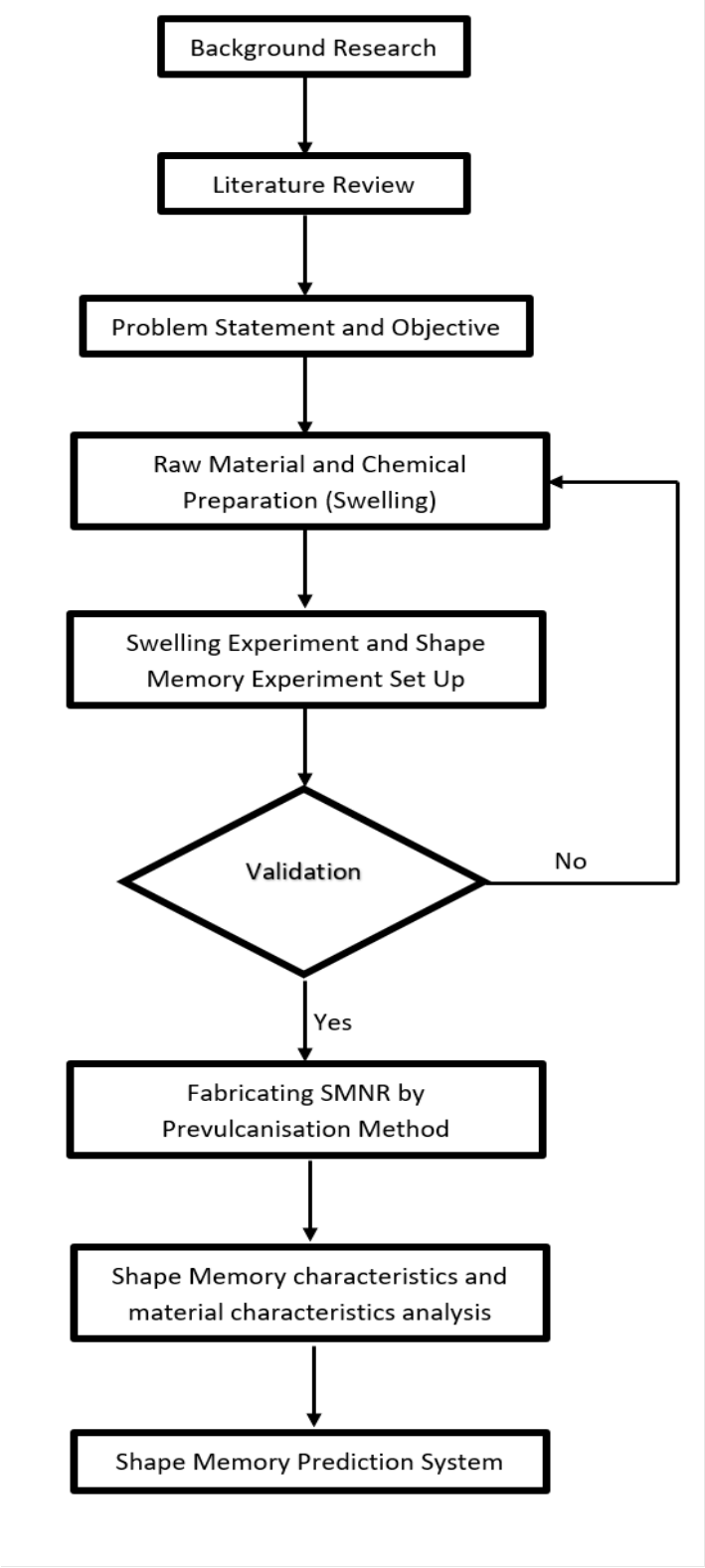

Figure 3.1:The flowchart of the research works

3.1 Material

Commercial grade vulcanised dry NR (CGNR) is provided by Central Elastic Corporation Sdn Bhd, and liquid natural rubber latex (NRL) is purchased from Getahindus Sdn Bhd. The compositions detail of CGNR and NRL are shown in Table 3.1 and Table 3.2 respectively. Synthesis grade of palmitic acid (Merck) is purchased from Synergy Scientific Sdn Bhd, and its material properties are listed in Table 3.3. The crosslink agents, sulphur and accelerators, zinc Diethylithiocarbamate (ZDEC), zinc 2-mercaptobenzothiazole (ZMBT), Zinc oxide (ZnO), and potassium hydroxide (KOH) ware provided by Excelkos Sdn Bhd in dispersion form.

Table 3.1: Formulation of CGNR

Material	Percentage (%)
NR Content	95.0
Activator	1.5
Antiozonant	0.5
Rubber Accelerator	0.5
Vulcanizing Agent	2.5

Table 3.2: The composition and material properties of the liquid NRL

Properties	Value
Total Solid Content (%)	61.5
Dry Rubber Content (%)	60.0
Alkalinity (%)	0.3
Coagulum Content(ppm)	30.0
Viscosity at 26^{o}C (cps)	50.0
pH Value	10.1
Density (kg/m^{3})	950.0

Table 3.3: The chemical and thermal properties of palmitic acid

Properties	Value
Chemical Formula	$CH_3(CH_2)_{14}COOH$
Molar mass	256.43 g/mol
Density	0.852 g/cm^{3}
Boiling point	271.4^{o}C
Melting Point	63^{o}C (upper ≤64^{o}C, lower ≥62^{o}C)
Physical form	Solid (crystal powder)
Saponification Value	218-221 mg KOH/g

3.2 Fabrication of SMNR

3.2.1 Preparation of Rubber Specimen

To fabricate a NRL specimen, 20g of liquid NRL is poured into a rectangular mould to form a NRL film with 2mm thickness. Before the NRL film drying process, the oven is preheated to 50^{o}C for two hours to ensure thermal equilibrium during drying process. Subsequently, the specimen is dried in the oven for 5 hours at 50^{o}C. Next, the dried NRL film is stored at room temperature for seven days to remove remaining water content. A rectangular NRL strip with a dimension of 30mm x 10mm is cut from the dried NRL film.

While for the CGNR specimen, the rectangular shape CGNR strips with a dimension of 30mm x 10mm is cut from a CGNR sheet of 2mm thickness received.

3.2.2 Fabrication of SMNR through Swelling Process

Swollen SMNR specimens are prepared by swelling the strips of NRL and CGNR in the molten palmitic acid under various swelling temperatures (65ºC, 70ºC, and 75ºC) and swelling durations (20,40,60,80,100 and 120 minutes). 200g of palmitic acid powder are poured into a 500ml beaker and heated up to the T_m of palmitic acid. To achieve the thermal equilibrium, palmitic acid is stirred in a water bath shaker machine (Memmert WNB 45), with a speed of 15 rpm for 5 minutes at respective swelling temperatures. A thermometer is used to monitor the solvent temperature to ensure a steady swelling temperature during the swelling process. Rectangular rubber specimens are fully immersed into the palmitic acid solvent to allow palmitic acid to diffuse into the rubber specimen. According to the desired swelling duration, the swollen specimen is taken out from breaker. And then, the excess palmitic acid crystal on the rubber surface is cleaned by filter paper. Afterward, the swollen specimen is sent for quenching at room temperature for 10 minutes. The sample code in Table 3.4 is organized by swelling temperature and rubber source.

Table 3.4: The sample codes of swollen SMNR at respective swelling temperature and rubber source

Sample Code	Swelling Temperature (ºC)	Raw Material
NRL65	65	Liquid natural rubber latex
NRL70	70	Liquid natural rubber latex
NRL75	75	Liquid natural rubber latex
CGNR65	65	Commercial grade vulcanised dry natural rubber
CGNR70	70	Commercial grade vulcanised dry natural rubber
CGNR75	75	Commercial grade vulcanised dry natural rubber

3.2.3 Fabrication of SMNR through Prevulcanisation Process

To investigate the effect of sulphur content and palmitic acid loadings on the shape memory behaviour of SMNR, SMNR is fabricated through prevulcanisation process with different sulphur contents (0.2pphr, 0.5pphr, 1.0pphr, and 1.5pphr) and palmitic acid loading (20pphr,30pphr,40pphr, and 50pphr).

3.2.3.1 Preparation of Potassium Palmitate Soap

Potassium palmitate soap is prepared to incorporate palmitic acid into NRL to reduce coagulation when directly mixing palmitic acid into NRL. According to the saponification value, each gram of palmitic acid can react with approximately 219.4mg of KOH [157], but high pH will prolong the saponification process. To overcome this issue, the ratio of KOH to palmitic acid is reduced to 0.2. Table 3.5 shows the formulation of potassium palmitate soap. Figure 3.2 shows the chemical reaction of potassium palmitate soap.

Table 3.5: Formulation of potassium palmitate soap

Chemical	Weight (g)
Palmitic acid	90.00
Potassium hydroxide (KOH)	18.00
Deionized water (dissolving KOH)	54.00
Deionized water (diluting potassium palmitate soap)	324.00

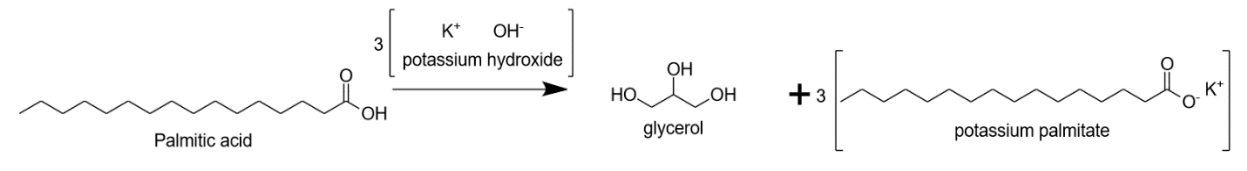

Figure 3.2: The chemical reaction of potassium palmitate

The fabrication process of potassium palmitate soap is described as followed:

1. KOH is dissolved in distilled water and heated to 70^{o}C

2. Palmitic acid is melted at 70^{o}C

3. KOH solution is poured slowly into molten palmitic acid and stirred with 45 rpm at 80^{o}C for 2 hours.

4. The water content is slowly evaporated during the stirring process, and the mixture becomes more viscous.

5. The potassium palmitate soap is allowed to quench and solidify into room temperature for at least one day.

6. Potassium palmitate soap is reheated to the temperature of 70^{o}C until the solution become transparent

7. The potassium palmitate solution is transferred into new 1 litre breaker and further diluted into desired concentration.

3.2.3.2 Fabrication Procedure of Prevulcansied SMNR

Prevulcanised SMNR fabrication is modified from NRL fabrication which the compounding process is undergone in dispersion form. The approach concentration potassium palmitate soap solution is mixed with liquid NRL to achieve the desired content of palmitic acid. The material formulation of each prevulcanised SMNR and its associated sample code is listed in Table 3.6. To highlight the influence from palmitic acid, another three prevulcanised SMNR specimens with no palmitic acid (0.2SNR), stearic acid (0.2SSA20), and high sulphur content (2.0SPA20) are fabricated. Prevulcanised SMNR specimens are prepared according to the following procedures:

1. Liquid NRL is stirred with 100 rpm for five minutes.

2. Chemical substances are poured into liquid NRL and stirred for another 15 minutes

3. Mixtures are diluted with water (40% of total weight) and heated to 70^{o}C

4. Potassium palmitate solution is added to mixture and stirred with 100 rpm for 1 hour

5. The mixture is removed from heat, and continuously stirred for at least 4 hours with 45 rpm.

6. The mixture is poured into the mould for drying process at room temperature for a week to get a fully drained latex film.

7. Drained latex film is demoulded and immersed into clean water for 12 hours to remove chemical substances (unbonded sulphur and unreacted accelerator).

8. SMNR is dried at 100^{o}C for 30 minutes to remove the undesired residue stress that is imposed during demoulding process.

9. SMNR is allowed to quench at room temperature for another 16 hours to stabilise the shape.

Table 3.6: The Formulation and sample code of prevulcanised SMNR

Sample code	Liquid NR (pphr)	Sulphur (pphr)	ZDEC (pphr)	ZMBT (pphr)	Zinc Oxide (pphr)	Palmitic acid (pphr)
0.2SPA20	100	0.200	0.225	0.225	0.200	20
0.2SPA30	100	0.200	0.225	0.225	0.200	30
0.2SPA40	100	0.200	0.225	0.225	0.200	40
0.2SPA50	100	0.200	0.225	0.225	0.200	50
0.5SPA20	100	0.500	0.563	0.563	0.563	20
0.5SPA30	100	0.500	0.563	0.563	0.563	30
0.5SPA40	100	0.500	0.563	0.563	0.563	40
0.5SPA50	100	0.500	0.563	0.563	0.563	50
1.0SPA20	100	1.000	1.125	1.125	1.000	20
1.0SPA30	100	1.000	1.125	1.125	1.000	30
1.0SPA40	100	1.000	1.125	1.125	1.000	40
1.0SPA50	100	1.000	1.125	1.125	1.000	50
1.5SPA20	100	1.500	1.688	1.688	1.500	20
1.5SPA30	100	1.500	1.688	1.688	1.500	30
1.5SPA40	100	1.500	1.688	1.688	1.500	40
1.5SPA50	100	1.500	1.688	1.688	1.500	50
2.0SPA20	100	2.000	2.250	2.250	2.000	20
0.2SNR	100	0.200	0.225	0.225	0.200	0
0.2SSA20	100	0.200	0.225	0.225	0.200	0

*0.2SNR = 0.2pphr sulphur prevulcanised NR (without any fatty acid)

**0.2SSA20= 0.2pphr sulphur and 20pphr stearic acid (from potassium stearate soap)

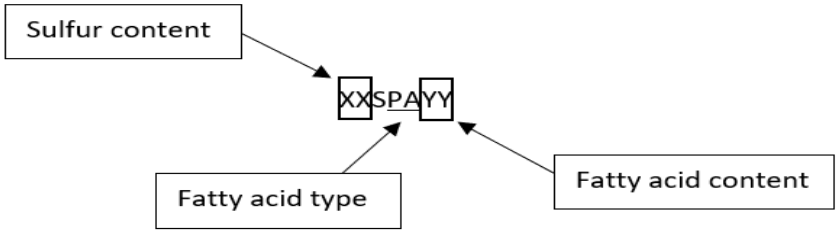

3.3 Composition Characterization of SMNR

This section is to identify the composition content of each SMNR specimen group. According to the TGA/DSC analyser, the TGA and DTG results are able to obtain simultaneously for both swollen SMNR and prevulcanised SMNR specimens. The former records the mass percentage at each temperature, the latter determines the degradation section by measuring the mass percentage change as a temperature function. The composition content can be determined by measuring the mass loss at a particular degradation temperature. Due to the fact that the rubber sheet of CGNR was provided by third party company, swelling experiment is conducted under swollen SMNR to cross-check the palmitic acid loading with the TGA results. Instead of comparing the weight fraction of respective component only, TGA result also is adopted to measure the volume fraction of corresponding compound as simulating the shape memory behaviour.

3.3.1 Swelling Measurement

At the beginning of the swelling process, the initial weight of the rubber specimen is obtained and recorded as W_a. Every twenty minutes of swelling duration, three specimens are removed from the solvent and quenched for 5 minutes to await the palmitic acid crystal formed on rubber surface. Subsequently, the swollen weight is measured by the digital weighing scale machine and recorded as W_b. The swelling ratio is calculated with Equation (3.1),

$$Swelling\ ratio, S = \frac{W_b - W_a}{W_a} x100\% \qquad \text{Equation (3.1)}$$

3.3.2 Thermal Gravimetric Analysis (TGA) and Derivative Thermogravimetry (DTG) Experiments

Mettler-Toledo TGA/DSC 1 analyser is used to examine the composition content in swollen and prevulcanised SMNR with the weight below 15mg. The experiment is conducted at a heating rate of 10°C/min from 30°C to 700°C under a nitrogen gas (20ml/min) environment.

To compare the swelling ratio of palmitic acid between the swelling measurement and TGA results, the weight fraction of the swollen SMNR specimen converts to swelling ratio as following:

According to Equation (3.1), swelling ratio equation could be rewritten as in Equation (3.2),

$$S = \frac{W_p}{W_r} \qquad \text{Equation (3.2)}$$

where W_p is weight fraction of palmitic acid, W_r is the weight fraction of rubber

Equation (3.2) can be restructured to Equation (3.3),

$$W_r S = W_p \qquad \text{Equation (3.3)}$$

Substitute Equation (3.3) into the weight fraction equation, $wt\% = \frac{w_p}{W_{p+W_r}}$ will obtain Equation (3.4) as following,

$$wt\% = W_r(\frac{S}{1+S}) \qquad \text{Equation (3.4)}$$

3.4 Trigger Temperature, T_c

The T_c for SMP is usually around the T_g or T_m of the additive polymer [158]. To verify this hypothesis, the thermal behaviour of the swollen SMNR is conducted with differential scanning calorimetry (DSC). Due to the fact that prevulcanised SMNR contains less palmitic acid amount, it is difficult to determine the T_c under the DSC experiment. Hence, the T_c of selected prevulcanised SMNR samples is validated under DMA machine by looking at the temperature that shows the onset peak in storage modulus.

3.4.1 Differential Scanning Calorimetry (DSC) Experiment

Mettler-Toledo TGA/DSC 1 analyser is used to examine the T_c of swollen SMNR with the weight below 15mg. The experiment is conducted at a heating rate of 10^{o}C/min from 30^{o}C to 700^{o}C under a nitrogen gas (20ml/min) environment.

3.4.2 Dynamic Mechanical Analysis (DMA)

Perkin Elmer DMA 8000 is used to determine the T_c of prevulcanised SMNR under tensile mode. The experiment is set up at the frequency of 1Hz and heating rate of 5^{o}C/min as a function of temperature from 25^{o}C to 100^{o}C

3.5 Custom-made Stretching Apparatus

To study the shape memory behaviour of both swollen and prevulcanised SMNR, a custom-made stretching apparatus is developed to conduct the shape memory experiment under strain-control mode, as shown in Figure 3.3. This apparatus is utilised to observe and record the length change during the shape memory experiment. To have a flexible testing temperature range, a water bath system is adopted to simulate the environment temperature. As illustrated in Figure 3.4, the deformation and temperature control processes are carried out independently. The features of the stretching apparatus and water bath system are described as below:

1. The custom-made stretching apparatus is used to elongate the length of the sample to specific deformed strain. At the same time, the water bath takes responsible for tuning and maintaining the temperature at the desired temperature.

2. The stretching apparatus is made with two threaded rods, two clamps, and a fixing basement plate.

3. The threaded rod is acted as the holding platform to maintain the deformed strain by constraining the height of both clamp blocks.

4. The threaded rod is also utilised to constrain the deformed angle in $0^{o,}$ which to have a uniaxial tensile mode during the deformation process.

5. The clamping block is made of light solid wood instead of metal block to avoid generates an undesired weight load that would compromise the accuracy of the length change recording.

6. Flexible deformation is feasible by adjusting the gap length between two clamping blocks

7. The roughness of the clamping surface is increased by brushing the clamping site to prevent the occurrence of slippage.

8. The water bath allows the specimen to reach the desired temperature by immersing the SMNR specimen into a water bath with a specific temperature range.

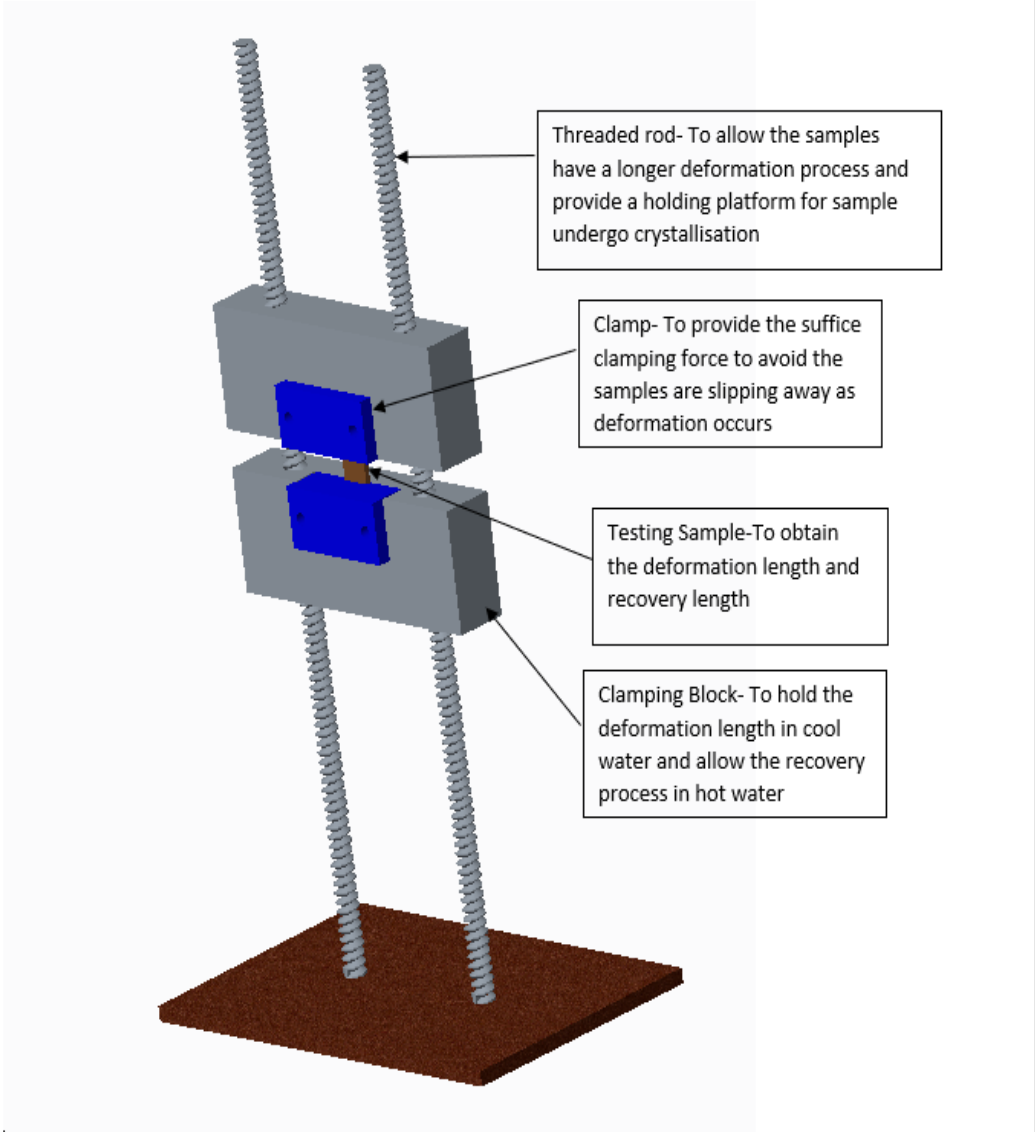

Figure 3.3: Custom-made stretching apparatus

Figure 3.4: The equipment of shape memory experiment (water bath machine for heating process while ice water for quenching process)

3.6 Shape Memory Experiment

To investigate the shape memory behaviours of the SMNR developed, shape memory capabilities are evaluated under various experimental settings, as shown in Table 3.7. Two shape memory parameters which are proposed by Lendlein and Kelch [159], are adopted to determine the shape memory capability. They are shape fixity and shape recovery: the former defines the percentage of holding the deformed length to the original length while the latter is the percentage of recover length to the deformed length. Figure 3.5 shows the entire shape memory experiment by using custom-made stretching apparatus. The equations of shape fixity (S_f) and shape recovery (S_r) of the specimen are shown in Equation (3.5-6)

$$S_f = \frac{\varepsilon_f}{\varepsilon_l} \text{x} 100\% \qquad \text{Equation (3.5)}$$

$$S_r = \frac{\varepsilon_l - \varepsilon_r}{\varepsilon_l - \varepsilon_i} \text{x} 100\% \qquad \text{Equation (3.6)}$$

where $\varepsilon_i$is defined as the strain level during the initial point, $\varepsilon_l$is defined as the strain level during the deformation stage, ε_f is defined as the strain level during the unloading stage, ε_r is defined as the strain level during the recovery stage

Table 3.7: The shape memory experimental setting

Testing parameter	Types of specimens	Testing Temperature	Deformation strain
Shape memory capability	Swollen SMNR	$T_p = T_r = 70^oC$	100% ,200%, 300%
Composition content	Prevulcanised SMNR	$T_p = T_r = 70^oC$	200%
Working temperature	Prevulcanised SMNR	T_p= 40^oC,50^oC,60^oC,70^oC T_r=40^oC,50^oC,60^oC,70^oC	200%
Shape memory cycle	Prevulcanised SMNR	$T_p = T_r = 70^oC$	200%

where T_p is the programming temperature, T_r is the recovery temperature

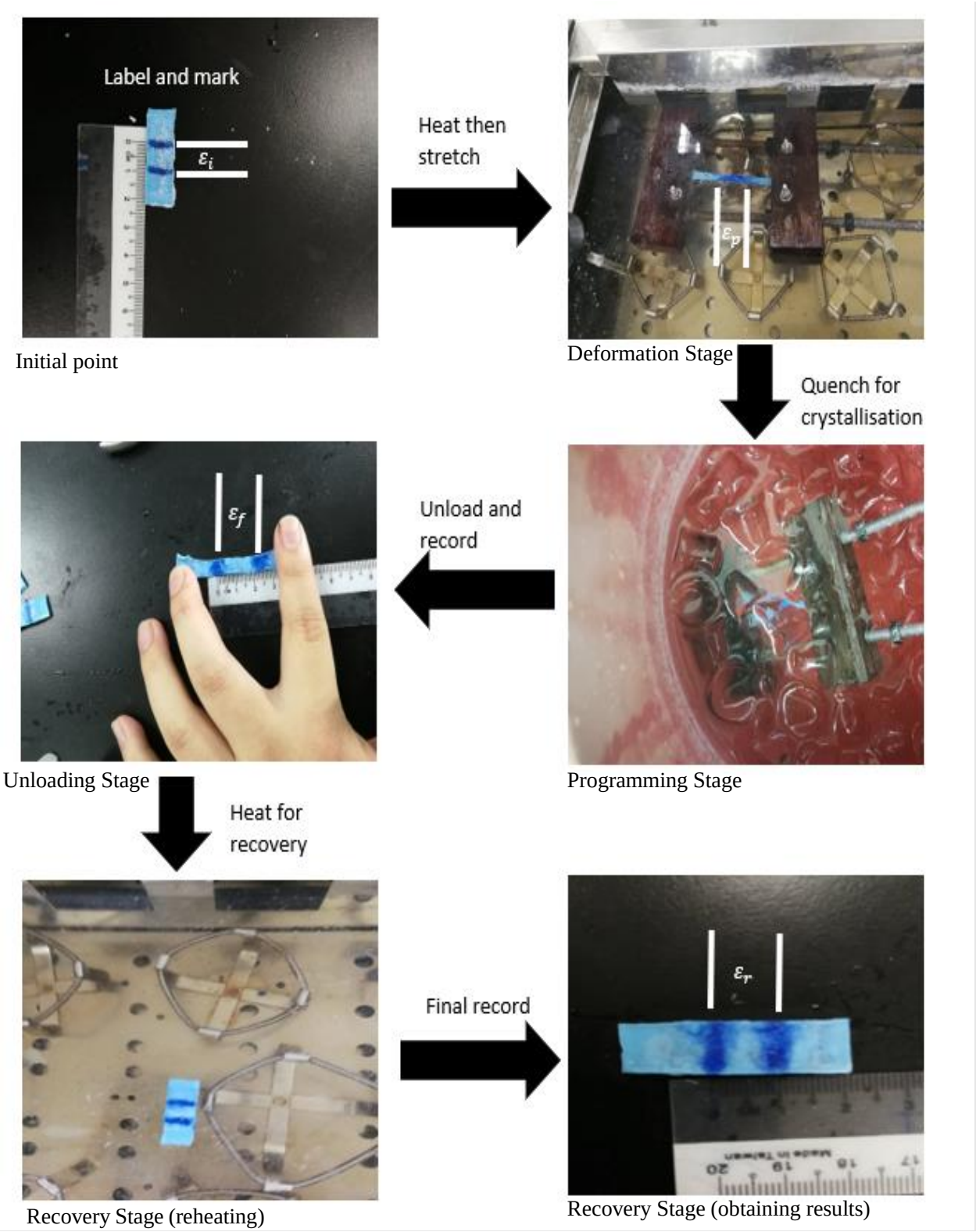

Figure 3.5: Procedure pictures of the shape memory experiment

3.6.1 Thermomechanical Test on SMNR Specimen Fabricated through Swelling Process

This test is conducted to evaluate the relationship between the swelling temperature and shape memory properties of the swollen SMNR. To begin, each swollen specimen is labelled with a 10 mm gap line on the rubber surface and the initial strain is recorded as, ε_i. Afterward, the swollen sample is clamped and immersed in hot water at a temperature of 70°C of hot water to soften it. After two minutes, the swollen sample is elongated into 100% of strain level and the deformed strain is recorded as loaded strain, ε_l. Then, the deformed sample is quenched in ice water for 180 seconds to stabilise crystal structure, the strain is recorded as programming strain, ε_p. To avoid the occurrence of slipping during the programming process, the experiment is restarted if the difference between the ε_p and ε_l more than 5%. Next, the swollen SMNR is released, and the unloaded strain is recorded as fixed strain, ε_f. Lastly, the rubber strip is soaked into hot water bath for another 180 seconds and the recovery strain, ε_r is recorded. 200% and 300% of strain level are repeated for the next swollen SMNR specimens. Figure 3.6 depicts the shape memory capability experiment in the 2D graph.

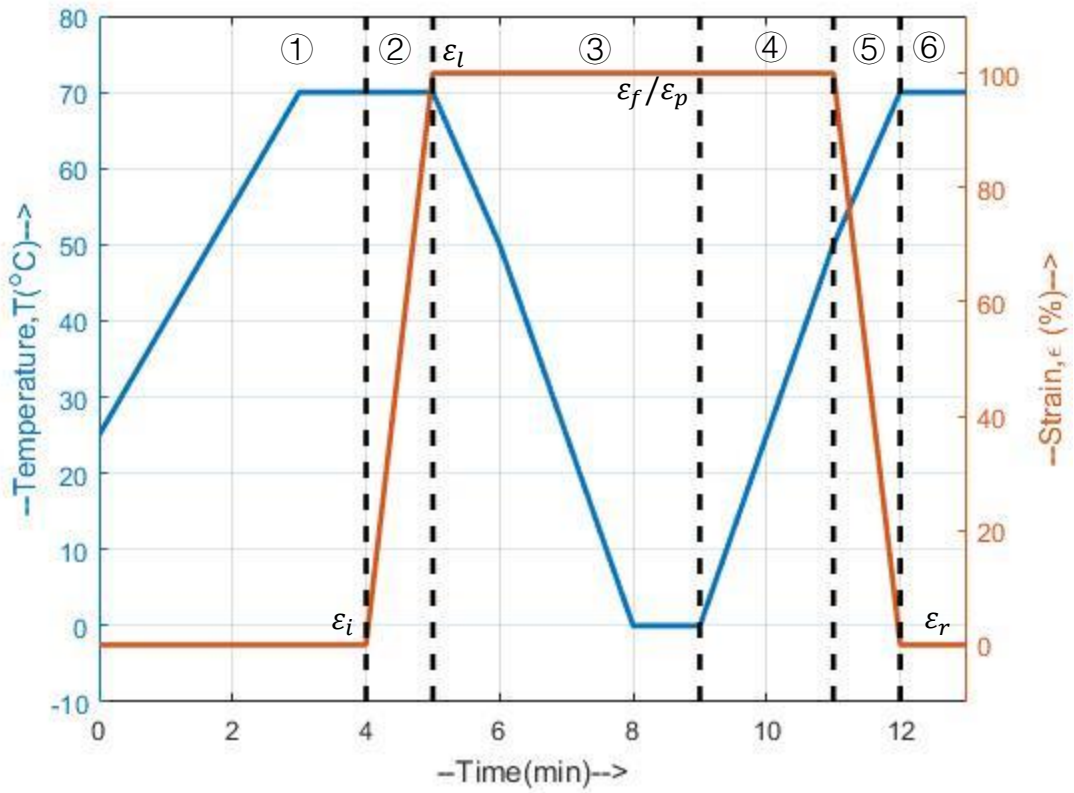

Figure 3.6: 2D of shape memory capability test under 100% of strain ratio and their corresponding strains. Specimen is deformed under a particular loaded strain, ε_l (100%,200% and 300%) to examine their fixed strain, ε_f and recovery strain, ε_r

① softens the specimen (first time heating process), ② is to entangle the molecular to undergo SIC (deformation stage), ③ stabilise the SIC structure and halts the mobility of molecular (unloading and programming process), ④ reheats the molecule to vanish the SIC (reheating process), ⑤ triggers SME and the high entropy energy imposes the recovery process (recovery process-beginning) , ⑥ is the end of the recovery process (recovery process- completed).

3.6.2 Thermomechanical Test under Various Formulation and Working Temperature on SMNR Fabricated through Prevulcanisation Process

This test is conducted to evaluate the effect of material formulation and working temperatures on the prevulcanised SMNR. The prevulcanised SMNR is clamped on the custom-made stretching apparatus with 10 mm initial length, and it is recorded as initial strain, ε_i. First, the specimen is heated at the T_p of 40°C for three minutes. Afterward, the specimen is stretched to the deformed strain of 200%, and the elongation strain is recorded as loaded strain, ε_l. The quenching process is done with temperature range of 0~2°C for another 180 seconds, and the strain is recorded as programming strain, ε_p. Then, the specimen is released by removing the weight load, and unloaded strain is recorded as fixed strain, ε_f. The recovery process is initiated by heating the specimen to 40°C for three minutes and its recovered strain is recorded as recovery strain, ε_{r40}. For every increment of 10°C up to a maximum of 70°C, the recovered strain is measured and recorded for the particular T_r. The shape memory experiment is repeated with T_p in 50°C, 60°C and 70°C. Figure 3.7 shows a 3D graph of shape memory experiment. Figure 3.8 demonstrates the experiment setting to investigate the effect of T_c.

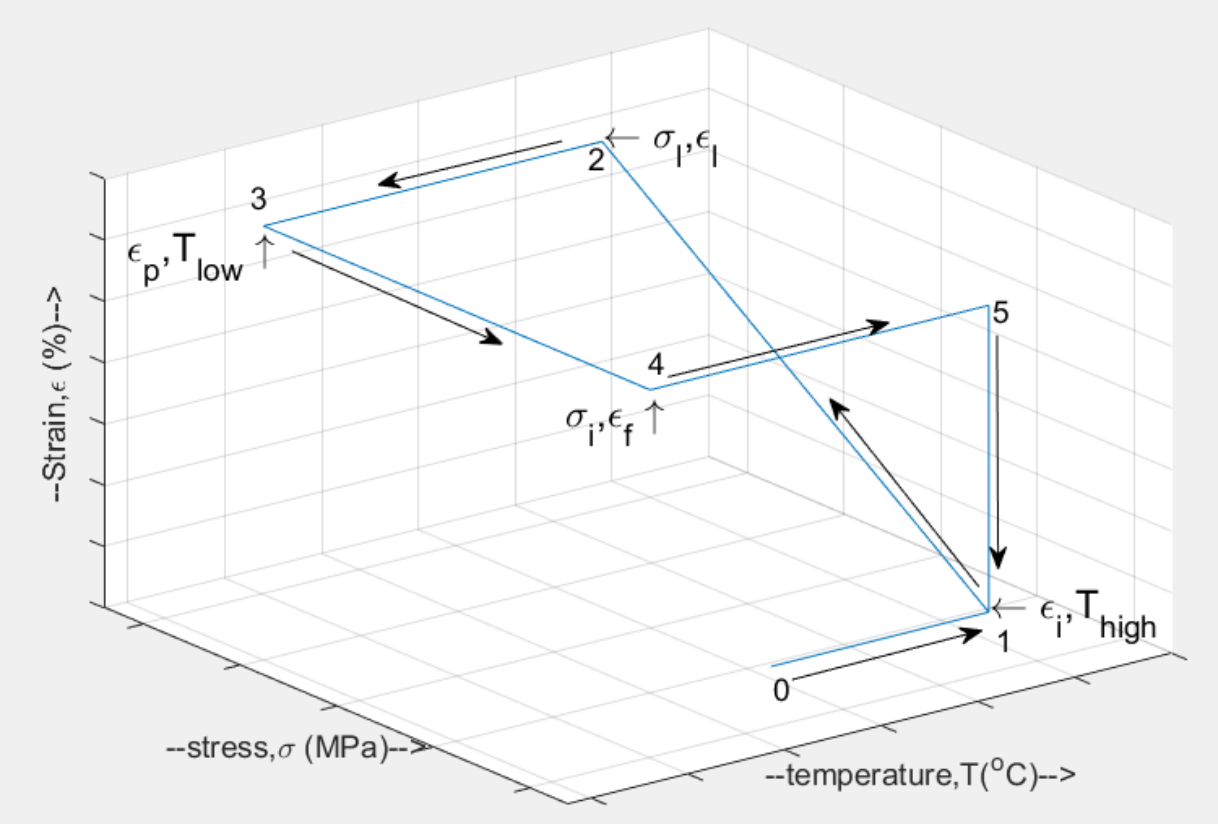

Figure 3.7: 3D graph of SME with corresponding stress and strain

where T_{high} expresses as heating temperature while T_{low} defines as lower temperature range.

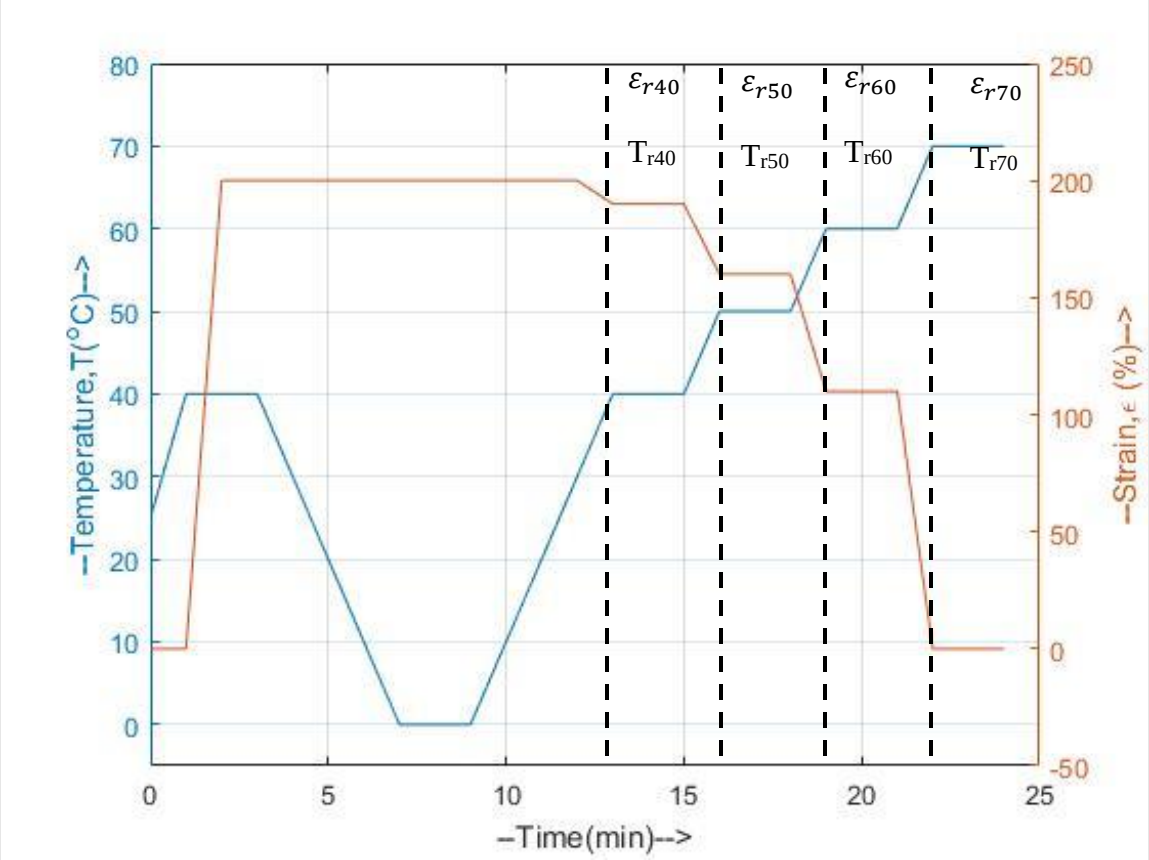

Figure 3.8: The experiment setting for T_c test (dotted lines represent the recovery strains upon heating to the corresponding recovery temperature). Specimen is deformed under 200% of strain ratio to obtain their recovery strain, ε_r at vary recovery temperature, T_r

3.6.3 Multi Cycles Thermomechanical Test on Prevulcanised SMNR

This test evaluates the repeatability of prevulcanised SMNR. The prevulcanised specimen is clamped on the stretching apparatus with a gap of 10 mm between the clamping blocks, and it is recorded as initial strain, ε_i . The specimen is softened by immersing it into 70°C of hot water for three minutes. Subsequently, the specimen is elongated in 200% deformed strain and the loaded strain, ε_l is recorded. Then, the specimen is quenched in ice water for another 180 seconds. After three minutes, the specimen is released, and the unloaded strain is recorded as fixed strain, ε_f. Afterward, the specimen is reheated to 70°C for three minutes, and the recovery strain, ε_r is measured and recorded. The entire process is repeated 3 times on similar specimen. Figure 3.9 describes the shape memory cycle procedure in 2 D graph.

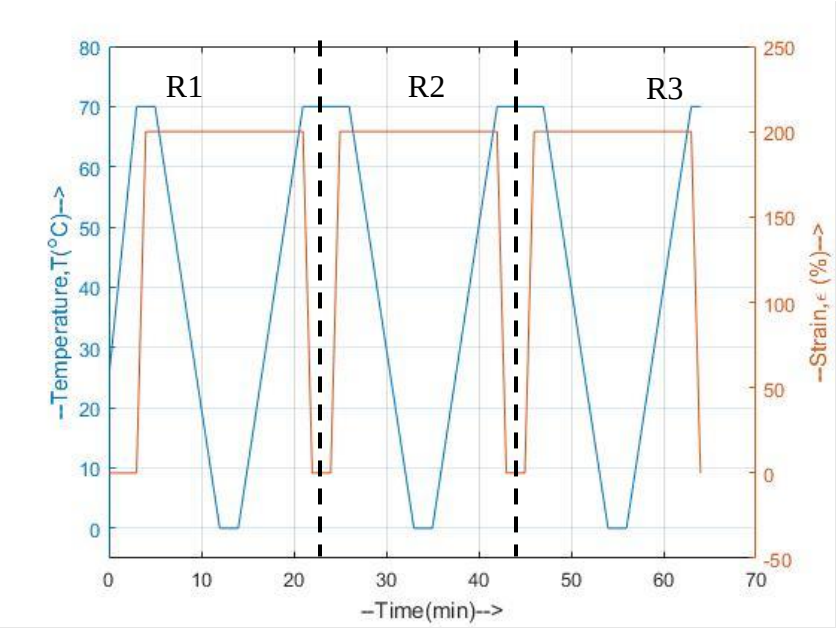

Figure 3.9: 2D procedure of shape memory cycle test. Specimen repeats the shape memory experiment for 3 cycles under the similar strain ratio, 100% with 70°C of programming and recovery temperature to obtain fixed strain and recovery strain for each cycle (R1, R2 and R3).

3.7 Mechanical Characterization

The mechanical characteristics of prevulcanised SMNR with different palmitic acid loading are further characterised in this section to gain insight into the viscoelastic behaviour of the SMNR developed.

3.7.1 Tensile Test Experiment at Room Temperature

Tensile strength of SMNR specimen is determined by the tensile test instrument LLOYD Instruments LR50k Plus at room temperature. The experiment follows the ASTM D412 standard, which the sample is prepared by the ASTM 412 type C die cutter and conducts under a constant crosshead speed of 50mm/min. Figure 3.10 shows the tensile tester is operated at room temperature. The tensile test is conducted at least three times for each specimen batch.

3.7.2 Tensile Test Experiment At 70^{o}C (with heat chamber)

The tensile test is undertaken with a controlled heat chamber on an MTS 831 servo-hydraulic testing machine. The experimental procedures are executed by a Multi-Purpose Testware (MPT). The tensile experiment is conducted under the 50mm/min crosshead speed at temperature of 70^{o}C. The displacement strain limit of the tensile test is 200%. Figure 3.11 shows the tensile machine with a controlled temperature chamber.

Figure 3.10: Tensile test conducted at room temperature

Figure 3.11: Tensile machine with a controlled temperature chamber (70^{o}C)

3.7.3 Viscoelastic Experiment under Stress Relaxation mode (without Temperature Ramp)

Viscoelastic properties of the prevulcanised SMNR are obtained under a MTS 831 servo-hydraulic testing machine with a controlled heat chamber. The specimen is examined under stress relaxation mode by maintaining the deformed strain of 500% for 30 minutes at the temperature of 70^{o}C. To have an isothermal environment, the specimen is heated to a similar temperature range for 5 minutes before the experiment is started.

3.7.4 Viscoelastic Experiment under Stress Relaxation mode (with Temperature Ramp)

A stress relaxation experiment is conducted under Perkin Elmer DMA 8000 machine with tensile mode to determine the stress-strain behaviour during the temperature change. Due to the machine limitations, the maximum deformed strain for this experiment is confined to 1.5% and the specimen is cut with the dimension of 5mmx10mm (below 0.5mm thickness). Before the experiment is conducted, the specimen is heated to 70^{o}C for 5 minutes. Subsequently, the specimen is held to the maximum deformed strain for one hour. During the stress relaxation experiment, the temperature of the first 20 minutes is set to 70^{o}C, then it is quenched at room temperature for another 20 minutes. Lastly, the specimen is reheated to 70^{o}C for the remaining 20 minutes.

3.8 Shape Memory Behaviours Prediction Modelling

Hyun Kim's phenomenological model [160] is adopted to predict the shape memory behaviours of this SMNR developed. The mechanical approach of the shape memory behaviour is demonstrated under the 'three-phases' model: one hard segment phase to domain the viscoelastic behaviour of SMNR and two soft segment phases (active and frozen phase) reflect the microstructure phase transition behaviour at respective temperatures. A thermal responsive strain algorithm is also included in the shape memory behaviours prediction model to account for the thermal effect during shape morphing and shape programming. According to the phase transition model, the volume fraction of palmitic acid formulations is incorporated into the thermal model equation. Hence, the composition results from the TGA experiment are utilised to determine the volume fraction of the soft and hard segment phase. Figure 3.12 shows the shape memory behaviours prediction model of SMNR is established using both mechanical and thermal approach and their coefficients of each element labelled above the respective model.

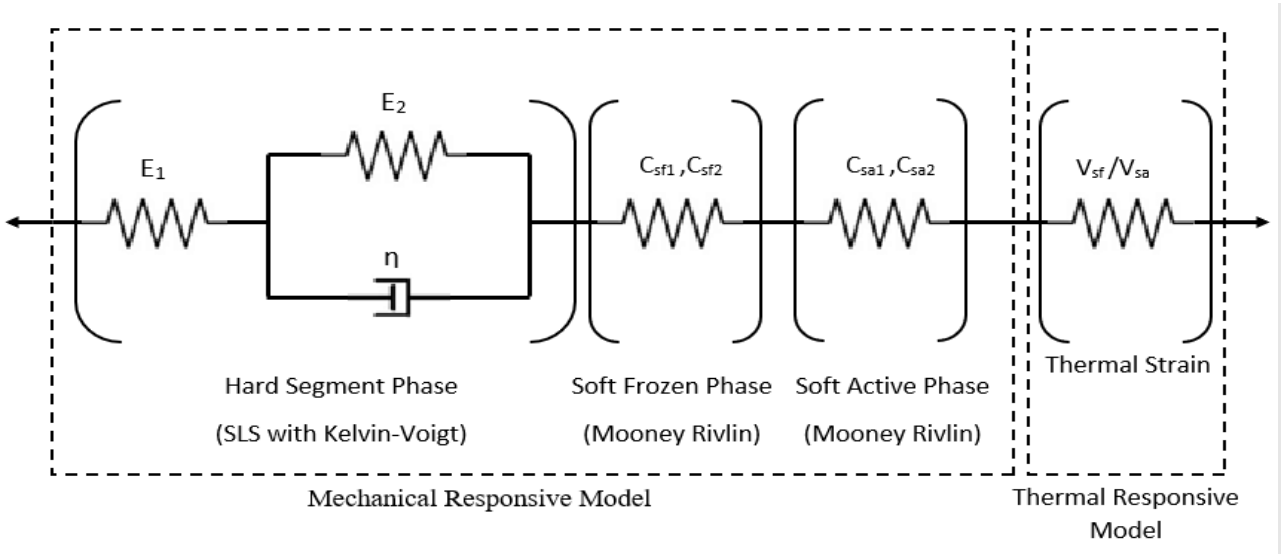

Figure 3.12: The shape memory behaviours prediction model under three-phase mode with their coefficient constants

3.8.1 The Description of Hard Segment Phase

The standard linear solid (SLS) describes the viscoelastic behaviour of the hard segment phase by two material stiffness, E_1 and E_2, and one material viscosity, η. Following the Kelvin-Voigt model arrangement, the general SLS model equation can be written as follows:

$$\varepsilon E_1 E_2 + \eta E_1 \dot{\varepsilon} = (E_1 + E_2)\sigma + \eta\dot{\sigma} \quad \text{Equation (3.7)}$$

where ε is the total strain, $\dot{\varepsilon}$ is strain rate, σ is the total stress, $\dot{\sigma}$ is the stress rate

Since strain is fixed during the shape programming, the Equation (3.7) governs the stress relaxation behaviour in this constitutive model. The unrelaxed modulus, E_U, relaxed modulus, E_R and relaxation time, τ' are derived in Equation (3.8a-c),

$$E_U = E_1 \quad \text{Equation (3.8a)}$$

$$E_R = \frac{E_1 E_2}{E_1 + E_2} \quad \text{Equation (3.8b)}$$

$$\tau' = \frac{\eta}{E_1 + E_2} \quad \text{Equation (3.8c)}$$

Boundary conditions of stress relaxation is given by:

$$\varepsilon = \varepsilon(t) \; for \; t > 0 \quad \text{Equation (3.9a)}$$

$$\dot{\varepsilon} = 0 \; for \; t > 0 \quad \text{Equation (3.9b)}$$

Under the boundary condition of Equation (3.9a-b), the general equation of the viscoelastic model under stress relaxation is expressed as:

$$E(t) = (E_R + (E_U - E_R)\exp\left(-\frac{t}{\tau'}\right)) \quad \text{Equation (3.10a)}$$

$$\sigma = E(t)\varepsilon_0 \quad \text{Equation (3.10b)}$$

where $E(t)$ is the total material stiffness at a particular time, ε_0 is the initial strain

To have a continuous form of the shape memory behaviours prediction model, the stress-strain relationship of the viscoelastic equation is expressed under Boltzmann Superposition Principle and given as:

$$\sigma(t) = \int E(t - t_i) \frac{d\varepsilon(t_i)}{dt_i} dt_i \quad \text{Equation (3.11a)}$$

$$\varepsilon(t) = \frac{\sigma(t)}{[\int E(t-t_i) dt_i]}\ dt_i + \varepsilon(t-1) \quad \text{Equation (3.11b)}$$

where t_i is the particular time for undergoing strain change

3.8.2 The Description of Soft Segment Phase

The strength reinforcement and shape morphing properties are undertaken by soft segment phases consisting of active and frozen phases. Both soft segment phases are considered to exhibit hyperelastic properties during the shape memory response. Thereby, their mechanical properties are demonstrated under the Mooney Rivlin equation [161] with the following forms:

$$W = C_1(I_1 - 3) + C_2(I_2 - 3) \quad \text{Equation (3.12a)}$$

where W is the strain energy, C_1 and $C_2$are the material constants of Mooney Rivlin

Assuming the material is incompressible and isotropic under uniaxial tension, the deformation gradient, F, right and left Cauchy-Green deformation tensor, respectively C and B are defined by:

$$\mathrm{F} = \begin{bmatrix} \lambda & 0 & 0 \\ 0 & \lambda^{-0.5} & 0 \\ 0 & 0 & \lambda^{-0.5} \end{bmatrix} \quad \text{Equation (3.12b)}$$

$$\mathrm{B} = \mathrm{C} = \begin{bmatrix} \lambda^2 & 0 & 0 \\ 0 & \lambda^{-1} & 0 \\ 0 & 0 & \lambda^{-1} \end{bmatrix}$$ Equation (3.12c)

where for the deformation under uniaxial extension,

$\lambda = \varepsilon_s + 1$

$\lambda_1 = \lambda$

$\lambda_2 = \lambda_3 = \lambda^{-0.5}$

where λ is the extension ratio, $\varepsilon_s$is the strain of soft segment phase

To express as a set of independent strain invariants of C and B, denoted as I_1, I_2, and I_3 and following by:

$I_1 = tr(\mathrm{C}) = \lambda^2 + 2\lambda^{-1}$ Equation (3.12d)

$I_2 = \frac{1}{2}\left[(tr(C))^2 - tr(\mathrm{C}^2)\right] = 2\lambda + \lambda^{-2}$ Equation (3.12e)

$I_3 = det(\mathrm{C}) = 1$ due to incompressible properties Equation (3.12f)

In the general theory of hyperelasticity, the stress response can be derived from the strain energy function which written as:

$$\begin{bmatrix} \sigma_{11} & 0 & 0 \\ 0 & \sigma_{22} & 0 \\ 0 & 0 & \sigma_{33} \end{bmatrix} = \begin{bmatrix} -p & 0 & 0 \\ 0 & -p & 0 \\ 0 & 0 & -p \end{bmatrix} + 2\left(\frac{\partial W}{\partial I_1} + I_1\frac{\partial W}{\partial I_2}\right)B - 2\frac{\partial W}{\partial I_2}B^2$$ Equation (3.12g)

where p is the hydrostatic process due to incompressibility

Boundary condition of uniaxial extension is given by:

$\sigma_{22} = \sigma_{33} = 0$ Equation (3.12h)

Under the boundary condition of Equation (3.12h), the stress principle can be determined by denoting λ (Equation (3.12d-e)), which can be expressed by:

$$\sigma = 2\left(\lambda - \frac{1}{\lambda^2}\right)\left(\frac{dW}{dI_1} + \frac{dW}{dI_2}\frac{1}{\lambda}\right) \text{ for uniaxial extension} \qquad \text{Equation (3.12i)}$$

Substituting the strain energy of Mooney Rivlin function at Equation (3.12a) into Equation (3.12i), the algorithm derived as:

$$\frac{\sigma}{2} = C_1\lambda - \frac{C_1}{\lambda} + C_2\lambda^3 - C_2 \qquad \text{Equation (3.12j)}$$

where λ is the extension ratio, $\varepsilon_s$is the strain of soft segment phase

To determine the extension ratio under a given stress condition, the roots of the quartic equation from Equation (3.12j) are solved by Matlab with the boundary conditions of $\lambda > 1$, and the roots should be in real numbers. Although both soft segment phase models adopt similar hyperelastic model, they have different coefficient constant values to reflect the stress-strain response at their respective temperature ranges.

3.8.3 Determination of the Volume Fraction of Hard and Soft Segment Phase

According to the characteristic of the hard and soft segment phases, the prevulcanised NR structure is responsible for the hard segment phase, while the soft segment phase (active and frozen) is attributed to the palmitic acid. Thereby, the volume fraction of both segment phases is determined by the mass fraction obtained from TGA experiments and written as follow:

$$V_p = \frac{W_p}{W_p + (1 - W_p)\frac{\rho_{nr}}{\rho_p}} \quad \text{Equation (3.13a)}$$

$$V_p = V_{sa} + V_{sf} \quad \text{Equation (3.13b)}$$

$$V_h = 1 - V_p \quad \text{Equation (3.13c)}$$

where V is the volume fraction, W is the mass fraction from TGA results, ρ is the density while the subscripts of 'p', 'nr', 'sa', 'sf' and 'h' are defined as palmitic acid, NR, soft active segment phase, soft frozen segment phase, and hard segment phase, respectively. For example, ρ_{nr} is the density of NR (920kg/m^3), ρ_p is the density of palmitic acid (853kg/m^3),

The volume fraction of the soft active segment and frozen segment phases are interchangeable and corresponding to the thermomechanical properties of palmitic acid. An algorithm for volume fraction change in temperature is required and will be discussed in Section 5.1. However, as shown in Equation (3.13b), the total volume fraction of the soft segment phase equals the volume fraction of palmitic acid. It could be determined by the TGA results from Section 4.1.3.

3.8.4 The Description of Thermal Strain Model

Besides the stress effect, a thermal strain model is involved in the shape memory model algorithm. According to the researches in shape memory prediction models [140], [147], [162] on the SMP, thermal strain is irrelevant to mechanical stress but corresponds to the testing temperature range. This non-mechanical strain is often generated during the programming process and eliminated during shape recovery. According to the thermal strain from Hyun Kim [160], the continuum form of the thermal strain across various temperature ranges is written as follows:

$$\varepsilon_t(t) = \varepsilon_t(t-1) + C_f(V_{sa}(t-1) - V_{sa}(t))\varepsilon_{sa}(t-1) \quad T>T_g \qquad \text{Equation (3.14a)}$$

$$\varepsilon_t(t) = \varepsilon_t(t-1) + C_r \frac{(V_{sf}(t-1) - V_{sf}(t))}{(V_{sf}(t-1))}\varepsilon_t(t-1) \quad T<T_g \qquad \text{Equation (3.14b)}$$

where $\varepsilon_t(t)$ is the thermal strain in a particular time, $\varepsilon_{sa}$is the strain of soft active segment phase, C_f and C_r are the fixed coefficient and recovery efficient, respectively.

3.8.5 The Algorithm of Constitutive Models

As seen in Figure 3.12, a SLS model with Kelvin-Voigt element is extended with two Mooney Rivlin models to account for the shape memory behaviour of SMNR in mechanical approach and a thermal strain model referred to the change of length during the programming process and recovery process. Since the connection of these model elements is series arrangement, the strain response of each segment phase is simulated under similar stress behaviour. Hence, the overall shape memory prediction algorithms are obtained as follows:

$$\sigma = \sigma_h = \sigma_{sa} = \sigma_{sf} \qquad \text{Equation (3.15a)}$$

$$\varepsilon = V_h\,\varepsilon_h + V_{sa}\,\varepsilon_{sa} + V_{sf}\varepsilon_{sf} + \varepsilon_t \qquad \text{Equation (3.15b)}$$

where $\varepsilon_h(t) = \frac{\sigma(t)}{[\int E(t-t_i)dt_i]}\, dt_i + \varepsilon(t-1)$

$$\varepsilon_{sa}(t) = \sqrt[3]{\frac{C_{sa1}\lambda(t)+C_{sa2}}{C_{sa1}\lambda(t)+C_{sa2}-\frac{\sigma(t)}{2}}} - 1$$

$$\varepsilon_{Sf}(t) = \sqrt[3]{\frac{C_{sf1}\lambda(t)+C_{sf2}}{C_{sf1}\lambda(t)+C_{sf2}-\frac{\sigma(t)}{2}}} - 1$$

where σ is the stress, ε is the strain, $C_1$and C_2 is the material coefficients of the Mooney Rivlin equation while the subscripts of '*sa*', '*sf*', '*h*' and 't' are defined as soft active segment phase, soft frozen segment phase, hard segment phase, and thermal, respectively

4 Experimental Results and Discussion

This chapter presents the experimental results which are obtained throughout this project and draws the discussions for each experimental works. Both composition of the SMNR which are swollen and prevulcanised specimens are inspected and characterised in section 4.1. Subsequently, the shape memory behaviour of the SMNR with various material formulations under different working temperatures are reported. The mechanical responses such as hyperelastic and viscoelastic behaviours are examined to determine the material coefficient of respective segment phase as establishing a constitutive model system to predict the shape memory behaviour of prevulcanised SMNR.

4.1 Determination of Chemical Composition

4.1.1 Swelling

To investigate the relationship between palmitic acid loading and SME, the swollen SMNR is prepared with various swelling duration and swelling temperatures. The variance in the swelling ratio of CGNR and NRL specimens as a function of swelling duration with different swelling temperatures is shown in Figure 4.1. Both rubber specimens exhibit a dramatic rise in solvent absorption (>20% of swelling ratio) during the first twenty minutes, but the diffusion rate decreases significantly with an increment of the swelling duration and slowly plateau after 100 minutes. Compared with the CGNR specimens, the NRL specimen allows for greater solvent penetrates into the rubber molecule, and the penetration rate increases with elevating swelling temperature. In contrast, the CGNR specimens show a similar solvent uptake of around 70% of swelling ratio even in different swelling temperatures.

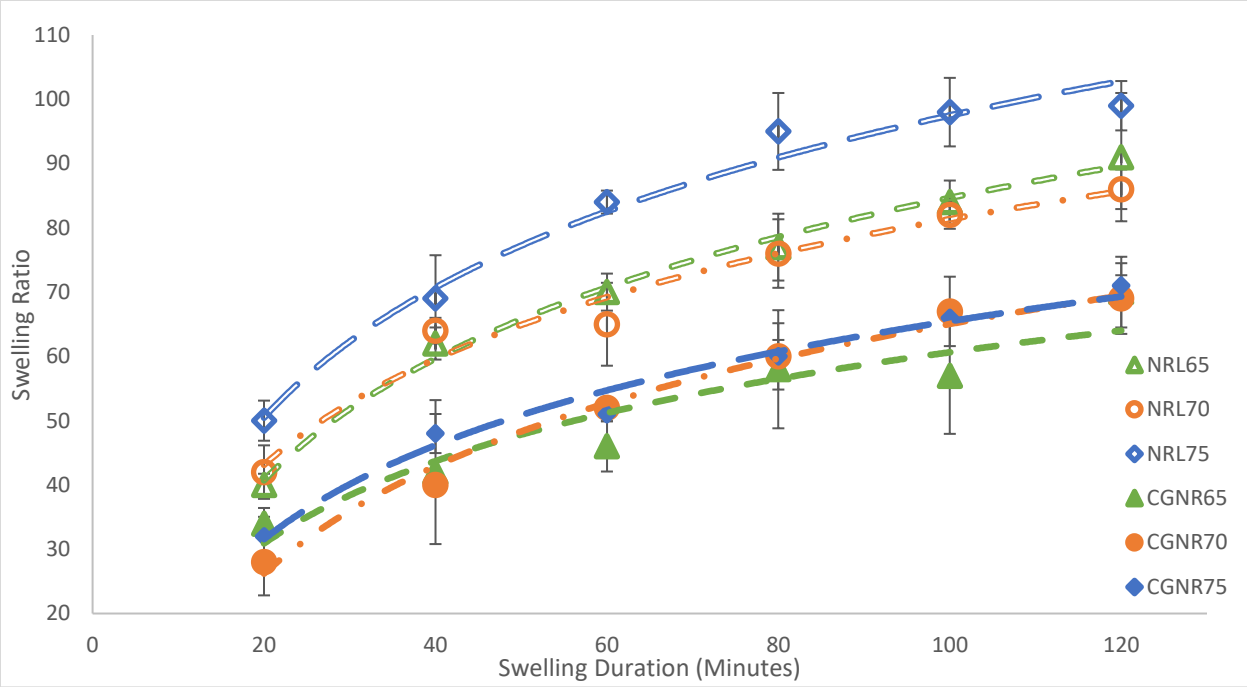

Figure 4.1: The swelling ratio of CGNR and NRL specimens on different swelling durations and swelling temperatures

There are three factors influencing the solvent diffusion rate. Firstly, the concentration gradient of palmitic acid in rubber molecular is the prime factor. The initial increment occurs in the swelling ratio for both rubber specimens during the first twenty minutes because the specimens are exposed to high solvent stress [163]. The large concentration gradient between rubber molecular and surrounding allows more palmitic acid solvent to flow into the low concentration region during the early swelling process. Nevertheless, the diffusion rate decreases with increasing swelling duration as a consequence of elevating rubber density [164]. Due to less void within the rubber network, palmitic acid forms a precoated layer on the rubber molecular. This layer acts as a barrier to hinder the solvent's movement. Thereby, solvent uptake is gradually plateaued by prolonging the swelling period after 100 minutes.

By considering the chain effects of rubber structure (sulphur network), the diffusion rate is not the only factor to be constrained, but also the solvent uptake is reduced [165]. Adding filler or additive is the general method for enhancing the mechanical properties of rubber products, such as improves thermal resistance or enhances the strength of rubbers [166]–[168]. The CGNR specimen is made of vulcanised rubber, which contains sulphur crosslinks the rubber molecular layer structure to limit swelling capability [169]. In contrast, the NRL specimen is prepared with pure NRL without any filler or additive. It has the greater volume capability for storing palmitic acid solvent compared to the CGNR specimen. In consequence, the CGNR specimen achieves the equilibrium swelling of 70%±2%, which is lower than the NRL specimen (92.5%±6.5%).

In addition, the CGNR specimens show similar solvent uptake after 120 minutes regardless of swelling temperatures. This is because all the CGNR specimens have the same crosslink density to limit their solvent absorption, achieving equilibrium swelling at 70%±2% of swelling ratio. The degree of crosslink density significantly influences the porosity formation in the network structure of the CGNR specimen [170]. In consequence, the maximum solvent uptake is similar under the same crosslink density. Once the equilibrium swelling ratio is achieved, the solvent no longer penetrates the rubber molecule. Any further solvent uptake occurs on the rubber surface, as illustrated in Figure 4.2, rather than precoating on the rubber molecule itself.

Figure 4.2: Crystal palmitic acid formed on the surface of NRL specimen (swelling duration >120 minutes)

Although crosslink density appears to confine the maximum solvent uptake in the CGNR regardless of the swelling temperatures, increasing the swelling temperature accelerates the penetration rate. Figure 4.1 shows the swelling ratio of CGNR at 70^{o}C and 75^{o}C of swelling temperature require 100 minutes to reach the equilibrium swelling while CGNR at 65^{o}C only achieves equilibrium swelling of 70% after 120 minutes. This indicates that more thermal energy is converted to the entropy and internal energy for palmitic acid solvent, which speeds up the swelling process at higher swelling temperature [117], [171]. NRL specimens have a similar trend which the NRL75 has the highest swelling ratio (99%) at a similar swelling duration compared to the NRL 65 and the NRL70. Obviously, the swelling capability of the NRL specimen is higher than the CGNR specimen because of the low crosslink density in the NRL rubber molecule. Combining the thermal effect, the penetrability of solvent is further increased, and more solvent is bound to rubber molecular. Therefore, there is a huge swelling ratio gap between the CGNR and NRL specimens, even at similar swelling temperature.

4.1.2 Thermogravimetric Analysis (TGA) and Derivative Thermogravimetry (DTG) Analysis for Swollen SMNR Specimens

By observing the TGA and DTG results, the composition element of each SMNR specimen can be determined by validating the material decomposition temperature. Figure 4.3, Figure 4.4, and Figure 4.5 describe the TGA and DTG results of the palmitic acid swollen SMNR specimens which are prepared from NRL and CGNR. To highlight the NR decomposition temperature ranges, dry rubber sources from NRL and CGNR are also subjected to TGA studies. DTG results reveal that the rubber decomposition is involved in three temperature ranges, which are 198^{o} to 330^{o}C, 330^{o}C to 450^{o}C, and above 450^{o}C. Due to the primary mass drop of both dry rubber specimens occur in middle temperature range, the second degradation section is attributed to the NR and unbonded latex molecular [115]. Generally, the organic compound will decompose first, and it is followed by inorganic compound. Hence, the initial mass loss percentage is contributed by the palmitic acid and other organic accelerators. While the single mass leftover after 450^{o}C should belong to the residual ash or other non-organic additives such as carbon black or zinc oxide.

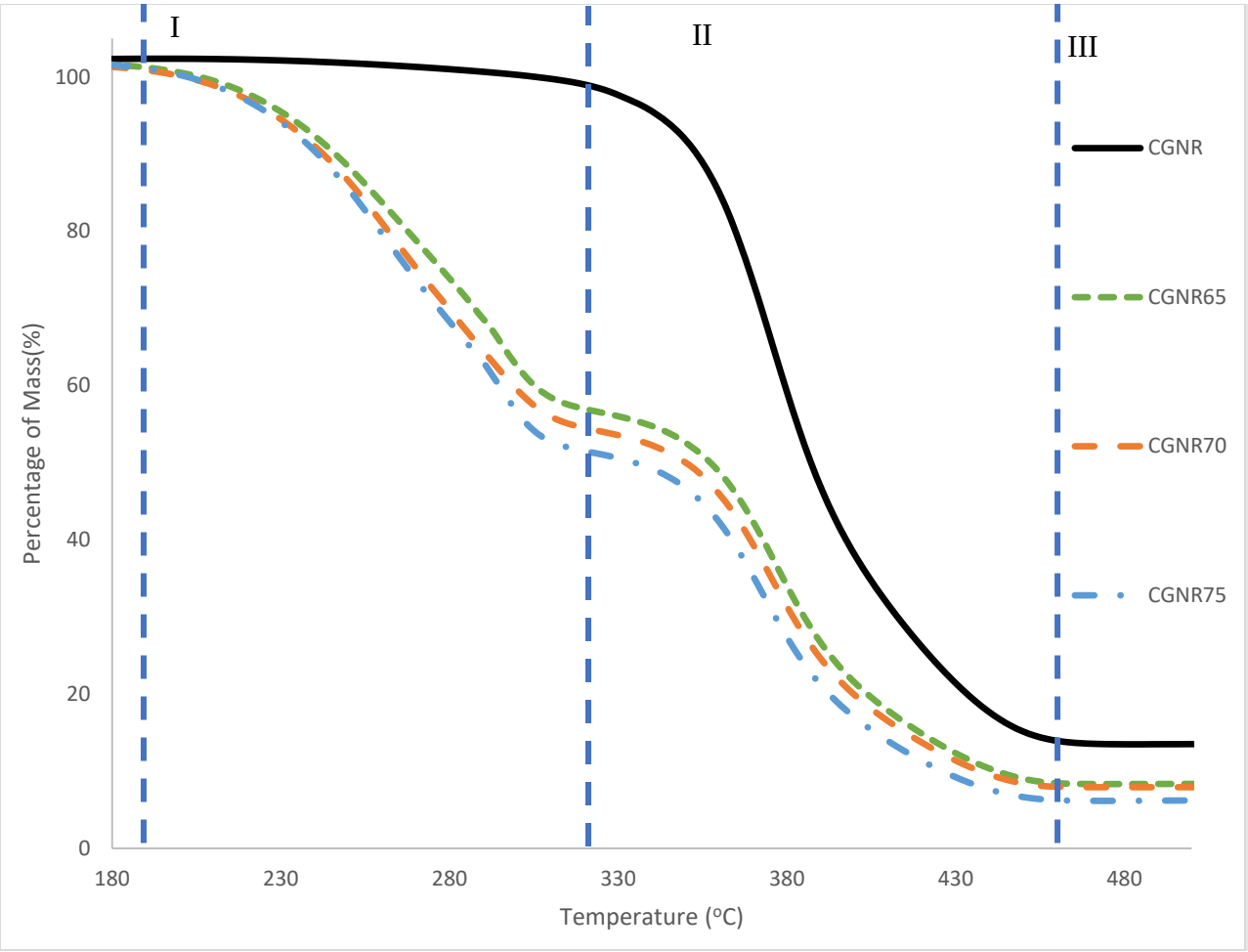

Figure 4.3: TGA result for swollen SMNR with CGNR

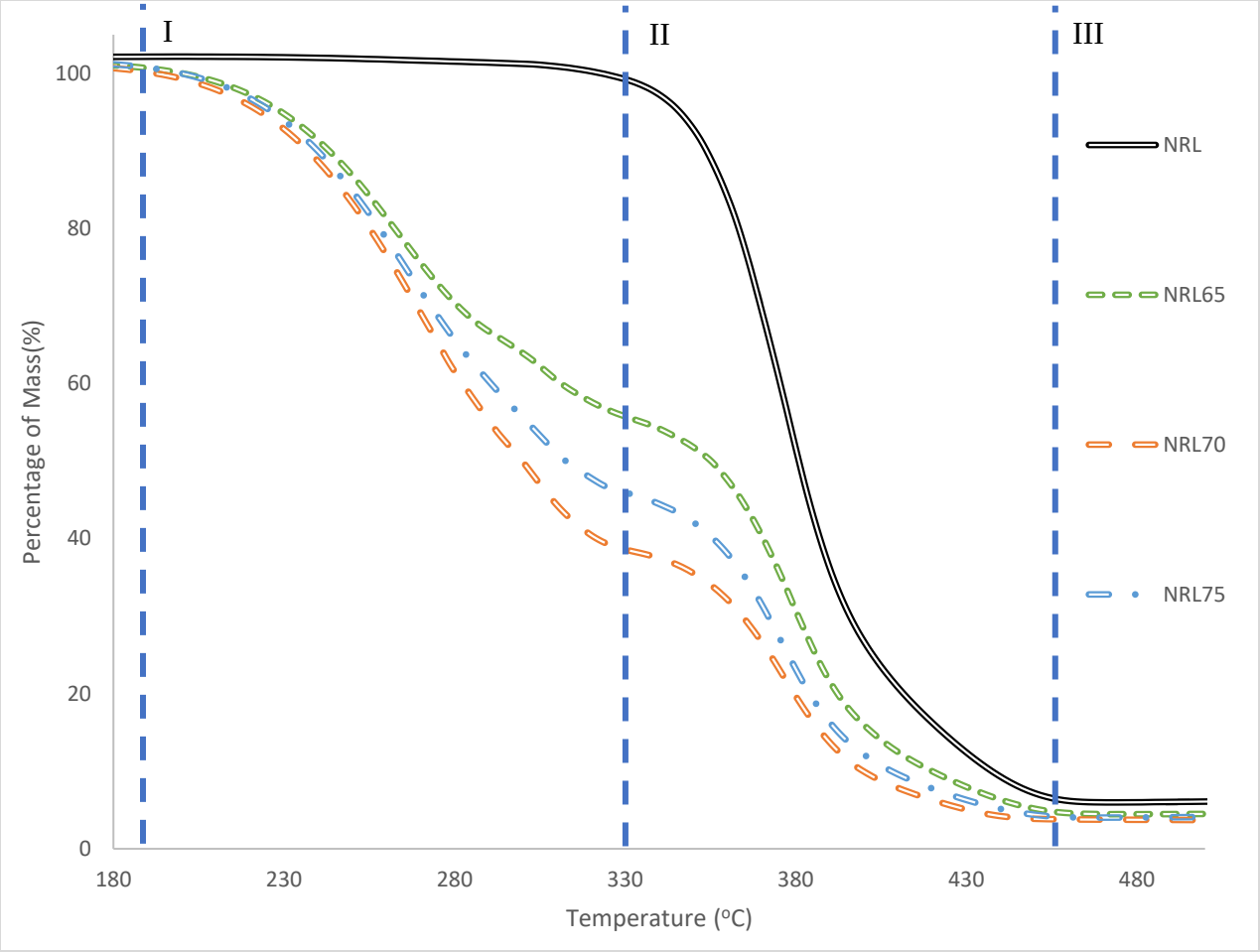

Figure 4.4: TGA result for swollen SMNR with NRL

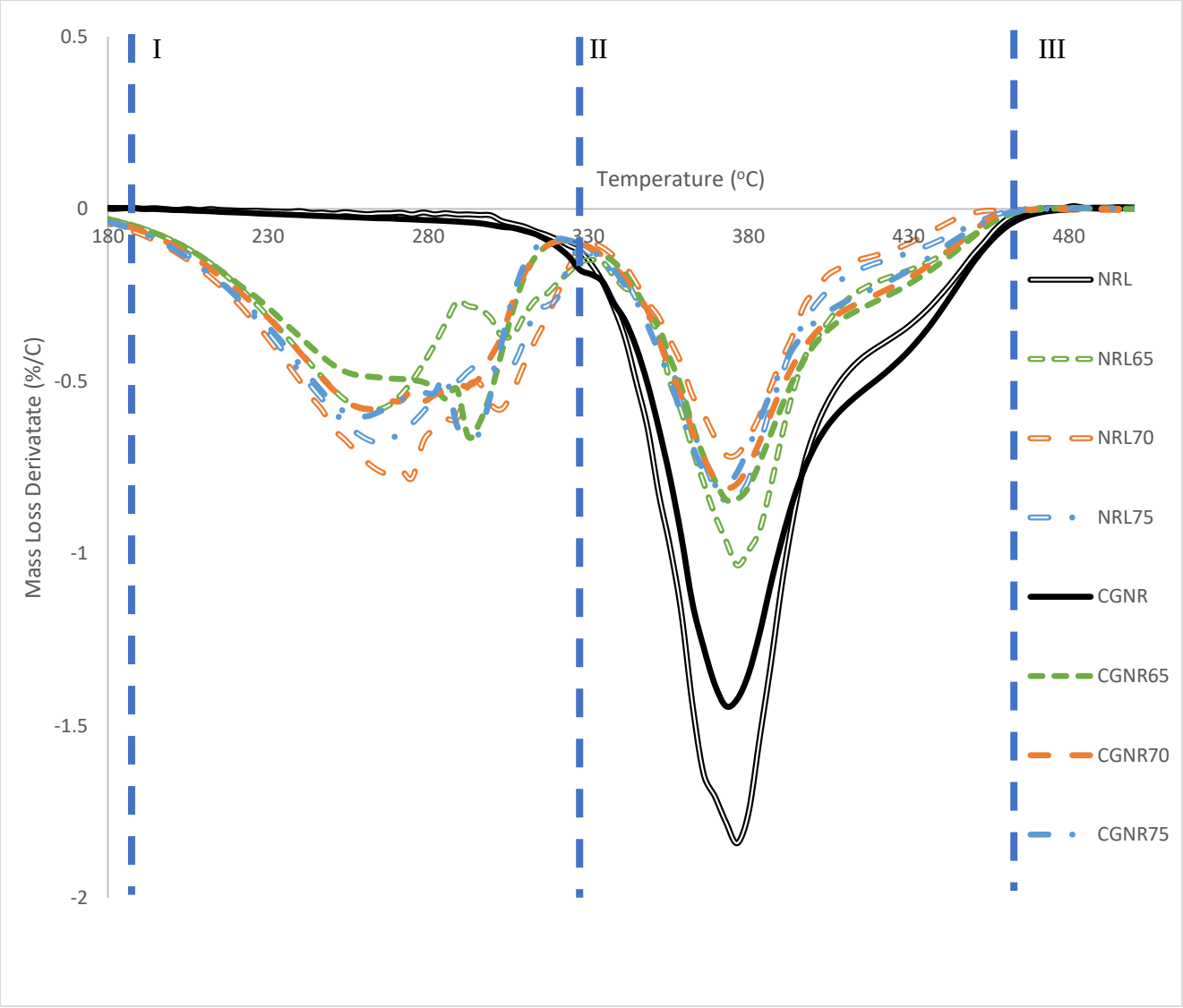

Figure 4.5: DTG results for both swollen rubber sources CGNR and NRL

According to the TGA results in Figure 4.3 and Figure 4.4 from both rubber sources, the CGNR65 has the least mass loss percentage in the initial decomposition section, which contains the lowest palmitic acid. Moreover, the mass loss scheme of each CGNR group is similar and increases with the swelling temperature. While NRL has a chaotic mass loss tendency, which the NRL70 has the highest palmitic acid content, and the NRL 75 contains the lowest palmitic acid

loading. This implies that the crosslink density stands as the barrier to limit palmitic acid movement. The mass loss pattern for both rubber sources is consistent with the swelling experiment finding. Table 4.1 summarizes the palmitic acid loading in various specimens based on the TGA and swelling experiment.

Although TGA experiments for both rubber sources have a varied magnitude on the weight fraction of palmitic acid with the swelling experiment results, they have a similar ascent behaviour with respect to the swelling temperature except the NRL 70. This is because excess palmitic acid forms the crystal structure on the rubber surface like Figure 4.2 to mislead the TGA result. Due to the fact that the swelling temperature of the NRL 70 is closer to the T_m of palmitic acid, palmitic acid is rapidly solidified on the rubber surface before being wiped off. Although the NRL 70 group specimen has a huge difference between the TGA and swelling experiment, the amount of palmitic acid for prevulcanised SMNR could be determined by the mass loss trend. In agreement with identifying the specimen composition by the degradation temperature, the next subsection discusses component characterization of the prevulcanised SMNR with a similar experimental setting.

Table 4.1: Palmitic acid weight fraction from TGA (obtaining from TGA analyser) and swelling experiment (measured from Equation (3.4))

Sample Code	TGA	Swelling experiment
NRL65	44%	48%
NRL70	62%	44%
NRL75	54%	50%
CGNR65	44%	41%
CGNR70	47%	41%
CGNR75	50%	42%

4.1.3 Thermogravimetric Analysis (TGA) and Derivative Thermogravimetry (DTG) Experiment for Prevulcanised SMNR

To identify the chemical composition of each prevulcanised SMNR, the TGA and DTG results are inspected with respect to the palmitic acid content. The results are shown from Figure 4.6 to Figure 4.11. The DTG results demonstrate the decomposition section is separated into four temperature ranges which are 190^{o}C to 300^{o}C, 300^{o}C to 450^{o}C, 450^{o}C to 530^{o}C, and above 530^{o}C. Referring to the TGA results of swollen SMNR specimen (Figure 4.3 and Figure 4.4), the unreacted palmitic acid and the NRL own the major mass loss percentage of the first and second decomposition sections, respectively. Hence, the remaining section is attributed to an inorganic component such as unreacted KOH, ash, and potassium palmitate. To determine the decomposition temperature of potassium palmitate, the 0.2SNR (without potassium palmitate) is examined under the DTG experiment. Figure 4.6 indicates that the third decomposition temperature range is attributed to potassium palmitate. Although the stearic acid has a higher T_m, it has a similar decomposition section with palmitic acid depicted in Figure 4.8. Therefore, the weight fraction of stearic acid could be determined similar decomposition section.

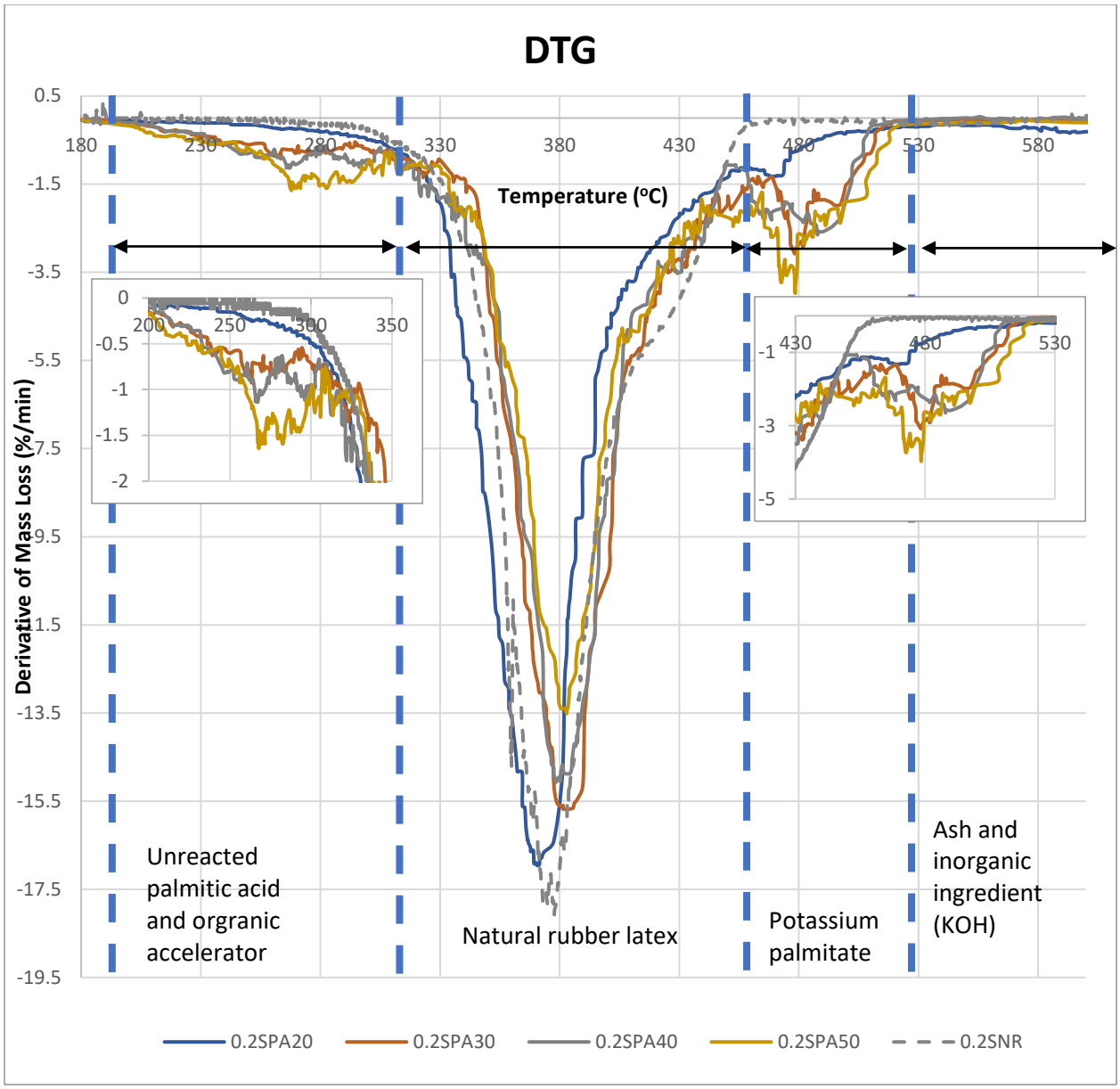

Figure 4.6:DTG result for prevulcanised SMNR with different palmitic acid loading

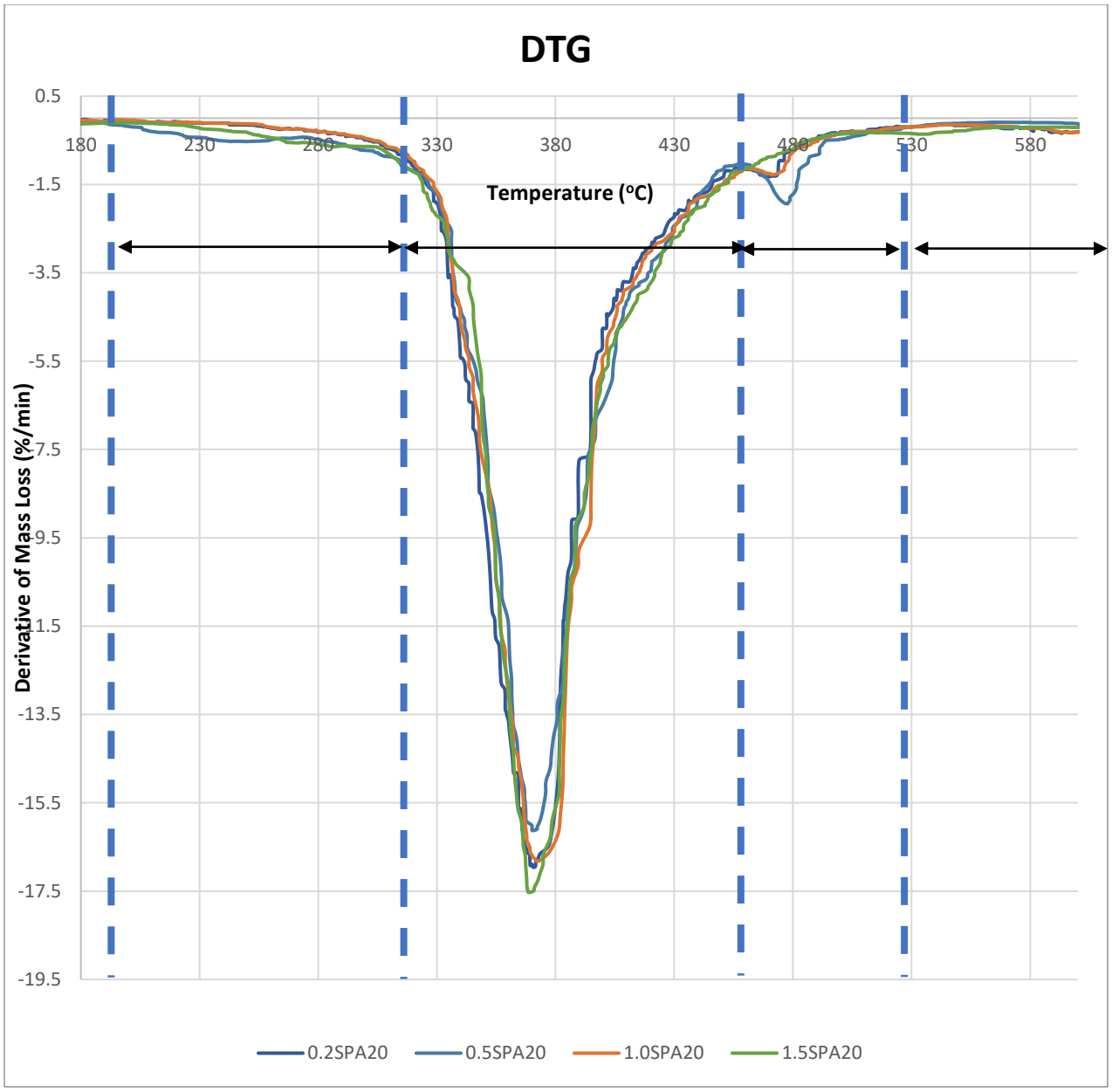

Figure 4.7: DTG result for prevulcanised SMNR with different sulphur content

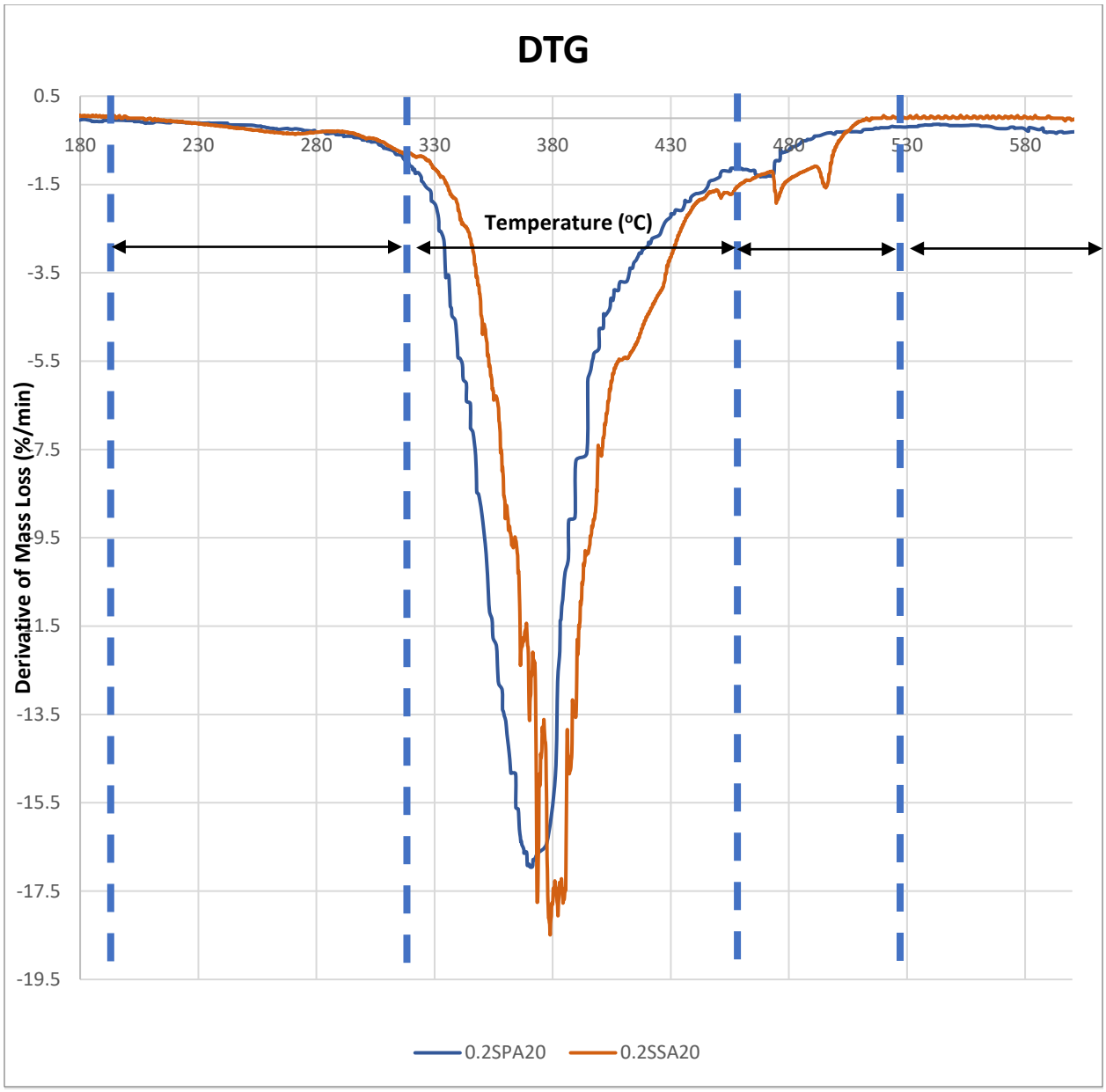

Figure 4.8: DTG results for prevulcanised SMNR with different fatty acids

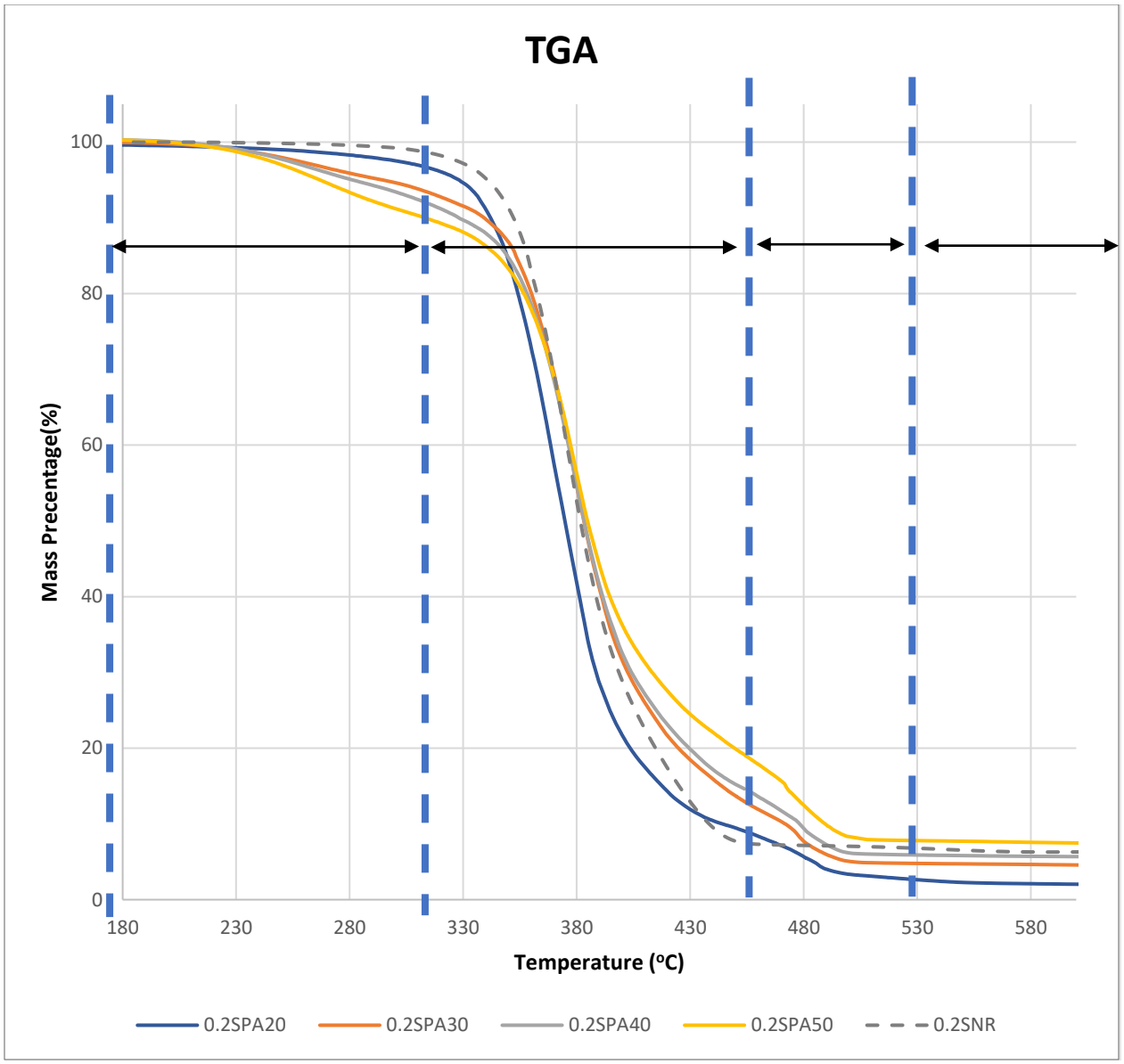

Figure 4.9: TGA result for prevulcanised SMNR with different palmitic acid loading

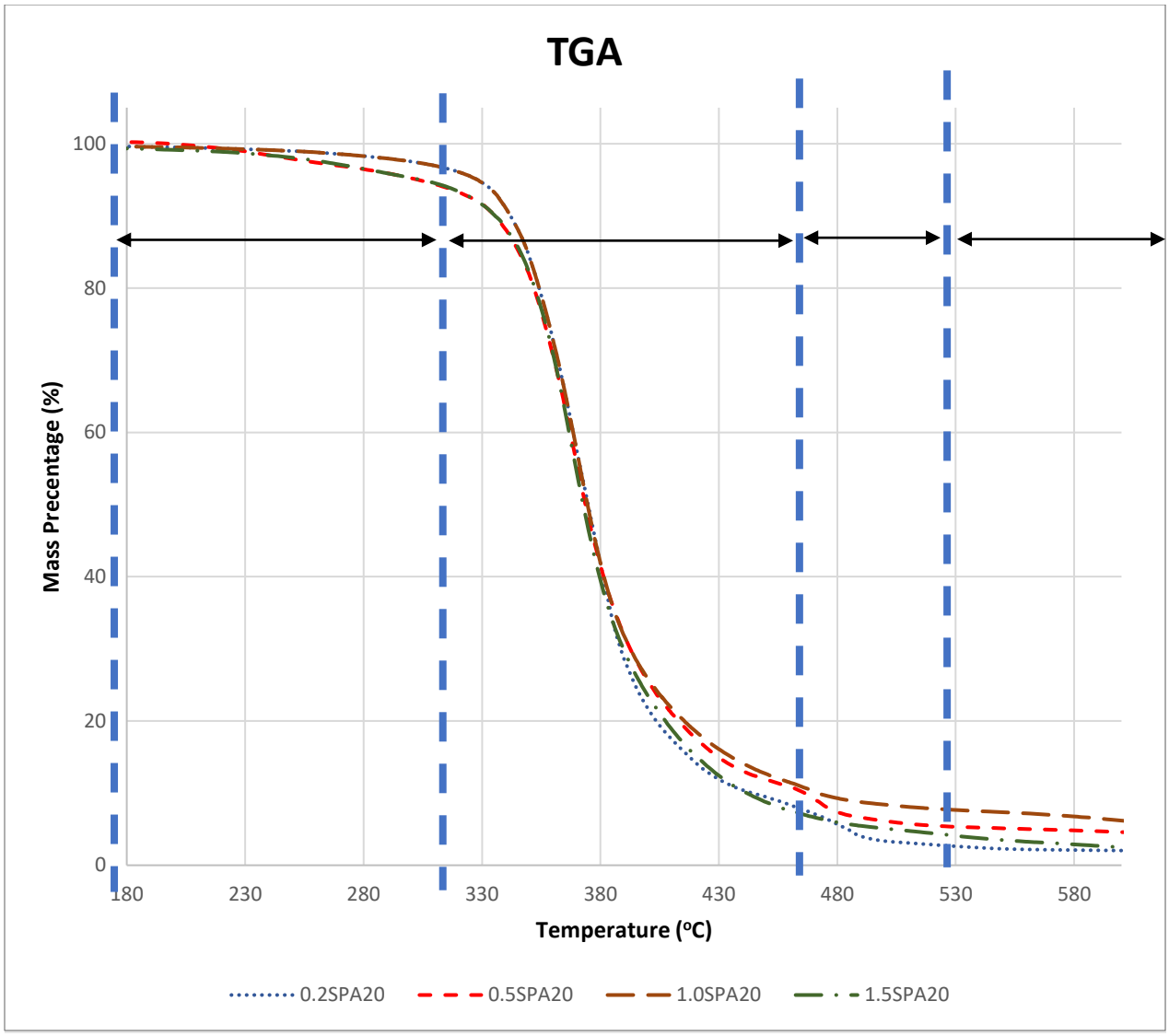

Figure 4.10: TGA result for prevulcanised SMNR with different sulphur content

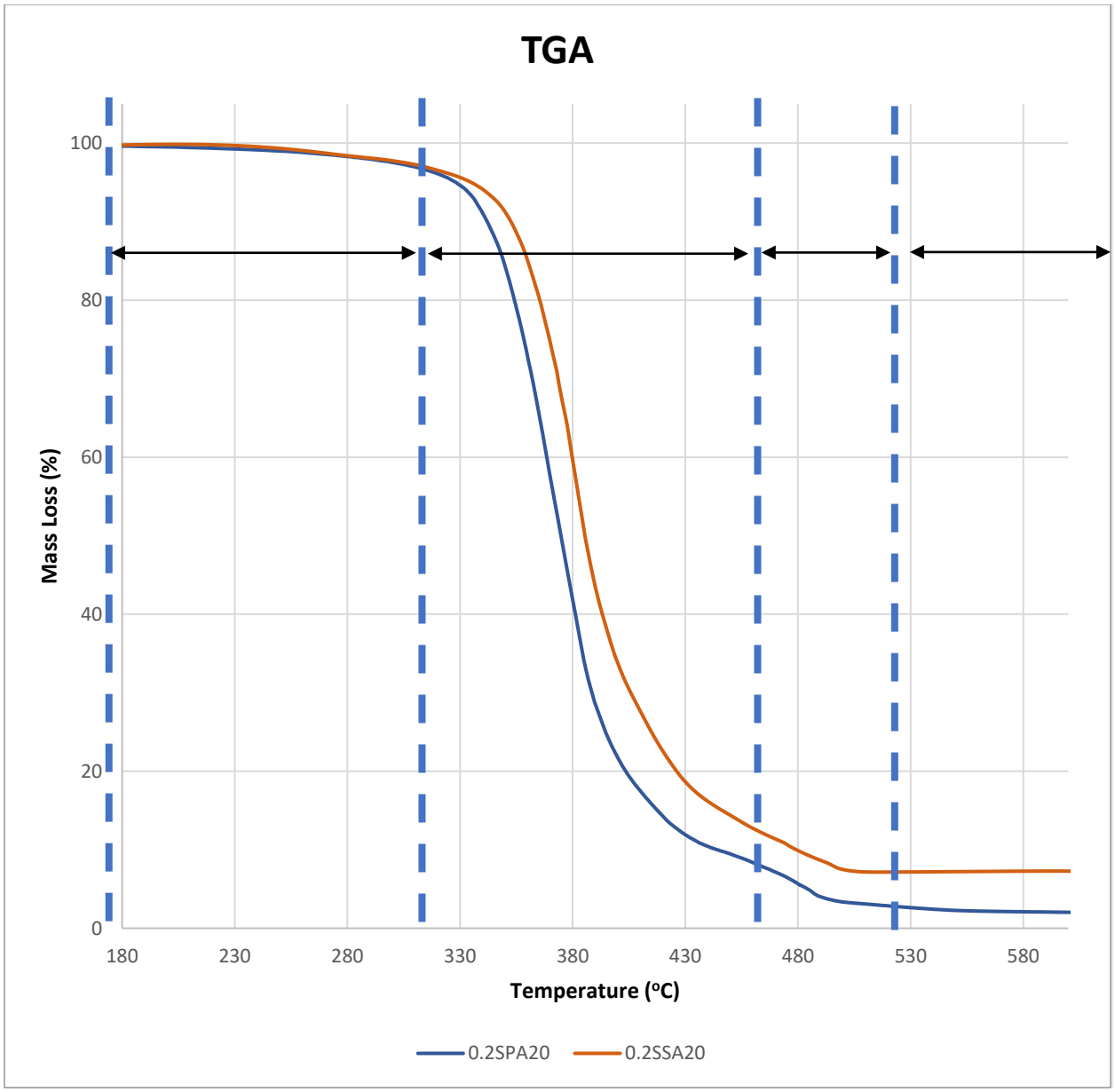

Figure 4.11: TGA results for prevulcanised SMNR under different fatty acids

After classifying the decomposition section, the content of SMNR components could be determined by their respective decomposition temperature. For example, palmitic acid content of each formulation configuration is obtained from the first and third decomposition sections while the weight fraction for NRL is determined by mass loss percentage in the second temperature range. The component content of SMNR is listed in Table 4.2. While the comparison graphs between

respective component for each specimen group are shown from the Figure 4.12 to Figure 4.15. The TGA results from Table 4.2 shows that NRL contains about 80%±8% of each prevulcanised SMNR while palmitic acid content just comprises for 12%±6% of total weight. By observing Figure 4.12 and Figure 4.13, they show that NRL content decreases by increasing palmitic acid content but the total palmitic acid amount fluctuates even mixing under the same sulphur content in Figure 4.15, especially for the 1.0S and 1.5S specimen groups. Palmitic acid is physically crosslinking to the rubber molecular, which easily diffuses out as flashing with water during the specimen preparation process. It is reasonable to assume that more palmitic acid is bound with rubber molecular as the higher concentration of potassium palmitate is involved during the compounding process. Nevertheless, potassium palmitate is soluble in water which easily permeates through rubber during the water flashing process. Consequently, the remaining palmitic acid in the SMNR specimen is much less than the absolute palmitic acid added during the compounding process. This is also the reason for the 1.0S and 1.5S specimen groups have the lower potassium palmitate content than other sulphur content group (0.2S and 0.5S) even they are mixed under similar concentration of potassium palmitate.

Table 4.2: The weight fraction of each component SMNR fabricated under prevulcanised process

	Weight fraction of each component (%)			
Sample code	Unreacted palmitic acid	Latex	Potassium palmitate soap	Total palmitic acid
0.2SPA20	3.107	88.547	5.540	7.723
0.2SPA30	6.180	82.048	6.982	11.998
0.2SPA40	7.581	78.859	7.613	13.925
0.2SPA50	9.780	72.528	9.840	17.980
0.5SPA20	5.594	83.505	5.392	10.087
0.5SPA30	7.941	81.286	5.794	12.769
0.5SPA40	9.806	79.721	7.721	16.240
0.5SPA50	11.565	77.659	9.562	19.534
1.0SPA20	2.992	85.552	3.641	6.026
1.0SPA30	7.341	76.773	8.895	14.754
1.0SPA40	5.727	78.567	10.152	14.187
1.0SPA50	3.116	75.998	12.885	13.854
1.5SPA20	5.476	86.922	3.126	8.081
1.5SPA30	5.818	84.360	7.260	11.868
1.5SPA40	3.908	82.699	6.431	9.267
1.5SPA50	4.798	75.966	9.260	12.515
2.0SPA20	0.235	84.315	6.214	5.413
0.2SNR	0.000	93.623	0.000	0.000
0.2SSA20	(Stearic Acid)2.747	84.534	(Potassium Stearate)5.561	(Stearic acid)7.382

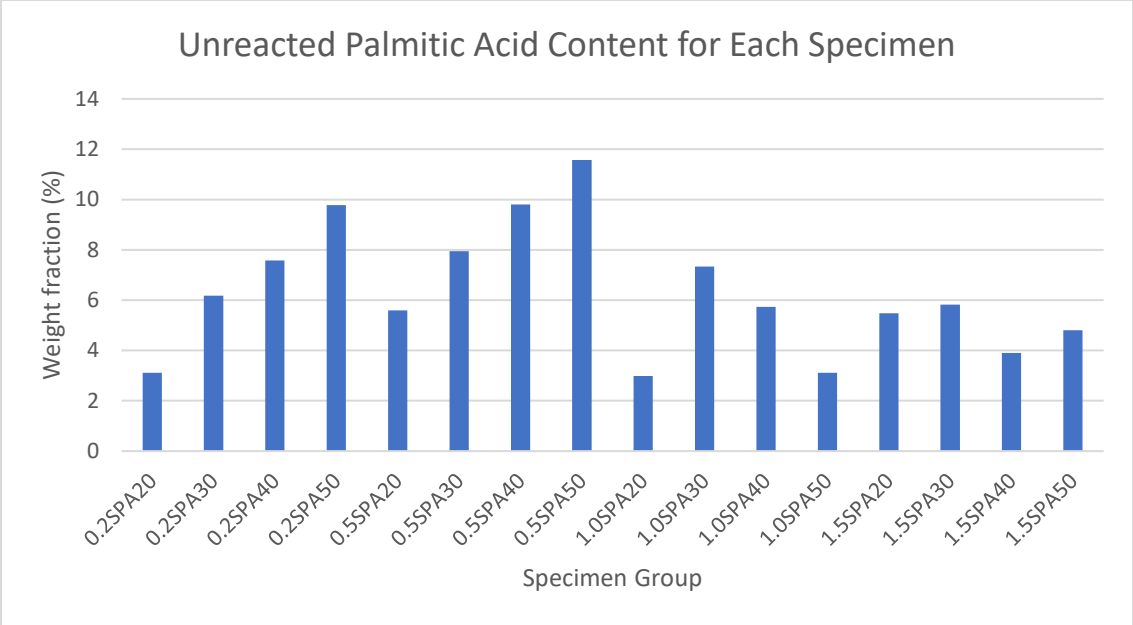

Figure 4.12: Weight fraction of unreacted palmitic acid content for each prevulcanised SMNR specimen (for 0.2S to 1.5S specimen groups)

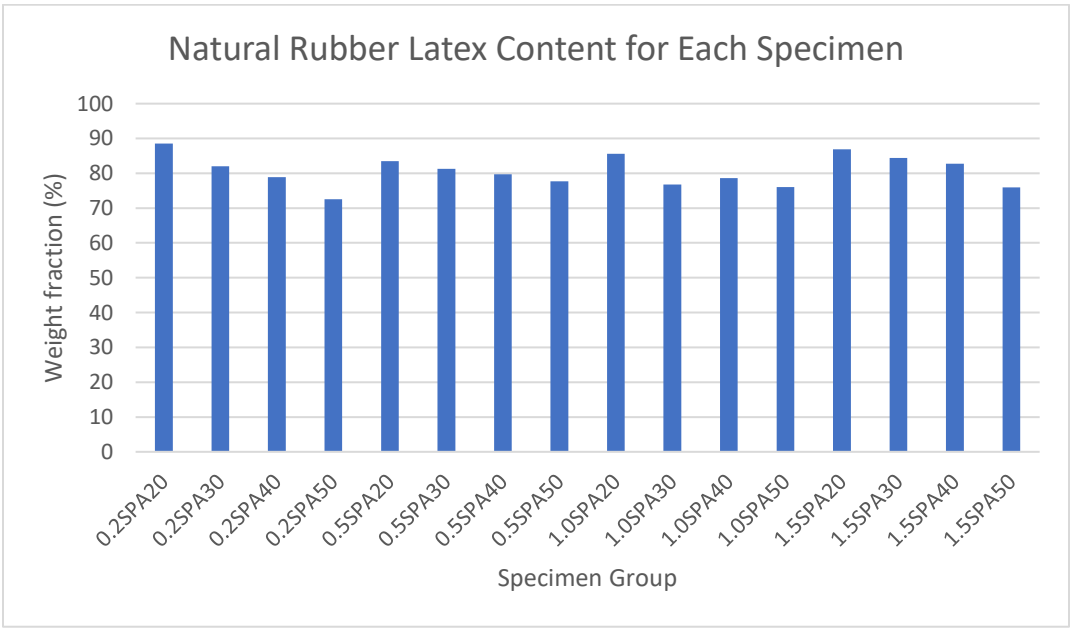

Figure 4.13: Weight fraction of natural rubber latex content for each prevulcanised SMNR specimen (for 0.2S to 1.5S specimen groups)

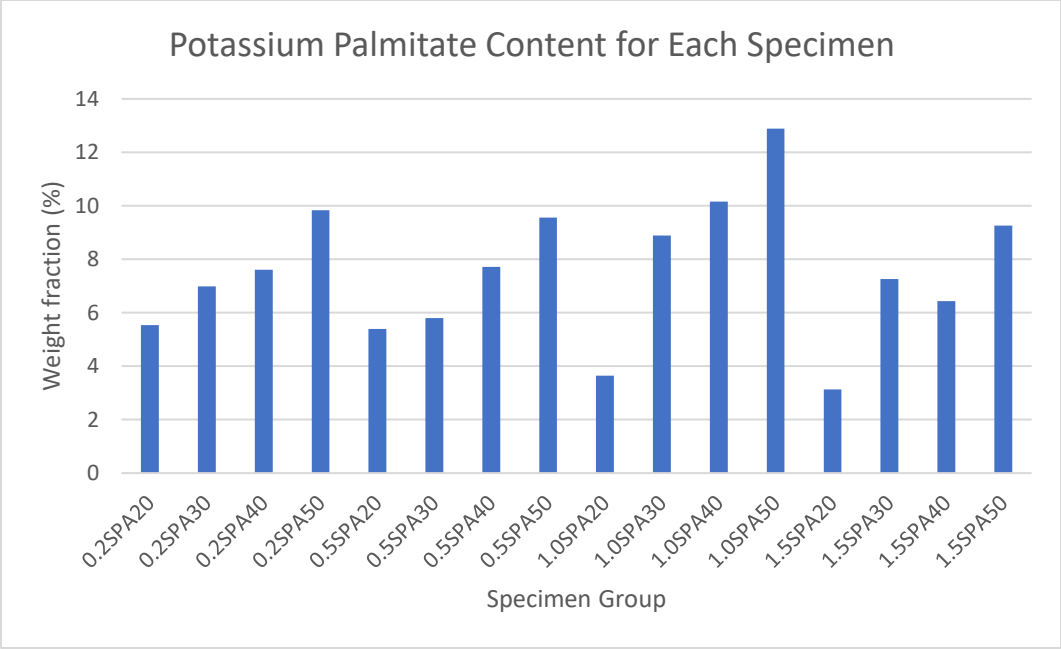

Figure 4.14: Weight fraction of potassium palmitate content for each prevulcanised SMNR specimen (for 0.2S to 1.5S specimen groups)

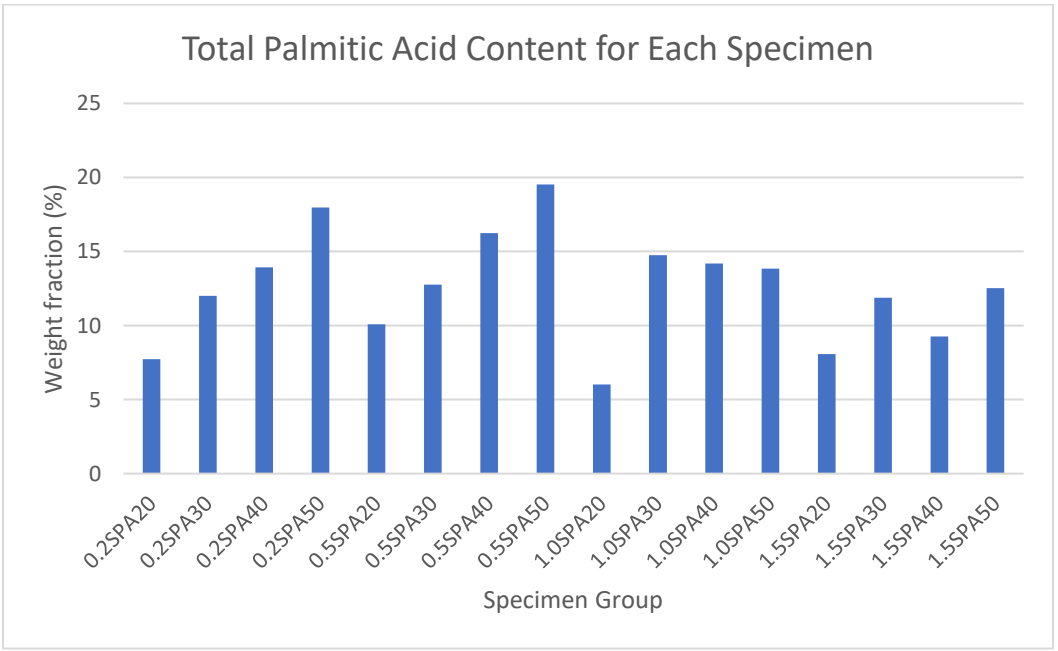

Figure 4.15: Weight fraction of total palmitic acid content for each prevulcanised SMNR specimen (for 0.2S to 1.5S specimen groups)

However, the ascent trend of palmitic acid content is spotted in the similar sulphur content group in low sulphur content specimen groups which are the 0.2S and 0.5S specimen groups. Comparing the total palmitic acid content of the 0.2S and 0.5S specimen groups, they slightly increase by adding higher potassium palmitate concentration. The unreacted palmitic acid is responsible for this outcome. According to the DTG results in Figure 4.6, partly unreacted palmitic acid is discovered, accounting for 50% of the total palmitic acid content in prevulcanised SMNR molecular. Due to the incomplete saponification process, partial palmitic acid is remained in the potassium palmitate soap and mixed with NRL during the compounding process. Moreover, palmitic acid is an insoluble fatty acid, which is still attached to rubber molecular even after water flashing and drying processes. Comparing the TGA results in Figure 4.12, the 1.0S and 1.5S specimen group have lower unreacted palmitic acid content within their rubber network. It is believed that the crosslink density limits the porosity structure within rubber molecule which constrains the permeability of rubber network for unreacted palmitic acid. Hence, less unreacted palmitic acid content is spotted on these two specimen groups (1.0S and 1.5S).

To conclude this section, the crosslink density constrain the penetrability of palmitic acid during the swelling process. Although increasing the swelling duration and swelling temperature could improve the swelling ratio, it might lead to another critical issue such as increasing the brittleness of rubber specimen or thermal degradation due to exposure to a high temperature environment for a long time. These issues are considered and inspected in other mechanical tests. For prevulcanised SMNR, the total palmitic acid content is increasing as mixing with a higher concentration of potassium palmitate but unreacted palmitic acid contributes large amount (39%~68%) of the weight fraction of total palmitic acid content. According to TGA result, majority specimen groups contain less than half of the palmitic acid added within rubber molecule.

4.2 Trigger temperature, T_c

4.2.1 Trigger temperature of Swollen SMNR Specimens under DSC Experiment

The shape transition temperature of swollen SMNR with CGNR and NRL specimens is determined under the DSC experiment, and the results are summarised in Figure 4.16. To emphasise the difference between rubber specimens with and without palmitic acid, the DSC results of dry rubber samples are also depicted in Figure 4.17 and Figure 4.18. To compare the trigger temperature between CGNR and NRL specimen, Figure 4.19 are enlarged the DSC results of each swollen SMNR specimen on first endothermic activity.

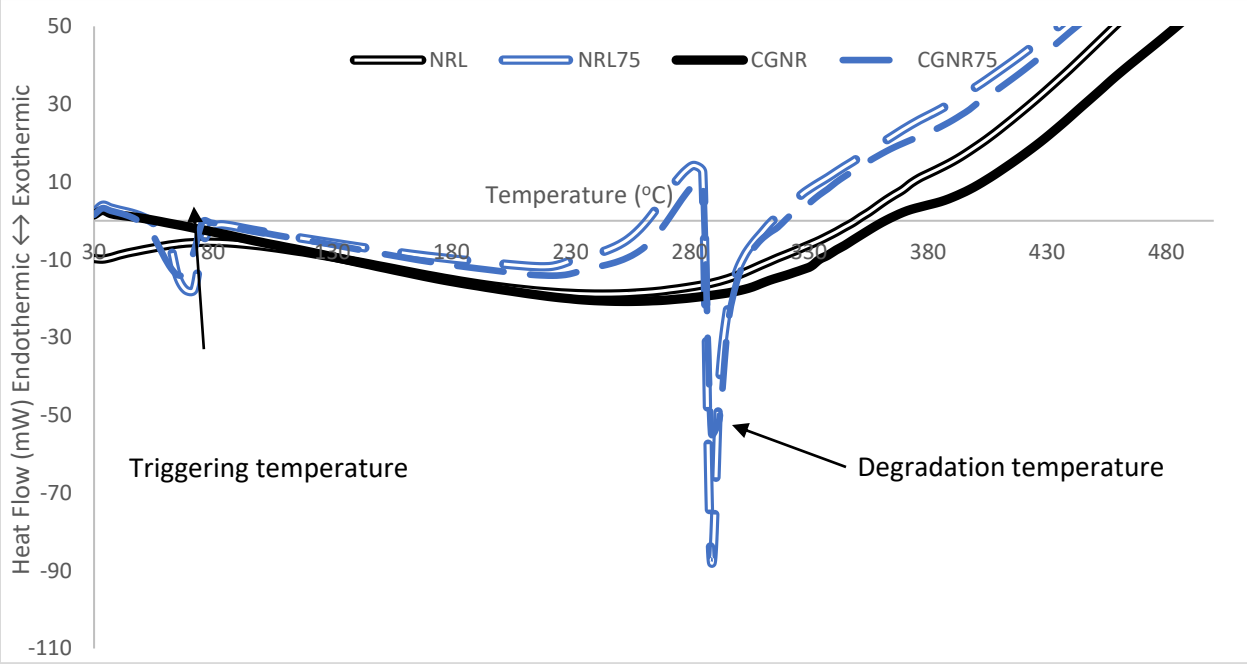

Figure 4.16: The DSC result in between 30°C and 500°C

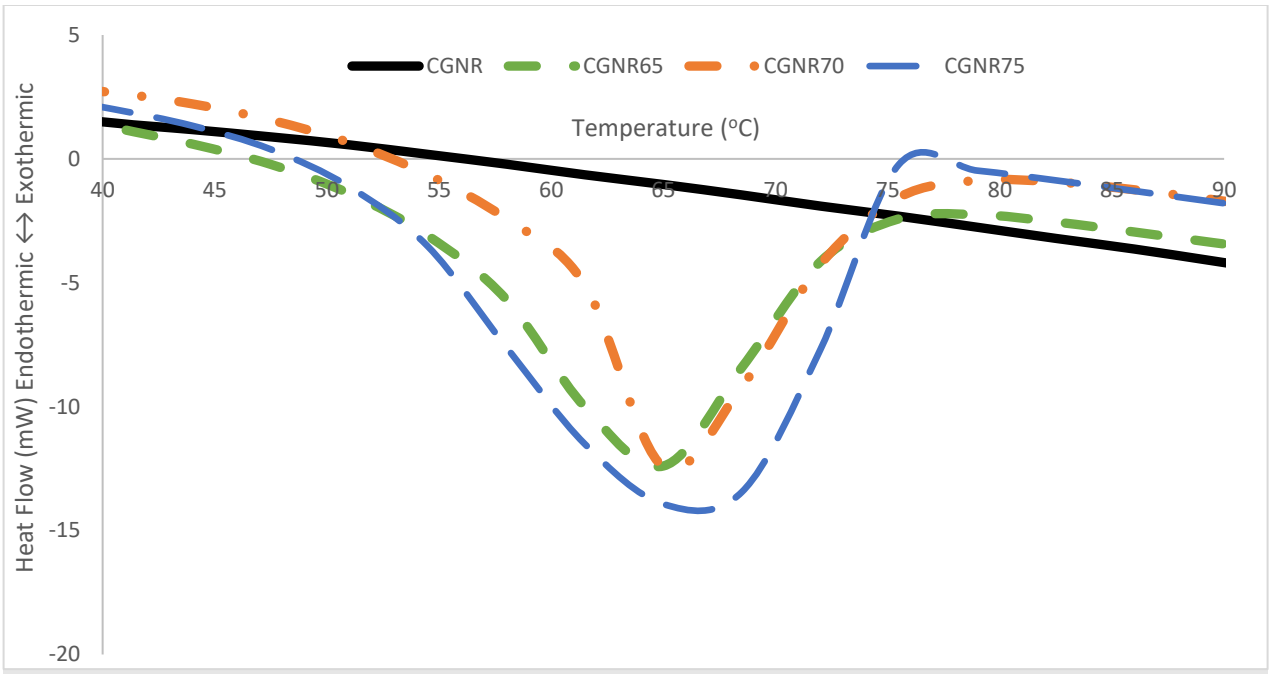

Figure 4.17: The DSC results for CGNR specimens (with dry rubber specimen, CGNR)

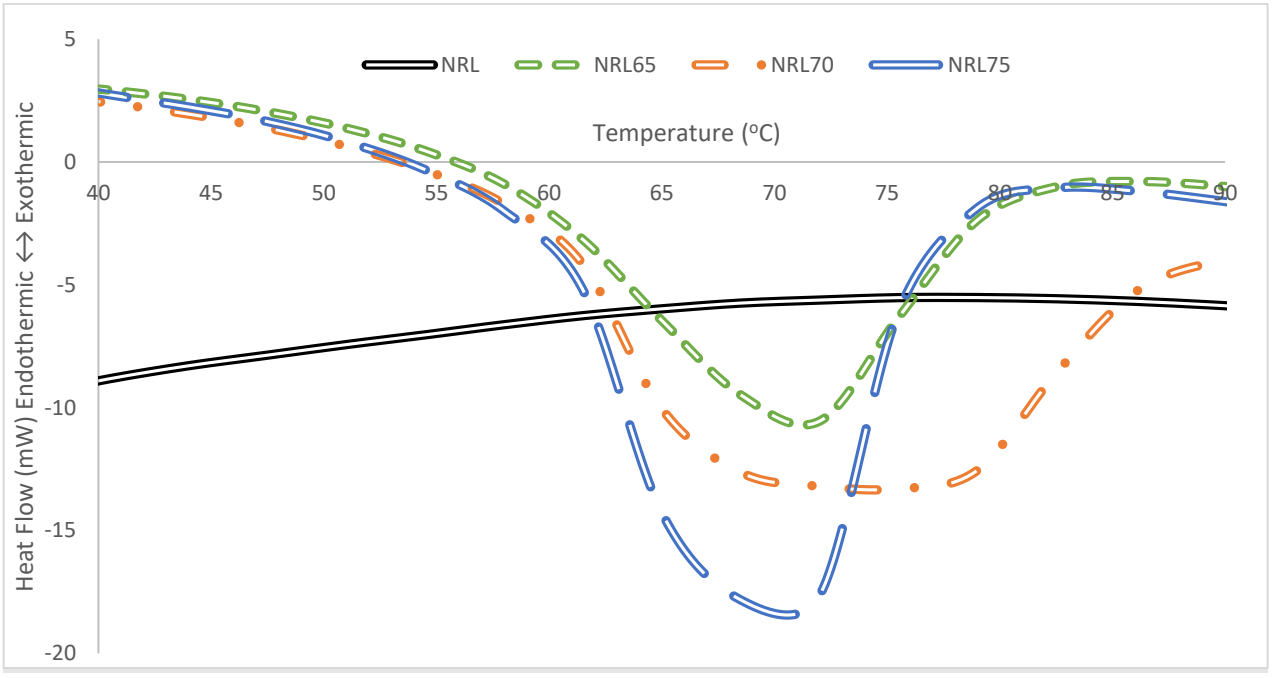

Figure 4.18: The DSC results for NRL specimens (with dry rubber specimen, NRL)

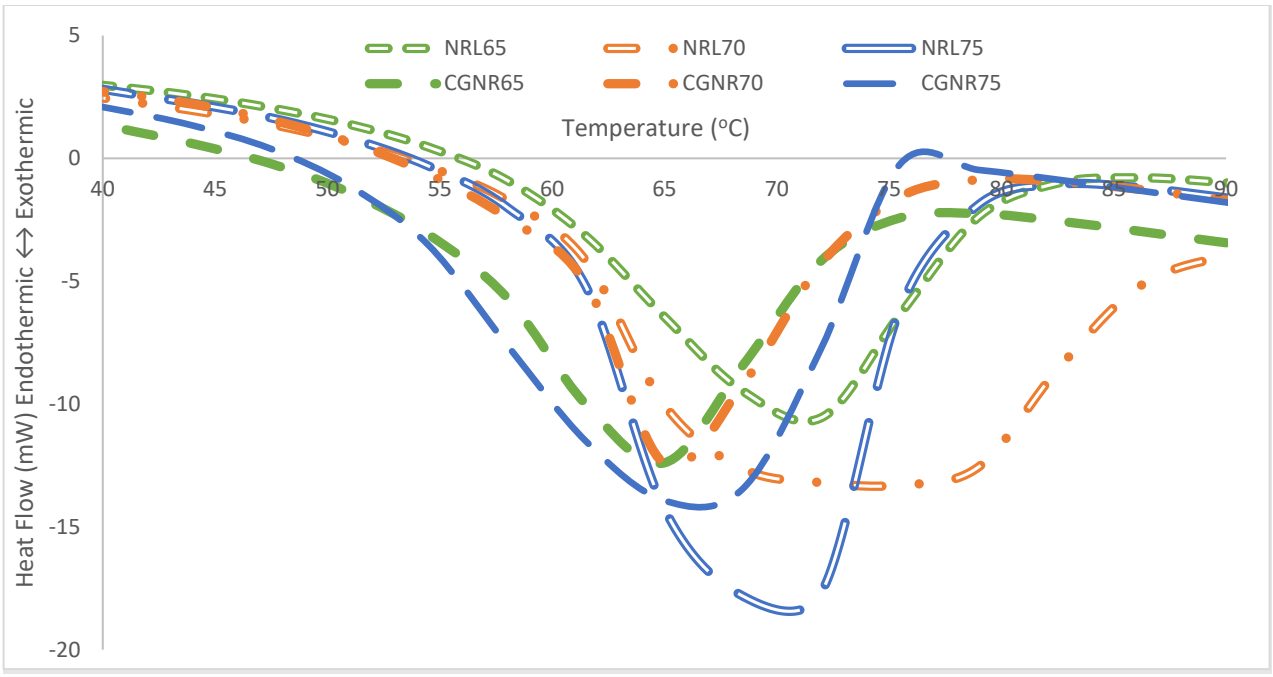

Figure 4.19: The DSC results for both rubber sources under different swelling temperature

From Figure 4.16, specimens with palmitic acid are found to have two endothermic activities which are in temperature range of 64°C to 75°C and 285°C to 310°C. It is obvious that the second endothermic temperature belongs to the degradation temperature of palmitic acid. It is in line with the finding from the TGA experiment in which palmitic acid undergoes decomposition below 330°C. Therefore, the first endothermic temperature range is attribute to the T_c of swollen SMNR.

Figure 4.17 and Figure 4.18 show that the T_c of swollen SMNR specimens is spotted between 64°C~80°C, close to the T_m of palmitic acid (~63°C). This indicates that the T_c is aligned with the choice of the fatty acid [172]. Moreover, the DSC results show that the T_c of swollen rubber corresponds to the swelling ratio [173]. Figure 4.19 describes that NRL specimens have a wider T_c range and shift the heat flow peak to higher temperature zone. This is attributed to the

homogeneity in the swelling process [174]. Due to the overflow of palmitic acid absorption during the swelling process, an uneven physically crosslink bond exists between the NRL specimen group. They also dominate the thermal characteristic of the swollen SMNR specimens. In consequence, the T_c is increased due to more thermal energy is required for the melting process. According to Table 4.1, CGNR specimens have a similar outcome to NRL specimens, in which T_c is shifted to higher temperature range by increasing the palmitic acid content. The sequence of T_c for CGNR is 65ºC (CGNR65) → 68.5ºC (CGNR70) → 69ºC (CGNR75). Therefore, the T_c corresponds to the palmitic acid content.

4.2.2 Trigger Temperature of Prevulcanised SMNR from DMA Experiment

Prevulcanised SMNR specimens contain less than a quarter of palmitic acid amount by comparing with swollen SMNR specimens. Combining the degradation effect from NRL, T_c is difficult to determine under the DSC experiment for SMNR fabricated through prevulcanisation. To address this issue, the T_c of prevulcanised SMNR specimens is determined from DMA machine under tension mode. Due to the crystalline nature of fatty acid, T_c can be determined by referring to the onset of storage modulus drop under a particular temperature [175]. To determine the T_c, the storage modulus of prevulcanised SMNR specimens is shown in Figure 4.20. DMA results show a significant difference in storage modulus between the specimen with and without fatty acid. Within the 25ºC to 100ºC of the temperature range for the specimen containing fatty acid, only one distinct transition is observed, which is ~65ºC for palmitic acid (0.2SPA20 and 2.0SPA20) and ~73ºC for stearic acid (0.2SSA20). Since both onsets drop temperatures are closer to their T_m of fatty acid, this indicates that the choice of the fatty acid is responsible for T_c for prevulcanised SMNR. After the temperature above their T_m, the crystalline structure of fatty acid is began to vanish and went through decrystallisation process. In consequence, the SMNR specimens return

to a rubbery plateau state that is soft and viscous. In this stage, the fatty acid in SMNR molecular contributes negligibly to load bearing and begins to exhibit a severe decrease in storage modulus. At the same time, the 0.2SNR has another dynamic behaviour without any onset drop on its storage modulus result between testing temperature ranges. It is obvious that the 0.2SNR is just a crosslinked NR sample with a T_g at -70°C, which is far below the testing temperature range.

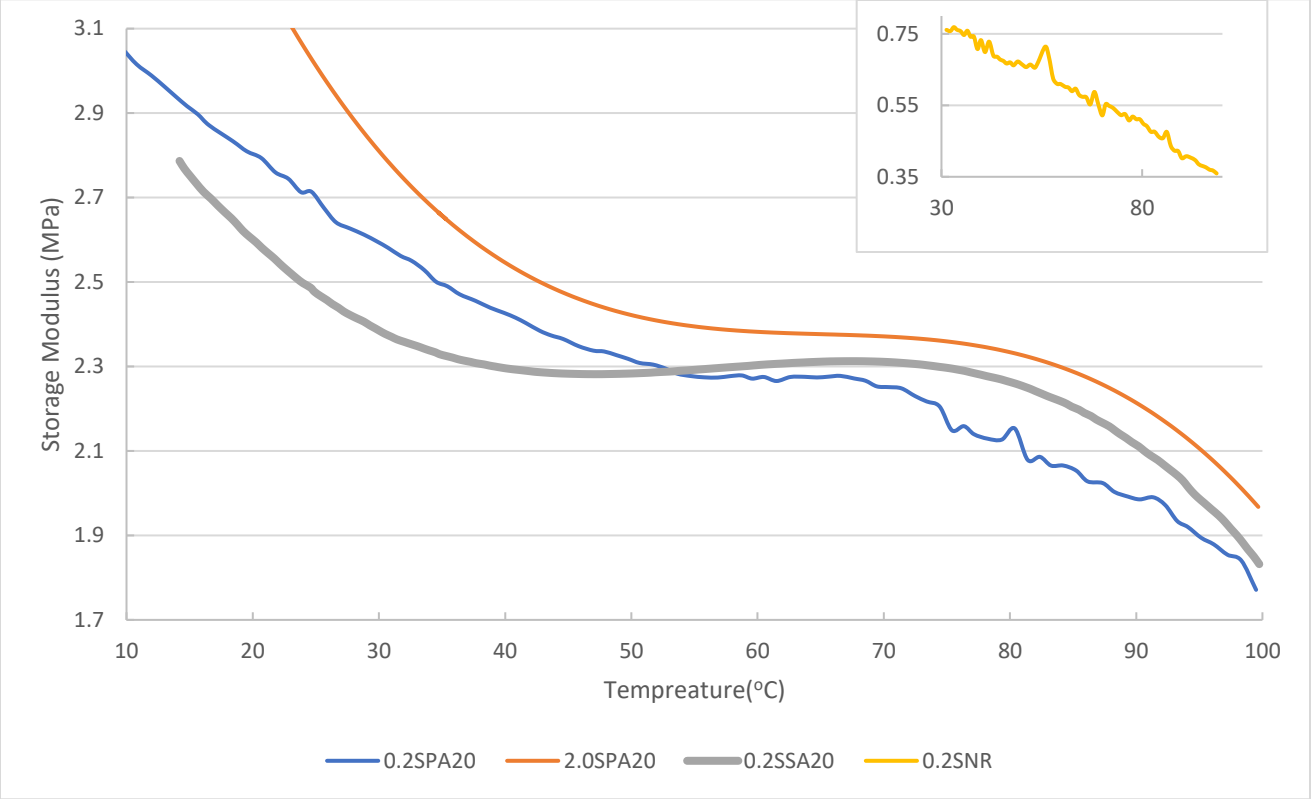

Figure 4.20: DMA results for prevulcanised SMNR

According to the T_c experiment results in swollen SMNR specimen, it believes that the T_c corresponds to the palmitic acid content. The higher palmitic acid required more thermal energy to vanish the linkage between the molecular, which resulted in the Tc shifting to a higher temperature range. In addition, it is found that the T_c depends on the choice of the fatty acid and is irrelevant to sulphur content.

4.3 Shape Memory Behaviour

4.3.1 Effect of Swelling Temperature and Solvent Loading on the Shape Memory Behaviours of the Swollen SMNR

To investigate the effect of swelling temperature and solvent loading on the shape memory behaviours. NRL and CGNR swollen under three swelling temperatures (65^{o}C, 70^{o}C, and 75^{o}C) at various swelling durations (20, 40, 60, 80, 100, and 120 minutes) are evaluated under three deformed strains of 100%, 200%, and 300% at the T_r of 70^{o}C. Figure 4.21 shows the shape fixity and shape recovery of swollen SMNR specimens from two rubber sources with different deformed strains. These results are also tabulated in Table 4.3 and Table 4.4.

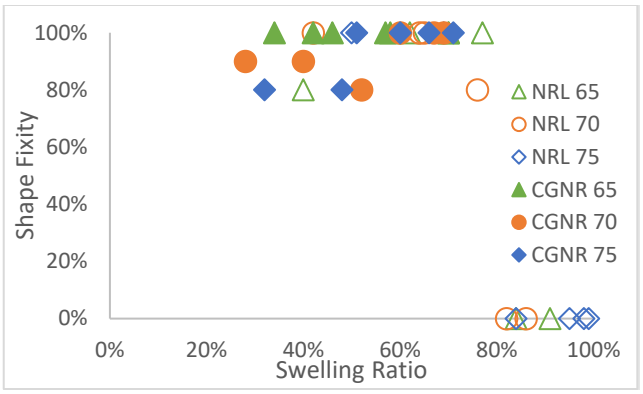

a) 100% strain

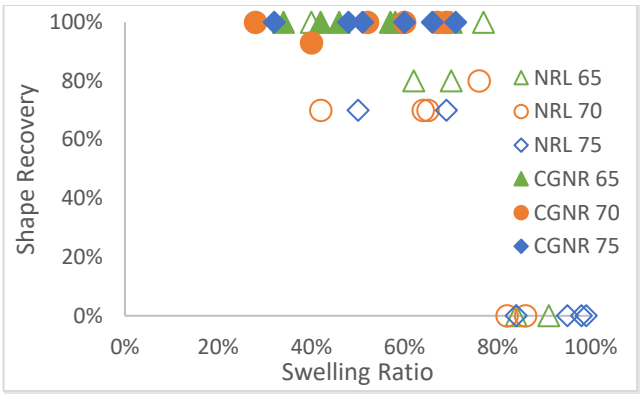

d) 100% strain

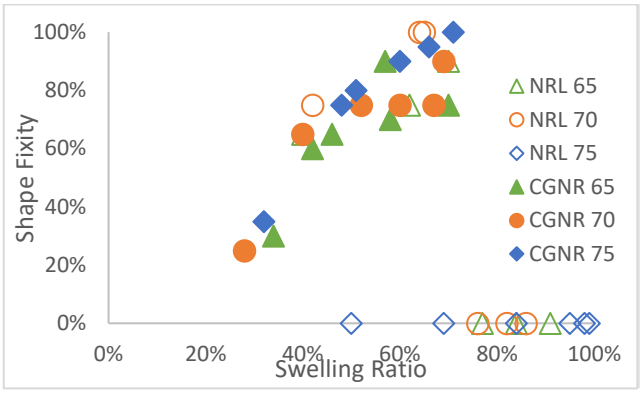

b) 200% strain

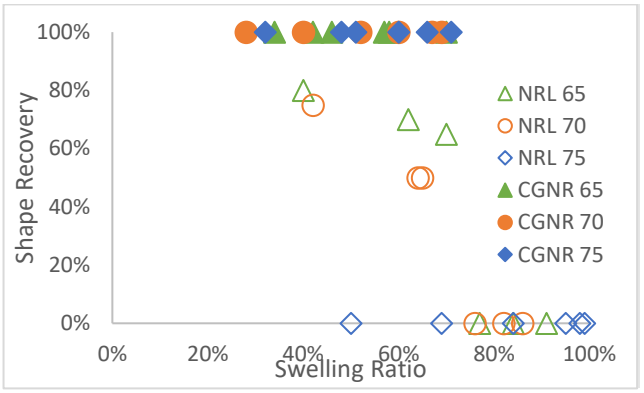

e) 200% strain

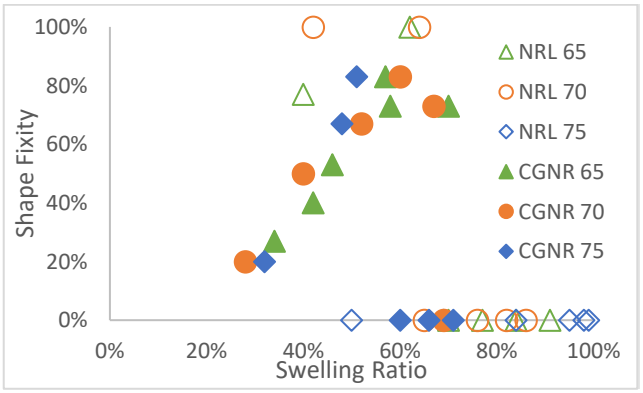

c) 300% strain

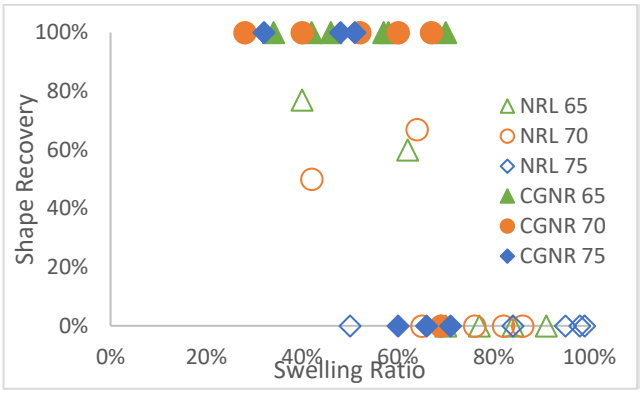

f) 300% strain

Figure 4.21: The shape fixity (a,b,c) and shape recovery(d,e,f) versus swelling ratio for two swollen SMNR rubber sources with different swelling temperatures and deformed strain

Table 4.3: The shape fixity of swollen SMNR

			Shape fixity					
NRL65	Swelling Duration (min)		20	40	60	80	100	120
	Swelling Ratio		40%	62%	70%	77%	84%	91%
	Deformed Strain	100%	80%	100%	100%	100%	break	break
		200%	65%	75%	90%	break	break	break
		300%	77%	100%	break	break	break	break
NRL70	Swelling Duration (min)		20	40	60	80	100	120
	Swelling Ratio		42%	64%	65%	76%	82%	86%
	Deformed Strain	100%	100%	100%	100%	80%	break	break
		200%	75%	100%	100%	break	break	break
		300%	100%	100%	break	break	break	break
NRL75	Swelling Duration (min)		20	40	60	80	100	120
	Swelling Ratio		50%	69%	84%	95%	98%	99%
	Deformed Strain	100%	100%	100%	break	break	break	break
		200%	break	break	break	break	break	break
		300%	break	break	break	break	break	break
CGNR 65	Swelling Duration (min)		20	40	60	80	100	120
	Swelling Ratio		34%	42%	46%	58%	57%	70%
	Deformed Strain	100%	100%	100%	100%	100%	100%	100%
		200%	30%	60%	65%	70%	90%	75%
		300%	27%	40%	53%	73%	83%	73%
CGNR 70	Swelling Duration (min)		20	40	60	80	100	120
	Swelling Ratio		28%	40%	52%	60%	67%	69%
	Deformed Strain	100%	90%	90%	80%	100%	100%	100%
		200%	25%	65%	75%	75%	75%	90%
		300%	20%	50%	67%	83%	73%	break
CGNR 75	Swelling Duration (min)		20	40	60	80	100	120
	Swelling Ratio		32%	48%	51%	60%	66%	71%
	Deformed Strain	100%	80%	80%	100%	100%	100%	100%
		200%	35%	75%	80%	90%	95%	100%
		300%	20%	67%	83%	break	break	break

Table 4.4: The shape recovery of swollen SMNR

			Shape Recovery					
NRL65	Swelling duration		20	40	60	80	100	120
	Swelling Ratio		40%	62%	70%	77%	84%	91%
	Deformed Strain	100%	100%	80%	80%	100%	break	break
		200%	80%	70%	65%	break	break	break
		300%	77%	60%	break	break	break	break
NRL70	Swelling duration		20	40	60	80	100	120
	Swelling Ratio		42%	64%	65%	76%	82%	86%
	Deformed Strain	100%	70%	70%	70%	80%	break	break
		200%	75%	50%	50%	break	break	break
		300%	50%	67%	break	break	break	break
NRL75	Swelling Duration (min)		20	40	60	80	100	120
	Swelling Ratio		50%	69%	84%	95%	98%	99%
	Deformed Strain	100%	70%	70%	break	break	break	break
		200%	break	break	break	break	break	break
		300%	break	break	break	break	break	break
CGNR 65	Swelling Duration (min)		20	40	60	80	100	120
	Swelling Ratio		34%	42%	46%	58%	57%	70%
	Deformed Strain	100%	100%	100%	100%	100%	100%	100%
		200%	100%	100%	100%	100%	100%	100%
		300%	100%	100%	100%	100%	100%	100%
CGNR 70	Swelling Duration (min)		20	40	60	80	100	120
	Swelling Ratio		28%	40%	52%	60%	67%	69%
	Deformed Strain	100%	100%	93%	100%	100%	100%	100%
		200%	100%	100%	100%	100%	100%	100%
		300%	100%	100%	100%	100%	100%	break
CGNR 75	Swelling Duration (min)		20	40	60	80	100	120
	Swelling Ratio		32%	48%	51%	60%	66%	71%
	Deformed Strain	100%	100%	100%	100%	100%	100%	100%
		200%	100%	100%	100%	100%	100%	100%
		300%	100%	100%	100%	break	break	break

It can be seen that both rubber sources have distinct advantages, such as CGNR specimens possess superior recovery ability even when it is subjected to higher elongation strain and swelling temperatures. In contrast, NRL specimens achieve 100% shape fixity, even specimens with lower swelling ratios (42% under 300% deformed strain). Despite the high degree of crosslinking

providing excellent shape recovery in CGNR specimens, the shape fixity is constrained by high elastic force especially for high deformed strain. Table 4.3 shows that the CGNR 70 specimen has achieved 90% of shape fixity under 100% percentage strain but it is deteriorated to 20% as the deformed strain increased to 300%. It is because the crosslink density results in a high elastic force, inhibiting the entanglement between rubber molecular and constraining the growth of the SIC. Moreover, the elastic force is proportional to the deformed strain. Due to sparse crystallites formation is insufficient to withstand the high elastic force from high elongation strain, the SIC structure is vanished and lead to elastic retraction occurred in the CGNR specimens upon removing the weight load [152]. In consequence, lower shape fixity is shown in similar swelling ratio under the CGNR 70.

Although the low degree of SIC is unable to withstand the elastic force from sulphur crosslinking, the shape fixity could improve by increasing palmitic acid content. Table 4.3 shows that increasing the swelling duration significantly enhances the shape fixity of the CGNR 75 from 35% to 100% under 200% of deformed strain. Due to the swelling ratio increases following with the swelling duration, palmitic acid is able to secure more SIC remaining in the CGNR molecular during shape programming process. High portion of the palmitic acid generates more retaining force to store the elastic strain for shifting the recovery process to higher temperature range. By combining the elastic load from crosslink density and reversible strain of palmitic acid, the overall shape memory performance on the CGNR specimen is dramatically improved. It indicates that the content of palmitic acid is responsible for the retaining force within swollen SMNR. Therefore, higher palmitic acid content could improve the growth and nucleation of SIC to retain more deformed length.

The NRL specimen groups have a similar outcome on the low deformed strain. Compared to specimens from both rubber sources, the NRL specimens exhibit less shape recovery at all deformed strains, which is attributed to plastic deformation during the shape programming process. Without the sulphur crosslink bond in the NRL molecular, they have a relatively low elastic modulus that easily distorts the rubber molecular at high deformed strain (>100%). This residue strain on the NRL molecule is irreversible, halting the shape recovery process, as shown in Figure 4.22. The increment on shape recovery of the NRL specimens under 100% deformed strain is attributed to more reversible strain is preserved from the precoated rubber structure. The high portion of palmitic acid precoats on the rubber molecule to prevent molecular from distortion. It also retains most entangled length (shape programming) even when the load is removed. Hence, this block copolymer not only improves the elastic limit of the NRL specimens but also imposes a new feature, SME, on them.

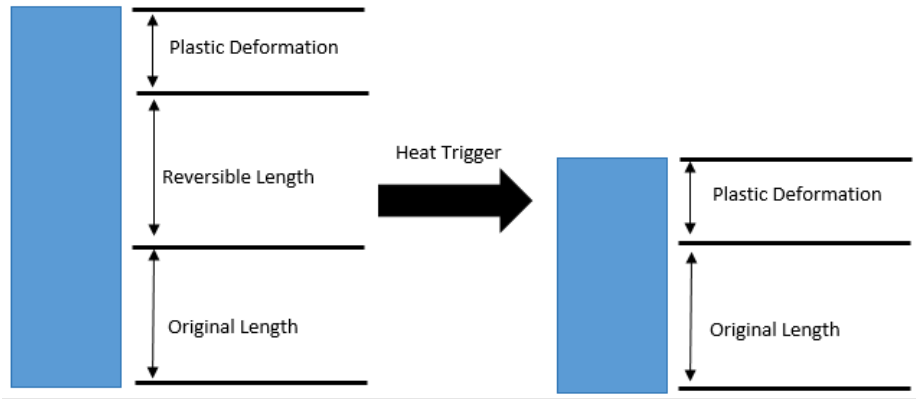

Figure 4.22: Residual strain on NRL specimen (Due to distortion occurred, partly deformed strain become irreversible length)

Despite both shape memory parameters are increased with palmitic acid content on both rubber sources, but they are loss their elastic properties when the palmitic acid is excess into the

rubber molecule. By observing the results of the shape memory experiment, the rubber network failure in the NRL rubber source occurs particularly when the swelling ratio of NRL is greater than 64% under 300% deformed strain. The reduction in the elastically effective chain is attributed to the high concentration of palmitic acid that dominates the mechanical properties of the NRL specimen [48]. Further increasing the solvent uptake will cause the NRL specimens to become more brittle, but this solvent degradation is insignificant for CGNR specimens. It is because the vulcanisation has improved the chemical resistance by sulphur crosslinking. Sulphur crosslink bond between CGNR molecular dominates the mechanical properties in terms of high elasticity and withstanding the high tensile stress. Therefore, CGNR specimens retain the outstanding shape recovery in high strain load with a high swelling ratio.

CGNR specimens have higher chemical resistance to solvent degradation than the NRL specimen group, but thermal degradation brings an undesired deterioration effect on the sulphur crosslink band. Figure 4.21 describes that the network failure for the CGNR 75 is occurred after 60 minutes of swelling duration with 300% deformed strain, while the CGNR70 is up to 100 minutes at a similar elongation. This thermal degradation attributes to the occurrence of chain scission because the specimen exposed to a high temperature environment for a long period. High temperature with a long ageing time decreases the crosslink density of the CGNR specimen [120]. Due to less sulphur crosslink bond between the rubber molecule, the elastic modulus of CGNR specimen is reduced, rendering the incapable of withstanding high deformed load. Generally, high swelling temperature not only accelerates the swelling process but also speeds up the overcure process [176], [177]. In addition, the initial design purpose of CGNR rubber source (rubber band) is to operate at room temperature, without any thermal resistance additives. Combining the solvent

degradation effect, the high strain loading distorts the CGNR molecule and stretches beyond its elastic limit, resulting in its breakup into two pieces.

According to the shape memory experiment of swollen SMNR, palmitic acid content significantly influences the SME under NRL and CGNR. Despite the overflow of palmitic acid might lead the SMNR to fail catastrophically, palmitic acid can enhance the shape memory capability as it is below 64% of the swelling ratio. Palmitic acid not only retains deformed length under CGNR specimen but also reduces the residue strain for NRL specimen in the result of preventing molecule distortion. Besides that, the 200% of deformed strain is the maximum elongation length to verify the shape memory experiment under low sulphur crosslink density (sulphur weight <2.5% of total weight). The occurrence of network failure on rubber specimen might cause beyond this elongation length. Hence, 200% of deformed strain is selected as the elongation length for prevulcanised SMNR.

4.3.2

4.3.2 Shape Memory Experiment for Prevulcanised SMNR under Custom Made Stretching Apparatus

To investigate the shape memory response on prevulcanised SMNR, the specimen formulation is prepared regarding sulphur and palmitic acid content. The shape memory experiment is conducted under 200% deformed strain with different T_p and T_r ranges. The shape memory parameters are measured by custom-made stretching apparatus. The shape memory results are summarised in Table 4.5 and Table 4.6.

Table 4.5: Shape fixity for prevulcanised SMNR (with various sulphur configurations and palmitic acid configurations)

Sample Code	Shape Fixity			
	T_p=40°C	T_p =50°C	T_p =60°C	T_p =70°C
0.2SPA20	38%	47%	48%	56%
0.2SPA30	48%	48%	65%	94%
0.2SPA40	82%	73%	67%	92%
0.2SPA50	70%	68%	78%	85%
0.5SPA20	13%	19%	28%	28%
0.5SPA30	12%	20%	42%	43%
0.5SPA40	25%	30%	48%	57%
0.5SPA50	32%	45%	52%	60%
1.0SPA20	8%	13%	22%	25%
1.0SPA30	5%	9%	13%	8%
1.0SPA40	15%	12%	15%	15%
1.0SPA50	21%	19%	53%	47%
1.5SPA20	5%	3%	5%	5%
1.5SPA30	4%	5%	5%	7%
1.5SPA40	8%	8%	10%	10%
1.5SPA50	8%	12%	13%	12%
2.0SPA20	3%	4%	7%	7%
0.2SNR	5%	7%	10%	10%
0.2SSA20	65%	70%	80%	92%

Table 4.6: Shape recovery for prevulcanised SMNR (with various sulphur configuration and palmitic acid configurations)

Sample Code	Shape Recovery															
	T_p=40°C				T_p =50°C				T_p =60°C				T_p =70°C			
	T_r= 40°C	T_r= 50°C	T_r = 60°C	T_r= 70°C	T_r= 40°C	T_r= 50°C	T_r = 60°C	T_r= 70°C	T_r= 40°C	T_r= 50°C	T_r = 60°C	T_r= 70°C	T_r= 40°C	T_r= 50°C	T_r = 60°C	T_r= 70°C
0.2SPA20	78%	85%	91%	93%	74%	81%	87%	90%	73%	81%	88%	91%	74%	82%	89%	91%
0.2SPA30	77%	86%	93%	97%	79%	85%	94%	97%	70%	87%	95%	95%	75%	86%	92%	94%
0.2SPA40	45%	60%	65%	73%	55%	64%	77%	82%	60%	75%	88%	90%	65%	78%	88%	92%
0.2SPA50	63%	70%	78%	87%	69%	75%	85%	90%	62%	81%	94%	99%	65%	72%	80%	85%
0.5SPA20	94%	98%	99%	100%	95%	95%	98%	100%	86%	93%	98%	100%	85%	93%	94%	98%
0.5SPA30	93%	98%	100%	100%	90%	95%	98%	99%	78%	88%	95%	95%	79%	88%	93%	96%
0.5SPA40	85%	96%	100%	100%	83%	90%	97%	100%	71%	85%	95%	95%	68%	82%	92%	93%
0.5SPA50	79%	85%	100%	100%	79%	89%	96%	100%	69%	83%	92%	100%	65%	81%	91%	100%
1.0SPA20	97%	98%	99%	99%	93%	97%	98%	100%	95%	95%	98%	100%	90%	94%	95%	95%
1.0SPA30	100%	100%	100%	100%	95%	97%	99%	100%	95%	98%	100%	100%	98%	99%	100%	100%
1.0SPA40	93%	98%	98%	99%	93%	94%	98%	99%	95%	98%	100%	100%	93%	96%	98%	100%
1.0SPA50	89%	94%	95%	96%	90%	94%	95%	97%	82%	87%	93%	94%	86%	90%	95%	95%
1.5SPA20	98%	100%	100%	100%	98%	99%	100%	100%	98%	99%	100%	100%	100%	100%	100%	100%
1.5SPA30	98%	98%	98%	100%	98%	98%	98%	99%	95%	98%	98%	100%	90%	91%	93%	94%
1.5SPA40	98%	99%	99%	99%	94%	98%	100%	100%	95%	96%	100%	100%	95%	95%	100%	100%
1.5SPA50	98%	99%	100%	100%	93%	96%	98%	100%	97%	100%	100%	100%	98%	99%	100%	100%
2.0SPA20	92%	96%	98%	100%	93%	94%	96%	100%	95%	98%	98%	100%	96%	98%	98%	100%
0.2SNR	91%	96%	97%	98%	92%	93%	94%	95%	93%	94%	95%	98%	95%	98%	100%	100%
0.2SSA20	39%	63%	77%	84%	34%	62%	76%	80%	33%	60%	73%	78%	19%	57%	71%	76%

4.3.2.1 Effect of Sulphur Content on Shape memory Behaviours of Prevulcanised SMNR

Figure 4.23 and Figure 4.24 show the shape memory parameters of prevulcanised SMNR with 20 pphr palmitic acid with various sulphur content (0.2 pphr, 0.5pphr 1.0pphr, 1.5pphr and 2.0pphr) at various T_p ranges (40^{o}C, 50^{o}C, 60^{o}C and 70^{o}C) and T_r ranges(40^{o}C, 50^{o}C, 60^{o}C and 70^{o}C). From Figure 4.23, the shape fixity declines with increasing the sulphur content under the same T_p. 0.2SPA20 specimens always show the highest shape fixity under the same fatty acid specimen. Whereas the 1.5SPA20 and 2.0SPA20 specimens contain common sulphur content in the commercial NRL compounding process, they shows poor shape fixity (<10%) at every T_p. While swollen SMNR experiences similar shape memory behaviour, the specimen with higher crosslink density exhibits low shape fixity under similar palmitic acid content. Due to the higher sulphur content involves in the specimen, the crosslink bond between the rubber molecule exhibits a high elastic force during the deformation process. Although the degree of SIC increases with the sulphur content [155], high elastic force vanishes the SIC during the unloading process. In consequence, poor shape fixity is exhibited for high crosslink density specimens under similar deformed strain [178]. This is also the typical reason for non or poor SME exhibited in crosslinked NR.

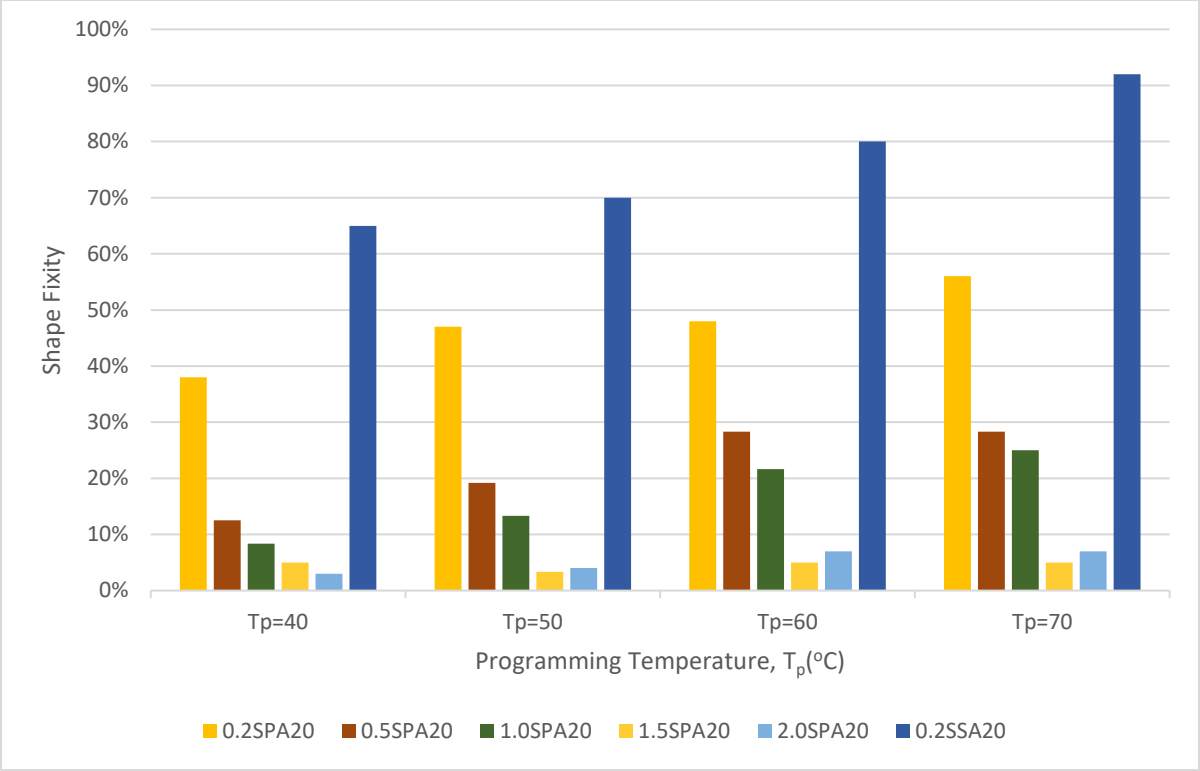

Figure 4.23: The shape fixity of prevulcanised SMNR with various sulphur content at various T_p

Apart from the effect on sulphur content, higher shape fixity is observed as T_p is near the T_c. The 1.0SPA20 and 0.5SPA20 have increased more than double the shape fixity by elevating the T_p from 40°C to 70°C. Generally, NR molecule is crystallised upon strained, but they dissipate during the unloading process at room temperature. Due to the molten palmitic acid attaches to the SIC structure during the programming process, the vanishing temperature has been shifted above the T_m of palmitic acid with consequence of more deformed strain retained above room temperature. Referring to the DSC results, The T_c of palmitic acid specimens is above 65°C for prevulcanised SMNR. Low T_p lead to partial palmitic acid coating on deformed rubber molecular. As a result, it generates less retaining force [179]. Hence, low shape fixity is found as the programming process occurs at low temperature range.

To highlight the effect of T_p on shape recovery, Figure 4.24 compiles the shape recovery at different T_r ranges (40^{o}C, 50^{o}C, 60^{o}C, and 70^{o}C) with respect to four T_p ranges (40^{o}C, 50^{o}C, 60^{o}C, and 70^{o}C). It can be seen that each prevulcanised SMNR specimen exhibits high shape recovery at all T_r except 0.2SSA20. Referring to shape fixity results, the specimens with palmitic acid exhibits poor shape fixity (<80%), and shape retainability is deteriorated with increasing the sulphur content (0.2SPA20> 0.5SPA20> 1.0SPA20> 1.5SPA20> 2.0SPA20). Since the scattered palmitic acid provides less retaining force to withstand the large elastic load from sulphur crosslink bond, most deformed strain is recovered immediately after weight is removed. However, as shown in Figure 4.24c and Figure 4.24d, the increment trend persists at higher T_p and the shape recovery increases with T_r. By increasing the T_r from 40^{o}C to 70^{o}C, the shape recovery of 0.2SPA20 is increased from 74% to 91% at T_p of 70^{o}C. The entropy energy increases within the rubber molecule to vanish the palmitic acid crystal at elevated T_r. As a result, more entangled rubber molecular are released, and more deformed strain is restored to its original position.

a) Programming process progressed at T_p =40°C

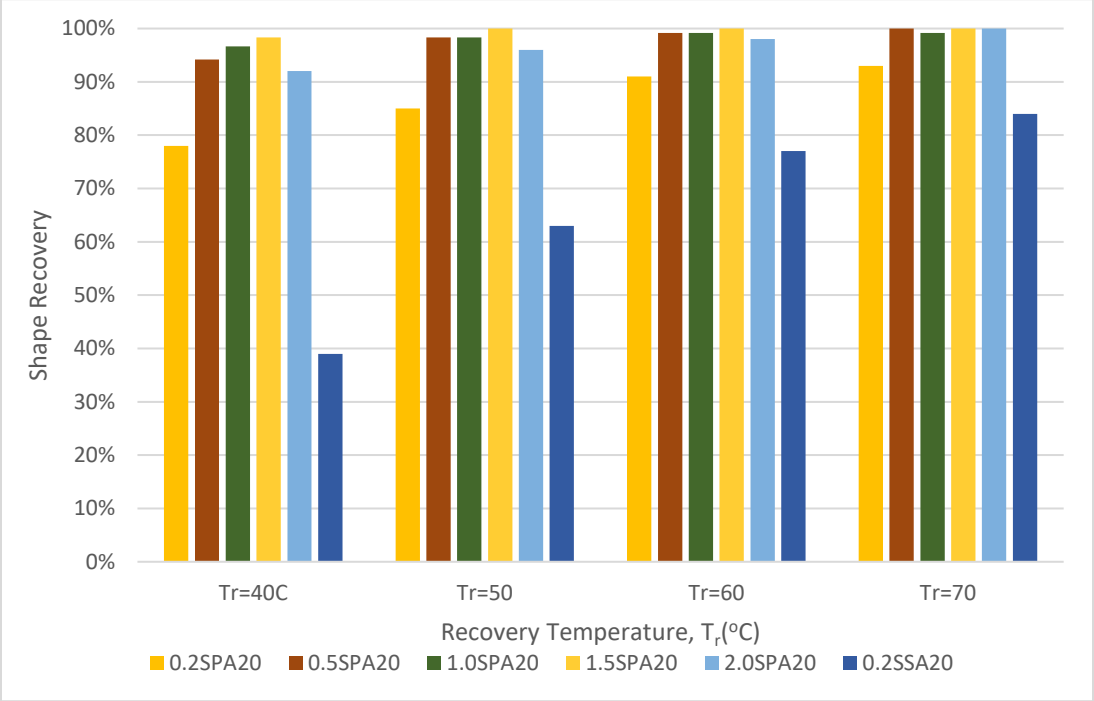

b) Programming process progressed at T_p =50°C

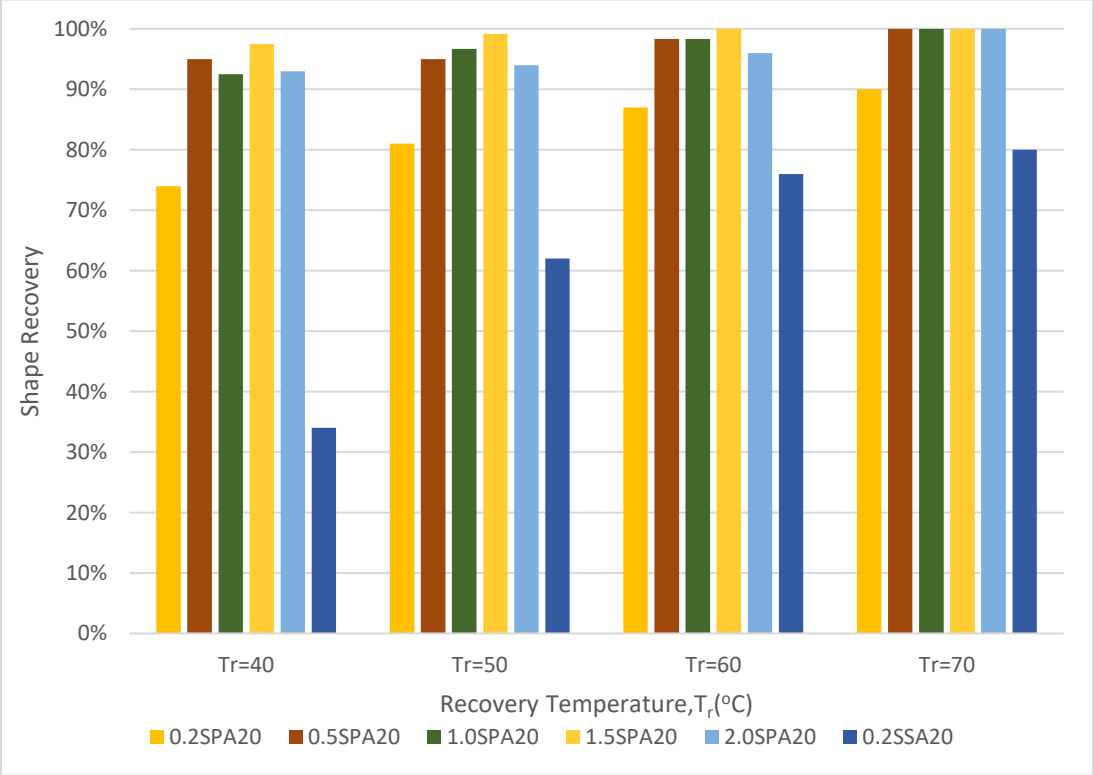

c) Programming process progressed at T_p =60°C

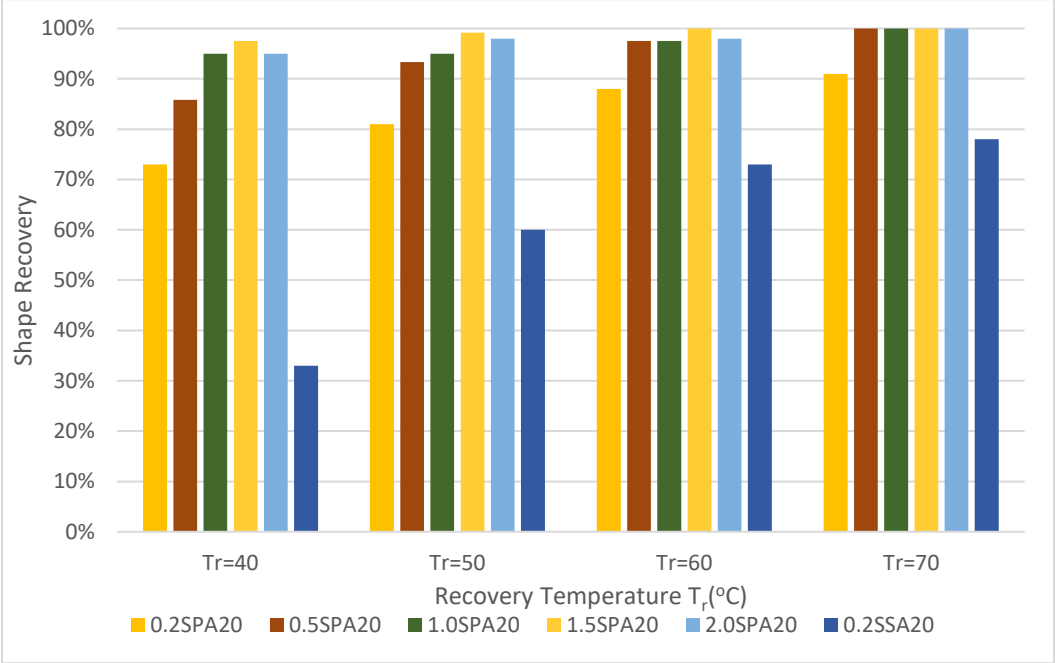

d) Programming process progressed at T_p =70°C

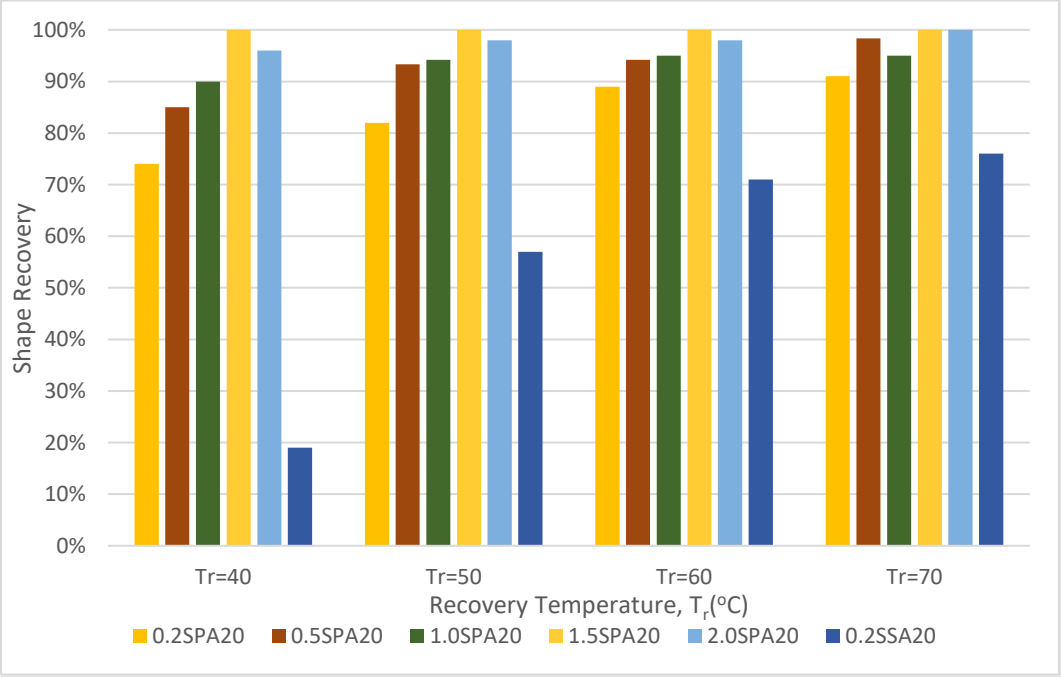

Figure 4.24: The shape recovery of prevulcanised SMNR with variable of sulphur content (a,b,c,d graphs are respected to the T_p of 40°C, 50°C, 60°C, and 70°C)

Although the 0.2SSA20 contains a different fatty acid, stearic acid, it shows a similar outcome to the 0.2SPA20 specimen. The results are in line with the finding from Marcos [44], in which the working temperature significantly influences on the shape memory parameter. The stearic acid specimen increases almost 40% of shape fixity (65%→92%) when the T_p is elevated from 40^{o}C to 70^{o}C. Besides that, it dramatically increases in shape recovery as a result of boosting the T_r value. Compared with the 0.2SSA20 at each T_p, less than 40% of shape recovery is found at the first T_r. By elevating the T_r to 70^{o}C, its shape recovery has risen to triple the initial T_r (19% → 76%) at T_p of 70^{o}C. Due to the large temperature gap between the working temperature and T_c for the stearic acid specimen, this huge change in shape memory parameters is observed during this experiment. It indicates that shape fixity corresponds to T_p while Tr is responsible for shape recovery [180], [181]. Hence, the tunable SME is feasible by manipulating the working temperature range.

4.3.2.2 Effect Of Palmitic Acid Loadings on Shape Memory Behaviours of Prevulcanised SMNR

To investigate the relationship between the palmitic acid loadings and shape memory parameters, the prevulcanised SMNR specimens with different concentrations of potassium palmitate solutions (0,20,30,40,50pphr of palmitic acid) are conducted shape memory experiments under various working temperatures (T_p and T_r ranges of 40^{o}C, 50^{o}C, 60^{o}C and70^{o}C). Their shape memory parameters are obtained under the same deformed strain, 200%, as in Figure 4.25 and Figure 4.26. To highlight the shape recovery capability from T_r, the shape recovery at room temperature is also included in Figure 4.26. From Figure 4.25, it is obvious that the shape fixity is increased with the palmitic acid content. Compared with the 0.2SNR (without palmitic acid), the specimen with palmitic acid content could retain more than four times of deformed length (>40% of shape fixity). Due to the presence of palmitic acid, the SIC vanishing process is retarded by shifting the T_c to a higher temperature range. Hence, high shape fixity can be achieved readily on these prevulcanised SMNR with a high palmitic acid content [182].

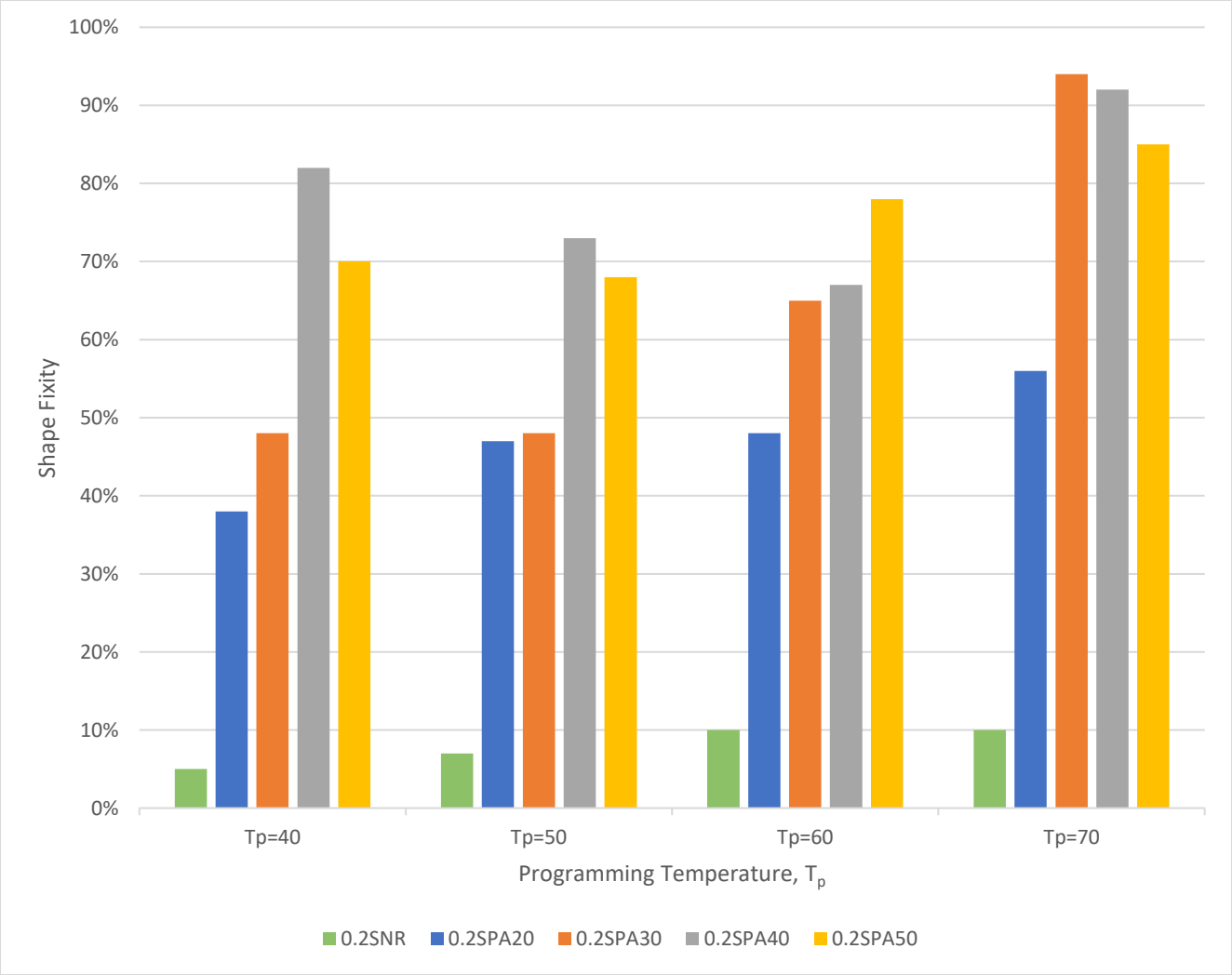

Figure 4.25: The shape fixity of prevulcanised SMNR with various of palmitic acid content

a) Shape recovery for at T_p =40°C under various T_r

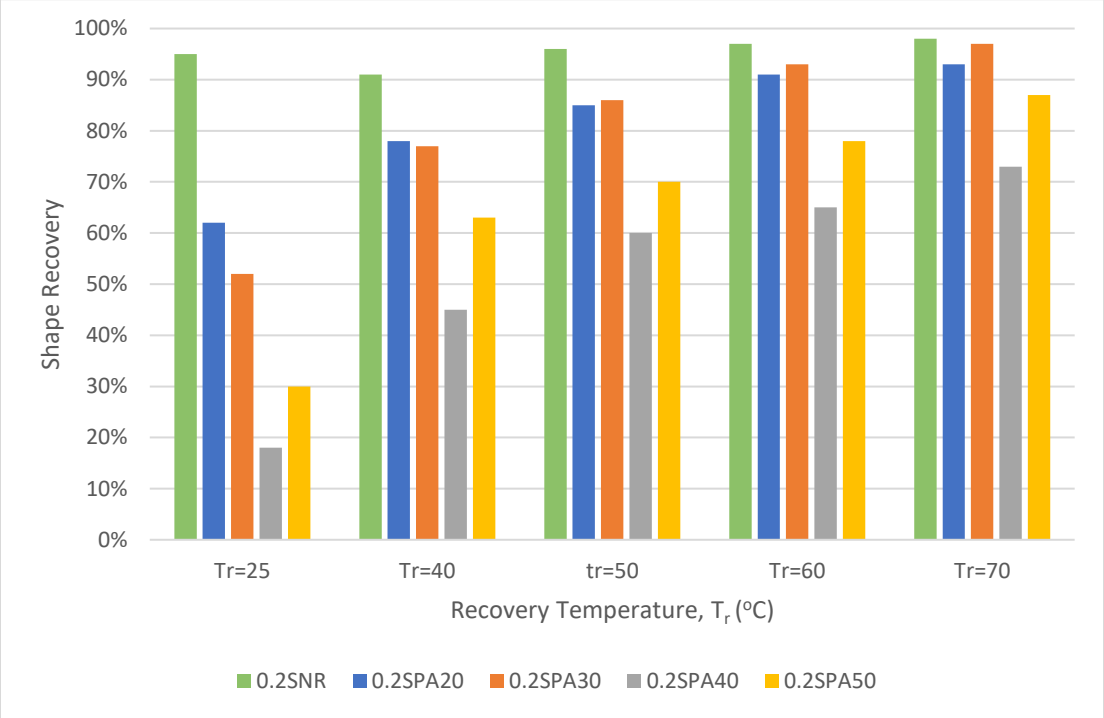

b) Shape recovery for at T_p =50°C under various T_r

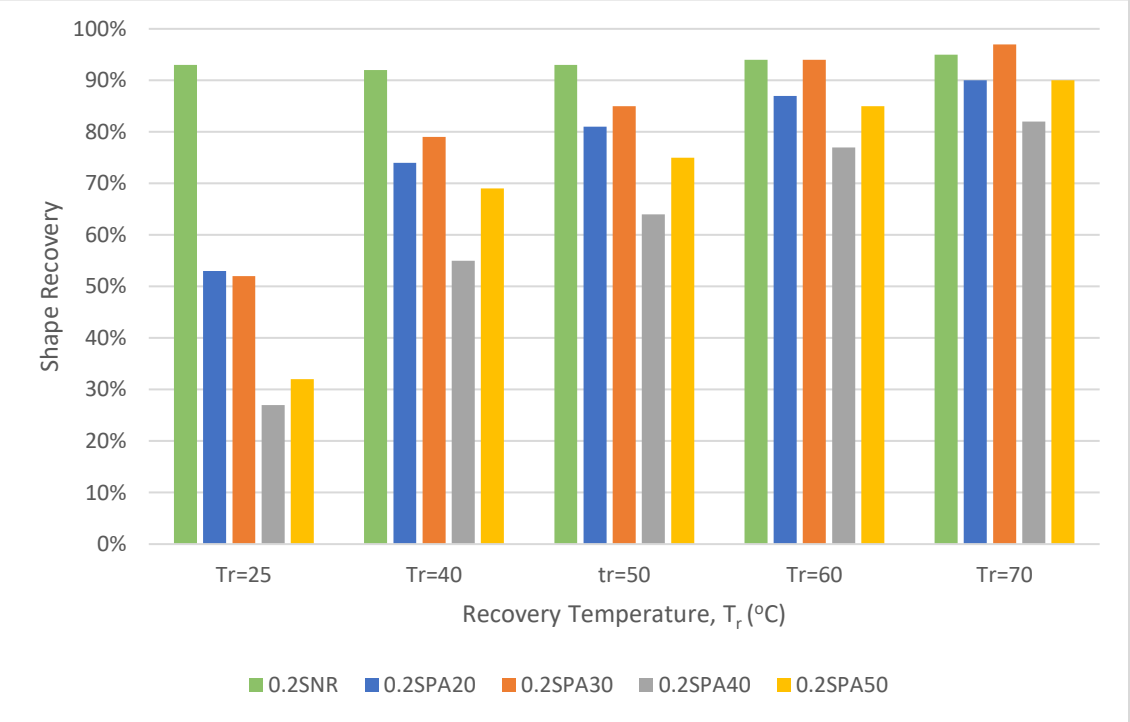

c) Shape recovery for at T_p =60°C under various T_r

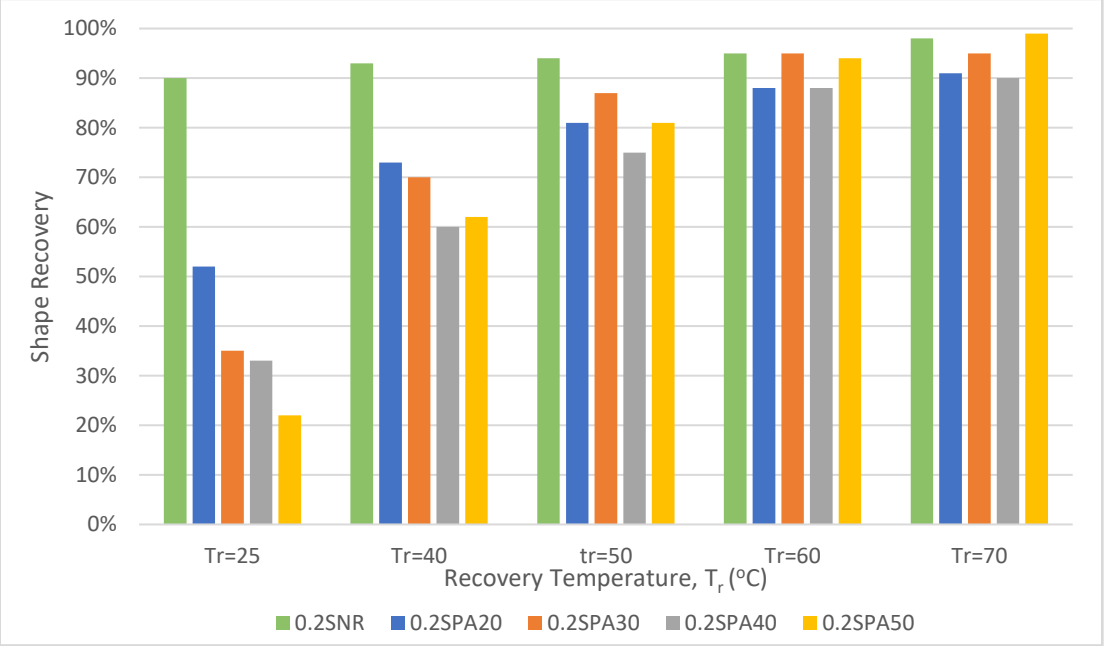

d) Shape recovery for at T_p =70°C under various T_r

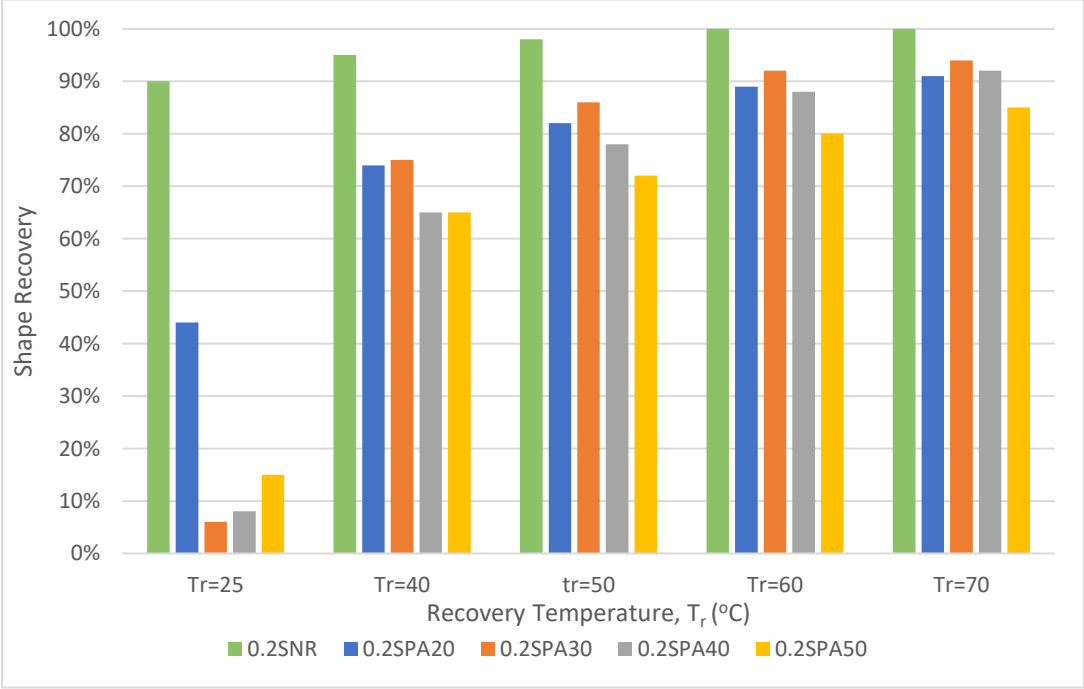

Figure 4.26: The shape recovery of prevulcanised SMNR with variable of palmitic acid content (a,b,c,d graphs are respected to the T_p)

Moreover, increasing the palmitic acid content is not the sole way to enhance the shape fixation. Superior shape fixity is observed when T_p near the T_c. Figure 4.25 shows that the shape fixity of the 0.2SPA30 and 0.2SPA50 increases with elevating the T_p value, and they have over 80% of shape fixity (above 80%) at T_p of 70^{o}C. Due to the increased conversion of thermal energy to entropy energy, a higher T_p results in more SIC being coated with palmitic acid, which halts the decrystallisation process during the unloading process. In consequence, more deformed length is preserved, which directly benefits the shape fixity at higher T_p. Referring to Figure 4.23, the similar shape memory tendency is observed as comparing the shape fixity under various sulphur content. T_p is proven once again that it has a significant influence on the shape fixity.

Compared to the shape recovery results in Figure 4.26, it indicates that the prevulcanised SMNR specimen with lower palmitic acid content has higher shape recovery at similar T_r, especially for the 0.2SPA20 and 0.2SNR. High shape recovery is generally attributed to two circumstances: low retaining force is maintained across T_r range or retaining force decreases with elevating T_r. Since both specimens have a low degree of shape fixity (<80%) even at 70 ^{o}C of T_p, they belong to the former. With less palmitic acid, the retaining force is insufficient to withstand the recovery load for the sulfur network with consequence of partial deformed length being recovered before the reheating process. Hence, high shape recovery is maintained throughout the T_r range under the 0.2SPA20 and 0.2SNR. In contrast, the remaining three specimens have a different shape recovery behaviour, which is corresponding to the T_r value. Due to the high retaining force between the rubber molecular, their shape recovery is poor at low temperature range, which is consistent with the finding from Dawei [183]. As elevating the Tr value, more thermal energy is consumed to vanish the SIC to release the entangled molecular back to the initial position.

As a result, the shape recovery increases with the T_r value. While 70°C of Tr is closest to the T_c of prevulcanised specimen, they have the highest shape recovery on this particular T_r range.

Observing the shape recovery at different T_p, it is clear that the prevulcanised SMNR has a great recovery ratio on the first thermal process (T_r of 25°C→T_r of 40°C), but the increment of shape recovery has dramatically dropped for the subsequent thermal process. For example, the 0.2SPA50 increases the shape recovery from 15% to 65% for the initial thermal recovery process at 70°C of T_p, and then the shape recovery increment is almost 6%±1% for another three T_r ranges. In general, high palmitic acid content allows the specimen to hold more deformed length during the quenching process and progressively release those entangled shapes by raising the T_r value [184]. Nevertheless, the initial retaining force of SMNR is contributed by the growth condition of SIC, which is the result of T_p under a similar deformed strain. This is also the reason why the higher shape fixity is always exhibited at higher T_p and leads to a higher recovery ratio for the first thermal recovery process.

4.3.2.3 Effect of Shape Memory Cycle on Prevulcanised SMNR

To highlight the SME in shape memory cycle, the 0.2SPA20 and the 0.2SPA30 specimens are selected to conduct this experiment under the temperature of 70°C for shape programming and shape recovery. Both shape memory parameters are obtained with respected to three shape memory cycles (R1, R2, and R3) and summarised in Figure 4.27 and Figure 4.28. Figure 4.29 is TGA results, and Table 4.7 lists the weight fraction of each compound element before and after the shape memory cyclic test. Figure 4.27 shows that the shape fixity for both prevulcanised SMNR declines with the number of cycles. Compared to the first shape memory cycle, both specimens retain a shape fixity of 50% after the third cycle. Nevertheless, shape recovery shows an opposite trend with shape fixity, increasing with the number of cycles in Figure 4.28. This indicates that both specimens regained their elastic properties, leading to the deterioration on the shape memory capability.

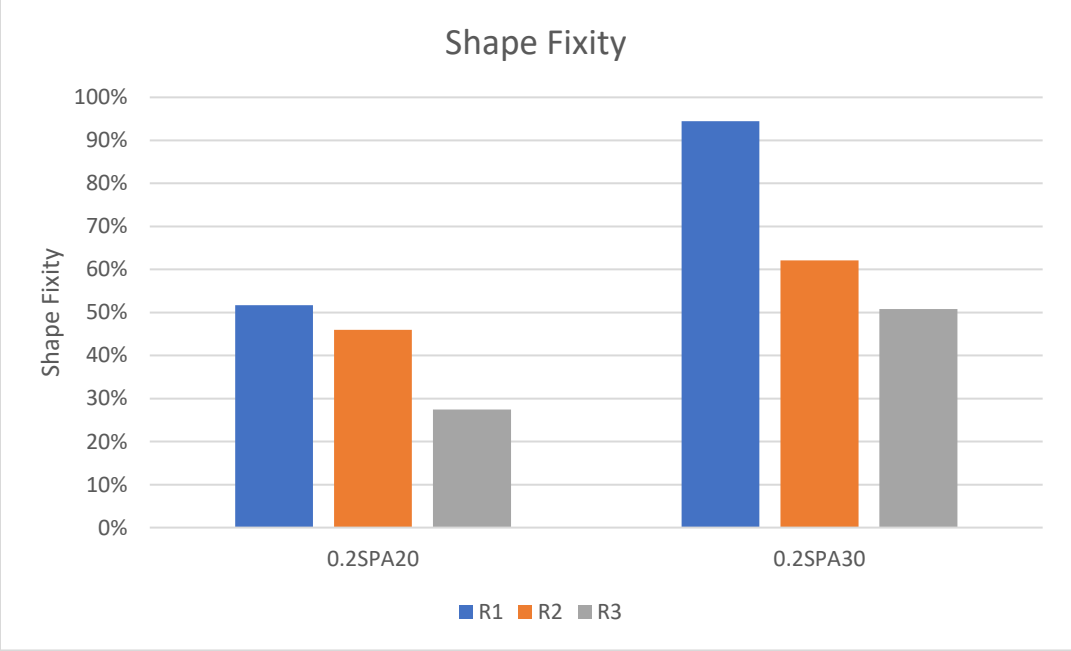

Figure 4.27: The shape fixity of prevulcanised SMNR under cycle test

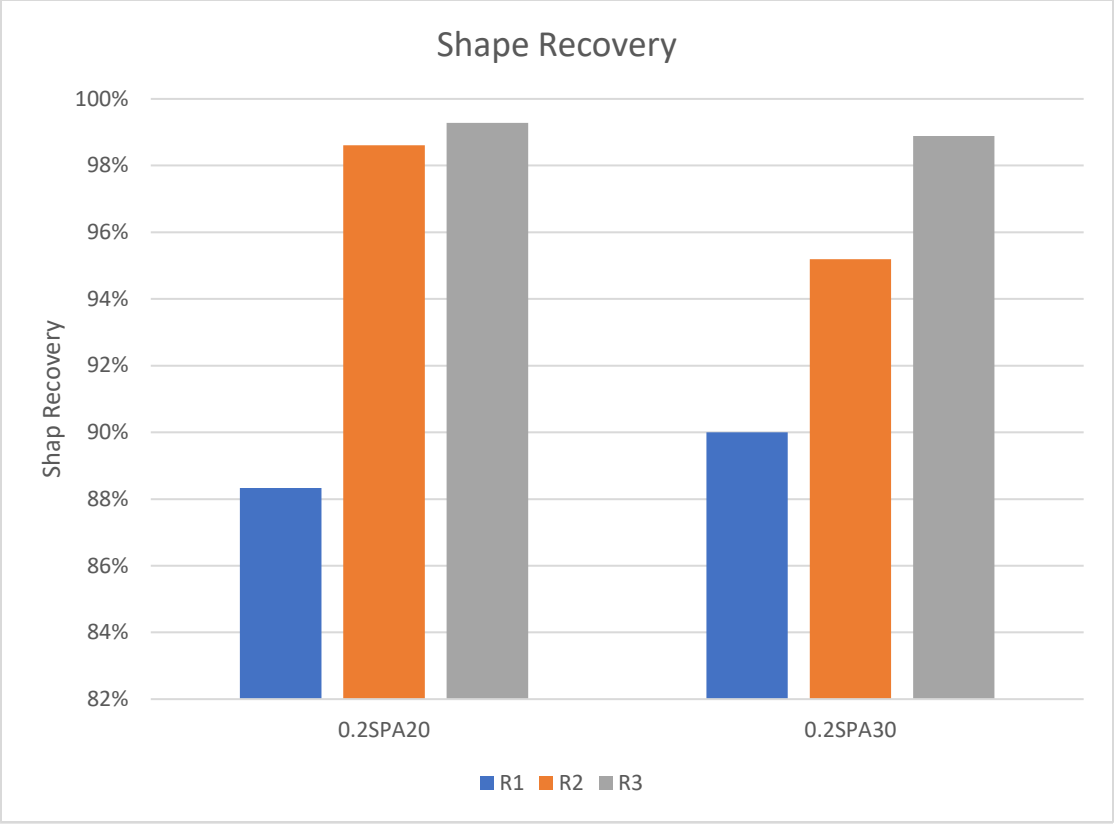

Figure 4.28: The shape recovery of prevulcanised SMNR under cycle test

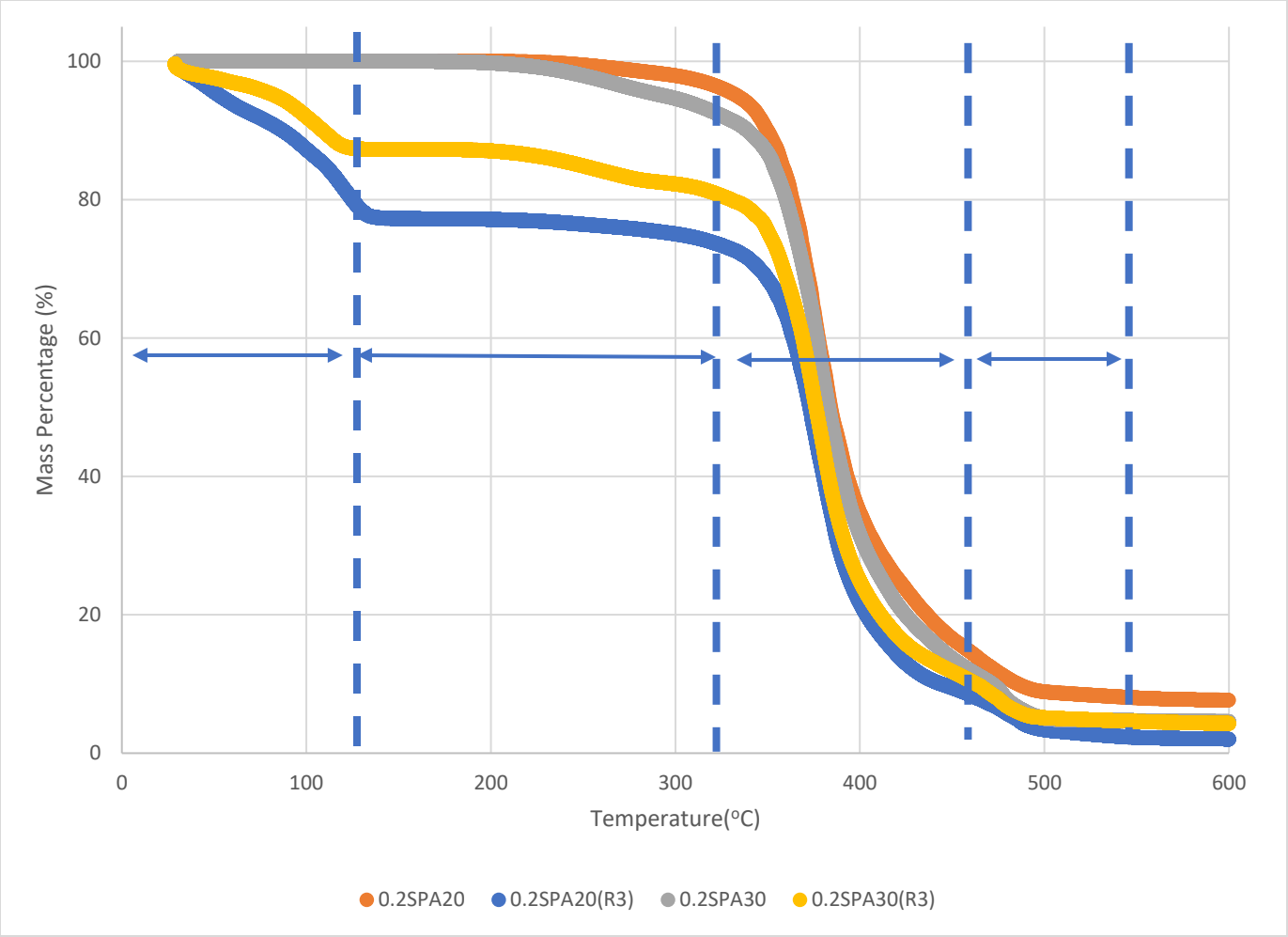

Figure 4.29: The TGA results of the prevulcanised SMNR after and before the shape memory cycle test.

Table 4.7: The weight fraction of the prevulcanised SMNR after and before the shape memory cycle test

Sample code	Water content (%)	Unreacted palmitic acid (%)	Latex (%)	Potassium palmitate soap (%)	Total palmitic acid content (%)
0.2SPA20	0	3.11	88.55	5.54	7.72
0.2SPA20 (R3)	22.48	2.94	67.18	2.93	5.38
0.2SPA30	0	6.18	82.05	6.98	12.00
0.2SPA30 (R3)	12.49	5.65	72.66	3.60	8.65

The specimens before and after the shape memory cycle are conducted under TGA experiment to investigate the root of declining on shape fixity. As a result, the weight fraction of total palmitic acid is reduced after the three-shape memory cycle test. According to Figure 4.29, the weight fraction of palmitic acid content in the 0.2SPA20 drops from 7.72% to 5.38%, while for the 0.2SPA30 is decreased from 12% to 8.65%. Although the overall palmitic acid reduces with the shape memory cycle, potassium palmitate is primarily responsible for this loss. Table 4.7 shows that the loss of palmitic acid content from the unreacted palmitic acid component is less than 9%, but potassium palmitate just remains half of the original weight fraction after three cycles test. Potassium palmitate is soluble in water and easily diffuses out from rubber molecular as the shape memory experiment is conducting under water bath for shape fixing and recovery purposes. This is consistent with the TGA results in the Section 4.2.2 , which found that potassium palmitate is lost during the specimen preparation process. In addition, the TGA results (the thermal degradation section below 140^{o} of temperature) also show that high water content is contained in the SMNR specimen after the shape memory cycle test. This is proven that the specimen regains the elastic properties after the shape memory cycle because the palmitic acid content is lost in the water bath, leading to less retaining force to withstand the recovery load during the unloading process. Hence, the fabrication process of prevulcanised SMNR needs to be further improved in the future to ensure repeatability of SMNR.

4.4 Mechanical Characteristic of Low Crosslinked Prevulcanised SMNR with Various Palmitic Acid Loadings

Since low crosslinked prevulcanised SMNR (0.2 pphr sulphur) shows the most promising shape memory response, only mechanical characteristics of low crosslinked prevulcanised SMNR with various palmitic acid content is reported in Section 4.4.

4.4.1 Uniaxial Stress-Strain Behaviour

Figure 4.30 and Figure 4.31 show the stress-strain response of low crosslinked prevulcanised SMNR at room temperature (25^{o}C) and high temperature (70^{o}C), and their elongations on break are summarised in Table 4.8. Both figures demonstrate that the tensile strength of prevulcanised SMNR increases with palmitic acid content, but only the 0.2SPA20 specimen can be stretched to above 600% of deformed strain at room temperature. From Figure 4.30, the elongation at break for most of prevulcanised SMNR is between 400% and 600% at ambient temperature

Table 4.8: The tensile modulus with 400% of deformed strain and the elongation at break for low crosslinked prevulcanised SMNR at room temperature

Specimen Code	Tensile Modulus with 400% of deformed strain (MPa)	Elongation at break
0.2SPA20	0.450	651.583%
0.2SPA30	0.715	411.172%
0.2SPA40	0.870	537.090%
0.2SPA50	1.160	482.450%

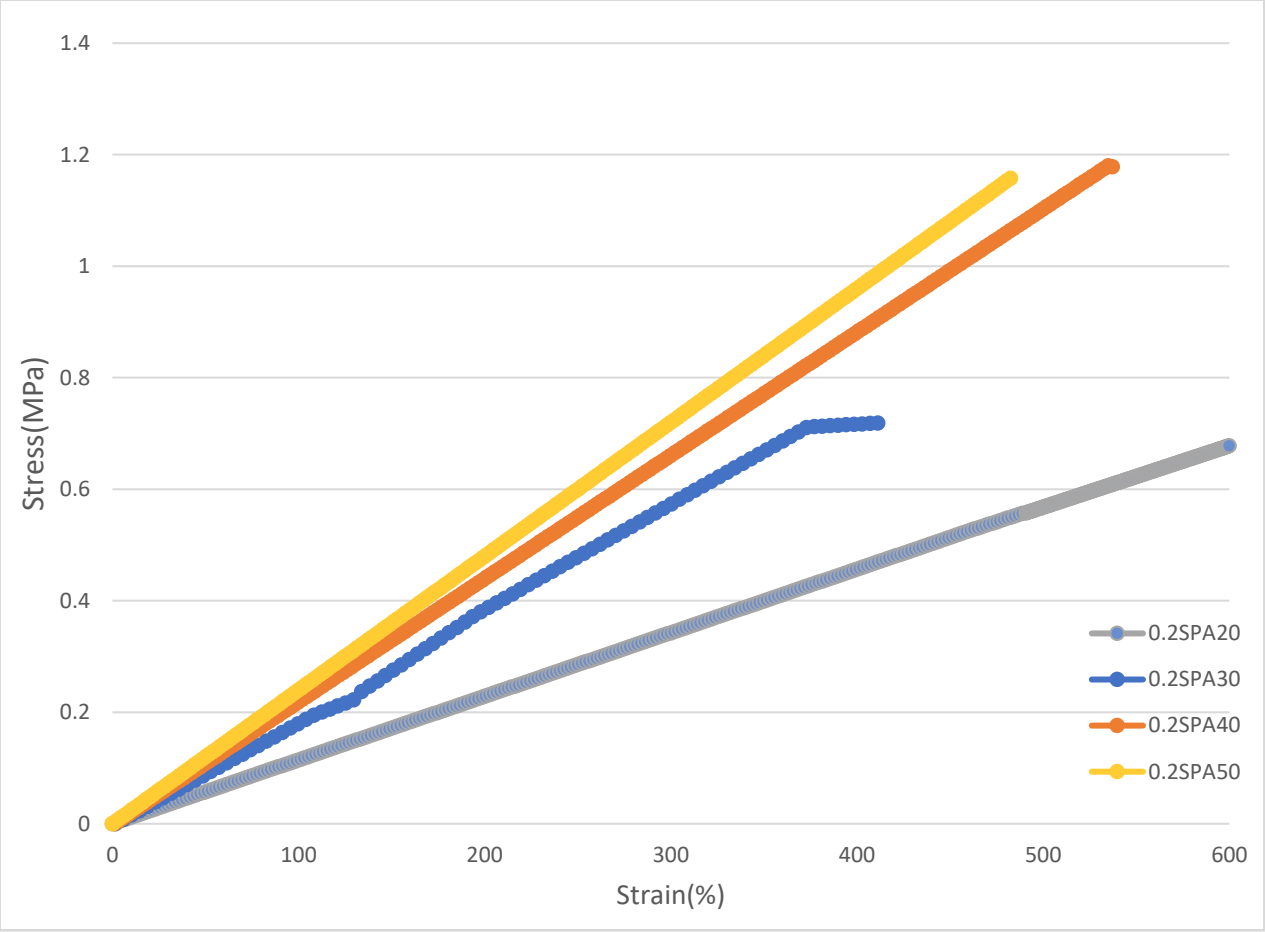

Figure 4.30: Stress-strain curves of prevulcanised SMNR at room temperature

Compared to the tensile modulus at elongation strain of 400%, the 0.2SPA50 has the highest tensile modulus (1.16MPa), subsequence is the 0.2SPA40 (0.87MPa) then is the 0.2SPA30 (0.715MPa). While the 0.2SPA20 has the lowest tensile modulus (0.45MPa), its elongation at break is achieved above 600%. It is obvious that palmitic acid has enhanced the tensile strength of the specimens by reducing the elastic properties and flexibility of SMNR. The binding force is generated during the deformed process to constrain the elongation strain of the rubber molecule [185]. Nevertheless, the network failure is initiated once the tensile load exceeds the binding force.

In general, binding force corresponds to palmitic acid content. It leads to higher stiffness by increasing palmitic acid amount, but it also reduces the elastic limit on the elongation stain. In consequence, tensile failure is easily promoted at low deformed strain with higher palmitic content.

Due to the high palmitic acid amount within the rubber molecule, the tensile modulus of prevulcanised SMNR specimen is linear at room temperature, contradicting the high non-linearity of typical rubber stress-strain response [186]. However, the response is completely different at high temperature of 70^{o}C. The stress-strain response of low crosslinked prevulcanised SMNR at 70^{o}C is shown as Figure 4.31. It describes that the specimens exhibit dramatically increment in tensile stress during the initial deformation process. Still, the increment is less and reaches a plateau once the deformed strain excess 50%, which is consistent with the findings from Shigeyuki Toki et al. [187] and Abbas et al. [188]. It is well known that rubber is the ductile material, and its elasticity corresponds to the sulphur content, but the sulphur content of prevulcanised SMNR (0.2 pphr) is much lower than the commercial grade (1.5 pphr to 2.5pphr sulphur). Combining the effect of a high portion of palmitic acid, the prevulcanised SMNR experiences the brittle-to-ductile transition at 70^{o}C [189]. The early deformation process (<50% deformed strain) is represented the specimen still involves in glass state deformation, which has the linear and sharp stress-strain behaviour. After it reaches the deformed strain of 50%, the specimen transforms to rubbery state, and the rubber molecule is free for entanglement under low tensile stress. However, the tensile modulus increases with palmitic acid loading. No elongation at break is observed for all specimens even deformed to 500% of elongation strain at the elevated temperature range.

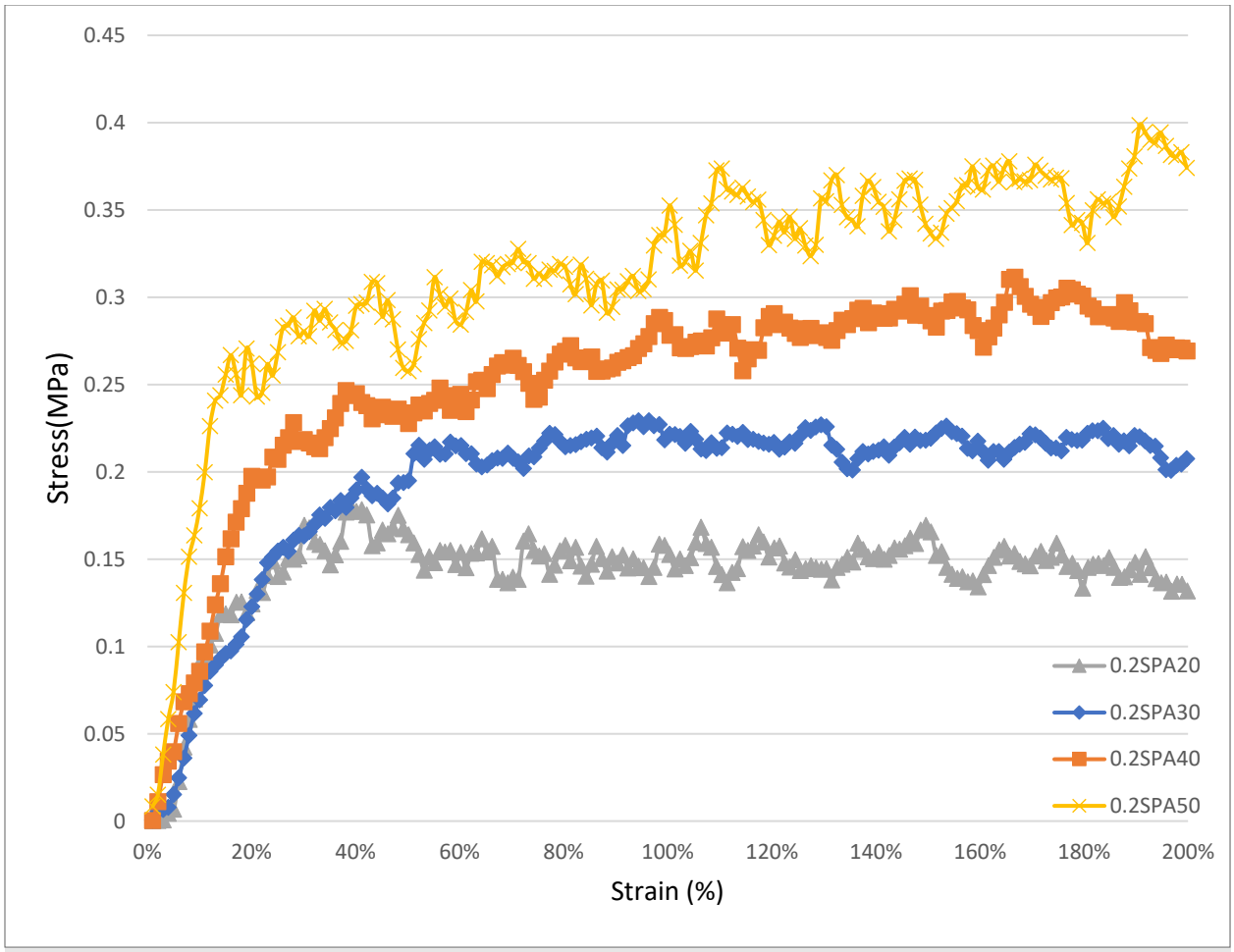

Figure 4.31: Stress-strain curve of prevulcanised SMNR at the temperature of 70 ^{o}C

4.4.2 Stress Relaxation under Tensile Machine with Heat Chamber

To study the stress behaviour during the programming process, the stress relaxation of prevulcanised SMNR with various palmitic acid content is conducted under a tensile machine at 70°C. To highlight the viscoelastic behaviour, the stress ratio of prevulcanised SMNR specimen as a function of the time are shown in Figure 4.32. It can be seen that the stress ratio has a gradually drop at the early period of the stress relaxation experiment. Especially for the 0.2SPA20, the stress ratio has achieved an equilibrium of 60% after 600 seconds.

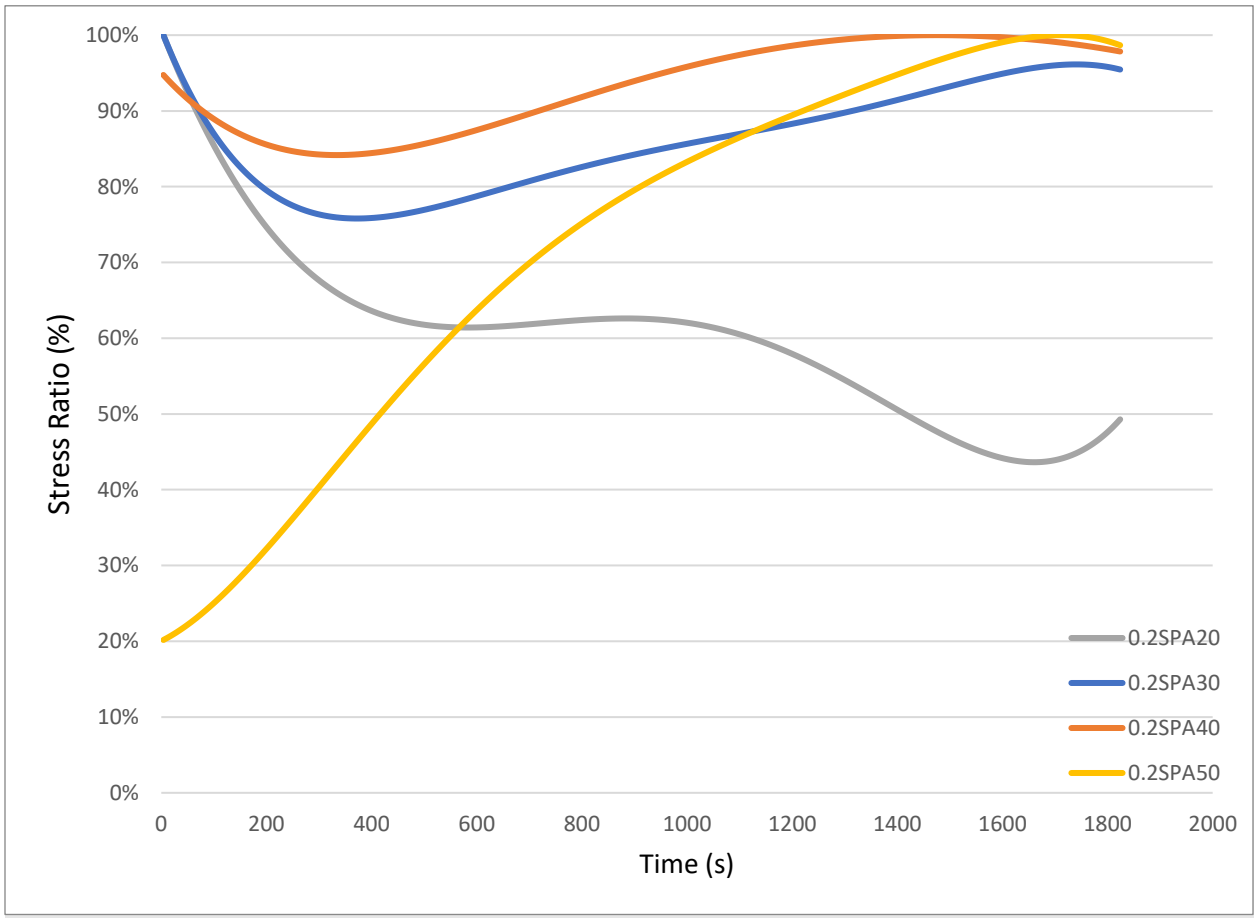

Figure 4.32: Stress relaxation results for prevulcanised SMNR under the tensile machine at 70°C

While for the 0.2SPA40 and 0.2SPA30, their stress ratios gradually increase after 400 seconds. This indicates the SME presents during this viscoelastic experiment [190]. Due to the retention force is released during the viscoelastic experiment, it overlays the stress relaxation effect and dominates the stress behaviour in the intermedia period. Nevertheless, the accumulating stress relaxation effect regains the dominance of stress behaviours by increasing the experiment duration. For the 0.2SPA20, less retaining force is generated from the palmitic acid; its stress ratio had reached the offset peak at 950 seconds. While for the 0.2SPA30 and the 0.2SPA40, the equilibrium condition achieves at 1756 seconds, and their stress ratio back to decline trend. The 0.2SPA50 has the highest palmitic acid content, which no stress relaxation sign is observed, and the stress ratio increases from the beginning of the experiment until the end. However, the stress relaxation corresponds to the time function; the stress relaxation has a minimum effect within a short shape programming period and accumulates with experimental duration.

4.4.3 Stress Relaxation under DMA Machine

To reveal the stress behaviour during the quenching process, stress relaxation with temperature ramps is performed on prevulcanised SMNR in DMA machine and shown in Figure 4.33. Figure 4.33 shows that the stress ratio of each prevulcanised specimen decreases at the beginning of the experiment. As the specimen begin with the quenching process, the stress ratio is decreased dramatically by 21%±7% and slowly increased after the temperature is stable. Similar stress reduction with temperature is also reported by Riccardo [191], but his specimen is recovering its stress ratio by elevating the temperature. As the temperature is reheated to the temperature of 70^{o}C, the stress ratio have a dramatical increment at the beginning of reheating process but it starts to another declining tendency after the temperature is stable at 70^{o}C. It is obvious that the declining trends observed at the early and late end of the experiment period are attributed to stress relaxation [192]. Due to the stress relaxation effect involves, the entangled force between the molecule decreases over time, resulting in less stress is required to maintain a similar strain level. While the SME is responsible for the stress ratio shifting during the quenching and reheating process [193]. Due to the retaining force from palmitic acid is holding partial deformed strain during the quenching process, less elastic force is required to maintain the same elongated strain at low temperature range. The retaining force is released, and the stress ratio is rebounded during the reheating process by vanishing the SIC structure. Combining with the elastic load, most stress ratio is restored at the high temperature range. Therefore, it is proven that the stress reduction corresponds to the temperature, and it is required a thermal algorithm to describe this particular stress reduction response for establishing the shape memory behaviour prediction model.

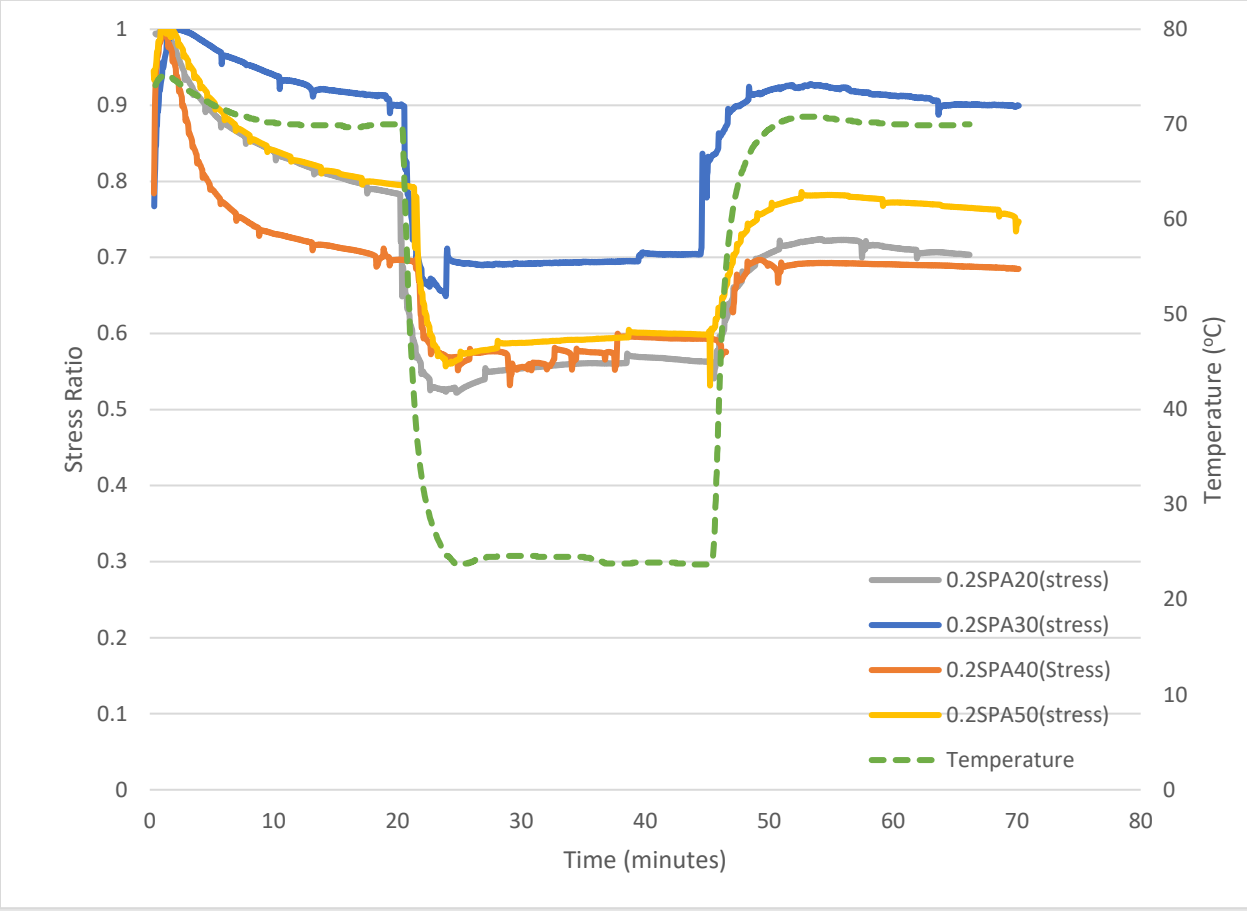

Figure 4.33: Stress relaxation with involved temperature ramp under DMA machine

5 Shape Memory Behaviours Prediction Modelling Results and Discussion

From Chapter 4, it can be seen that the shape memory behaviours of prevulcanised SMNR are complex because multiple intermolecular phase transitions are involved during the shape memory process. In addition, composition formulation and the rubber structure of SMNR also significantly influence the SME. To model the shape memory behaviours of SMNR, not only the stress-strain behaviours and composition are considered. The thermal effects occurring throughout shape memory process are also taken into account for the model algorithm. This chapter identifies the material constant and compares experimental and modelling results of the proposed constitutive model. Since SMNR with 0.2S sulphur loading incorporated with various palmitic acid loadings shows the best shape memory response, only this group of specimens is involved in this chapter.

5.1 Identification of Material Coefficient

As mentioned previously in the methodology section, the constitutive model is established using mechanical and thermal approaches. The mechanical approach is formed by one SLS model with Kelvin-Voigt element to describe the viscoelastic properties (hard segment phase) and two Mooney Rivlin equations to represent the hyperelastic behaviours at respective temperature range (soft active and frozen segment phase). At the same time, a single thermal strain model respects to the volume change of both soft segments in temperature takes the thermal effect into account during the shape programming and recovery process. Each segment phase and thermal model consist of at least two material constants. The material coefficient of each model element is

characterised by the composition and mechanical response result at room temperature (25^{o}C) and high temperature (70^{o}C) which are obtained in experiment work at previous section.

5.1.1 Determination of Volume Fraction (Hard and Soft Segment Phase)

Referring to the material characteristic of prevulcanised SMNR in the Section 4.1.3, the prevulcanised NR compound is emerged as the hard segment phase while palmitic acid material is classified as the soft segment phase (active and frozen stage). The mass fraction obtained from TGA results is utilised to measure the volume fraction of respective material with different formulations and summarised in Table 5.1.

Table 5.1: The volume fraction of each composition with their specimen group

Specimen code	Mass fraction		Volume fraction	
	Palmitic acid	Prevulcanised NR compound	Palmitic acid	Prevulcanised NR compound
0.2SPA20	0.0723	0.9300	0.0720	0.9280
0.2SPA30	0.1200	0.8800	0.1189	0.8811
0.2SPA40	0.1393	0.8600	0.1379	0.8621
0.2SPA50	0.1798	0.8200	0.1775	0.8225

Along with the volume fraction for individual material, a law of governing the change of volume fraction by temperature is also introduced in this subsection. Due to the thermal characteristic of palmitic acid, prevulcanised SMNR possesses the ability to constrain the mobility of rubber molecular at low temperature and promotes the recovery process at high temperature by interchanging the soft active and frozen segment phases. To determine the volume fraction of both soft segment phase at specific temperature range, the heat flow of DSC experiment around T_c

(35~80°) is depicted in Figure 5.1. To highlight the phase change effect from palmitic acid, the DSC result of the 0.2SNR is also included in Figure 5.1.

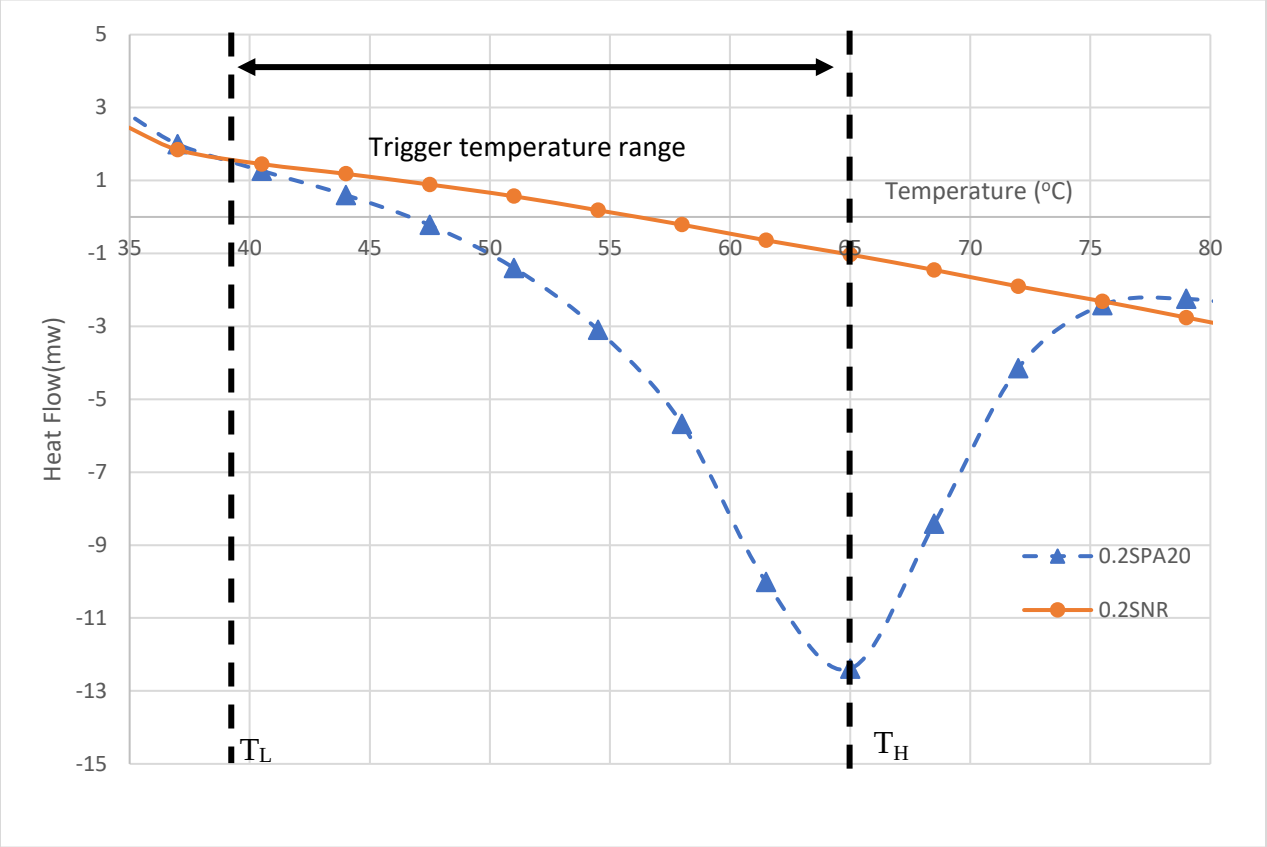

Figure 5.1: DSC result of 0.2SPA20 and 0.2SNR (within 35°C to 80°C)

By inspecting the DSC thermogram, an onset peak of heat flow is found between the temperature of 39°C to 75.5°C on 0.2SPA20. It is obvious that the change of heat flow at this specific temperature range is attributed to the microstructural phase change of palmitic acid. Due to the endothermic reaction occurring within palmitic acid molecular, additional thermal energy is absorbed and converted into entropy to increase the mobility of molecular. Once the frozen soft segment phase has been completely transformed as active phase, the heat flow in the process is terminated and slowly recover to a normal heat flow rate like the 0.2SNR at 75.5°C. Hence, the T_L

is determined as the temperature where the beginning of heat flow changes (39°C) while the T_H is defined as the temperature with the heat flow peak (65°C).

To model the shape memory behaviours of prevulcanised SMNR, an algorithm to govern volume fraction change for both soft segment phases is required. According to the DSC result, a regression equation (Equation (5.1a-d) respected to temperature is established to model the volume fraction change between the soft active and frozen segment phase in the SMNR molecule during the shape memory process (shape programming and shape recovery). The regression line of the temperature algorithm is shown in Figure 5.2, and their coefficients are written as follows:

$$V_s = 1 - V_h \qquad \text{Equation (5.1a)}$$

$$V_{sf} = V_s \qquad \text{For } T_L \leq T(t) \qquad \text{Equation (5.1b)}$$

$$V_{sf} = V_s(C_{T1} + C_{T2}T + C_{T3}T^2 + C_{T4}T^3 + C_{T5}T^4 + C_{T6}T^5) \qquad \text{For } T_H \leq T(t) \leq T_L \qquad \text{Equation (5.1c)}$$

$$V_{sf} = 0 \qquad \text{For } T_H \geq T(t) \qquad \text{Equation (5.1d)}$$

where T_L and T_H are the lower and upper boundary of temperature, respectively, and the C is the coefficients of the temperature algorithm. (C_{T1}= -442.377, C_{T2}=44.527, C_{T3}= -1.776, C_{T4}= 0.035, C_{T5}= -3.459e^{-4} and C_{T6}=1.350e^{-6})

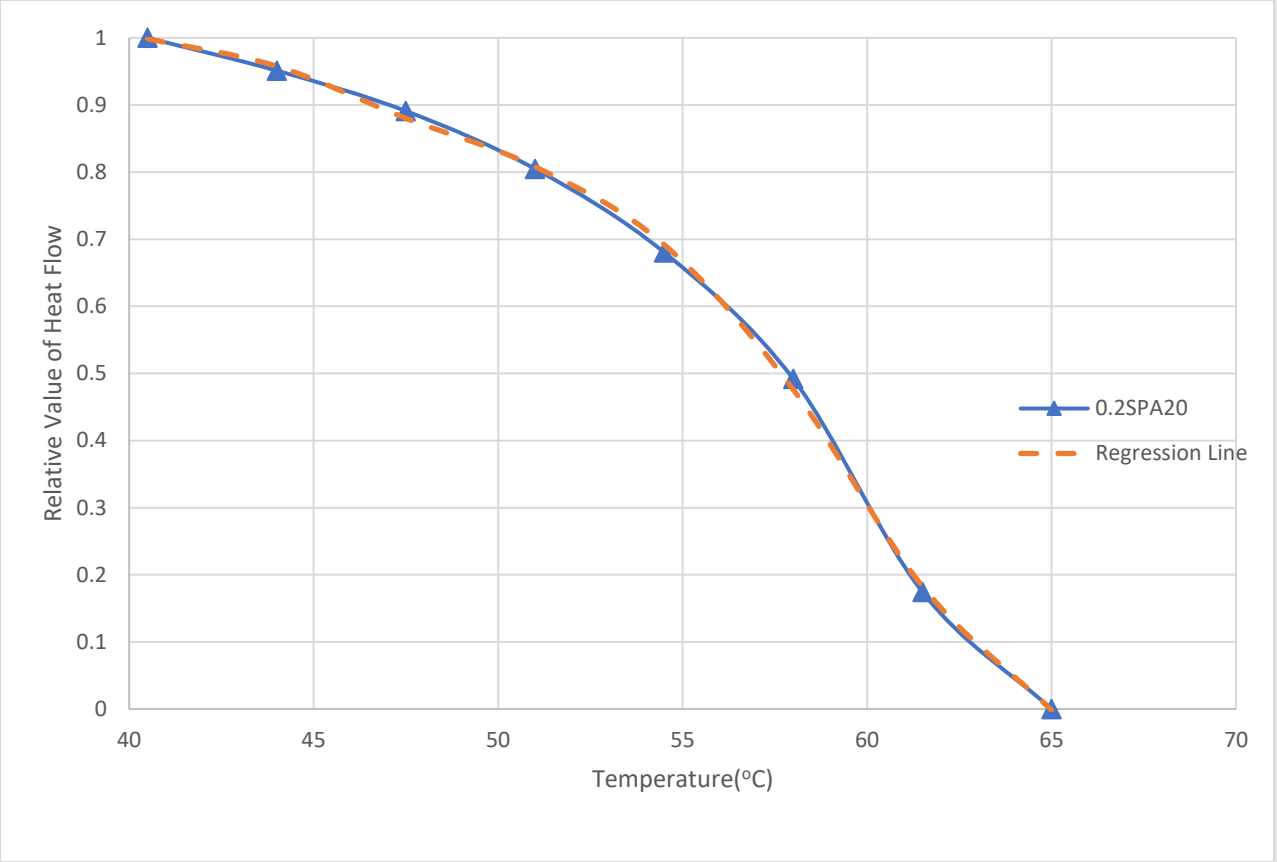

Figure 5.2: Relative value of heat flow on 0.2SPA20 and its regression line

5.1.2 Determination of Material Coefficient (Hard and Soft Segment)

The mechanical response of prevulcanised SMNR presented in Section 4.4 is utilised to determine the material constant of each mechanical segment mode. The experimental data of prevulcanised SMNR under a similar testing temperature is modelled by combining viscoelastic (SLS) and hyperelastic (Mooney Rivlin) models. Table 5.2 lists the material coefficient of each prevulcanised SMNR in the mechanical segment model. The comparison of experimental and modelling stress-strain results from the tensile test of SMNR at room temperature and 70^{o}C are demonstrated from Figure 5.3 to Figure 5.6. Moreover, the behaviours of the respective strain from the related segment model at room temperature and 70^{o}C are also presented.

Table 5.2: Material constants of the prevulcanised SMNR with different palmitic acid content

Specimen Code	Viscoelastic model			Soft frozen segment model		Soft active segment model	
	E_1 (MPa)	E_2 (MPa)	η (MPa s)	C_{sf1}(MPa)	C_{sf2}(MPa)	C_{sa1}(MPa)	C_{sa2}(MPa)
0.2SPA20	10	0.25	3.5	0.0275	0.001	0.0036	0.0452
0.2SPA30	10	0.40	4.0	0.0400	0.001	0.0048	0.0890
0.2SPA40	10	0.50	5.0	0.0435	0.002	0.0065	0.0835
0.2SPA50	10	0.55	6.0	0.0540	0.001	0.0092	0.1000

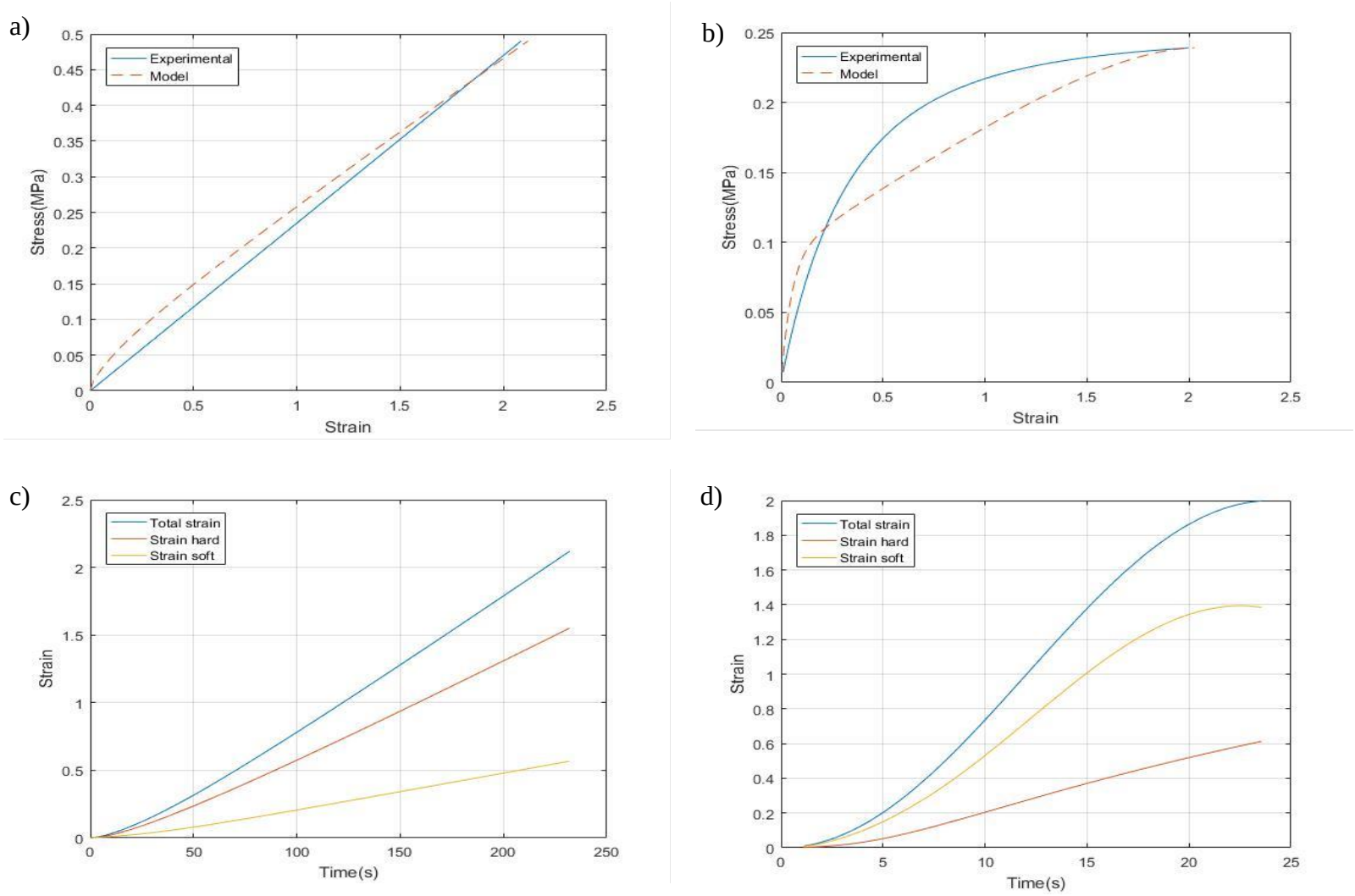

Figure 5.3: The experimental and modelling of stress-strain behaviours of 0.2SPA20 at a) room temperature and b)70^{o}C, the strain behaviours of each segment model at c) room temperature and d)70^{o}C

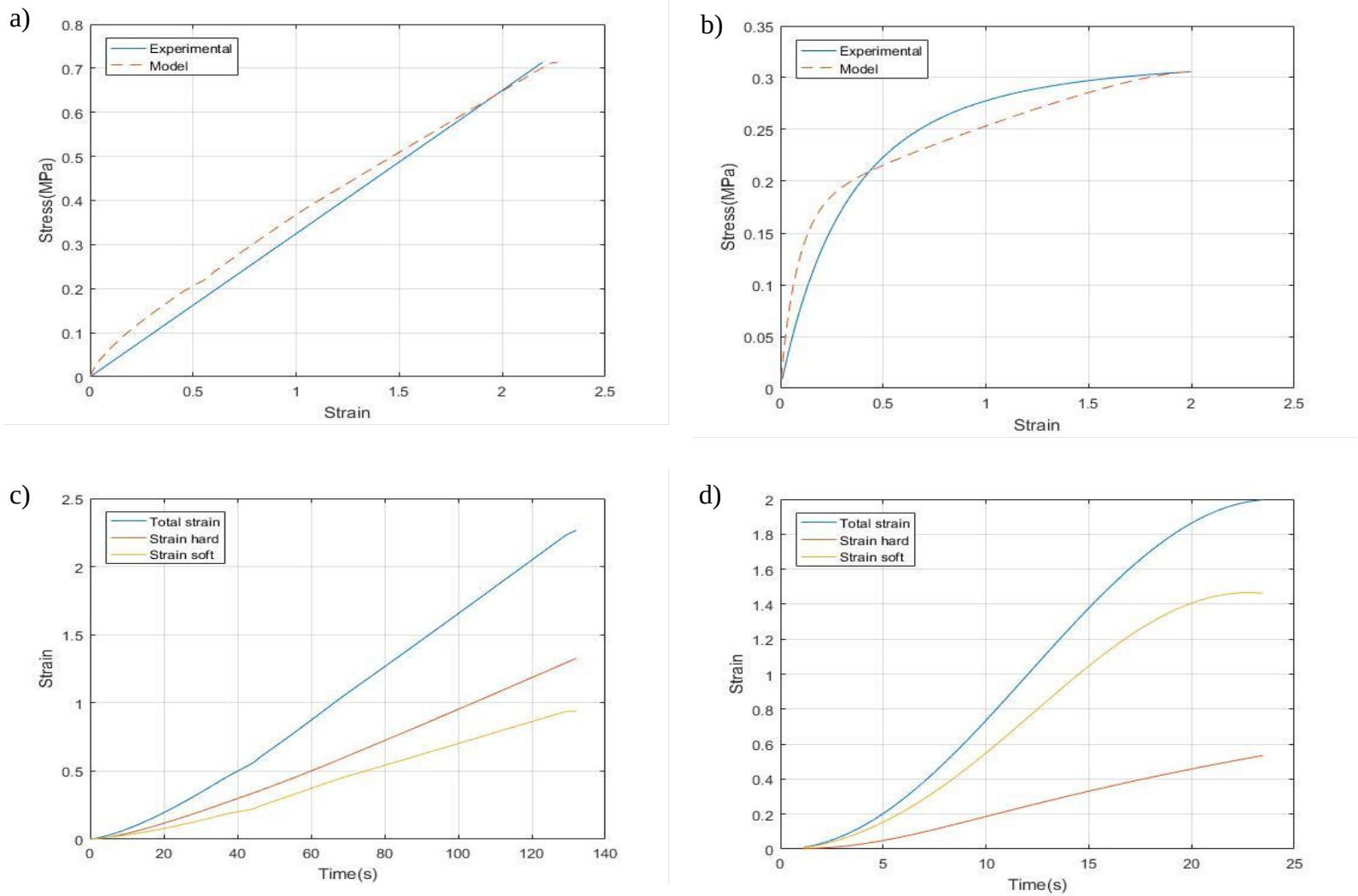

Figure 5.4: The experimental and modelling of stress-strain behaviours of 0.2SPA30 at a) room temperature and b)70^{o}C, the strain behaviours of each segment model at c) room temperature and d)70^{o}C

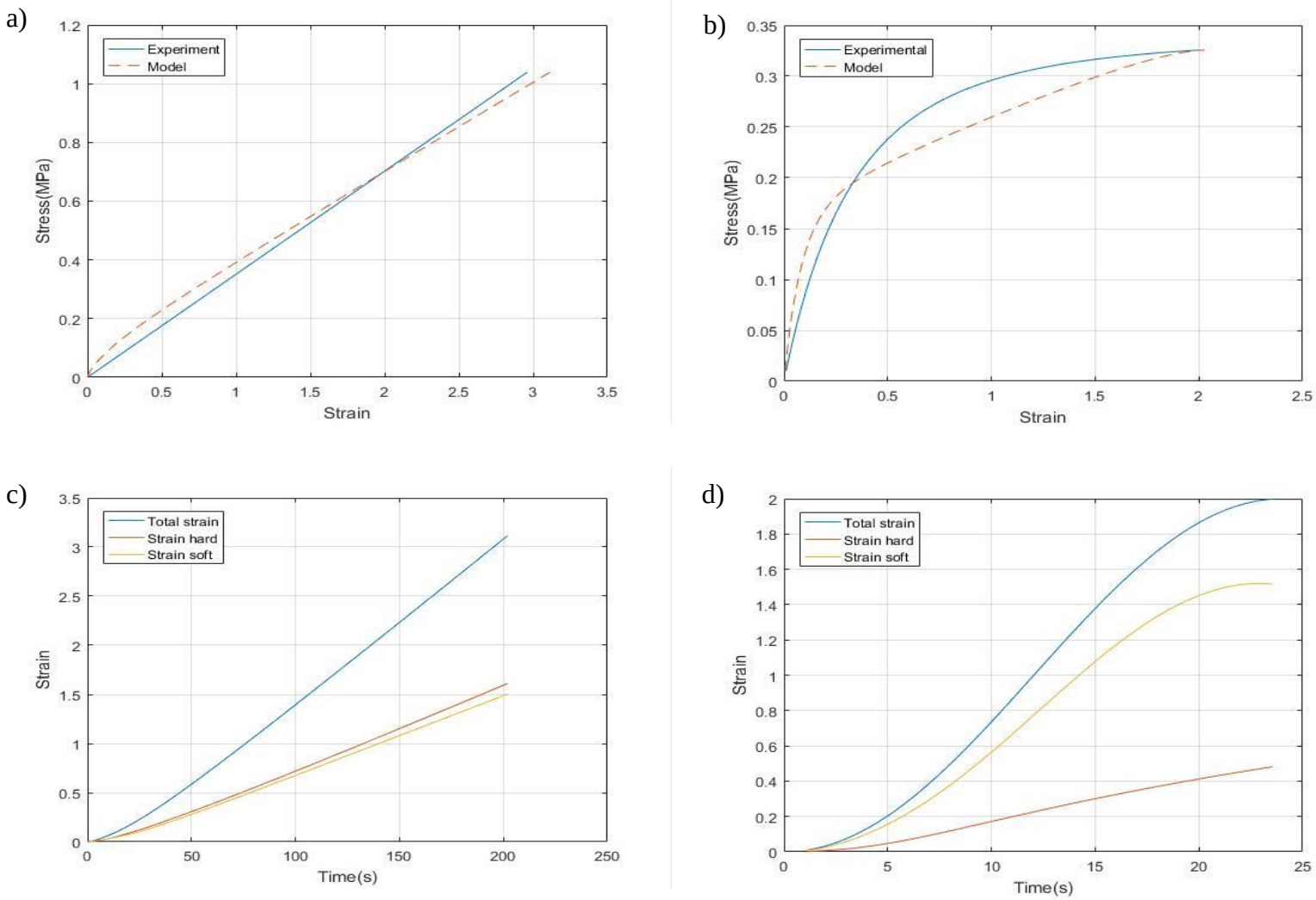

Figure 5.5: The experimental and modelling of stress-strain behaviours of 0.2SPA40 at a) room temperature and b)70^{o}C, the strain behaviours of each segment model at c) room temperature and d)70^{o}C

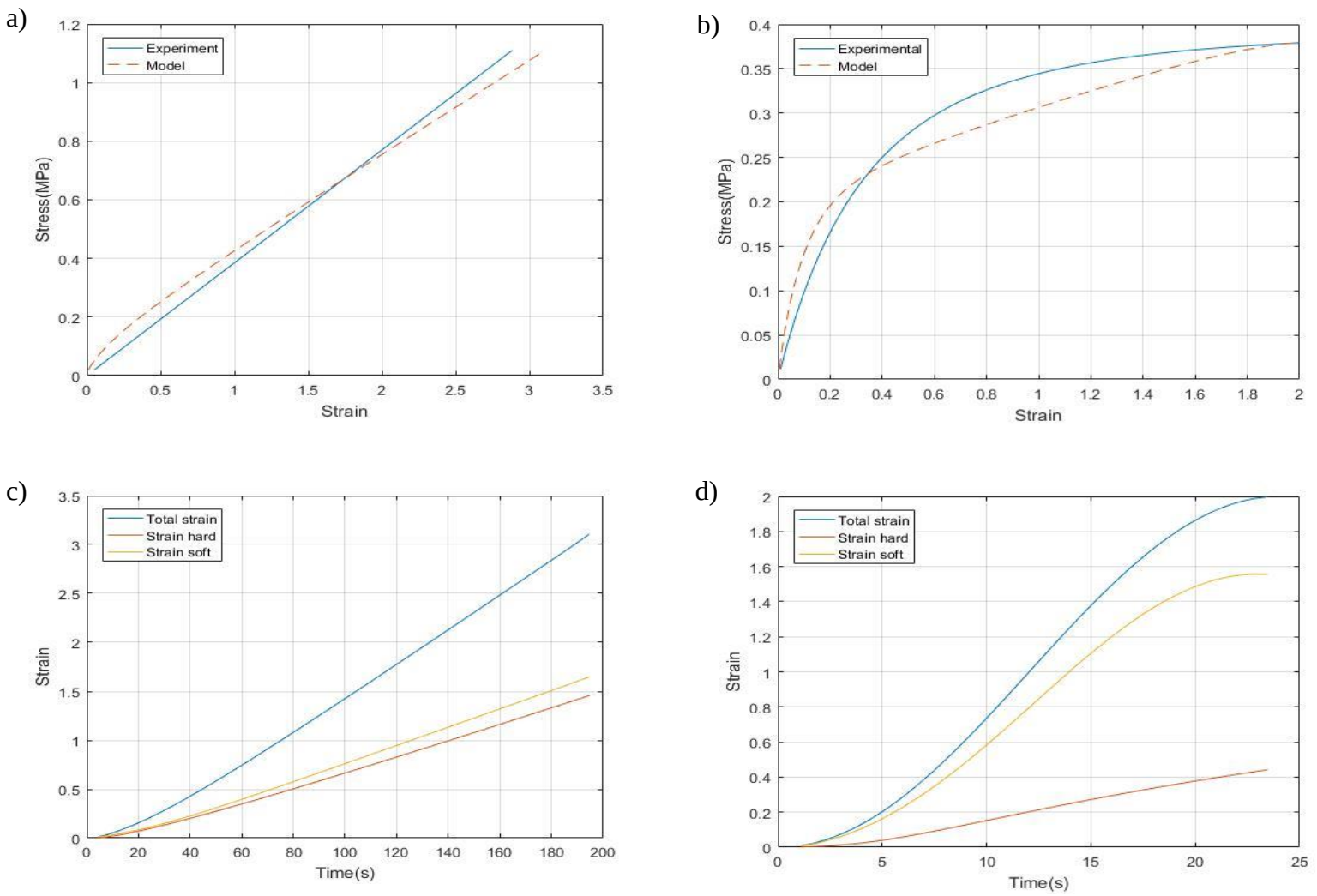

Figure 5.6: The experimental and modelling of stress-strain behaviours of 0.2SPA50 at a) room temperature and b)70^{o}C, the strain behaviours of each segment model at c) room temperature and d)70^{o}C

By inspecting the stress-strains behaviours of each prevulcanised SMNR, the constitutive model is capable of simulating the mechanical response at both temperatures. According to the strain evolution of both segments, the soft segment phase always provided the higher deformed strain than the hard segment phase at 70^{o}C, and the 'S' deformation trend is found on the soft segment phase of each prevulcanised SMNR at high temperature range. Nevertheless, it experiences different circumstances at room temperature, in which the soft segment phase has a linear deformation. It contributes less deformed strain than hard segment under similar stress levels for specimen with low palmitic acid loading (0.2SPA20 and 0.2SPA30). This indicates that the soft segment offers the stiffness properties at room temperature and exhibits the rubbery properties trend at the high temperature [194]. As the soft segment phase, palmitic acid has a T_m of ~64^{o}C [195]; it changes the polymer properties from a glass state to a rubbery state within the testing temperature range. Due to the soft segment having higher flexibility on the molecule movement at high temperature, higher deformed strain is generated at low stress levels. Nonetheless, the soft segment has low entropy energy at room temperature, limiting polymer chain mobility. In consequence, less strain is contributed to similar stress behaviour.

Moreover, the strain evolution of each prevulcanised SMNR shows that the soft segment phase gradually increases the tensile strain by raising the palmitic acid content. For example, the tensile strain of the soft segment phase is above the hard segment in Figure 5.5 and Figure 5.6. Due to the increased palmitic acid amount in the prevulcanised molecule, the soft segment generates more tensile strain than other prevulcanisation SMNR (0.2SPA20 and 0.2SPA30) at a similar stress level. Further increasing the palmitic acid content, the soft segment will gradually dominate the stress-strain behaviour at room temperature. However, both strain behaviours are consistent with the finding from the tensile experiment of prevulcanised SMNR at room

temperature and temperature of 70^{o}C. Therefore, similar material coefficients are adopted to model the shape memory behaviour of prevulcanised SMNR

5.1.3 Determination of the Stress Reduction on Temperature change

The investigation of stress-strain behaviour during the shape memory process is important because it reflects the specimen condition and reveals the thermal effect on prevulcanised SMNR at the programming and recovery stage. Due to the limitations of the testing machines, the stress-strain behaviour of each shape memory process is obtained independently. For example, tensile test results are responsible for shape deformation. In contrast, the shape programming process is inspected under the DMA machine with a stress relaxation test with a temperature ramp.

Referring to the stress relaxation results in the Section 4.4.3, it indicates that the stress behaviour of the prevulcanised SMNR corresponds to the temperature during the shape programming. To highlight the stress reduction associates with temperature change, the stress reduction region of the 0.2SPA20 is pointed out and shown in Figure 5.7. To establish a stress reduction algorithm, the stress ratio is redefined using the initial tensile stress, σ_H is the upper boundary of stress where the temperature change occurs, while the lower boundary stress at the stress reduction section is recorded as σ_L. Since the early stress reduction is attributed to the stress relaxation during the isothermal process, the upper boundary of the stress reduction due to temperature change is started at 20 minutes (end of isothermal process) and the lower boundary stress defined as the minimum stress ratio for low temperature (room temperature). A law of governing the stress reduction respects to temperature for each specimen listed, and its regression line is shown in Figure 5.8 to Figure 5.11.

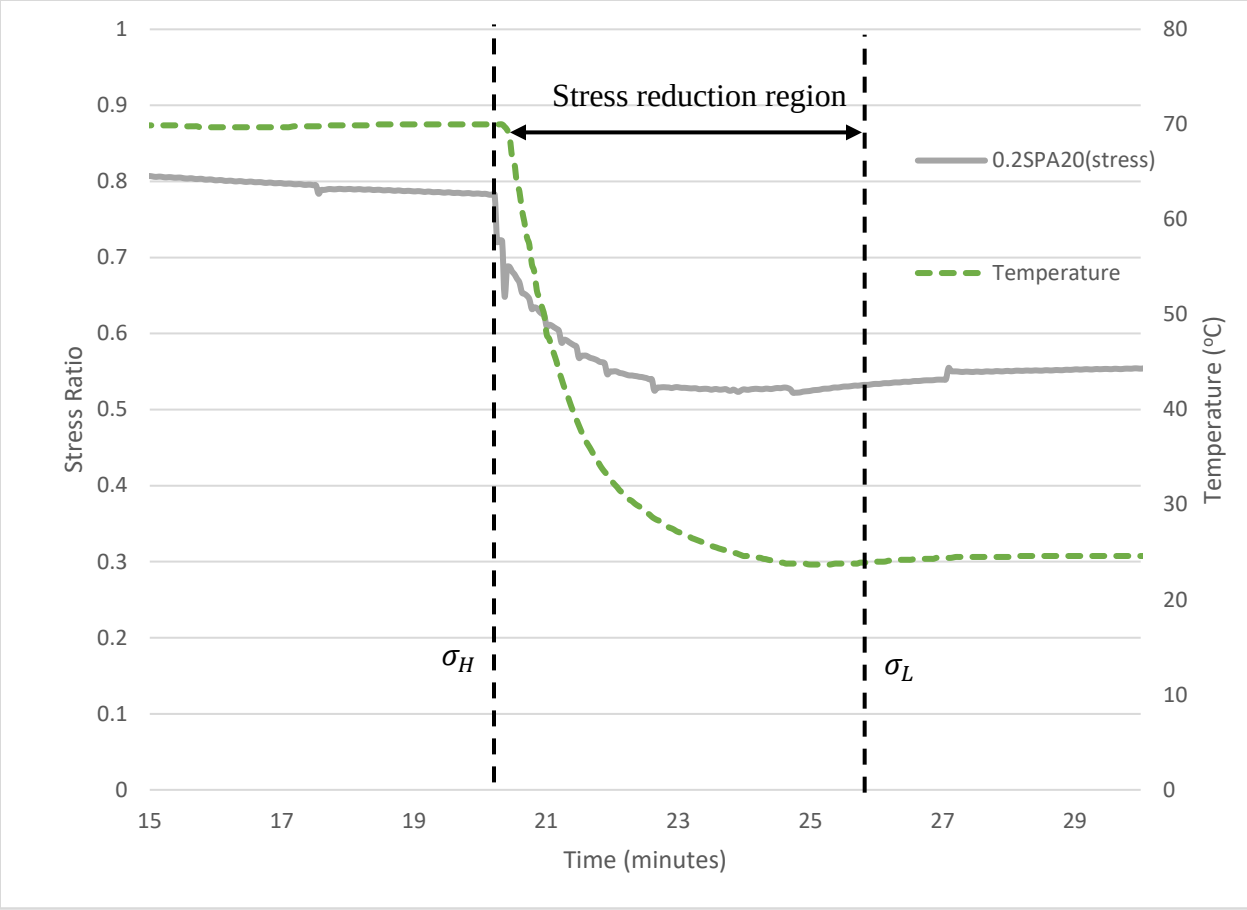

Figure 5.7: Remarking the stress reduction region of 0.2SPA20

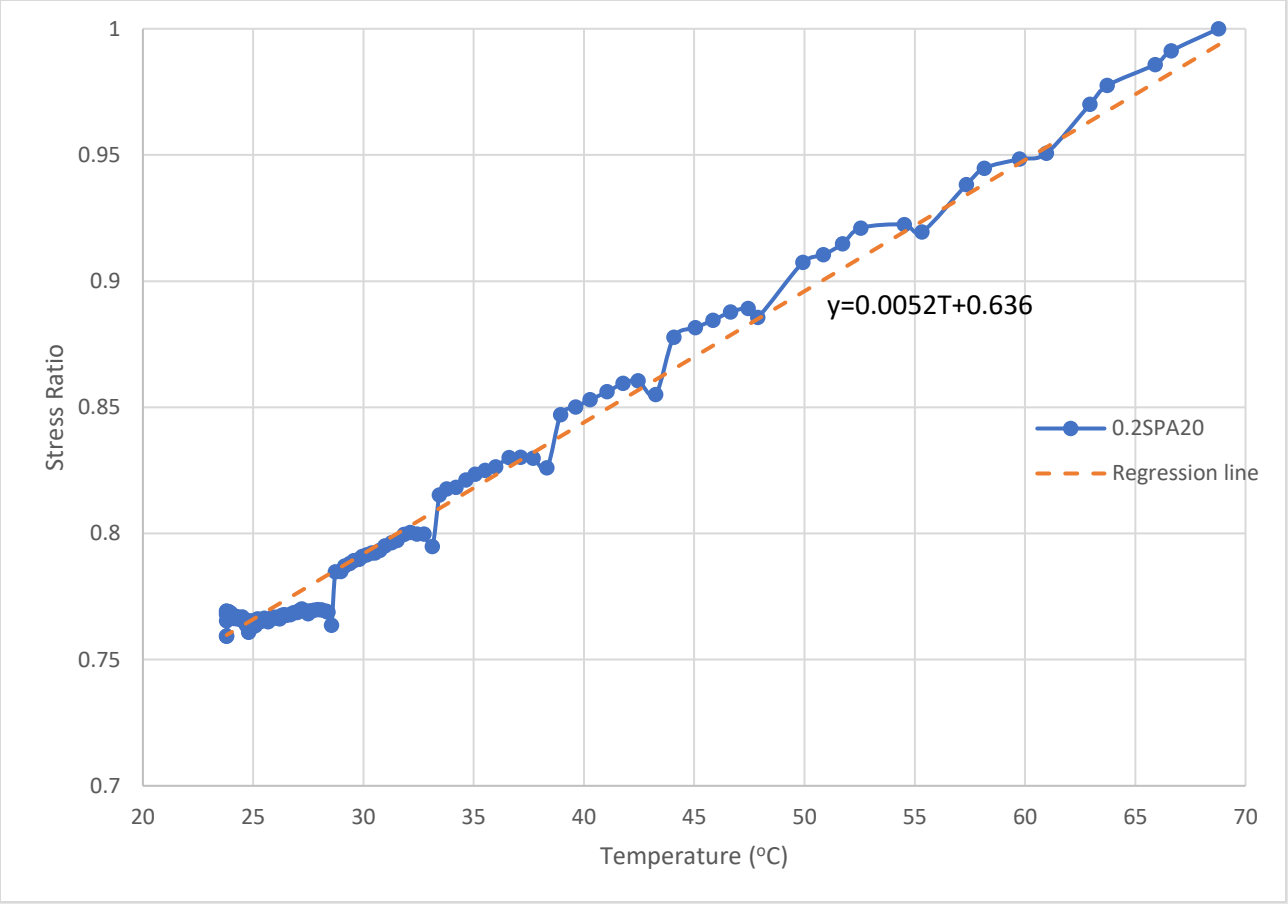

Figure 5.8: The experiment data and regression line of 0.2SPA20 for the stress reduction

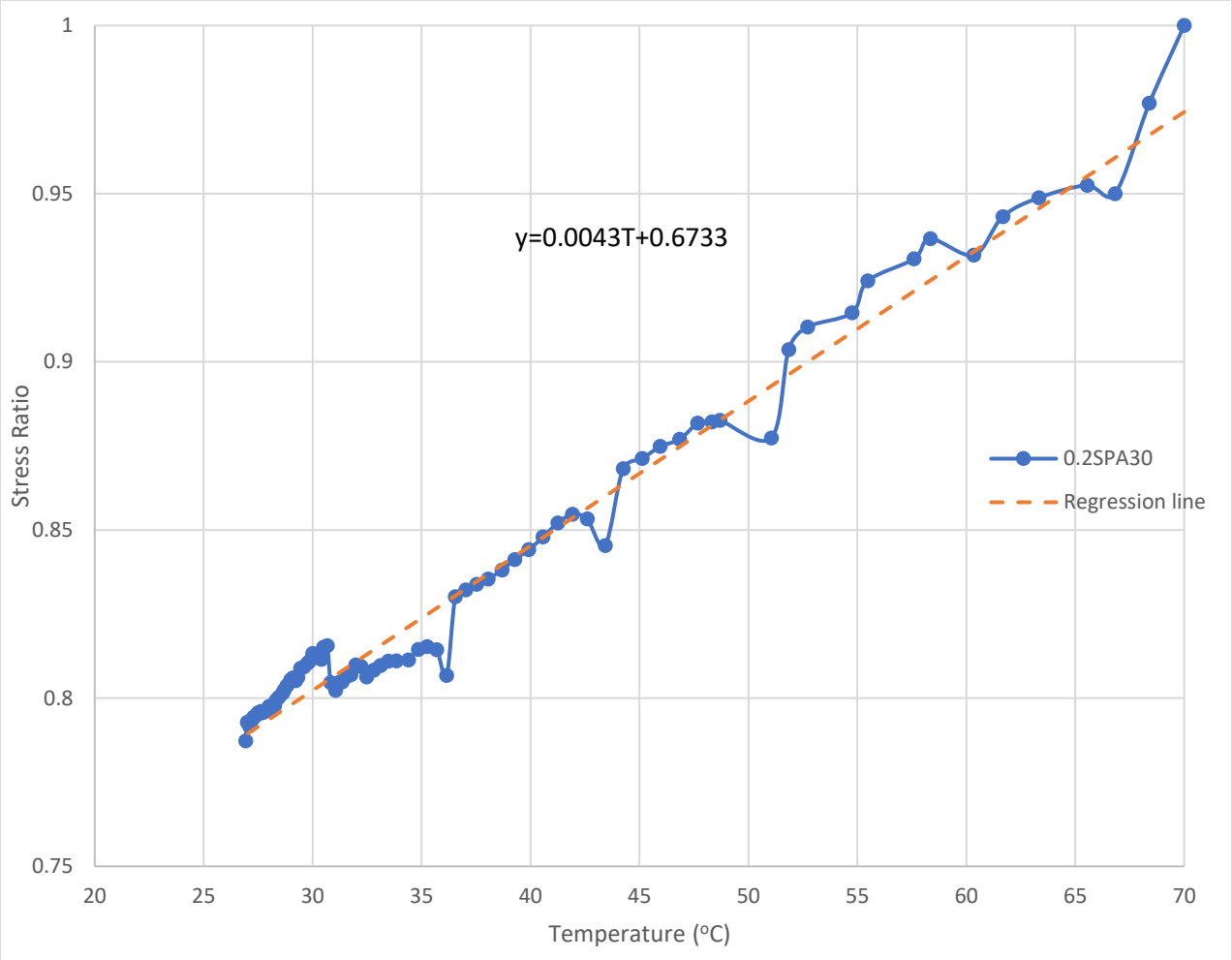

Figure 5.9: The experiment data and regression line of 0.2SPA30 for the stress reduction

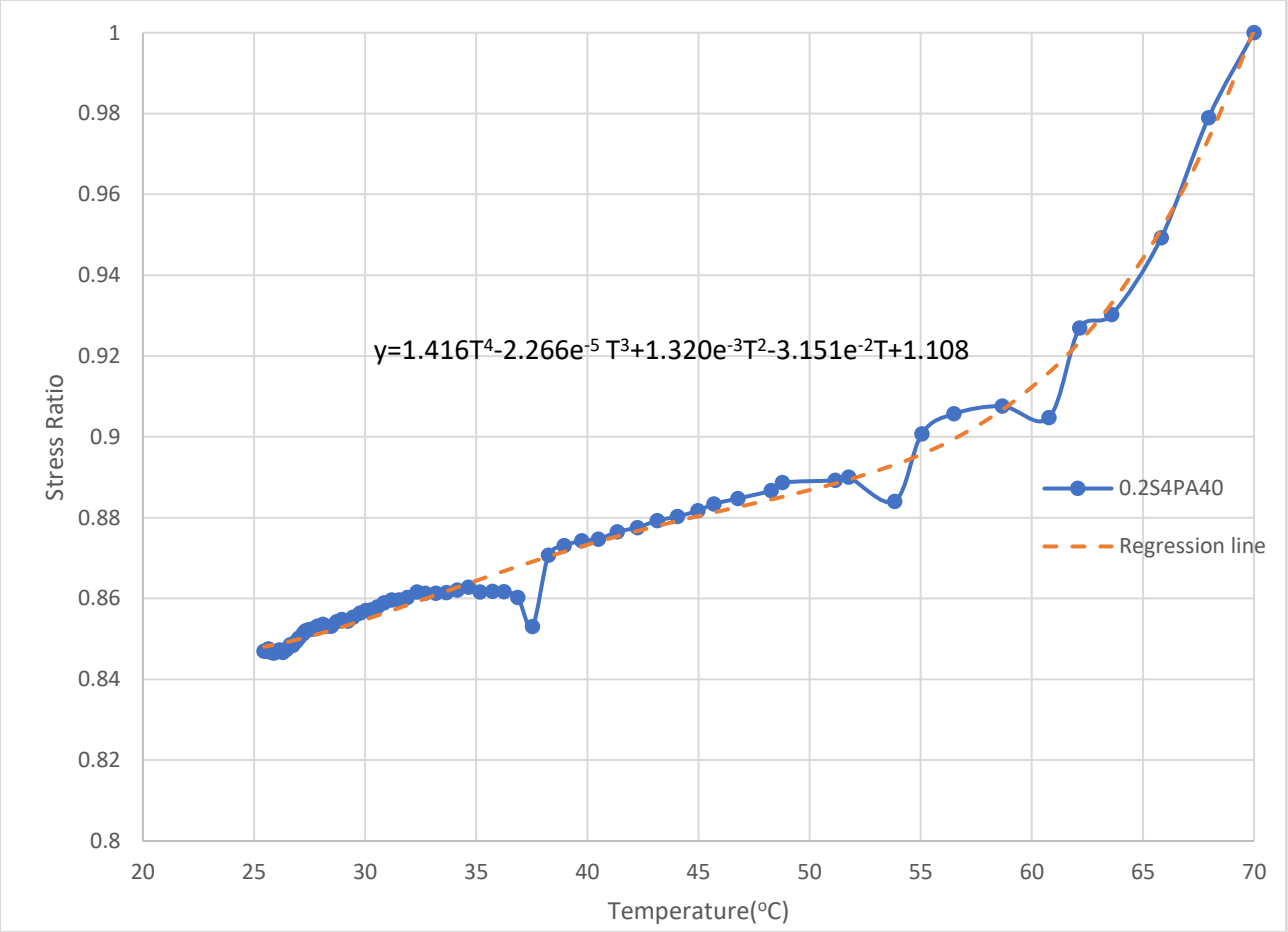

Figure 5.10: The experiment data and regression line of 0.2SPA40 for the stress reduction

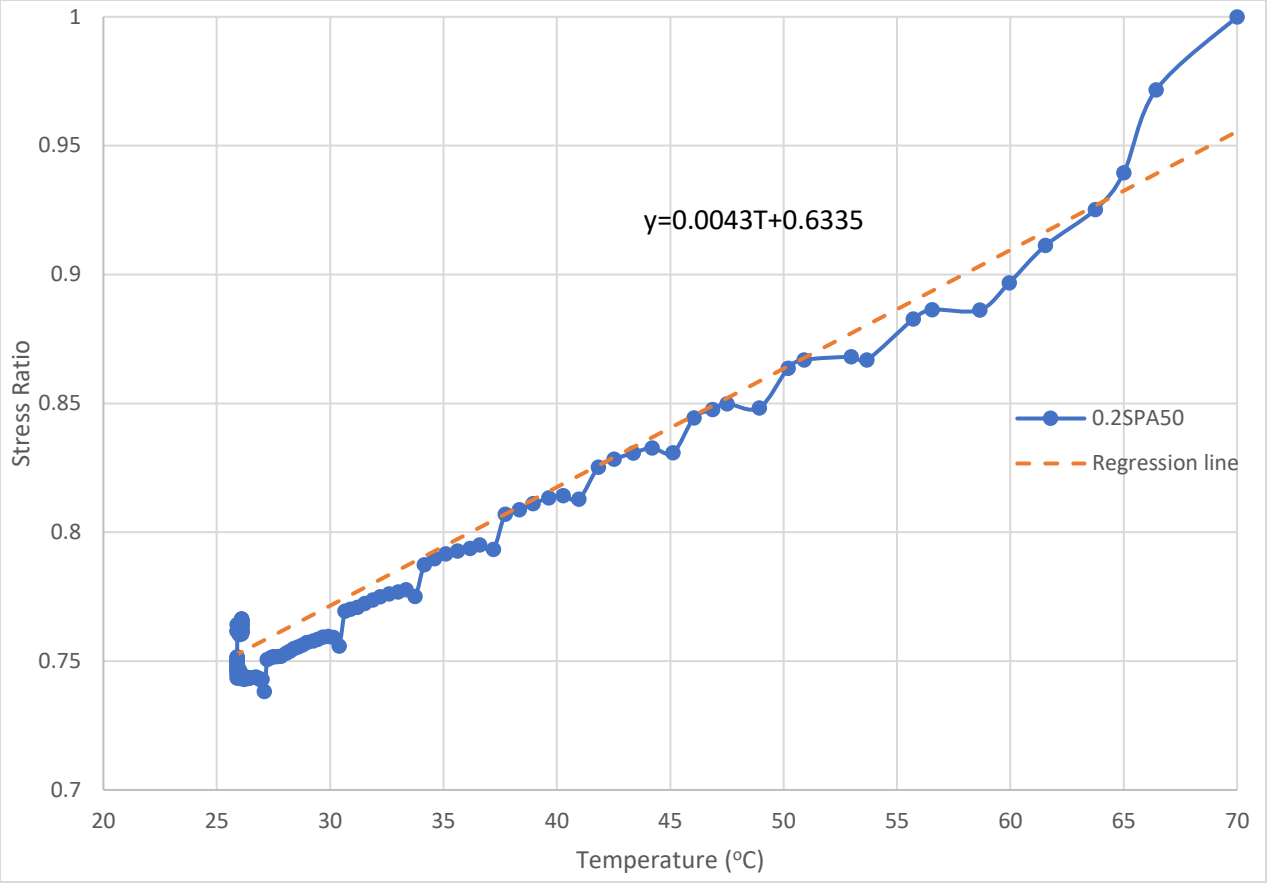

Figure 5.11: The experiment data and regression line of 0.2SPA40 for the stress reduction

5.2 Implementation and Validation of Shape Memory Behaviours Prediction Model

The shape memory prediction model of prevulcanised SMNR is examined under Matlab with the material coefficients shown in Table 5.2 and their validation condition summarised in Table 5.3. Due to machine limitations, real-time stress-strain behaviour during the shape memory experiment is not available. To model the shape memory behaviours, the experimental stress behaviours of the entire shape memory process are collected from the results of the mechanical response experiment, which tensile test at the temperature of 70°C (initial deformation process) and stress relaxation with temperature change (programming process). The remaining material coefficients, C_f and C_r are obtained during the model validation process. The comparison of the experimental modelling results for each prevulcanised SMNR is shown from Figure 5.12 to Figure 5.15.

Table 5.3: The validation condition for shape memory prediction model

Shape Memory Process	Strain	Stress (MPa)	Temperature	Duration (s)
Deformation Process	0→2	0→σ_{TH}	70°C→70°C	24
Programming Process	2→2	σ_{TH}→σ_{SR}	70°C→0°C	180
Unloading Process	Free	σ_{SR}→0	0°C→0°C	120
Recovery Process	Free	0→0	0°→70°C	180

where σ_{TH} is stress value under the deformed strain of 200% at the temperature of 70°C, σ_{SR} is the stress value measured from the stress reduction equation.

By observing the stress-strain behaviour graph of each specimen, it shows that the shape memory behaviours prediction model is capable of modeling the experimental stress-strain results. Rather than just inspecting the total strain behaviour of SMP by phenomenological approach, the model measured the respective segment strains by stress behaviour obtained during the mechanical

response experiments. Hence, the duplicated stress behaviour of experimental and modelling results is shown in Figure 5.12b, Figure 5.13b, Figure 5.14b, and Figure 5.15b.

Moreover, this constitutive model has successfully reflected the component effect of each specimen group. By measuring the volume fraction of composition, the strain response of each segment phase is demonstrated in the strain evolution graphs (Figure 5.12d, Figure 5.13d, Figure 5.14d, and Figure 5.15d). Compared to the strain evolution graphs for each prevulcanised group, the deformed strain in both soft segments increases with the palmitic acid content. For example, the maximum deformed strain of the soft frozen segment phase is 37.87% in 0.2SPA50, while the least deformed strain in the soft frozen segment phase is found at 0.2SPA20, which has 19.67%. Due to the formation of the soft segment phase as a result of increased palmitic acid loading, more deformed strain is generated by the soft segment phase under the same stress level

Although the model accurately predicted the stress-strain behaviour of prevulcanised SMNR, it did not adequately capture the shape fixity. Table 5.4 shows the shape memory parameters obtained from experimental and modelling results under 200% deformed strain. It is clearly shown that only the 0.2SPA20 has similar shape memory parameters for experimental and modelling results. Although both shape recovery values from experimental and modelling are close, there are huge discrepancies in shape fixity for other prevulcanised SMNR specimen (0.2SPA30, 0.2SPA40 AND 0.2SPA50) at Table 5.4. According to the strain evolution graph (Figure 5.12d, Figure 5.13d, Figure 5.14d, and Figure 5.15d), the thermal strain and the hard segment strain are responsible for shape fixity values. Due to zero stress on the unloading process, the majority of the deformed strain is preserved by the thermal strain and hard segment strain. Nevertheless, the hard segment is governed by the viscoelastic model, which the strain is recovering with time. Beside a suddenly decrease on the strain response of hard segment phase (due to unloading process), the

strain is recovered slowly over time and the recovery behaviour is irrelevant to the temperature change. With the consequence, partly of the hard segment is started to restore before reheating process. The shape fixity of numerical model is increasing with the palmitic acid content (the total volume faction of the soft segment) but the gap between experimental and simulation result still stand a large difference on the shape recovery. Hence, an external thermally sensitive model is required to consistently simulate the recovery strain after unloading process.

Table 5.4: Comparison of experiment result and simulation result in shape memory parameters

	Experiment result		Simulation result	
Sample Code	Shape Fixity	Shape Recovery	Shape Fixity	Shape Recovery
0.2SPA20	56%	91%	57%	100%
0.2SPA30	94%	94%	62%	94%
0.2SPA40	92%	92%	64%	95%
0.2SPA50	85%	85%	64%	95%

With the agreement of the thermal strain model, the recovery process is started as the temperature reaches the phase transition temperature (>40^{o}C). Compared with other segment strains, thermal strain retains the highest deformed strain during the programming process. In consequence, a swiftly recovering process is exhibited once the temperature reaches the phase transition temperature. Although the shape fixity can be simply adjusted by increasing the C_f value, it will ruin the strain balancing at the programming stage. Thereby, the improvement on the thermal coefficient model, which changes to a non-linear algorithm, will be the future work for this project.

Other than the limitation on the thermal model, another factor that is the stress relaxation experiment issue might lead to the incorrect shape fixity value obtained in the modelling results.

Due to the machine limitation, the stress relaxation experiment is done at a low strain value (1.5%) within the temperature range of 25^{o}C to 70^{o}C. This might influence the accuracy of the stress ratio calculation due to the difference between the strain ratio and testing temperature (experimental setting is 200% at 0^{o}C to 70^{o}C). To overcome this issue, the real-time stress-strain behaviour during shape memory experiments should be obtained in the future research works.

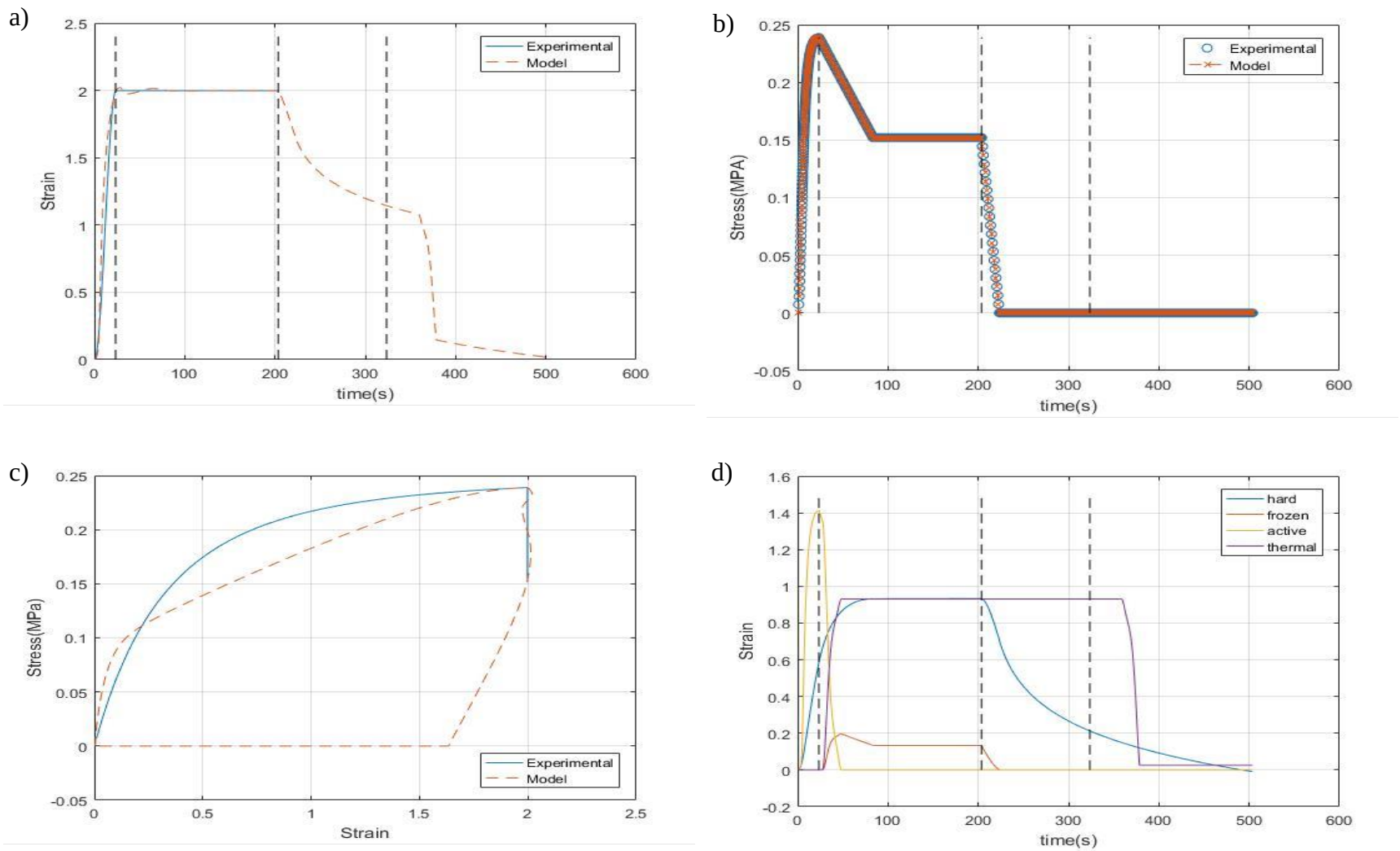

Figure 5.12: Comparison of the experimental data and prediction model at (a) total strain behaviour, (b) stress behaviour and (c) stress-strain behaviour, and d) the respective segment strain in 0.2SPA20 (C_f =0.75 and C_r=0.9)

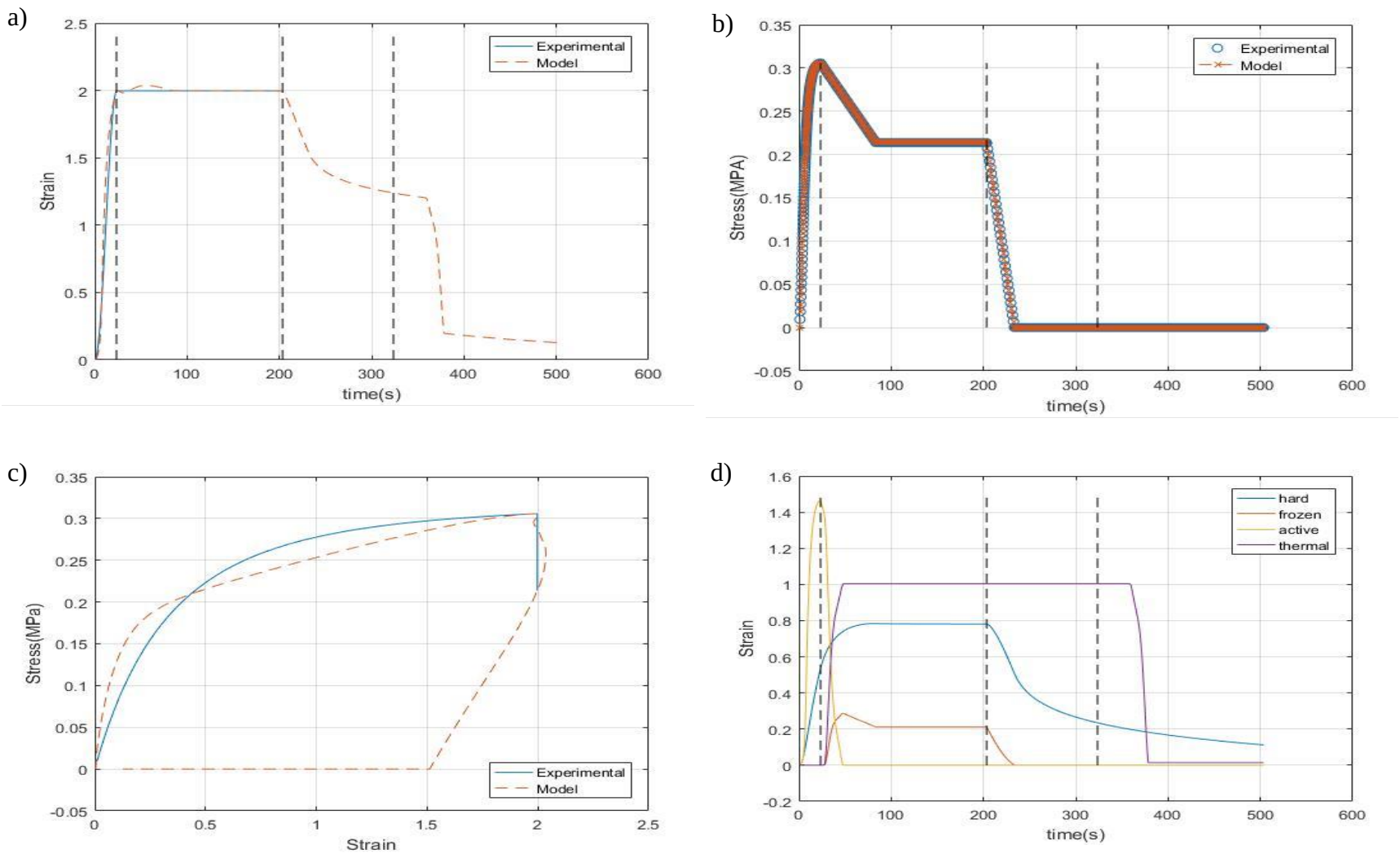

Figure 5.13: Comparison of the experimental data and prediction model at (a) total strain behaviour, (b) stress behaviour and (c) stress-strain behaviour, and d) the respective segment strain in 0.2SPA30 (C_f =0.8 and C_r=1)

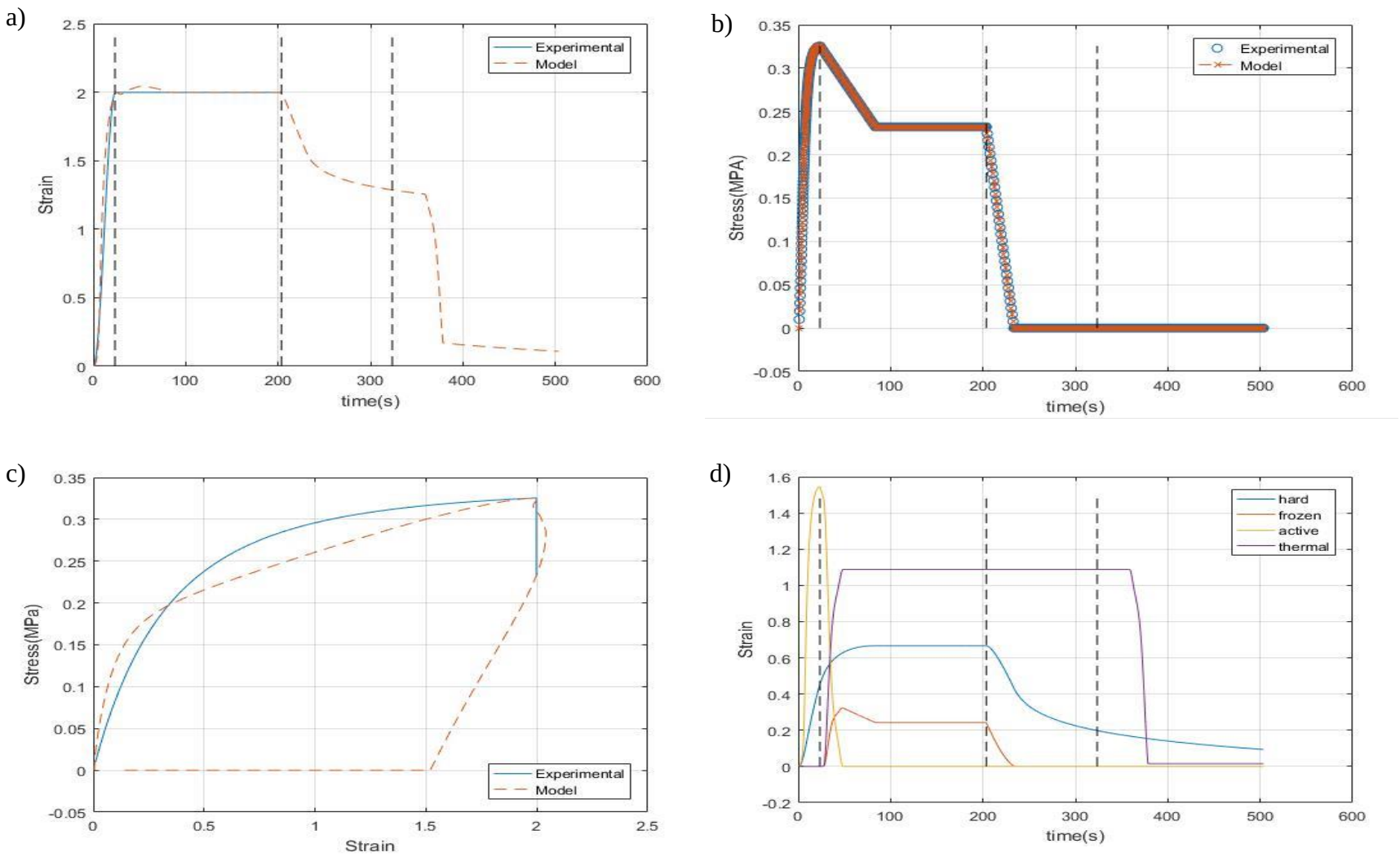

Figure 5.14: Comparison of the experimental data and prediction model at (a) total strain behaviour, (b) stress behaviour and (c) stress-strain behaviour, and d) the respective segment strain in 0.2SPA40 (C_f =0.8 and C_r=1)

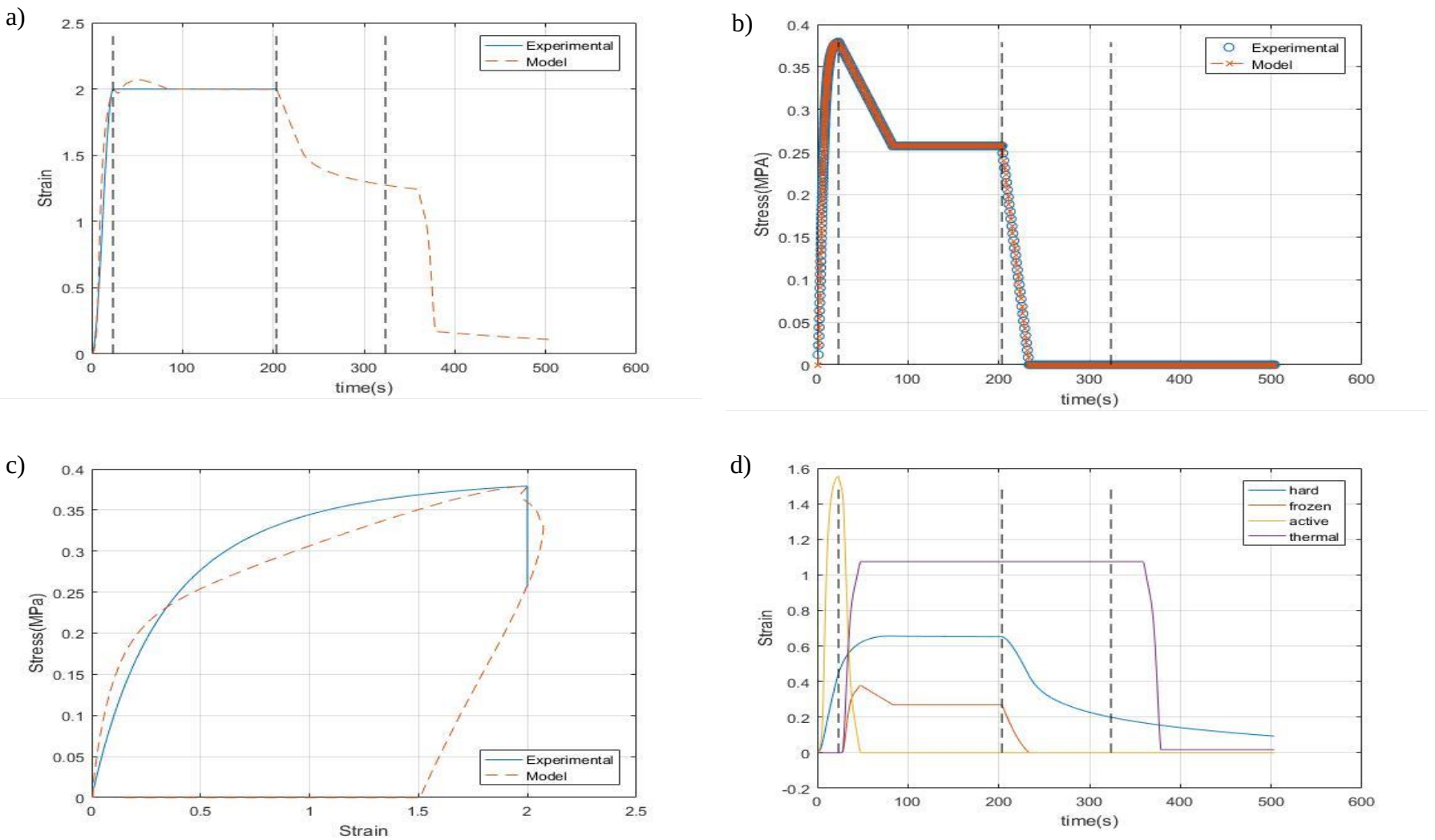

Figure 5.15: Comparison of the experimental data and prediction model at (a) total strain behaviour, (b) stress behaviour and (c) stress-strain behaviour, and d) respective segment strain in 0.2SPA50 (C_f =0.8 and C_r=1)

6 Conclusion and Future works

6.1 Contributions of Present Works

To conclude, the objectives layout in Chapter 1 have been achieved, and the findings are detailed as follow:

1. Development of a thermal responsive palmitic acid-based SMNR:

   A novel SMNR fabrication technique was developed based on prevulcanisation process. Compared with swollen SMNR, the prevulcanised SMNR possesses the shape memory capability with reduced palmitic acid loadings. Instead of the permeability issue from the swelling temperature and crosslink density, the palmitic acid content of the prevulcanised SMNR was adjusted by the concentration of potassium palmitate under dispersion mixing. Different fatty acid content was considered in the T_c experiment. It was found that the T_c of the SME was correlated to the choice of the fatty acid and is also influenced by the homogeneity of fatty acid in the rubber molecular. Various crosslink densities on swollen SMNR and prevulcanised SMNR were inspected, but T_c was irrelevant to sulphur content.

2. Characterisation of the shape memory response of SMNR

   A custom-made stretching apparatus was developed to measure the shape fixity and shape recovery of the SMNR under stain-control mode. The test device validated the SME of SMNR under uniaxial tensile mode with various deformed strains. To fulfill the shape memory experiment testing condition, the tensile device was designed with high portability and lightweight for transferring the SMNR specimen into the desired testing environment, such as different testing temperature ranges. The preliminary shape memory experiments were conducted on swollen SMNR to standardise the deformed strain for validating SME in prevulcanised SMNR. The shape memory experiments of prevulcanised SMNR under 200% of deformed strain were conducted with three different experimental settings: different formulations, various working temperatures, and shape memory cycle test.

2.1. Effect of the SMNR formulation on the shape memory capability:

The test was conducted under prevulcanised SMNR with various sulphur content and palmitic acid loading. It was found that increasing the palmitic acid amount could improve the shape fixity by converting the residue strain to a reversible strain, but high sulphur content confined the shape fixity. At the same time, the shape recovery was enhanced by increasing reversible strain resulting from increasing sulphur content and palmitic acid.

2.2 Effect of working temperatures on the shape memory capability:

The SME of prevulcanised SMNR corresponded to the testing temperature, which tuneable SME is feasible by manipulating the working temperature. It was found that by increasing the T_p and T_r, higher shape memory performance was exhibited. Both working temperatures significantly influenced the respective shape memory parameter. For example, higher shape fixity as the T_p was near T_c whereas higher shape recovery was exhibited as the temperature gap between the T_c and T_r is small.

2.3 Effect of shape memory cycle on the shape memory capability

Under the shape memory cyclic test, it was observed that the shape fixity was decreased with increasing the number of cycles. Due to the potassium palmitate was soluble in water, the palmitic acid amount in prevulcanised SMNR was lost during the programming and quenching process in the cycle test. Less retaining force was generated to secure the temporary shape, which led to more deformed strain being recovered instantly upon removal of the load.

3. Characterisation of the mechanical response of the SMNR

The stress-strain behaviour during the deformed was investigated under uniaxial tensile mode at room temperature and temperature of 70^{o}C. It was found that the prevulcanised SMNR possessed the hyperelastic behaviour at room temperature. Although the tensile modulus at room temperature increased with the palmitic acid

content, the elongation at break was reduced. For the tensile test at high temperature range, it was found that the specimen experienced brittle-to ductile transition after it reached 50% deformed strain, but no elongation at break was spotted even the elongation strain increased to 500%. The viscoelastic response and SME were exhibited during the stress relaxation experiment. The stress relaxation mode with temperature ramp was conducted in DMA to investigate the stress reduction on temperature change. It was found that the stress behaviour corresponds to the temperature change when the strain was constrained in a fixed value.

4. Development of a shape memory behaviours prediction model in SMNR

The shape memory behaviour modelling of prevulcanised SMNR was simulated by mechanical and thermal approaches using a combination algorithm. A SLS model with Kelvin-Voigt element extended with two Mooney Rivlin models and a thermal strain model were adopted to model the shape memory behaviour. The prediction model was capable of modelling the stress-strain response contributed by each segment phase during the shape memory process.

6.2 Suggestion for Future Works

Based on the experimental results, it is suggested that further improvement on the shape memory repeatability and the shape fixity with high sulphur content are needed. The suggestion will aid in extending the application of prevulcanised SMNR and further investigate the other shape memory feature such as self-healing properties and multiple way SME. This can be done by redesigning the chemical structure or the linkage between the palmitic acid and rubber molecular. To obtain the real time stress strain behaviours during shape memory experiment, a flexible and reliable automatic testing machine with a combination of the stretching apparatus and temperature monitoring feature is suggested. This can minimize human error and investigate the SIC formation

on each shape memory process. Although this action can be done by modifying the current custom-made stretching machine, the accuracy and consistency of the result are difficult to guarantee.

The constitutive model is established on the shape memory behaviour prediction modeling under the linear mechanical response models: SLS and Mooney Rivlin equation and thermal responsive strain. The nonlinear model development and further thermal response validation are required, such as the shape memory response on various heating and quenching rates. The nonlinear models could reduce those parameters involved in the model and have a more precise shape memory behaviour prediction algorithm. Other rubber behaviours such as Mullin's effect and hysteresis could also be considered in the model algorithm in the future.

7 References

[1] D. Tarniţă, D. N. Tarniţă, N. Bîzdoacă, I. Mîndrilă, and M. Vasilescu, "Properties and medical applications of shape memory alloys," *Rom. J. Morphol. Embryol.*, vol. 50, no. 1, pp. 15–21, 2008.

[2] N. B. Morgan, "Medical shape memory alloy applications - The market and its products," *Mater. Sci. Eng. A*, vol. 378, no. 1-2 SPEC. ISS., pp. 16–23, 2004, doi: 10.1016/j.msea.2003.10.326.

[3] L. Petrini and F. Migliavacca, "Biomedical Applications of Shape Memory Alloys," *J. Metall.*, vol. 2011, no. Figure 1, pp. 1–15, 2011, doi: 10.1155/2011/501483.

[4] L. Sun *et al.*, "A brief review of the shape memory phenomena in polymers and their typical sensor applications," *Polymers (Basel).*, vol. 11, no. 6, 2019, doi: 10.3390/polym11061049.

[5] M. A. A. Kazemi-Lari, A. D. Dostine, J. Zhang, A. S. Wineman, and J. A. Shaw, "Robotic jellyfish actuated with a shape memory alloy spring," in *Bioinspiration, Biomimetics, and Bioreplication IX*, 2019, vol. 10965, pp. 1–17, doi: 10.1117/12.2513456.

[6] W. Wu *et al.*, "Snake-Inspired, Nano-Stepped Surface with Tunable Frictional Anisotropy Made from a Shape-Memory Polymer for Unidirectional Transport of Microparticles," *Adv. Funct. Mater.*, vol. 31, no. 19, 2021, doi: 10.1002/adfm.202009611.

[7] K. Saito, K. Iwata, Y. Ishihara, K. Sugita, M. Takato, and F. Uchikoba, "Miniaturized rotary actuators using shape memory alloy for insect-type MEMS microrobot," *Micromachines*, vol. 7, no. 4, pp. 1–11, 2016, doi: 10.3390/mi7040058.

[8] W. Yuan *et al.*, "Stress-free two-way shape memory effects of semicrystalline polymer networks enhanced by self-nucleated crystallization," *ACS Macro Lett.*, vol. 9, no. 9, pp. 1325–1331, 2020, doi: 10.1021/acsmacrolett.0c00571.

[9] P. S. Yao, H. Y. Huang, Y. J. Su, and J. X. Xie, "Two-way shape memory effect induced by tensile deformation in columnar-grained Cu71.7Al18.1Mn10.2 Alloy," *Materials (Basel).*, vol. 11, no. 11, 2018, doi: 10.3390/ma11112109.

[10] G. Chen *et al.*, "Converse two-way shape memory effect through a dynamic covalent network design," *J. Mater. Chem. A*, vol. 10, no. 19, pp. 10350–10354, 2022, doi: 10.1039/d2ta01540d.

[11] X. Xiao, T. Xie, and Y. T. Cheng, "Self-healable graphene polymer composites," *J. Mater. Chem.*, vol. 20, no. 17, pp. 3508–3514, 2010, doi: 10.1039/c0jm00307g.

[12] R. P. Wool, "Self-healing materials: A review," *Soft Matter*, vol. 4, no. 3, pp. 400–418, 2008, doi: 10.1039/b711716g.

[13] M. D. Hager, P. Greil, C. Leyens, S. Van Der Zwaag, and U. S. Schubert, "Self-healing materials," *Adv. Mater.*, vol. 22, no. 47, pp. 5424–5430, Dec. 2010, doi: 10.1002/ADMA.201003036.

[14] Y. Yang, X. Ding, and M. W. Urban, "Chemical and physical aspects of self-healing materials," *Prog. Polym. Sci.*, vol. 49–50, pp. 34–59, 2015, doi: 10.1016/j.progpolymsci.2015.06.001.

[15] M. Scheiner, T. J. Dickens, and O. Okoli, "Progress towards self-healing polymers for composite structural applications," *Polymer (Guildf).*, vol. 83, pp. 260–282, 2016, doi:

10.1016/j.polymer.2015.11.008.

[16] H. M. Jonkers, A. Thijssen, G. Muyzer, O. Copuroglu, and E. Schlangen, “Application of bacteria as self-healing agent for the development of sustainable concrete,” *Ecol. Eng.*, vol. 36, no. 2, pp. 230–235, 2010, doi: 10.1016/j.ecoleng.2008.12.036.

[17] F. B. Silva, N. Boon, N. De Belie, and W. Verstraete, “Industrial application of biological self-healing concrete: Challenges and economical feasibility,” *J. Commer. Biotechnol.*, vol. 21, no. 1, pp. 31–38, 2015, doi: 10.5912/jcb662.

[18] Y. Cheng, X. Xiao, K. Pan, and H. Pang, “Development and application of self-healing materials in smart batteries and supercapacitors,” *Chem. Eng. J.*, vol. 380, no. May 2019, p. 122565, 2020, doi: 10.1016/j.cej.2019.122565.

[19] M. A. Zainal and M. S. Mohamed Ali, “Wireless shape memory polymer microactuator for implantable drug delivery aplication,” *IECBES 2016 - IEEE-EMBS Conf. Biomed. Eng. Sci.*, pp. 76–79, 2016, doi: 10.1109/IECBES.2016.7843418.

[20] F. Liang, R. Sivilli, J. Gou, Y. Xu, and B. Mabbott, “Electrical actuation and shape recovery control of shape-memory polymer nanocomposites,” *Int. J. Smart Nano Mater.*, vol. 4, no. 3, pp. 167–178, 2013, doi: 10.1080/19475411.2013.837846.

[21] X. Wu, W. M. Huang, Y. Zhao, Z. Ding, C. Tang, and J. Zhang, “Mechanisms of the shape memory effect in polymeric materials,” *Polymers (Basel).*, vol. 5, no. 4, pp. 1169–1202, 2013, doi: 10.3390/polym5041169.

[22] C. M. Yakacki, R. Shandas, D. Safranski, A. M. Ortega, K. Sassaman, and K. Gall, “Strong, tailored, biocompatible shape-memory polymer networks,” *Adv. Funct. Mater.*, vol. 18, no.

16, pp. 2428–2435, Aug. 2008, doi: 10.1002/ADFM.200701049.

[23] J. J. Song, H. H. Chang, and H. E. Naguib, “Biocompatible shape memory polymer actuators with high force capabilities,” *Eur. Polym. J.*, vol. 67, pp. 186–198, 2015, doi: 10.1016/j.eurpolymj.2015.03.067.

[24] J. J. Song, H. H. Chang, and H. E. Naguib, “Design and characterization of biocompatible shape memory polymer (SMP) blend foams with a dynamic porous structure,” *Polymer (Guildf).*, vol. 56, pp. 82–92, 2015, doi: 10.1016/j.polymer.2014.09.062.

[25] C. N. Aiza Jaafar, I. Zainol, N. S. Ishak, R. A. Ilyas, and S. M. Sapuan, “Effects of the liquid natural rubber (LNR) on mechanical properties and microstructure of epoxy/silica/kenaf hybrid composite for potential automotive applications,” *J. Mater. Res. Technol.*, vol. 12, pp. 1026–1038, 2021, doi: 10.1016/j.jmrt.2021.03.020.

[26] T. T. Nga Dang, J. K. Kim, and K. J. Kim, “Organo bifunctional silane effects on the vibration, thermal, and mechanical properties of a vinyl-group-containing silicone rubber/natural rubber/silica compound,” *J. Vinyl Addit. Technol.*, vol. 16, no. 4, pp. 254–260, Dec. 2010, doi: 10.1002/VNL.20240.

[27] G. Craciun, E. Manaila, and M. D. Stelescu, “New elastomeric materials based on natural rubber obtained by electron beam irradiation for food and pharmaceutical use,” *Materials (Basel).*, vol. 9, no. 12, 2016, doi: 10.3390/ma9120999.

[28] N. B. M. Azahar, N. B. A. Hassan, R. P. Jaya, M. A. B. A. Kadir, N. Z. B. M. Yunus, and M. Z. H. Mahmud, “An overview on natural rubber application for asphalt modification,” *Int. J. Agric. For. Plant.*, vol. 2, pp. 212–218, 2016.

[29] M. Coja and L. Kari, “Using waveguides to model the dynamic stiffness of pre-compressed natural rubber vibration isolators,” *Polymers (Basel).*, vol. 13, no. 11, 2021, doi: 10.3390/polym13111703.

[30] C. W. Lee, I. H. Kim, and H. J. Jung, “Fabrication and Characterization of Natural Rubber-Based Magnetorheological Elastomers at Large Strain for Base Isolators,” *Shock Vib.*, vol. 2018, 2018, doi: 10.1155/2018/7434536.

[31] X. Xu, H. Wang, Y. Sun, J. Han, and R. Huang, “Sound absorbing properties of perforated composite panels of recycled rubber, fiberboard sawdust, and high density polyethylene,” *J. Clean. Prod.*, vol. 187, pp. 215–221, 2018, doi: 10.1016/j.jclepro.2018.03.174.

[32] M. I. Seth A Rahim, K. V. Horoshenkov, J. Rongong, H. Ahmadi, and J. Picken, “Epoxidized natural rubber for vibro-acoustic isolation,” *Polym. Test.*, vol. 67, no. February, pp. 92–98, 2018, doi: 10.1016/j.polymertesting.2018.02.018.

[33] J. Weisman and G. P. Warn, “Stability of Elastomeric and Lead-Rubber Seismic Isolation Bearings,” *J. Struct. Eng.*, vol. 138, no. 2, pp. 215–223, 2012, doi: 10.1061/(asce)st.1943-541x.0000459.

[34] X. D. Nguyen and L. Guizani, “Analytical and numerical investigation of natural rubber bearings incorporating U-shaped dampers behaviour for seismic isolation,” *Eng. Struct.*, vol. 243, no. January, p. 112647, 2021, doi: 10.1016/j.engstruct.2021.112647.

[35] D. Rus and M. T. Tolley, “Design, fabrication and control of soft robots,” *Nature*, vol. 521, no. 7553, pp. 467–475, 2015, doi: 10.1038/nature14543.

[36] A. A. Khin, R. L. L. Bin, S. B. Kai, K. L. L. Teng, and F. Y. Chiun, “Challenges of the

Export for Natural Rubber Latex in the ASEAN Market," *IOP Conf. Ser. Mater. Sci. Eng.*, vol. 548, no. 1, 2019, doi: 10.1088/1757-899X/548/1/012024.

[37] P. E. Hurley, "History of Natural Rubber," *J. Macromol. Sci. Part A - Chem.*, vol. 15, no. 7, pp. 1279–1287, 1981, doi: 10.1080/00222338108056785.

[38] E. R. Grilli, "Natural rubber: a better future? - After the rise of oil prices, the economics of natural production have changed for the better vis-a-vis petroleum-based synthetics," *Finance Dev.*, vol. 0018, no. 002, Jun. 1981, doi: 10.5089/9781616353452.022.A008.

[39] S. Petsri, A. Chidthaisong, N. Pumijumnong, and C. Wachrinrat, "Greenhouse gas emissions and carbon stock changes in rubber tree plantations in Thailand from 1990 to 2004," *J. Clean. Prod.*, vol. 52, pp. 61–70, 2013, doi: 10.1016/j.jclepro.2013.02.003.

[40] Y. Jing-Cheng, H. Jian-Hui, T. Jian-Wei, P. Qing-Min, and H. Xing-Guo, "Carbon Sequestration in Rubber Tree Plantations Established on Former Arable Lands in Xishuangbanna, Sw China," *Chinese J. Plant Ecol.*, vol. 29, no. 2, pp. 296–303, 2005, doi: 10.17521/cjpe.2005.0038.

[41] W. Jawjit, C. Kroeze, and S. Rattanapan, "Greenhouse gas emissions from rubber industry in Thailand," *J. Clean. Prod.*, vol. 18, no. 5, pp. 403–411, 2010, doi: 10.1016/j.jclepro.2009.12.003.

[42] M. Kawano, "Changing Resource-Based Manufacturing Industry: The Case of the Rubber Industry in Malaysia and Thailand," in *Emerging Challenges for Emerging States*, 2019, pp. 145–162.

[43] F. Katzenberg and J. C. Tiller, "Shape memory natural rubber," *J. Polym. Sci. Part B Polym.*

Phys., vol. 54, no. 14, pp. 1381–1388, 2016, doi: 10.1002/polb.24040.

[44] J. M. Chenal, C. Gauthier, L. Chazeau, L. Guy, and Y. Bomal, "Parameters governing strain induced crystallization in filled natural rubber," *Polymer (Guildf).*, vol. 48, no. 23, pp. 6893–6901, 2007, doi: 10.1016/j.polymer.2007.09.023.

[45] S. Toki, T. Fujimaki, and M. Okuyama, "Strain-induced crystallization of natural rubber as detected real-time by wide- angle X-ray diffraction technique," *Polymer (Guildf).*, vol. 41, no. 14, pp. 5423–5429, 2000, doi: 10.1016/S0032-3861(99)00724-7.

[46] B. Huneau, "Strain-induced crystallization of natural rubber: A review of X-Ray diffraction investigations," *Rubber Chemistry and Technology*, vol. 84, no. 3. pp. 425–452, 2011, doi: 10.5254/1.3601131.

[47] X. Zhang, T. Lin, Z. Tang, K. Sun, and B. Guo, "Sustainable shape memory polymers based on epoxidized natural rubber cured by zinc ferulate via oxa-Michael reaction," *Int. J. Smart Nano Mater.*, vol. 6, no. 4, pp. 1–16, 2016, doi: 10.1080/19475411.2015.1129368.

[48] M. Pantoja, Z. Lin, M. Cakmak, and K. A. Cavicchi, "Structure–property relationships of fatty acid swollen, crosslinked natural rubber shape memory polymers," *J. Polym. Sci. Part B Polym. Phys.*, vol. 56, no. 8, pp. 673–688, 2018, doi: 10.1002/polb.24578.

[49] T. Lin, S. Ma, Y. Lu, and B. Guo, "New Design of Shape Memory Polymers Based on Natural Rubber Crosslinked via Oxa-Michael Reaction," *ACS Appl. Mater. Interfaces*, vol. 6, no. 8, pp. 5695–5703, 2014, doi: 10.1021/am500236w.

[50] A. Chakrabarti and S. R. Barman, "Theoretical prediction of shape memory behavior and ferrimagnetism in Mn2 NiIn," *Appl. Phys. Lett.*, vol. 94, no. 16, pp. 1–4, 2009, doi:

10.1063/1.3116618.

[51] S. R. Barman *et al.*, “Theoretical prediction and experimental study of a ferromagnetic shape memory alloy: Ga2MnNi,” *Phys. Rev. B - Condens. Matter Mater. Phys.*, vol. 78, no. 13, pp. 1–6, 2008, doi: 10.1103/PhysRevB.78.134406.

[52] M. Mehrpouya, A. Gisario, A. Rahimzadeh, M. Nematollahi, K. S. Baghbaderani, and M. Elahinia, “A prediction model for finding the optimal laser parameters in additive manufacturing of NiTi shape memory alloy,” *Int. J. Adv. Manuf. Technol.*, vol. 105, no. 11, pp. 4691–4699, 2019, doi: 10.1007/s00170-019-04596-z.

[53] E. Camposilvan, O. Torrents, and M. Anglada, “Small-scale mechanical behavior of zirconia,” *Acta Mater.*, vol. 80, pp. 239–249, 2014, doi: 10.1016/j.actamat.2014.07.053.

[54] X. M. Zeng, A. Lai, C. L. Gan, and C. A. Schuh, “Crystal orientation dependence of the stress-induced martensitic transformation in zirconia-based shape memory ceramics,” *Acta Mater.*, vol. 116, pp. 124–135, 2016, doi: 10.1016/j.actamat.2016.06.030.

[55] E. Moshkelgosha and M. Mamivand, “Phase field modeling of crack propagation in shape memory ceramics – Application to zirconia,” *Comput. Mater. Sci.*, vol. 174, no. December 2019, p. 109509, 2020, doi: 10.1016/j.commatsci.2019.109509.

[56] A. Firouzeh, M. Salerno, and J. Paik, “Stiffness Control with Shape Memory Polymer in Underactuated Robotic Origamis,” *IEEE Trans. Robot.*, vol. 33, no. 4, pp. 765–777, 2017, doi: 10.1109/TRO.2017.2692266.

[57] T. Mu, L. Liu, X. Lan, Y. Liu, and J. Leng, “Shape memory polymers for composites,” *Compos. Sci. Technol.*, vol. 160, pp. 169–198, 2018, doi:

10.1016/j.compscitech.2018.03.018.

[58] T. A. Schroeder and C. M. Wayman, “The two-way shape memory effect and other ‘training’ phenomena in CuZn single crystals,” *Scr. Metall.*, vol. 11, no. 3, pp. 225–230, 1977, doi: 10.1016/0036-9748(77)90058-8.

[59] L. Sun *et al.*, “Stimulus-responsive shape memory materials: A review,” *Mater. Des.*, vol. 33, no. 1, pp. 577–640, 2012, doi: 10.1016/j.matdes.2011.04.065.

[60] I. R. Crystal, A. Lai, and C. A. Schuh, “Cyclic martensitic transformations and damage evolution in shape memory zirconia: Single crystals vs polycrystals,” *J. Am. Ceram. Soc.*, vol. 103, no. 8, pp. 4678–4690, 2020, doi: 10.1111/jace.17117.

[61] Z. Du, X. M. Zeng, Q. Liu, C. A. Schuh, and C. L. Gan, “Superelasticity in micro-scale shape memory ceramic particles,” *Acta Mater.*, vol. 123, pp. 255–263, 2017, doi: 10.1016/j.actamat.2016.10.047.

[62] Z. Du *et al.*, “Size effects and shape memory properties in ZrO2 ceramic micro- and nano-pillars,” *Scr. Mater.*, vol. 101, pp. 40–43, 2015, doi: 10.1016/j.scriptamat.2015.01.013.

[63] J. Mohd Jani, M. Leary, A. Subic, and M. A. Gibson, “A review of shape memory alloy research, applications and opportunities,” *Mater. Des.*, vol. 56, pp. 1078–1113, 2014, doi: 10.1016/j.matdes.2013.11.084.

[64] M. Ahmad *et al.*, “High Performance Shape Memory Polyurethane Synthesized with High Molecular Weight Polyol as the Soft Segment,” *Appl. Sci.*, vol. 2, no. 4, pp. 535–548, 2012, doi: 10.3390/app2020535.

[65] D. Ratna and J. Karger-Kocsis, “Recent advances in shape memory polymers and

composites: A review," *J. Mater. Sci.*, vol. 43, no. 1, pp. 254–269, 2008, doi: 10.1007/s10853-007-2176-7.

[66] X. Huang, M. Panahi-Sarmad, K. Dong, R. Li, T. Chen, and X. Xiao, "Tracing evolutions in electro-activated shape memory polymer composites with 4D printing strategies: A systematic review," *Compos. Part A Appl. Sci. Manuf.*, vol. 147, p. 106444, 2021, doi: 10.1016/j.compositesa.2021.106444.

[67] H. Koerner, G. Price, N. A. Pearce, M. Alexander, and R. A. Vaia, "Remotely actuated polymer nanocomposites - Stress-recovery of carbon-nanotube-filled thermoplastic elastomers," *Nat. Mater.*, vol. 3, no. 2, pp. 115–120, 2004, doi: 10.1038/nmat1059.

[68] H. Meng and G. Li, "A review of stimuli-responsive shape memory polymer composites," *Polym. (United Kingdom)*, vol. 54, no. 9, pp. 2199–2221, 2013, doi: 10.1016/j.polymer.2013.02.023.

[69] Q. Meng and J. Hu, "A review of shape memory polymer composites and blends," *Compos. Part A Appl. Sci. Manuf.*, vol. 40, no. 11, pp. 1661–1672, 2009, doi: 10.1016/j.compositesa.2009.08.011.

[70] C. Liu, H. Qin, and P. T. Mather, "Review of progress in shape-memory polymers," *J. Mater. Chem.*, vol. 17, no. 16, pp. 1543–1558, 2007, doi: 10.1039/b615954k.

[71] D. Bartels *et al.*, "Defence R & D Canada," *Atlantic*, no. August, pp. 1–51, 2002, doi: 10.1080/10242690213507.

[72] J. Cederström, J. Van Humbeeck, J. Cederström, and J. Van Humbeeck, "Relationship Between Shape Memory Material Properties and Applications," 1995.

[73] M. Behl and A. Lendlein, “Shape-memory polymers,” *Mater. Today*, vol. 10, no. 4, pp. 20–28, 2007, doi: 10.1016/S1369-7021(07)70047-0.

[74] T. Chung, A. Romo-Uribe, and P. T. Mather, “Two-way reversible shape memory in a semicrystalline network,” *Macromolecules*, vol. 41, no. 1, pp. 184–192, 2008, doi: 10.1021/ma071517z.

[75] I. Bellin, S. Kelch, and A. Lendlein, “Dual-shape properties of triple-shape polymer networks with crystallizable network segments and grafted side chains,” *J. Mater. Chem.*, vol. 17, no. 28, pp. 2885–2891, 2007, doi: 10.1039/b702524f.

[76] I. Bellin, S. Kelch, R. Langer, and A. Lendlein, “Polymeric triple-shape materials,” *Proc. Natl. Acad. Sci. U. S. A.*, vol. 103, no. 48, pp. 18043–18047, 2006, doi: 10.1073/pnas.0608586103.

[77] J. Du *et al.*, “Dual-responsive triple-shape memory polyolefin elastomer/stearic acid composite,” *Polym. (United Kingdom)*, vol. 126, pp. 206–210, 2017, doi: 10.1016/j.polymer.2017.08.039.

[78] T. Xie, “Tunable polymer multi-shape memory effect,” *Nature*, vol. 464, no. 7286, pp. 267–270, 2010, doi: 10.1038/nature08863.

[79] X. Luo, R. Ou, D. E. Eberly, A. Singhal, W. Viratyaporn, and P. T. Mather, “A thermoplastic/thermoset blend exhibiting thermal mending and reversible adhesion,” *ACS Appl. Mater. Interfaces*, vol. 1, no. 3, pp. 612–620, 2009, doi: 10.1021/am8001605.

[80] E. D. Rodriguez, X. Luo, and P. T. Mather, “Linear/network poly(ε-caprolactone) blends exhibiting shape memory assisted self-healing (SMASH),” *ACS Appl. Mater. Interfaces*,

vol. 3, no. 2, pp. 152–161, 2011, doi: 10.1021/am101012c.

[81] J. Nji and G. Li, “Damage healing ability of a shape-memory-polymer-based particulate composite with small thermoplastic contents,” *Smart Mater. Struct.*, vol. 21, no. 2, 2012, doi: 10.1088/0964-1726/21/2/025011.

[82] T. Xie, “Recent advances in polymer shape memory,” *Polymer (Guildf).*, vol. 52, no. 22, pp. 4985–5000, 2011, doi: 10.1016/j.polymer.2011.08.003.

[83] N. Rattanasom, S. Prasertsri, and T. Ruangritnumchai, “Comparison of the mechanical properties at similar hardness level of natural rubber filled with various reinforcing-fillers,” *Polym. Test.*, vol. 28, no. 1, pp. 8–12, 2009, doi: 10.1016/j.polymertesting.2008.08.004.

[84] N. C. Restrepo-Zapata, T. A. Osswald, and J. P. Hernández-Ortiz, “Vulcanization of EPDM rubber compounds with and without blowing agents: Identification of reaction events and TTT-diagram using DSC data,” *Polym. Eng. Sci.*, vol. 55, no. 9, pp. 2073–2088, Sep. 2015, doi: 10.1002/PEN.24049.

[85] N. Candau *et al.*, “Strain-induced crystallization of natural rubber and cross-link densities heterogeneities,” *Macromolecules*, vol. 47, no. 16, pp. 5815–5824, 2014, doi: 10.1021/ma5006843.

[86] Y. Fukahori, “‘Mechanism of the self-reinforcement of cross-linked NR generated through the strain-induced crystallization,’” *Polymer (Guildf).*, vol. 51, no. 7, pp. 1621–1631, 2010, doi: 10.1016/j.polymer.2010.01.059.

[87] K. Brüning, K. Schneider, S. V Roth, and G. Heinrich, “Strain-induced crystallization around a crack tip in natural rubber under dynamic load,” *Polymer (Guildf).*, vol. 54, no. 22,

pp. 6200–6205, 2013, doi: 10.1016/j.polymer.2013.08.045.

[88] S. Trabelsi, P. A. Albouy, and J. Rault, “Stress-induced crystallization around a crack tip in natural rubber,” *Macromolecules*, vol. 35, no. 27, pp. 10054–10061, 2002, doi: 10.1021/ma021106c.

[89] J. B. Le Cam and E. Toussaint, “The mechanism of fatigue crack growth in rubbers under severe loading: The effect of stress-induced crystallization,” *Macromolecules*, vol. 43, no. 10, pp. 4708–4714, 2010, doi: 10.1021/ma100042n.

[90] P. Rublon *et al.*, “Multiaxial deformation and strain-induced crystallization around a fatigue crack in natural rubber,” *Eng. Fract. Mech.*, vol. 123, pp. 59–69, 2014, doi: 10.1016/j.engfracmech.2014.04.003.

[91] K. Brüning, K. Schneider, S. V Roth, and G. Heinrich, “Kinetics of strain-induced crystallization in natural rubber studied by WAXD: Dynamic and impact tensile experiments,” *Macromolecules*, vol. 45, no. 19, pp. 7914–7919, 2012, doi: 10.1021/ma3011476.

[92] S. Sun, Y. Lu, B. S. Hsiao, D. Wang, and L. Zhang, “Comprehensive study on temperature-induced crystallisation and strain-induced crystallisation behaviours of natural rubber/isoprene rubber blends,” *Plast. Rubber Compos.*, vol. 46, no. 7, pp. 290–300, 2017, doi: 10.1080/14658011.2017.1335481.

[93] J. Plagge and M. Klüppel, “Determining strain-induced crystallization of natural rubber composites by combined thermography and stress-strain measurements,” *Polym. Test.*, vol. 66, no. January, pp. 87–93, 2018, doi: 10.1016/j.polymertesting.2017.12.021.

[94] C. L. Lewis and E. M. Dell, “A review of shape memory polymers bearing reversible binding groups,” *Journal of Polymer Science, Part B: Polymer Physics*, vol. 54, no. 14. John Wiley and Sons Inc., pp. 1340–1364, 15-Jul-2016, doi: 10.1002/polb.23994.

[95] B. Yang, W. M. Huang, C. Li, and L. Li, “Effects of moisture on the thermomechanical properties of a polyurethane shape memory polymer,” *Polymer (Guildf).*, vol. 47, no. 4, pp. 1348–1356, 2006, doi: 10.1016/j.polymer.2005.12.051.

[96] B. Yang, W. M. Huang, C. Li, C. M. Lee, and L. Li, “On the effects of moisture in a polyurethane shape memory polymer,” *Smart Mater. Struct.*, vol. 13, no. 1, pp. 191–195, 2004, doi: 10.1088/0964-1726/13/1/022.

[97] B. Yang, W. M. Huang, C. Li, and J. H. Chor, “Effects of moisture on the glass transition temperature of polyurethane shape memory polymer filled with nano-carbon powder,” *Eur. Polym. J.*, vol. 41, no. 5, pp. 1123–1128, 2005, doi: 10.1016/j.eurpolymj.2004.11.029.

[98] J. Dong and R. A. Weiss, “Effect of crosslinking on shape-memory behavior of zinc stearate/ionomer compounds,” *Macromol. Chem. Phys.*, vol. 214, no. 11, pp. 1238–1246, 2013, doi: 10.1002/macp.201200145.

[99] W. M. Huang, B. Yang, L. An, C. Li, and Y. S. Chan, “Water-driven programmable polyurethane shape memory polymer: Demonstration and mechanism,” *Appl. Phys. Lett.*, vol. 86, no. 11, pp. 1–3, 2005, doi: 10.1063/1.1880448.

[100] X. Wang, J. Sparkman, and J. Gou, “Electrical actuation and shape memory behavior of polyurethane composites incorporated with printed carbon nanotube layers,” *Compos. Sci. Technol.*, vol. 141, pp. 8–15, 2017, doi: 10.1016/j.compscitech.2017.01.002.

[101] M. Y. Razzaq, M. Behl, and A. Lendlein, “Memory-effects of magnetic nanocomposites,” *Nanoscale*, vol. 4, no. 20, pp. 6181–6195, 2012, doi: 10.1039/c2nr31332d.

[102] H. Lu, Y. Yao, W. M. Huang, J. Leng, and D. Hui, “Significantly improving infrared light-induced shape recovery behavior of shape memory polymeric nanocomposite via a synergistic effect of carbon nanotube and boron nitride,” *Compos. Part B Eng.*, vol. 62, pp. 256–261, 2014, doi: 10.1016/j.compositesb.2014.03.007.

[103] M. Rogóż, H. Zeng, C. Xuan, D. S. Wiersma, and P. Wasylczyk, “Light-Driven Soft Robot Mimics Caterpillar Locomotion in Natural Scale,” *Adv. Opt. Mater.*, vol. 4, no. 11, pp. 1689–1694, 2016, doi: 10.1002/adom.201600503.

[104] B. Heuwers, A. Beckel, A. Krieger, F. Katzenberg, and J. C. Tiller, “Shape-memory natural rubber: An exceptional material for strain and energy storage,” *Macromol. Chem. Phys.*, vol. 214, no. 8, pp. 912–923, 2013, doi: 10.1002/macp.201200649.

[105] F. Katzenberg, B. Heuwers, and J. C. Tiller, “Superheated rubber for cold storage,” *Adv. Mater.*, vol. 23, no. 16, pp. 1909–1911, 2011, doi: 10.1002/adma.201100408.

[106] D. Quitmann, F. M. Reinders, B. Heuwers, F. Katzenberg, and J. C. Tiller, “Programming of shape memory natural rubber for near-discrete shape transitions,” *ACS Appl. Mater. Interfaces*, vol. 7, no. 3, pp. 1486–1490, 2015, doi: 10.1021/am507184c.

[107] B. Heuwers, D. Quitmann, F. Katzenberg, and J. C. Tiller, “Stress-induced melting of crystals in natural rubber: A new way to tailor the transition temperature of shape memory polymers,” *Macromol. Rapid Commun.*, vol. 33, no. 18, pp. 1517–1522, 2012, doi: 10.1002/marc.201200313.

[108] D. Quitmann, N. Gushterov, G. Sadowski, F. Katzenberg, and J. C. Tiller, “Solvent-sensitive reversible stress-response of shape memory natural rubber,” *ACS Appl. Mater. Interfaces*, vol. 5, no. 9, pp. 3504–3507, 2013, doi: 10.1021/am400660f.

[109] D. Quitmann, N. Gushterov, G. Sadowski, F. Katzenberg, and J. C. Tiller, “Environmental memory of polymer networks under stress,” *Adv. Mater.*, vol. 26, no. 21, pp. 3441–3444, 2014, doi: 10.1002/adma.201305698.

[110] A. D. I, C. P, A. K. R, and S. B, “Shape Memory Ceramic,” in *Shape Memory Materials*, Boca Raton, Florida : CRC Press ; Taylor & Francis, 2018, p. 34.

[111] D. Yuan, Z. Chen, C. Xu, K. Chen, and Y. Chen, “Fully Biobased Shape Memory Material Based on Novel Cocontinuous Structure in Poly(Lactic Acid)/Natural Rubber TPVs Fabricated via Peroxide-Induced Dynamic Vulcanization and in Situ Interfacial Compatibilization,” *ACS Sustain. Chem. Eng.*, vol. 3, no. 11, pp. 2856–2865, 2015, doi: 10.1021/acssuschemeng.5b00788.

[112] J.-H. C. and D.-K. K. Young-Wook Chang, Joy K Mishra, “Thermomechanical properties and shape memory effect of epoxidized natural rubber crosslinked by 3-amino-1,2,4-triazole,” *Polym. Int.*, vol. 56, no. december, pp. 694–698, 2006, doi: 10.1002/pi.

[113] R. A. Weiss, E. Izzo, and S. Mandelbaum, “New design of shape memory polymers: Mixtures of an elastomeric ionomer and low molar mass fatty acids and their salts,” *Macromolecules*, vol. 41, no. 9, pp. 2978–2980, 2008, doi: 10.1021/ma8001774.

[114] J. S. H. Wee, A. B. Chai, and J. H. Ho, “Fabrication of shape memory natural rubber using palmitic acid,” *J. King Saud Univ. - Sci.*, vol. 29, no. 4, pp. 494–501, 2017, doi: 10.1016/j.jksus.2017.09.003.

[115] N. R. Brostowitz, R. A. Weiss, and K. A. Cavicchi, “Facile Fabrication of a Shape Memory Polymer by Swelling Cross-Linked Natural Rubber with Stearic Acid,” *ACS Macro Lett.*, vol. 3, no. 4, pp. 374–377, Apr. 2014, doi: 10.1021/mz500131r.

[116] J. Park and D. Kim, “Effect of Polymer Solution Concentration on the Swelling and Mechanical Properties of Glycol Chitosan Superporous Hydrogels,” *J Appl Polym Sci*, vol. 115, pp. 3434–3441, 2010, doi: 10.1002/app.30632.

[117] A. M. Saeed, “Temperature effect on swelling properties of commercial polyacrylic acid hydrogel beads,” *Int. J. Adv. Biol. Biomed. Res.*, vol. 1, no. 12, pp. 1614–1627, 2013.

[118] N. M. Barkoula, B. Alcock, N. O. Cabrera, and T. Peijs, “Effect of Temperature on Hygroscopic Thickness Swelling Rate of Composites From Lignocellolusic Fillers and HDPE,” *Polym. Polym. Compos.*, vol. 16, no. 2, pp. 101–113, 2008, doi: 10.1002/pc.

[119] A. R. R. Menon, C. K. S. Pillai, and G. B. Nando, “Thermal degradation characteristics of natural rubber vulcanizates modified with phosphorylated cashew nut shell liquid,” *Polym. Degrad. Stab.*, vol. 52, no. 3, pp. 265–271, 1996, doi: 10.1016/0141-3910(96)00007-9.

[120] Y. S. R. Yahya, A. R. Azura, and Z. Ahmad, “Effect of curing systems on thermal degradation behaviour of natural rubber (SMR CV 60),” *J. Phys. Sci.*, vol. 22, no. 2, pp. 1–14, 2011, doi: 10.13140/RG.2.1.1419.5683.

[121] M. Porter, R. Rawi, and S. A. Rahim, “Chemistry of the latex prevulcanization process. Part 1. Migration of reactants from the solid phase into rubber particles.,” *J. Nat. Rubber Res.*, vol. 7, no. 2, pp. 85–101, 1992.

[122] K. K. Sasidharan, S. Palaty, K. S. Gopalakrishnan, K. E. George, and R. Joseph, “Room

temperature prevulcanization of natural rubber latex using xanthate," *J. Appl. Polym. Sci.*, vol. 94, no. 3, pp. 1164–1174, 2004, doi: 10.1002/app.21025.

[123] A. S. Siti Nuraya *et al.*, "Reinforcement of prevulcanised natural rubber latex films by banana stem powder and comparison with silica and calcium carbonate," *J. Rubber Res.*, vol. 15, no. 2, pp. 124–140, 2012.

[124] K. K. Sasidharan, R. Joseph, S. Palaty, K. S. Gopalakrishnan, G. Rajammal, and P. V. Pillai, "Effect of the vulcanization time and storage on the stability and physical properties of sulphur-prevulcanized natural rubber latex," *J. Appl. Polym. Sci.*, vol. 97, no. 5, pp. 1804–1811, 2005, doi: 10.1002/app.21918.

[125] S. Palaty, P. V. Devi, and J. Honey, "Effect of storage on the colloidal properties of room-temperature prevulcanised natural rubber latex," *Prog. Rubber, Plast. Recycl. Technol.*, vol. 27, no. 4, pp. 201–213, 2011, doi: 10.1177/147776061102700402.

[126] A. Paajanen, J. Vaari, and T. Verho, "Crystallization of cross-linked polyethylene by molecular dynamics simulation," *Polymer (Guildf).*, vol. 171, no. January, pp. 80–86, 2019, doi: 10.1016/j.polymer.2019.03.040.

[127] S. Toki, R. Takagi, M. Ito, and B. S. Hsiao, "Rupture, orientation and strain-induced crystallization of polymer chain and network in vulcanized polyisoprene during uniaxial deformation by in-situ Electron Spin Resonance (ESR) and synchrotron X-ray analysis," *Polymer (Guildf).*, vol. 52, no. 11, pp. 2453–2459, 2011, doi: 10.1016/j.polymer.2011.03.037.

[128] W. Sainumsai, K. Suchiva, and S. Toki, "Influence of sulphur crosslink type on the strain-induced crystallization of natural rubber vulcanizates during uniaxial stretching by in situ

WAXD using a synchrotron radiation," *Mater. Today Proc.*, vol. 17, pp. 1539–1548, 2019, doi: 10.1016/j.matpr.2019.06.179.

[129] K. L. Mok and A. H. Eng, "Characterisation of crosslinks in vulcanised rubbers: From simple to advanced techniques," *Malaysian J. Chem.*, vol. 20, no. 1, pp. 118–127, 2018.

[130] D. Y. Kim, J. W. Park, D. Y. Lee, and K. H. Seo, "Correlation between the crosslink characteristics and mechanical properties of natural rubber compound via accelerators and reinforcement," *Polymers (Basel).*, vol. 12, no. 9, pp. 1–14, 2020, doi: 10.3390/polym12092020.

[131] P. Tangboriboonrat and C. Lerthititrakul, "Morphology of natural rubber latex particles prevulcanised by sulphur and peroxide systems," *Colloid Polym. Sci.*, vol. 280, no. 12, pp. 1097–1103, 2002, doi: 10.1007/s00396-002-0654-7.

[132] M. Pantoja, T. Alvarado, M. Cakmak, and K. A. Cavicchi, "Stearic acid infused polyurethane shape memory foams," *Polymer (Guildf).*, vol. 153, no. August, pp. 131–138, 2018, doi: 10.1016/j.polymer.2018.08.002.

[133] G. Capiel, N. E. Marcovich, and M. A. Mosiewicki, "From the synthesis and characterization of methacrylated fatty acid based precursors to shape memory polymers," *Polym. Int.*, vol. 68, no. 3, pp. 546–554, 2019, doi: 10.1002/pi.5744.

[134] G. Capiel, N. E. Marcovich, and M. A. Mosiewicki, "Shape memory polymer networks based on methacrylated fatty acids," *Eur. Polym. J.*, vol. 116, no. April, pp. 321–329, 2019, doi: 10.1016/j.eurpolymj.2019.04.023.

[135] P. T. Mather, X. Luo, and I. A. Rousseau, "Shape memory polymer research," *Annu. Rev.*

Mater. Res., vol. 39, pp. 445–471, 2009, doi: 10.1146/annurev-matsci-082908-145419.

[136] C. S. Zhang and Q. Q. Ni, "Bending behavior of shape memory polymer based laminates," *Compos. Struct.*, vol. 78, no. 2, pp. 153–161, 2007, doi: 10.1016/j.compstruct.2005.08.029.

[137] H. Du, L. Liu, F. Zhang, J. Leng, and Y. Liu, "Triple-shape memory effect in a styrene-based shape memory polymer: Characterization, theory and application," *Compos. Part B Eng.*, vol. 173, no. April, p. 106905, 2019, doi: 10.1016/j.compositesb.2019.106905.

[138] Q. Ge *et al.*, "Thermomechanical behavior of shape memory elastomeric composites," *J. Mech. Phys. Solids*, vol. 60, no. 1, pp. 67–83, 2012, doi: 10.1016/j.jmps.2011.09.011.

[139] Y. Liu, K. Gall, M. L. Dunn, A. R. Greenberg, and J. Diani, "Thermomechanics of shape memory polymers: Uniaxial experiments and constitutive modeling," *Int. J. Plast.*, vol. 22, no. 2, pp. 279–313, 2006, doi: 10.1016/j.ijplas.2005.03.004.

[140] T. D. Nguyen, C. M. Yakacki, P. D. Brahmbhatt, and M. L. Chambers, "Modeling the relaxation mechanisms of amorphous shape memory polymers," *Adv. Mater.*, vol. 22, no. 31, pp. 3411–3423, 2010, doi: 10.1002/adma.200904119.

[141] T. D. Nguyen, "Modeling shape-memory behavior of polymers," *Polym. Rev.*, vol. 53, no. 1, pp. 130–152, 2013, doi: 10.1080/15583724.2012.751922.

[142] A. Ben Abdallah, A. Kallel, T. Hassine, F. Gamaoun, and A. Tcharkhtchi, "Modeling of viscoelastic behavior of a shape memory polymer blend," *J. Appl. Polym. Sci.*, vol. 139, no. 13, 2022, doi: 10.1002/app.51859.

[143] R. Akbari, G. Alamdarnejad, and M. Kokabi, "A constitutive model of thermoviscoelastic semicrystalline shape memory polymer considering viscous dissipation in the amorphous

phase," *J. Appl. Polym. Sci.*, vol. 137, no. 45, pp. 1–15, 2020, doi: 10.1002/app.49398.

[144] R. Rieder, A. Mehrle, A. Kallel, and A. Tcharkhtchi, "Modeling of the thermomechanical behavior of shape memory polymers," *AIP Conf. Proc.*, vol. 2289, no. November 2020, 2020, doi: 10.1063/5.0029075.

[145] C. Fang, J. Leng, H. Sun, and J. Gu, "A multi-branch thermoviscoelastic model based on fractional derivatives for free recovery behaviors of shape memory polymers," *Mech. Mater.*, vol. 120, no. October 2017, pp. 34–42, 2018, doi: 10.1016/j.mechmat.2018.03.002.

[146] H. R. Jarrah, A. Zolfagharian, R. Hedayati, A. Serjouei, and M. Bodaghi, "Nonlinear finite element modelling of thermo-visco-plastic styrene and polyurethane shape memory polymer foams," *Actuators*, vol. 10, no. 3, pp. 1–20, 2021, doi: 10.3390/act10030046.

[147] Y. Wang, J. Wang, and X. Peng, "Refinement of a 3D finite strain viscoelastic constitutive model for thermally induced shape memory polymers," *Polym. Test.*, vol. 96, p. 107139, 2021, doi: 10.1016/j.polymertesting.2021.107139.

[148] T. D. Nguyen, H. Jerry Qi, F. Castro, and K. N. Long, "A thermoviscoelastic model for amorphous shape memory polymers: Incorporating structural and stress relaxation," *J. Mech. Phys. Solids*, vol. 56, no. 9, pp. 2792–2814, 2008, doi: 10.1016/j.jmps.2008.04.007.

[149] H. J. Qi, T. D. Nguyen, F. Castro, C. M. Yakacki, and R. Shandas, "Finite deformation thermo-mechanical behavior of thermally induced shape memory polymers," *J. Mech. Phys. Solids*, vol. 56, no. 5, pp. 1730–1751, 2008, doi: 10.1016/j.jmps.2007.12.002.

[150] X. Guo, L. Liu, B. Zhou, Y. Liu, and J. Leng, "Constitutive model for shape memory polymer based on the viscoelasticity and phase transition theories," *J. Intell. Mater. Syst.*

Struct., vol. 27, no. 3, pp. 314–323, 2016, doi: 10.1177/1045389X15571380.

[151] P. Gilormini and J. Diani, “On modeling shape memory polymers as thermoelastic two-phase composite materials,” *Comptes Rendus - Mec.*, vol. 340, no. 4–5, pp. 338–348, 2012, doi: 10.1016/j.crme.2012.02.016.

[152] S. Reese, M. Böl, and D. Christ, “Finite element-based multi-phase modelling of shape memory polymer stents,” *Comput. Methods Appl. Mech. Eng.*, vol. 199, no. 21–22, pp. 1276–1286, 2010, doi: 10.1016/j.cma.2009.08.014.

[153] B. L. Volk, D. C. Lagoudas, and D. J. Maitland, “Characterizing and modeling the free recovery and constrained recovery behavior of a polyurethane shape memory polymer,” *Smart Mater. Struct.*, vol. 20, no. 9, p. 94004, Aug. 2011, doi: 10.1088/0964-1726/20/9/094004.

[154] Q. Yang and G. Li, “Temperature and rate dependent thermomechanical modeling of shape memory polymers with physics based phase evolution law,” *Int. J. Plast.*, vol. 80, pp. 168–186, 2016, doi: 10.1016/j.ijplas.2015.09.005.

[155] C. S. Jarali, S. Raja, and B. Kiefer, “Modeling the effective properties and thermomechanical behavior of SMA-SMP multifunctional composite laminates,” *Polym. Compos.*, vol. 32, no. 6, pp. 910–927, 2011, doi: 10.1002/pc.21110.

[156] C. S. Jarali, S. Raja, and A. R. Upadhya, “Constitutive modeling of SMA SMP multifunctional high performance smart adaptive shape memory composite,” *Smart Mater. Struct.*, vol. 19, no. 10, 2010, doi: 10.1088/0964-1726/19/10/105029.

[157] M. Rivai, E. Hambali, A. Suryani, R. Fitria, S. Firmansyah, and J. Pradesi, “Synthesis of

palm oil fatty acid as foaming agent for firefighting application," *IOP Conf. Ser. Earth Environ. Sci.*, vol. 65, no. 1, 2017, doi: 10.1088/1755-1315/65/1/012047.

[158] K. Kratz, S. A. Madbouly, W. Wagermaier, and A. Lendlein, "Temperature-memory polymer networks with crystallizable controlling units," *Adv. Mater.*, vol. 23, no. 35, pp. 4058–4062, 2011, doi: 10.1002/adma.201102225.

[159] A. Lendlein and S. Kelch, "Shape-Memory Polymers," *Angew. Chemie Int. Ed.*, vol. 41, no. 12, pp. 2034–2057, Jun. 2002, doi: https://doi.org/10.1002/1521-3773(20020617)41:12<2034::AID-ANIE2034>3.0.CO;2-M.

[160] J. H. Kim, T. J. Kang, and W. R. Yu, "Thermo-mechanical constitutive modeling of shape memory polyurethanes using a phenomenological approach," *Int. J. Plast.*, vol. 26, no. 2, pp. 204–218, 2010, doi: 10.1016/j.ijplas.2009.06.006.

[161] G. Marckmann and E. Verron, "Comparison of hyperelastic models for rubber-like materials," *Rubber Chem. Technol.*, vol. 79, no. 5, pp. 835–858, 2006, doi: 10.5254/1.3547969.

[162] Y. Wang, F. Zhu, Q. Rao, and X. Peng, "A 3D finite strain viscoelastic model with uncoupled structural and stress relaxations for shape memory polymers," *Polym. Test.*, vol. 103, no. July, p. 107373, 2021, doi: 10.1016/j.polymertesting.2021.107373.

[163] R. Stephen, S. Varghese, K. Joseph, Z. Oommen, and S. Thomas, "Diffusion and transport through nanocomposites of natural rubber (NR), carboxylated styrene butadiene rubber (XSBR) and their blends," *J. Memb. Sci.*, vol. 282, no. 1–2, pp. 162–170, 2006, doi: 10.1016/j.memsci.2006.05.019.

[164] W. Wang, J. Wang, Y. Kang, and A. Wang, “Synthesis, swelling and responsive properties of a new composite hydrogel based on hydroxyethyl cellulose and medicinal stone,” *Compos. Part B Eng.*, vol. 42, no. 4, pp. 809–818, 2011, doi: 10.1016/j.compositesb.2011.01.018.

[165] J. Hruljova, O. Järvik, and V. Oja, “Application of differential scanning calorimetry to study solvent swelling of kukersite oil shale macromolecular organic matter: A comparison with the fine-grained sample volumetric swelling method,” *Energy and Fuels*, vol. 28, no. 2, pp. 840–847, 2014, doi: 10.1021/ef401895u.

[166] F. M. Helaly, S. H. El Sabbagh, O. S. El Kinawy, and S. M. El Sawy, “Effect of synthesized zinc stearate on the properties of natural rubber vulcanizates in the absence and presence of some fillers,” *Mater. Des.*, vol. 32, no. 5, pp. 2835–2843, 2011, doi: 10.1016/j.matdes.2010.12.038.

[167] E. Sheng, I. Sutherland, R. H. Bradley, and P. K. Freakley, “Effects of a multifunctional additive on bound rubber in carbon black and silica filled natural rubbers,” *Eur. Polym. J.*, vol. 32, no. 1, pp. 35–41, 1996, doi: 10.1016/0014-3057(95)00107-7.

[168] P. L. Teh, Z. A. Mohd Ishak, A. S. Hashim, J. Karger-Kocsis, and U. S. Ishiaku, “Physical properties of natural rubber/organoclay nanocomposites compatibilized with epoxidized natural rubber,” *J. Appl. Polym. Sci.*, vol. 100, no. 2, pp. 1083–1092, 2006, doi: 10.1002/app.23452.

[169] H. Angellier, S. Molina-Boisseau, L. Lebrun, and A. Dufresne, “Processing and structural properties of waxy maize starch nanocrystals reinforced natural rubber,” *Macromolecules*, vol. 38, no. 9, pp. 3783–3792, May 2005, doi: 10.1021/ma050054z.

[170] P. S. K. Murthy, Y. M. Mohan, J. Sreeramulu, and K. M. Raju, “Semi-IPNs of starch and poly(acrylamide-co-sodium methacrylate): Preparation, swelling and diffusion characteristics evaluation,” *React. Funct. Polym.*, vol. 66, no. 12, pp. 1482–1493, 2006, doi: 10.1016/j.reactfunctpolym.2006.04.010.

[171] R. Shah, N. Saha, and P. Saha, “Influence of temperature, pH and simulated biological solutions on swelling and structural properties of biomineralized (CaCO3) PVP–CMC hydrogel,” *Prog. Biomater.*, vol. 4, no. 2–4, pp. 123–136, 2015, doi: 10.1007/s40204-015-0043-1.

[172] C. C. Hornat *et al.*, “Quantitative predictions of maximum strain storage in shape memory polymers (SMP),” *Polymer (Guildf).*, vol. 186, no. September 2019, p. 122006, 2020, doi: 10.1016/j.polymer.2019.122006.

[173] S. Gu, B. Yan, L. Liu, and J. Ren, “Carbon nanotube-polyurethane shape memory nanocomposites with low trigger temperature,” *Eur. Polym. J.*, vol. 49, no. 12, pp. 3867–3877, 2013, doi: 10.1016/j.eurpolymj.2013.10.007.

[174] N. A. Kinasih, M. I. Fathurrohman, and D. A. Winarto, “Swelling behaviour in n-pentane and mechanical properties of epoxidized natural rubber with different epoxide content,” *IOP Conf. Ser. Mater. Sci. Eng.*, vol. 223, p. 12002, 2017, doi: 10.1088/1757-899X/223/1/012002.

[175] S. Song, J. Feng, and P. Wu, “A new strategy to prepare polymer-based shape memory elastomers,” *Macromol. Rapid Commun.*, vol. 32, no. 19, pp. 1569–1575, 2011, doi: 10.1002/marc.201100298.

[176] S. S. Choi, “Influence of thermal aging on change of crosslink density and deformation of

natural rubber vulcanizates," *Bull. Korean Chem. Soc.*, vol. 21, no. 6, pp. 628–634, 2000.

[177] J. T. South, S. W. Case, and K. L. Reifsnider, "Effects of thermal aging on the mechanical properties of natural rubber," *Rubber Chem. Technol.*, vol. 76, no. 4, pp. 785–802, 2003, doi: 10.5254/1.3547772.

[178] X. Xiao *et al.*, "Shape memory polymers with high and low temperature resistant properties," *Sci. Rep.*, vol. 5, no. 1, p. 14137, 2015, doi: 10.1038/srep14137.

[179] X. L. Wu, S. F. Kang, X. J. Xu, F. Xiao, and X. L. Ge, "Effect of the crosslinking density and programming temperature on the shape fixity and shape recovery in epoxy-anhydride shape-memory polymers," *J. Appl. Polym. Sci.*, vol. 131, no. 15, Aug. 2014, doi: 10.1002/APP.40559.

[180] S. Chen, Q. Zhang, and J. Feng, "3D printing of tunable shape memory polymer blends," *J. Mater. Chem. C*, vol. 5, no. 33, pp. 8361–8365, 2017, doi: 10.1039/c7tc02534c.

[181] R. Hoeher, T. Raidt, C. Krumm, M. Meuris, F. Katzenberg, and J. C. Tiller, "Tunable multiple-shape memory polyethylene blends," *Macromol. Chem. Phys.*, vol. 214, no. 23, pp. 2725–2732, 2013, doi: 10.1002/macp.201300413.

[182] S. A. R. Hashmi, H. C. Prasad, R. Abishera, H. N. Bhargaw, and A. Naik, "Improved recovery stress in multi-walled-carbon-nanotubes reinforced polyurethane," *Mater. Des.*, vol. 67, pp. 492–500, 2015, doi: 10.1016/j.matdes.2014.10.062.

[183] D. Zhang, Y. Liu, K. Yu, and J. Leng, "Influence of cross-linking agent on thermomechanical properties and shape memory effect of styrene shape memory polymer," *J. Intell. Mater. Syst. Struct.*, vol. 22, no. 18, pp. 2147–2154, 2011, doi:

10.1177/1045389X11425282.

[184] G. Yang *et al.*, “Luminescent Poly(vinyl alcohol)/Carbon Quantum Dots Composites with Tunable Water-Induced Shape Memory Behavior in Different pH and Temperature Environments,” *ACS Appl. Mater. Interfaces*, vol. 8, no. 50, pp. 34744–34754, 2016, doi: 10.1021/acsami.6b11476.

[185] A. A. El-Gamal, “Effect of reinforcement filler on vulcanization, diffusion, mechanical, and electrical properties of natural rubber,” *J. Elastomers Plast.*, vol. 51, no. 6, pp. 512–526, 2019, doi: 10.1177/0095244318803750.

[186] A. M. Noor Azammi, S. M. Sapuan, M. R. Ishak, and M. T. H. Sultan, “Mechanical and Thermal Properties of Kenaf Reinforced Thermoplastic Polyurethane (TPU)-Natural Rubber (NR) Composites,” *Fibers Polym.*, vol. 19, no. 2, pp. 446–451, 2018, doi: 10.1007/s12221-018-7737-7.

[187] S. Toki *et al.*, “Entanglements and Networks to Strain-Induced Crystallization and Stress − Strain Relations in Natural Rubber and Synthetic Polyisoprene at Various Temperatures,” 2013.

[188] A. Tcharkhtchi, S. Abdallah-Elhirtsi, K. Ebrahimi, J. Fitoussi, M. Shirinbayan, and S. Farzaneh, “Some new concepts of shape memory effect of polymers,” *Polymers (Basel).*, vol. 6, no. 4, pp. 1144–1163, 2014, doi: 10.3390/polym6041144.

[189] O. A. Serenko, I. V. Tyun’kin, G. P. Goncharuk, E. S. Obolonkova, A. V. Efimov, and S. L. Bazhenov, “The effect of temperature on the stress-strain behavior of composites based on high-density polyethylene and rubber particles,” *Polym. Sci. - Ser. B*, vol. 50, no. 5–6, pp. 105–110, 2008, doi: 10.1134/S1560090408050011.

[190] R. Long *et al.*, “Work capacity of self-folding polymer origami,” *Proc. ASME 2021 Conf. Smart Mater. Adapt. Struct. Intell. Syst. SMASIS 2021*, pp. 6–11, 2021, doi: 10.1115/SMASIS2021-68384.

[191] R. Maddalena, L. Bonanno, B. Balzano, C. Tuinea-Bobe, J. Sweeney, and I. Mihai, “A crack closure system for cementitious composite materials using knotted shape memory polymer (k-SMP) fibres,” *Cem. Concr. Compos.*, vol. 114, no. May 2020, p. 103757, 2020, doi: 10.1016/j.cemconcomp.2020.103757.

[192] Y. He, S. Guo, Z. Liu, and K. M. Liew, “Pattern transformation of thermo-responsive shape memory polymer periodic cellular structures,” *Int. J. Solids Struct.*, vol. 71, pp. 194–205, 2015, doi: 10.1016/j.ijsolstr.2015.06.022.

[193] Q. Q. Ni, C. sheng Zhang, Y. Fu, G. Dai, and T. Kimura, “Shape memory effect and mechanical properties of carbon nanotube/shape memory polymer nanocomposites,” *Compos. Struct.*, vol. 81, no. 2, pp. 176–184, 2007, doi: 10.1016/j.compstruct.2006.08.017.

[194] C. Walters, D. Ballesteros, and V. A. Vertucci, “Structural mechanics of seed deterioration: Standing the test of time,” *Plant Sci.*, vol. 179, no. 6, pp. 565–573, 2010, doi: 10.1016/j.plantsci.2010.06.016.

[195] D. Zhou, Y. Zhou, J. Yuan, and Y. Liu, “Palmitic Acid-Stearic Acid/Expanded Graphite as Form-Stable Composite Phase-Change Material for Latent Heat Thermal Energy Storage,” *J. Nanomater.*, vol. 2020, 2020, doi: 10.1155/2020/1648080.